

**PL-TR-96-2033**

## **HAWKS (HITRAN Atmospheric Work Station)**

**Ontar Corporation  
9 Village Way  
North Andover, MA 01845**

**November 1995**

**Final Report  
August 1991 – June 1995**

**19980120 187**


**Approved for public release; distribution unlimited**

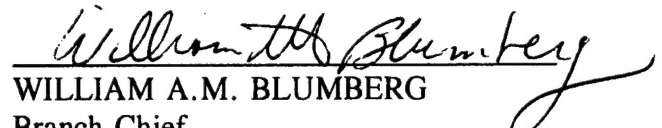


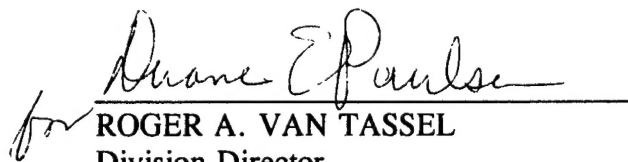
**PHILLIPS LABORATORY  
Directorate of Geophysics  
AIR FORCE MATERIEL COMMAND  
HANSCOM AFB, MA 01731-3010**

**[DTIC QUALITY INSPECTED 3]**

"This technical report has been reviewed and is approved for publication"

  
LAURENCE S. ROTHMAN  
Contract Manager

  
WILLIAM A.M. BLUMBERG  
Branch Chief

  
for ROGER A. VAN TASSEL  
Division Director  
Optical Environment Division

This report has been reviewed by the ESC Public Affairs Office (PA) and is releasable to the National Technical Information Service (NTIS).

Qualified requestors may obtain additional copies from the Defense Technical Information Center (DTIC). All others should apply to the National Technical Information Service (NTIS).

If your address has changed, or if you wish to be removed from the mailing list, or if the addressee is no longer employed by your organization, please notify PL/IM, 29 Randolph Road, Hanscom AFB, MA 01731-3010. This will assist us in maintaining a current mailing list.

Do not return copies of this report unless contractual obligations or notices on a specific document require that it be returned.



REPORT DOCUMENTATION PAGE			Form Approved OMB No. 0704-0188	
<small>Public reporting burden for this collection of information is estimated to average 1 hour per response, including the time for reviewing instructions, searching existing data sources, gathering and maintaining the data needed, and completing and reviewing the collection of information. Send comments regarding this burden estimate or any other aspect of this collection of information, including suggestions for reducing this burden, to Washington Headquarters Services, Directorate for Information Operations and Reports, 1215 Jefferson Davis Highway, Suite 1204, Arlington, VA 22202-4302, and to the Office of Management and Budget, Paperwork Reduction Project (0704-0188), Washington, DC 20503.</small>				
1. AGENCY USE ONLY (Leave blank)	2. REPORT DATE Nov 1995	3. REPORT TYPE AND DATES COVERED Final (August 1991 - June 1995)		
4. TITLE AND SUBTITLE HAWKS (HITRAN Atmospheric Work Station)		5. FUNDING NUMBERS PE 69120H PR 7670 TA 09 WU BI		
6. AUTHOR(S)		Contract F19628-91-C-0132		
7. PERFORMING ORGANIZATION NAME(S) AND ADDRESS(ES) ONTAR CORPORATION 9 Village Way North Andover, MA 01845		8. PERFORMING ORGANIZATION REPORT NUMBER  2032-02		
9. SPONSORING/MONITORING AGENCY NAME(S) AND ADDRESS(ES) Phillips Laboratory 29 Randolph Road Hanscom AFB, MA 01731-3010  Contract Manager: Laurence Rothman/GPOS		10. SPONSORING/MONITORING AGENCY REPORT NUMBER  PL-TR-96-2033		
11. SUPPLEMENTARY NOTES				
12a. DISTRIBUTION / AVAILABILITY STATEMENT  Approved for public release; distribution unlimited		12b. DISTRIBUTION CODE		
13. ABSTRACT (Maximum 200 words)  <p>The <b>HITRAN</b> database has been recognized for over 20 years as the international standard compilation of spectroscopic parameters for atmospheric gases. A comprehensive spectroscopic database of molecular parameters is required by all programs attempting to make line-by-line simulations. The next <b>HITRAN</b> release will be made under the <b>HAWKS</b> (HITRAN Atmospheric Work Station) umbrella. This new approach comes about because of the expanded nature of the current database. It will include an updated version of the traditional <b>HITRAN</b> compilation of spectral parameters for atmospheric gases. However, also included will be supplemental databases, greatly expanded cross-section databases, UV (both line-by-line, and cross-sections), aerosol indices of refraction, and the aforementioned <b>HITEMP</b>. The "old faithful" <b>SELECT.FOR.FORTRAN</b> source code is being superseded by <b>DOS/WINDOWS</b> and <b>UNIX</b>-based executable code for data handling. The makeover of <b>HITRAN</b>, represented by <b>HAWKS</b>, is a significant enhancement designed to meet the changing needs of the user community.</p>				
14. SUBJECT TERMS HAWKS Spectroscopy Molecular parameters		HITRAN UV		15. NUMBER OF PAGES 336
				16. PRICE CODE
17. SECURITY CLASSIFICATION OF REPORT Unclassified	18. SECURITY CLASSIFICATION OF THIS PAGE Unclassified	19. SECURITY CLASSIFICATION OF ABSTRACT Unclassified	20. LIMITATION OF ABSTRACT SAR	



## Table of Content

<b>1. INTRODUCTION</b>	<b>1</b>
<b>2.0 ACCOMPLISHMENT AND DELIVERABLES DURING THIS WORK</b>	<b>1</b>
<b>2.1 Accomplishments During this Work</b>	<b>2</b>
2.1.1 Assisted with the development of HITRAN92.	2
2.1.2 Assisted with the development of HITRAN96.	2
2.1.3 Development of the HAWKS workstation for DOS, DOS/WINDOWS and UNIX systems	4
2.1.4 Production of test CD-ROM's for the 1995/96 HITRAN database	4
2.1.5 Production and distribution of the HITRAN newsletter in 1992 through 1995	4
2.1.6 Assisted with the management of the HITRAN workshop in 1993	5
2.1.7 Presentation of a Paper at the 1995 SPIE meeting	5
2.1.8 Preparation of the MODTRAN technical report	5
<b>2.2 Deliverables During this Work</b>	<b>5</b>
2.2.1 Delivered HAWKS workstation to PL/GP	5
2.2.2 Delivered the HAWKS software for DOS, DOS/WINDOWS and UNIX	5
2.2.3 Delivered ~1200 CD-ROM's of the 1992 HITRAN database to PL/GP	5
2.2.4 Delivered ~5000 newsletter to PL/GP	6
<b>3.0 RECOMMENDATIONS FOR FUTURE WORK</b>	<b>6</b>
<b>APPENDIX A HAWKS SOFTWARE MANUAL</b>	<b>7</b>
<b>APPENDIX B SPIE PAPER (HITRAN, HAWKS AND HITEMP)</b>	<b>59</b>
<b>APPENDIX C MODTRAN TECHNICAL REPORT</b>	<b>66</b>

DTIC QUALITY INSPECTED 3



## **Acknowledgments**

Ontar is very fortunate to work with and develop software for the HITRAN database. The results of our work is described in this report. However the real work was done by a great many people outside of Ontar who are responsible for the success of this program. We would like to especially thank:

Dr. R. B. Wattson, Stewart Radiance Laboratory, Utah State University, Bedford, MA 01730 whose work with the Direct Numerical Diagonalization technique lead to the high temperature database for H<sub>2</sub>O and CO<sub>2</sub>.

Dr. R. R. Gamache, Univ. of Mass at Lowell, Lowell, MA 01854, whose contributions to the HITRAN database over the years are numerous.

All the contributors, worldwide, of data to the HITRAN database

Dr. L. S. Rothman, Geophysics Directorate, Simulations Branch, Hanscom AFB, MA 01731-3010 without whom there is no HITRAN.

Ms. Gail Anderson, Geophysics Directorate, Simulations Branch, Hanscom AFB, MA 01731-3010 for support with the MODTRAN report.

Mr. James Chetwynd Geophysics Directorate, Simulations Branch, Hanscom AFB, MA 01731-3010 for his help in putting together the MODTRAN manual.

Special thanks to the funding sources: The Air Force office of Scientific Research, The Department of Energy's ARM Program, The Phillips Laboratory, and The Naval Research Laboratory. The majority of this work was sponsored by the DOE's ARM program.

## **Database Distribution**

Distribution of the HAWKS/HITRAN databases and software is unlimited. They are currently distributed on a single CD-ROM. Copies may be obtained by contacting:

Dr. L. S. Rothman e-mail Rothman@PL9000.PLH.AF.MIL  
e-mail LRothman@CfA.Harvard.edu

or

The Ontar Corporation Tel: (USA)-508-689-9622  
Fax: (USA)-508-681-4585



# 1. Introduction

This report described work performed for the Phillips Laboratory, Geophysics Directorate under contract F19628-91-0132 from August 1991 through June 1995.

The primary purpose of this document is to review the contract accomplishments. The real "report" is the HAWKS/HITRAN database and associated software. **If you do not have the HAWKS/HITRAN 1996 database and software, our advise is to do so as quickly as you can and enjoy.**

The **HITRAN** database has been recognized for over 20 years as the international standard compilation of spectroscopic parameters for atmospheric gases. A new version is in beta testing and will be available for distribution within the next few months. Significant new additions have been made to the database to keep pace with the increasing requirements of the user community.

This report is divided into five parts:

- ◆ An description (thankfully brief) of the accomplishments and deliverables during the program. **Section 2**
- ◆ Recommendations for future work. **Section 3**
- ◆ The HAWKS/HITRAN software manual. **Appendix A**
- ◆ A paper describing the HITEMP database presented at the SPIE AeroSense Meeting, on 18 April 1995, in Orlando, Florida. **Appendix B**
- ◆ The MODTRAN Technical Report. **Appendix C**

## 2.0 Accomplishment and Deliverables During this Work

A great deal of work was accomplished during this contract. This included:

1. Assisted with the development of the 1992 HITRAN database.
2. Assisted with the development of the 1996 HITRAN database.
3. Development of the HAWKS workstation for DOS, DOS/WINDOWS and UNIX systems.
4. Production of test CD-ROM's for the 1995/96 HITRAN database.
5. Production and distribution of the HITRAN newsletter in 1992 through 1995.
6. Assisted with the management of the HITRAN workshop in 1993.
7. Presentation of a Paper at the 1995 SPIE meeting
8. Preparation of the MODTRAN technical report
9. Delivered a HAWKS workstation to PL/GP.
10. Delivered the HAWKS software for DOS, DOS/WINDOWS and UNIX systems to PL/GP

11. Delivered ~1200 CD-ROM's of the 1992 HITRAN database to PL/GP.
12. Delivered ~5000 newsletter to PL/GP.

## 2.1 Accomplishments During this Work



### 2.1.1 Assisted with the development of HITRAN92.

HITRAN92 was the first HITRAN database distributed on CD-ROM. Several significant additions over the previous database (HITRAN91) were made. Software programs were provided for simple data manipulations. Archival copies of the 1986 and 1991 database were included on the CD. Ontar both assisted the Phillips Laboratory in the preparation and validation of the data; and the overall design and production of the CD-ROM's

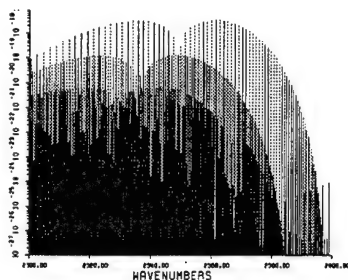


### 2.1.2 Assisted with the development of HITRAN96.

HAWKS/HITRAN96 will be the first total overhaul of the HITRAN database in the past 9 years. Significant data and software additions have been made. The databases in the 1996 release have been significantly improved and enhanced. New molecules added to the line-by-line database include: **CIONO<sub>2</sub>**  $\nu_4$  band of two isotopes plus one hot band, **HCOOH** in the 9  $\mu\text{m}$  region, **HO<sub>2</sub>** three fundamental bands  $\nu_1$ ,  $\nu_2$  and  $\nu_3$ , and **O** (atomic oxygen).

Improvements to existing line-by-line data include: **H<sub>2</sub>O** line positions have been corrected in the 720-1400  $\text{cm}^{-1}$  region and new data have been added on the isotope HDO; **O<sub>2</sub>** improved magnetic dipole transitions; **O<sub>3</sub>** updated 2.5  $\mu\text{m}$  band, updated 4.8  $\mu\text{m}$  data, replaced main bands at 3.3  $\mu\text{m}$  and added new hot lines at 10  $\mu\text{m}$ ; **OH** improved intensities for the pure rotational lines; **CH<sub>4</sub>** a new prediction of the CH<sub>3</sub>D triad  $\nu_3$ ,  $\nu_5$ , and  $\nu_6$ ; **CO** new and improved data at 10-480  $\text{cm}^{-1}$ ; **HCl** improved data; **HBr** improved data; **HF** improvements in the region 41-625  $\text{cm}^{-1}$ ; **NH<sub>3</sub>** major updates have been added; **NO** improved positions and intensities in the 2.5-7  $\mu\text{m}$  region; **HNO<sub>3</sub>** new and improved data for  $\nu_5$  and 2  $\nu_9$  bands; **N<sub>2</sub>O** two pure rotational bands have been added; **NO<sub>2</sub>** improved  $\nu_2$ , and hot  $\nu_2$  bands in the 10-17  $\mu\text{m}$  region, and new results for the  $\nu_3$  band in the 6-8.6  $\mu\text{m}$  region; **C<sub>2</sub>H<sub>2</sub>** new 3  $\mu\text{m}$  data added, and upgrades to the 14  $\mu\text{m}$  band; **CH<sub>3</sub>Cl** new  $\nu_3$  data and references have been added; **ClO** new data have been added; **COF<sub>2</sub>** the  $\nu_4$  and 2  $\nu_5$  bands have been added; **H<sub>2</sub>S** new data for the  $\nu_2$  region and the 2  $\nu_2$ ,  $\nu_1$  and  $\nu_3$  regions; **HOCl** updated line positions; **OCS** improved  $\nu_1$  data and additional  $\nu_1$  data for isotope 34; **SO<sub>2</sub>** new calculations of the 2  $\nu_3$  and 3  $\nu_3$  bands.





A major addition to the new database are data for aerosols. These include: **H<sub>2</sub>O** the real and imaginary indices of refraction for water at 27 C between 10 and 5000 cm<sup>-1</sup>; **H<sub>2</sub>O** the imaginary indices of refraction for water and ice in the 0.65 to 2.5 μm range; **H<sub>2</sub>O** the real and imaginary indices of refraction of ice at -7 C for the .043 to 167 μm range, and indices of ice at -1, -5, -20, and -60 C for the 167 to 8.6e6 μm range; **H<sub>2</sub>SO<sub>4</sub>** the real and imaginary indices of refraction of sulfuric acid solutions at 25, 38, 50, 75, 84.5, and 95.6% H<sub>2</sub>SO<sub>4</sub> by weight; **H<sub>2</sub>SO<sub>4</sub>** the real and imaginary indices of refraction of sulfuric acid solutions at 75 and 90% H<sub>2</sub>SO<sub>4</sub> by weight, plus the standard deviations of the measurements; **H<sub>2</sub>SO<sub>4</sub>** theoretical equilibrium composition (weight percentage of H<sub>2</sub>SO<sub>4</sub>) of sulfuric acid solutions, given as a function of temperature and H<sub>2</sub>O vapor pressure; **H<sub>2</sub>SO<sub>4</sub>** density (gm/cm<sup>3</sup>) values for solutions between 0 and 100% H<sub>2</sub>SO<sub>4</sub> (by weight) for temperatures between 0 and 60 C; **HNO<sub>3</sub>** the real and imaginary indices of refraction of nitric acid solutions at 68% HNO<sub>3</sub>, by weight, plus the standard deviations of the measurements; **HNO<sub>3</sub>** the real and imaginary indices of refraction of H<sub>2</sub>O-ice, amorphous nitric acid solutions, and nitric acid hydrates.

**Additional aerosols** include: the real and imaginary indices of refraction for water, ice, sodium chloride, sea salt, water soluble aerosol, ammonium sulfate, carbonaceous aerosol, volcanic dust, sulfuric acid, meteoric dust, quartz, hematite, sand, and dust-like aerosol. The tabulations start at 0.2 μm and extend out to 40 μm (or to longer wavelengths).

Cross-sections for **CFC11**, **CFC12** and **CFC22** have been improved and have been added for **CLONO<sub>2</sub>**. These data are now given for a range of temperatures and pressures.

High temperature (HITEMP) data for CO<sub>2</sub>, H<sub>2</sub>O and CO have been added and are discussed in more detail below in Section 3.

Finally, partition sum coefficients have been upgraded, partition sums are now either direct sum or formula, depending on molecule.

A high temperature datasets (HITEMP) for CO<sub>2</sub>, H<sub>2</sub>O and CO are a major addition and will be used in a variety of remote sensing applications ranging from exhaust gas monitoring to the investigation of stellar atmospheres. Traditionally, investigators have scaled the HITRAN database to estimate the absorption and emission spectra at elevated temperatures. Although the scaling from 296 K to higher temperatures is sufficiently accurate to estimate the line strength, etc. at the higher temperature, the additional spectral lines were missing from the simulation. This approach often leads to a significant underestimate of the source radiance.

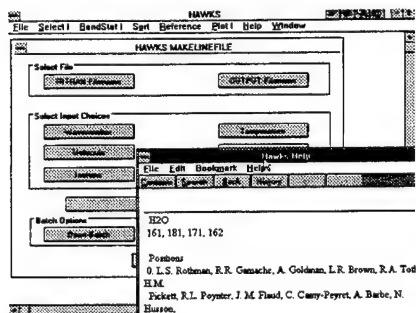
The data were scaled to a standard reference temperature of 296K for intensity and halfwidth to make database compatible with codes such as FASCODE. The dynamic range has also been limited by the choice of cutoff, for example limiting the total band intensities in the driver tables. The HITEMP database spectral coverage, number of lines for each molecule and calculational method are summarized in Table 3.

The line positions and intensities of water vapor were calculated from the Direct Numerical Diagonalization method [1]. For CO<sub>2</sub>, a table of spectroscopic constants, that is, distortion and higher order terms plus band intensities and Herman-Wallis factors was generated. However, very high weights were given to observed line positions from which lower order constants were established via a least-squares method. The final parameters were then calculated using the standard formulae [2]. Halfwidths were applied to the parameters in the same fashion as HITRAN. The CO parameters were generated with the application from solar atlas [3].

Molecules	Spectral Coverage	# of Lines	Temperature of Calculation
CO <sub>2</sub>	158 - 9648 cm <sup>-1</sup> 1 - 63 μm	1,032,269 1st. three isotopes	DND <sup>1</sup> @ 1000 K
H <sub>2</sub> O	500 - 5000 cm <sup>-1</sup> 2 - 20 μm	1,174,009 principal isotope	DND @ 1500 K
CO	850 -- 6418 cm <sup>-1</sup> 1.6 - 12 μm	113,022 all significant isotopes	Solar Atlas

<sup>1</sup> Direct Numerical Diagonalization

Table 3 Statistics HITEMP database



### 2.1.3 Development of the HAWKS workstation for DOS, DOS/WINDOWS and UNIX systems

Finally, totally new software has been developed for uses with the HITRAN and associated databases. The HAWKS software is designed to assist the user in easily adapting to the manipulation of the HITRAN molecular spectroscopic database and associated molecular databases. This edition is

the first in a MS Windows and UNIX environments. The many features are fully described in the manual given in Appendix A. The user now has many functions to examine and process the data on the compilation (or associated external data) than was previously available.

### 2.1.4 Production of test CD-ROM's for the 1995/96 HITRAN database

A beta version of HAWKS/HITRAN96 has been made. Approximately 9 test CD-Rom's were made and sent to selected individuals for evaluation.

### 2.1.5 Production and distribution of the HITRAN newsletter in 1992 through 1995

The HITRAN community has grown tremendously during the period of this work from approximately 300 to over 1100 users. It is important to maintain a sense of community which has been accomplished, in part, via a newsletter

Ontar published, in conjunction with Phillips Laboratory the HITRAN Newsletter. This has been an informative document covering specific details of the database, user applications, announcements of upcoming meetings, and other material related to the database. The newsletter has also served as a lightning rod to attract interest in this project.

#### **2.1.6 Assisted with the management of the HITRAN workshop in 1993**

The most recent HITRAN biennial workshop was held at Hanscom, AFB, MA in June 1993. Ontar assisted in the management and running of this meeting. Specifically, we prepared meeting announcements; collected a collated abstracts; prepared the conference proceedings; prepared name tags; arranged catering; and provided personnel during the meeting for management functions.

#### **2.1.7 Presentation of a Paper at the 1995 SPIE meeting**

A technical paper describing the next addition of the HITRAN/HAWKS database was presented at the SPIE AeroSense Meeting in Orlando FL, in April 1995. This paper is included as Appendix B of this report.

#### **2.1.8 Preparation of the MODTRAN technical report**

The MODTRAN technical report is a comprehensive manual discussing the theory and operation of the Phillips Laboratory's LOWTRAN and MODTRAN atmospheric radiance and transmission models. Ontar was responsible for assembling this document, which is Appendix C of this document.

### **2.2 Deliverables During this Work**

A number of deliverables were made over the period of this contract. They are briefly described below.

#### **2.2.1 Delivered HAWKS workstation to PL/GP**

A complete HAWKS was delivered to PL/GP during this contract. It consisted of a 66 mhz, Intel 486 based CPU, with 20 Mbytes of memory, a 1 gbytes hard disk, a CD-ROM drive, a 21" color monitor, and a 9-track tape drive. A fax machine was also delivered to PL/GP during the contract.

#### **2.2.2 Delivered the HAWKS software for DOS, DOS/WINDOWS and UNIX**

Three versions of the HAWKS software were delivered to PL/GP during this contract. One for MD-DOS, one for MD-DOS with Windows, and one for SUN/UNIX workstation. The latter two are more complete than the former. Finally, an upgraded version of Select (source code written in C) was delivered in PL/GP.

The Windows and UNIX softwares fully describe the HAWKS Software Manual, given in Appendix A.

#### **2.2.3 Delivered ~1200 CD-ROM's of the 1992 HITRAN database to PL/GP**

Approximately 1200 copies of the HITRAN92 CD-Rom were delivered to PL/GP.

#### **2.2.4 Delivered ~5000 newsletter to PL/GP**

Approximately 5000 HITRAN newsletter were delivered to PL/GP during this contract.

### **3.0 Recommendations for Future Work**

The **HITRAN** database is recognized as the international standard compilation of spectroscopic parameters for atmospheric gases. It is rapidly approaching the quarter century mark. HITRAN serves many diverse user communities. By far the largest number of users have DoD applications related to target detection through the atmosphere. Many do not use it directly, but access HITRAN via models such as FASCODE. At the other end of the spectrum is a smaller group of users performing basic research, both in the laboratory and in the atmosphere. It is a tribute to HITRAN that it can serve such a diverse group of users.

HITRAN must continue to serve all of these communities. New requirements in target detection (e.g. UV systems) are being investigated. Likewise, more complex atmospheric investigations are being undertaken which require high quality, reliable spectroscopic data. However, for HITRAN to remain vital it must continue to serve an expanding user base. There is a tremendous need for data (e.g. aerosols, organic molecules, different temperature regimes). The challenge for HITRAN over the next decade is to meet both the needs of its existing and new users.

## **Appendix A HAWKS Software Manual**

# **HAWKS**

## **HITRAN ATMOSPHERIC WORKSTATION**

### **FOR WINDOWS**

Laurence S. Rothman  
PL/GPOS  
23 Randolph Road  
Hanscom AFB, MA 01731-3010

Andrew McCann, Joseph Kristl, Len Abreu, Sabrina Harvey,  
Martine Voltaire, and Leslie Cox  
Ontar Corporation, 9 Village Way, North Andover, MA 01845-2000





**Table of Contents**

1. Software Installation .....	1
1.1 HAWKS PC Installation .....	1
1.2 HAWKS UNIX Installation .....	2
1.3 Setting up a DOS Text Editor .....	2
1.4 Setting up a UNIX Text Editor .....	5
2. HITRAN and HAWKS .....	5
3. Initiating the Operation of HAWKS .....	8
3.1 File Option .....	9
3.2 Select Option .....	9
3.2.1 Select Option: HITRAN Filename .....	10
3.2.2 Select Option: Output Filename .....	10
3.2.3 Select Option: Spectral Range .....	11
3.2.4 Select Option: Molecule .....	12
3.2.5 Select Option: Isotope .....	13
3.2.6 Select Option: Temperature .....	14
3.2.7 Select Option: Band .....	14
3.2.8 Select Option: Cutoff .....	16
3.2.9 Select Option: RUN SELECT .....	17
3.2.10 Select Option: RUN DESELECT .....	18
3.2.11 Select Option: Open Batch .....	18
3.2.12 Select Option: Save Batch .....	19
3.3 BandStat Option .....	20
3.4 Sort Option .....	21
3.4.1 Sort Option: Merge .....	23
3.5 Reference Option .....	24
3.5.1 Reference Option: Molecule .....	24
3.5.2 Reference Option: Wavenumber .....	26
3.5.3 Reference Option: Xsection .....	27
3.6 Plot Option .....	28
3.6.1 Difference Plots (Dif file) .....	31
3.6.2 Edit Plot .....	33
3.7 Help Option .....	33
3.7.1 Help Option: About .....	35
3.8 Window Option .....	36
4. Accessing other databases .....	36
5. Future Enhancements .....	37
6. Acknowledgments .....	37
7. References .....	38

APPENDIX A. Directories and Files on the CD-ROM .....	39
APPENDIX B. HITRAN Molecules with Associated Indices .....	46



This manual is designed to assist the user in easily adapting to the manipulation of the **HITRAN96** molecular spectroscopic database and associated molecular databases by proper utilization of the HAWKS software package.

## **1. Software Installation**

Installing HAWKS is a straightforward process of running the install program and then making a few manual (but optional) adjustments to the installation after you are done. Each of these steps is described in the following sections.

To use HAWKS, the following system requirements apply:

### **PC Hardware requirements:**

- ▶ Intel 80386 or higher PC running MS-Windows 3.x, Windows NT, or WINDOWS95
- ▶ 8 Mb of RAM (minimum)
- ▶ A numeric co-processor is needed for an 80386 processor
- ▶ 5 Mb of hard disk space (minimum), 100 Mb recommended
- ▶ A CD-ROM reader.

### **UNIX Hardware requirements:**

The UNIX hardware requirements are similar to that for the PC in terms of hard disk space, memory, and a CD-ROM reader. The software is currently available for systems using either Solaris 1 or Solaris 2. Additional versions will be available in the future.

## **1.1 HAWKS PC Installation**

You must have MS Windows 3.x (or WINDOWS95) running before you install HAWKS. Insert the CD-ROM into your CD-ROM reader (generally drive letter D: or E:). Use the Windows Program Manager menu option **File | Run** to run the installation program from the CD-ROM drive. For example, if your reader is drive D:, then run **D:\SOFTWARE\WINDOWS\SETUP** in the **File | Run** dialog box. The Setup program displays an information dialog box and then asks you what directory in which to install the software. This option lets you selectively install the HITRAN database and other data sets. The Setup program creates a Program Manager program group

for HAWKS and finishes. You are now ready to run the software by clicking on the HAWKS icon, or you can access the stand-alone help or view the README.DOC files by clicking the other icons.

You may want to configure your favorite DOS-based editor so that it can be used from within HAWKS to view and/or edit the very large ASCII files occasionally generated during select operations. For instructions on doing this, see Section 1.3.

## **1.2 HAWKS UNIX Installation**

The UNIX distribution presently supports SUNOS4 and Solaris2. Support for other UNIX systems are planned for a later date. The UNIX distributions are stored as compressed tar files in the directory: `\software\unix`. This directory has two files

`hawks_SUNOS4.tar.Z`

`hawks_Solaris2.tar.Z`

The first file is for Solaris 1 and the second file is for Solaris2. To install hawks, create a HAWKS home directory and copy the appropriate compressed tar file to the HAWKS home directory. Untar the compressed tar file with the following command

```
zcat hawks_SUNOS4.tar.Z | tar -xvf -           for SUNOS4
```

or

```
zcat hawks_Solaris2.tar.Z | tar -xvf -        for Solaris2
```

Run the hawks program with the following command

```
hawks &
```

The HAWKS distribution contains a file called **zApp**. This is a Motif resource file that must be copied to your home directory by typing:

```
cp Zapp~
```

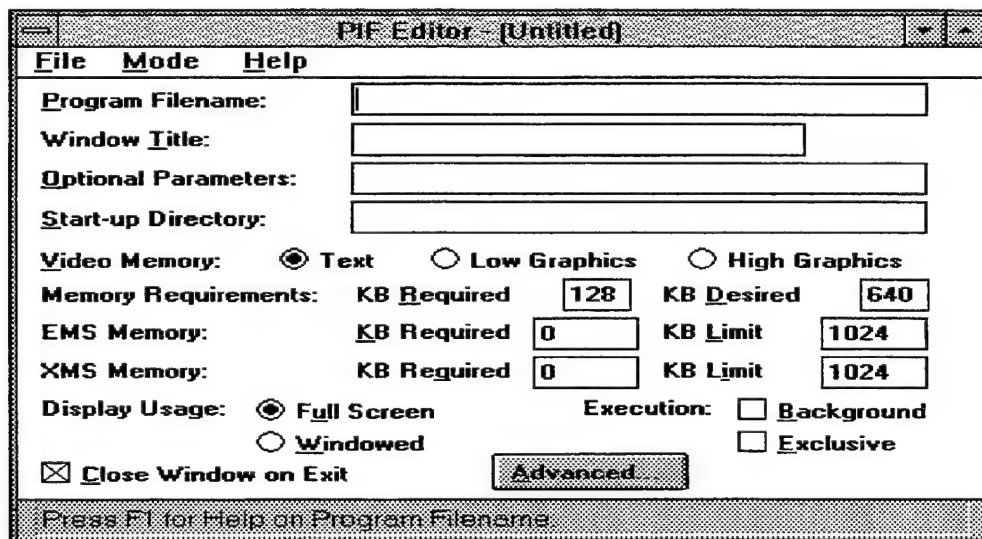
## **1.3 Setting up a DOS Text Editor**

HAWKS provides access to a DOS-based text editor from its command menus. This option has been offered because many HAWKS output files grow to many megabytes in size, and not many editors are capable of handling these large files. We have had good experience with

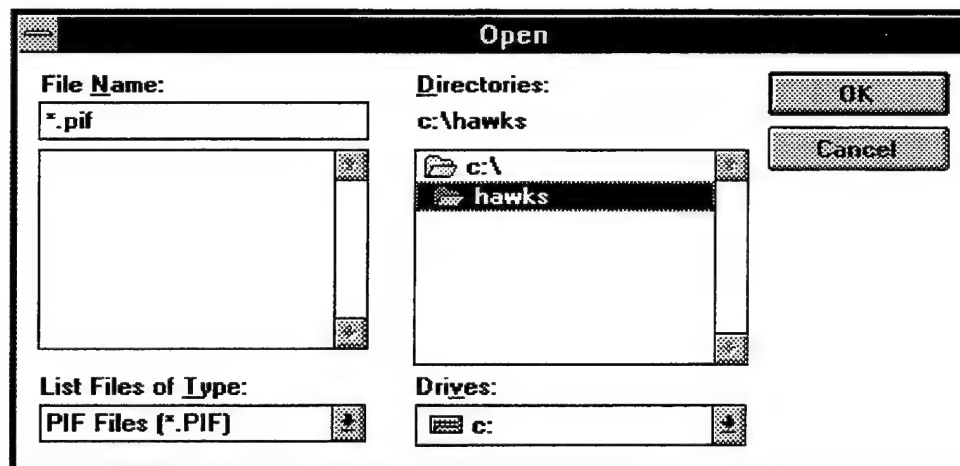
the Borland Brief editor. This option lets you hook your favorite DOS-based editor in, so that you do not have to learn a new set of viewing and editing commands. If you prefer to use a Windows-based editor, it cannot be hooked into the HAWKS menu system, but it does not need to be, since a Windows program can easily be run concurrently with HAWKS in its own window, and switched to when you want to view a file.

Setting up a text editor requires modification of the PIF (Program Information File) called B.PIF. This is done using the PIF editor that is supplied with MS Windows, and typically has an icon in the Main program group. If you have used the PIF editor before, all you have to do is change the program name and path in the PIF file to match the editor that you want to use. The B.PIF file supplied is set to work on the program B.EXE, at a default path of **C:\BRIEF**. If you have not used the PIF editor before, step-by-step instructions are provided below to walk you through the process. (In Windows95, use "Properties" to edit the b.pif file.)

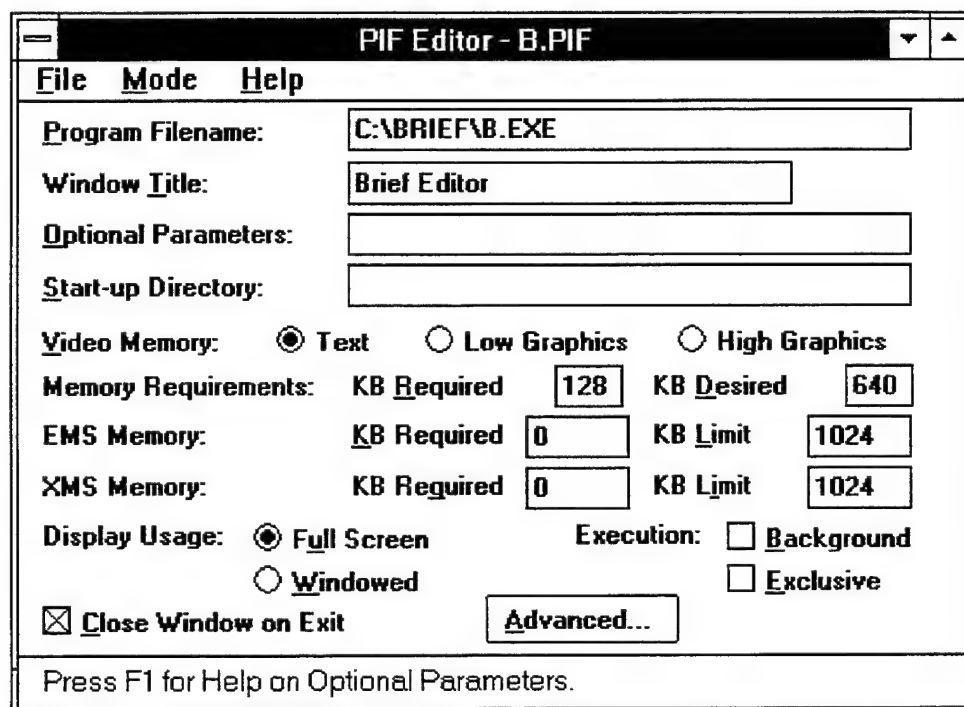
Start the PIF editor by double-clicking on its icon in the Main program group of the Windows Program Manager. You will see the following opening screen:



First you must load in the existing settings for the B.PIF file supplied with HAWKS. Use the **File** | **Open** command from the menu bar to select and load this file. After selecting **File**, and then **Open**, you will see a dialog box like the one below:



Use the 'Drives' box to select the drive that you have installed HAWKS on, and then use the 'directories' list box to change into the HAWKS directory. At that point, you will see B.PIF displayed in the list box on the left. Select the B.PIF file by clicking on its name in the list box. After the B.PIF name is displayed in the File Name box, click on the OK button on the upper right. You will be returned to the PIF editor main box, but now it should look like the one below:



At this point, you probably have to change only two items: the **Program Filename** (top box), and

the **Window Title** (second box). Edit these to match the text editor you will be using. If your editor has special instructions for running in a DOS window under MS Windows, you may have to change some other parameters as well. Consult the documentation for your editor to see if this is needed.

When the PIF file inputs are set, be sure to save the changed inputs away to the B.PIF file. This is done using the **File | Save** menu choice. If you use the **SaveAs** option, be sure to save the file as B.PIF in the HAWKS working directory. After this is done, you can exit the PIF editor using **File | Exit**, and you are now ready to give your HAWKS installation a trial run.

#### **1.4 Setting up a UNIX Text Editor**

HAWKS uses the shell script file view to run the text editor. The default text file view is

```
#!/bin/sh
```

```
fv $1
```

Edit this line to include your favorite editor. For example, to run the vi editor change file view to

```
#!/bin/sh, xterm -e vi $1
```

## **2. HITRAN and HAWKS**

The HITRAN Atmospheric Workstation is the latest version in a series of atmospheric molecular spectroscopic databases. These databases have a plethora of uses, the most prevalent one being as input to high-resolution transmission modeling codes of the atmosphere. Other examples of applications of HITRAN include laser propagation, hot gaseous source detection, pollution studies, background characterization, remote sensing in the atmosphere, climate assessment, greenhouse gas studies, ozone depletion, and laboratory spectroscopy.

HITRAN has traditionally supplied the necessary input for the molecular absorption part of the total attenuation in Lambert-Beer's law calculations. The other aspects of the attenuation are ascribed to aerosol extinction, continuum absorption, and scattering. The original public edition of the molecular spectroscopic database in a machine-readable form was in 1973 (the AFCRL Atmospheric Absorption Line Parameters Compilation<sup>1</sup>). This first edition was comprised

of the seven most infrared-active absorbers in the earth's atmosphere and only covered a spectral range of about 1 to 100 micrometers. In addition, the information for each available transition was essentially limited to the principal parameters: the line position (in wavenumbers, *i.e.* reciprocal centimeters,  $\text{cm}^{-1}$ ), the intensity of the transition (in  $\text{cm}^{-1}/(\text{molecule} \cdot \text{cm}^{-2})$  at 296K), the air-broadened halfwidth ( $\text{cm}^{-1}/\text{atm}$ ), and the energy of the lower state of the transition (in  $\text{cm}^{-1}$ ). Knowledge of the parameters at that time was limited, especially for the halfwidth which often simply was given a hard-sphere collision default value.

In the intervening decades, the molecular database has been substantially expanded, in terms of spectral coverage, molecular species, added parameters, increased number of molecular bands, and greatly improved accuracy. Details of the various editions and their enhancements are contained in Refs. 2-4.

The current edition contains 37 different species in the high-resolution portions, with the inclusion of many of their significant isotopomers as well. The spectral range is from the millimeter through the ultraviolet (0 to about  $60,000 \text{ cm}^{-1}$ ). From the initial inception of the database, the number of transitions has increased by an order of magnitude to about 1 million currently on the HITRAN line-by-line portion.

Another aspect of the development of the spectroscopic molecular database, or HITRAN as it is known, has been the improvement in user access. The initial versions were available on cards (a relic of the past, the cards held 80 characters of information and hence each 80-character HITRAN transition of the early editions was a single record) and on large magnetic tape. Tape became the principal means of distribution, but suffered from many inconveniences: slow sequential access, necessity of reading on mainframes, loss of integrity over time, damage, data corruption, etc. In 1992, HITRAN was made available on CD-ROM. This media enabled a great deal of data to be placed on a small, archival optical disk. More than 1000 copies of the 1992 edition have been distributed on CD-ROM as the revolution in the use of personal computers and workstations with attached CD-ROM readers mushroomed in the early '90s.

With the current edition of HITRAN, another major step has been made. HITRAN itself, the line-by-line portion of the compilation, is now part of a much larger ensemble of tools for modeling. First, the compilation includes HITRAN (significantly updated as always) and several other databases for the "matter" part of the modeling of the interaction of matter and radiation. The compilation has directories containing besides HITRAN, cross-section data of heavier species,

UV cross-sections, supplemental files (parameters in HITRAN-like format, but consigned to this section until further verification is made), aerosol indices of refraction, and HITEMP (the high-temperature analog of HITRAN). Table 1 illustrates the file structure of the compilation.

DIRECTORY	SUB-DIRECTORIES	MEGABYTES
SOFTWARE	WINDOWS	1.8
	UNIX	~2*(2.5)
	GENERIC	0.7
HITRAN96	By_Molecule	2*(101.9)
Supplemental		19.4
IR Cross-sections		18.0
UV	Line-by-line	1.1
	Cross-sections	2.5
Aerosols		0.2
HITEMP		236.6
MODELS	MODTRAN	~13.5
Total: ~500		

Table 1. File Structure of HAWKS

Equally important is the vastly improved user interface on the current compilation, HAWKS. This edition is the first in a WINDOWS environment. The many added features are described in the sections below, and it becomes apparent that the user now has many more functions to examine and process the data on the compilation (or associated external data) than was ever available before. Under the directory **\SOFTWARE**, are three subdirectories, **\WINDOWS**, **\UNIX**, and **\GENERIC**. The first subdirectory contains the ensemble of programs necessary for the DOS-based WINDOWS while the second subdirectory contains the analogous suite of programs for the UNIX operating system. The Generic software is described in Appendix A. The user still has the capability to query the data using a generic program, SELECT. In this case, the user must compile this program on his system and then proceed through the menu much like the previous

edition of 1992. However, the user will not have at his disposal all of the new features (such as sorting or plotting) that are available in the two Windows implementations. In addition, the search through the HITRAN database will likely be slower.

### **3. Initiating the Operation of HAWKS**

After proper installation of the software package as described in Section 1, the program is initiated by double clicking on the HAWKS icon. The initial HAWKS screen will then appear.



The following options are now available in the menu bar:

**File   Select   BandStat   Sort   Reference   Plot   Help   Window**

The choices produce pull-down screens or dialog boxes. Control is maintained either by clicking the left mouse button or by typing the underlined letter, as in popular programs in Windows. One can also use the tab key to cycle through choices in the dialog boxes.



### 3.1 File Option

By clicking on the FILE option, the user is given the option of performing five different tasks: Open, Print, Copy, Logo, and Exit. The choice of Open allows the user to edit any of the output files created by the HAWKS software (see discussion in Section 1.3). The Print option enables the printing out of sections of data or of whole files. This option also allows printing of a plot generated by HAWKS (see Section 3.6). The Copy option gives the user the ability to copy sections of data or plots to the clipboard for future use. This feature is particularly useful for pasting results into other WINDOWS applications, such as word processing. The Logo option simply returns the HITRAN logo to the main screen. The Exit option enables an easy exit from the HAWKS software.

### 3.2 Select Option

The most important and detailed optional screen is the second one, Select, which contains the 12 choices displayed below:

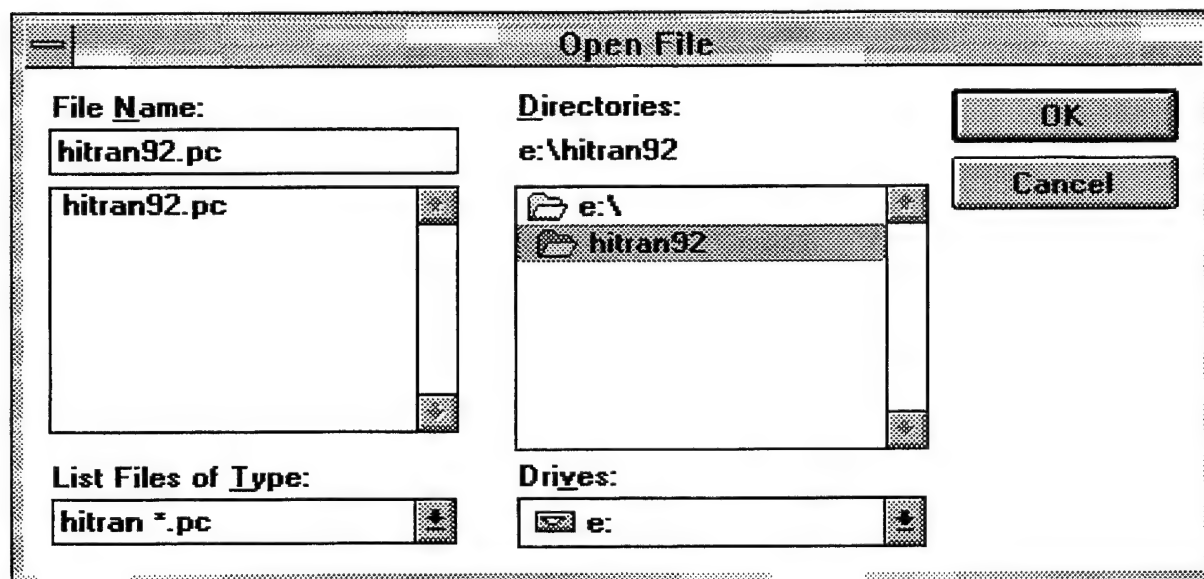
The screenshot shows a window titled "HAWKS SELECT". Inside the window, there are several sections of controls:

- Select File:** Contains two buttons, "HITRAN Filename" and "OUTPUT Filename".
- Select Input Choices:** Contains six buttons arranged in two columns: "Spectral Range", "Molecule", "Isotope" on the left, and "Temperature", "Band", "Cutoff" on the right.
- Batch Options:** Contains two buttons, "Open Batch" and "Save Batch".
- Other Buttons:** Between the "Select Input Choices" and "Batch Options" sections are two buttons: "RUN SELECT" and "RUN DESELECT". At the bottom center is a "Cancel" button.

Select is the principal operating program for a detailed manipulation of the HITRAN96 database, or any files in the HITRAN format. (The 100-character HITRAN molecular transition format is described in detail in Ref. 4.) When SELECT is started, a set of default parameters for all the selections is used. The set is stored in the "def.sel" file which is discussed below in Sections 3.2.11 and 3.2.12.

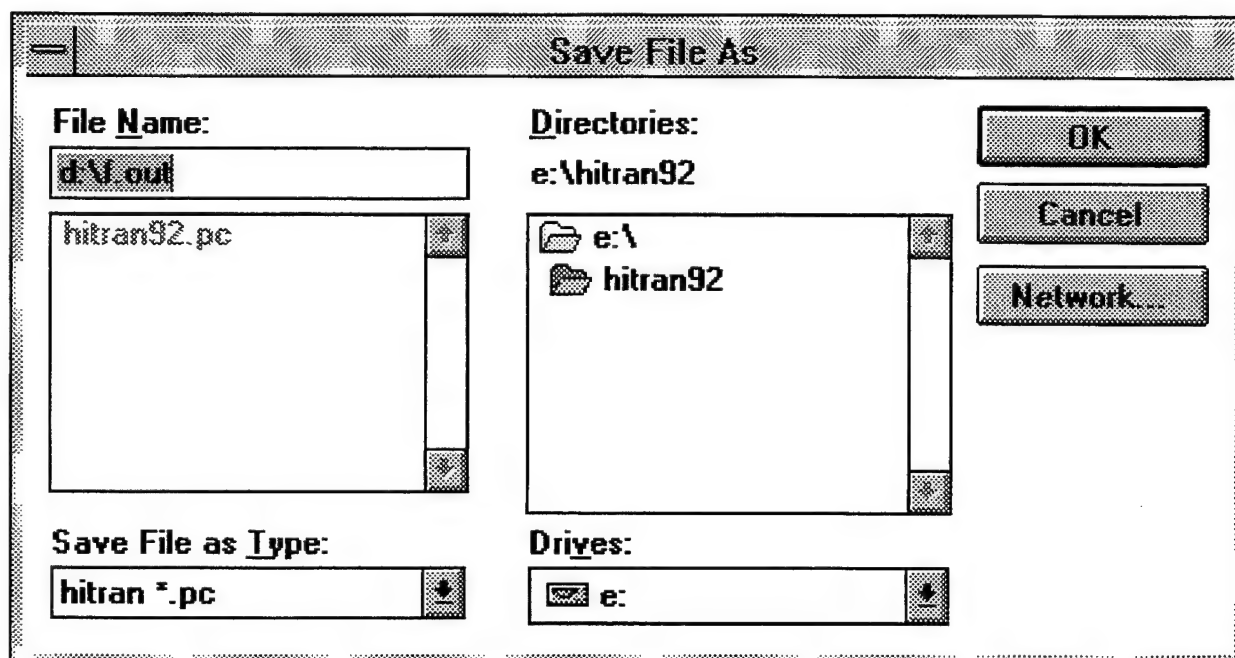
### 3.2.1 Select Option: HITRAN Filename

The first choice in the Select screen is HITRAN Filename, which permits the opening of the HITRAN96 database file at its stored location. This choice can also be used to bring up any HITRAN-like files. The dialog box that appears contains standard WINDOWS features for changing drives, browsing paths, or choosing common file types.



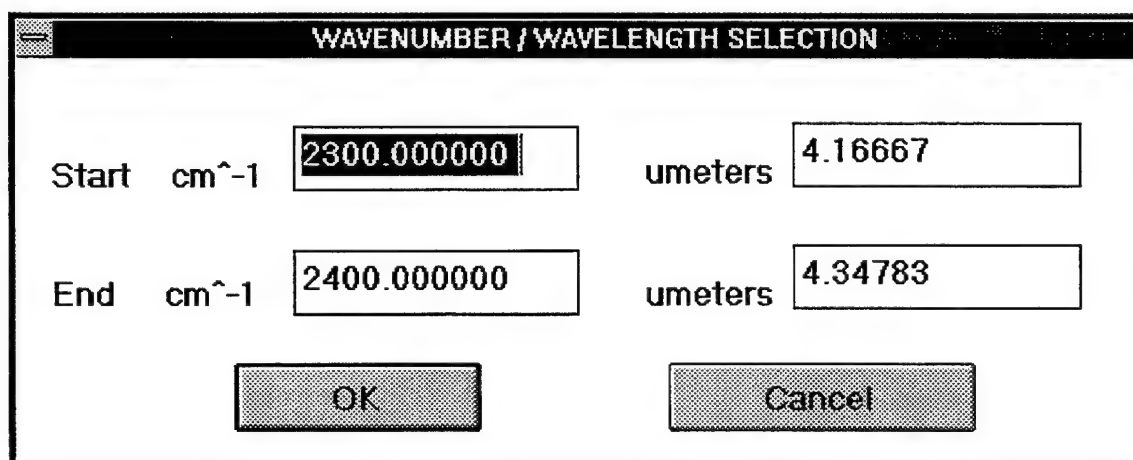
### 3.2.2 Select Option: Output Filename

The second choice in the Select screen is the OUTPUT Filename, which allows the user the option of storing the ASCII output file wherever it is desired.



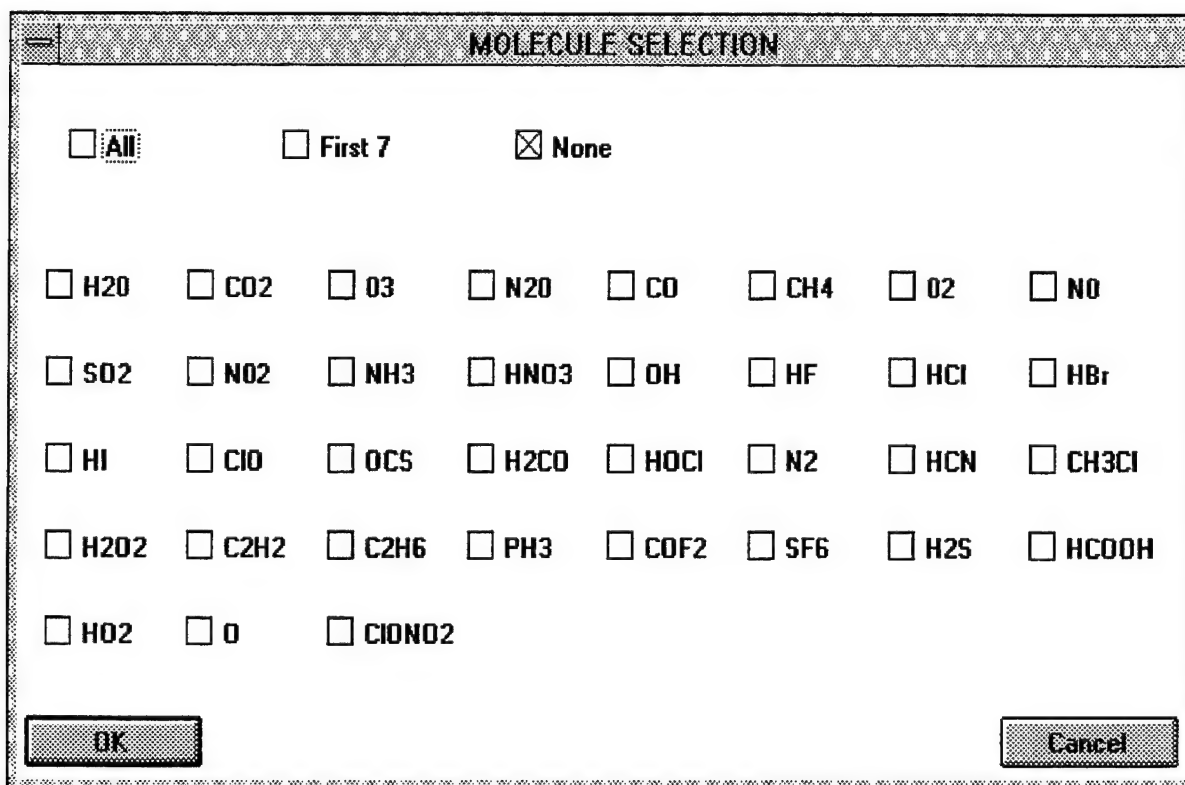
### 3.2.3 Select Option: Spectral Range

The third optional choice in this series is Spectral Range, which allows the user to identify the wavenumber (or wavelength) range of the data being gathered. One can choose the start and end of the selection in either wavenumbers ( $\text{cm}^{-1}$ ) or wavelength ( $\mu\text{m}$ ). This option is the essential choice (necessary and sufficient) in any SELECT procedure, but is ignored for DESELECT (see Section 3.2.10).



### 3.2.4 Select Option: Molecule

The fourth optional choice in the **Select** screen is Molecule, which gives the user the option of including All of the available molecules in the spectral range defined, the First 7 molecules (coinciding to the original HITRAN), or None. None is provided as a convenient button to allow the user to subsequently select various specific assortments of molecules; therefore, this latter choice is probably the most frequently employed.



A screenshot of a software dialog box titled "MOLECULE SELECTION". At the top, there are three radio buttons: "All" (unchecked), "First 7" (unchecked), and "None" (checked). Below these, there is a grid of checkboxes for various chemical species. The species are arranged in five rows: Row 1: H2O, CO2, O3, N2O, CO, CH4, O2, NO; Row 2: SO2, NO2, NH3, HNO3, OH, HF, HCl, HBr; Row 3: HI, ClO, OCS, H2CO, HOCl, N2, HCN, CH3Cl; Row 4: H2O2, C2H2, C2H6, PH3, COF2, SF6, H2S, HCOOH; Row 5: HO2, O, ClONO2. At the bottom left is an "OK" button and at the bottom right is a "Cancel" button.

MOLECULE SELECTION							
<input type="checkbox"/> All	<input type="checkbox"/> First 7	<input checked="" type="checkbox"/> None					
<input type="checkbox"/> H2O	<input type="checkbox"/> CO2	<input type="checkbox"/> O3	<input type="checkbox"/> N2O	<input type="checkbox"/> CO	<input type="checkbox"/> CH4	<input type="checkbox"/> O2	<input type="checkbox"/> NO
<input type="checkbox"/> SO2	<input type="checkbox"/> NO2	<input type="checkbox"/> NH3	<input type="checkbox"/> HNO3	<input type="checkbox"/> OH	<input type="checkbox"/> HF	<input type="checkbox"/> HCl	<input type="checkbox"/> HBr
<input type="checkbox"/> HI	<input type="checkbox"/> ClO	<input type="checkbox"/> OCS	<input type="checkbox"/> H2CO	<input type="checkbox"/> HOCl	<input type="checkbox"/> N2	<input type="checkbox"/> HCN	<input type="checkbox"/> CH3Cl
<input type="checkbox"/> H2O2	<input type="checkbox"/> C2H2	<input type="checkbox"/> C2H6	<input type="checkbox"/> PH3	<input type="checkbox"/> COF2	<input type="checkbox"/> SF6	<input type="checkbox"/> H2S	<input type="checkbox"/> HCOOH
<input type="checkbox"/> HO2	<input type="checkbox"/> O	<input type="checkbox"/> ClONO2					
OK				Cancel			

3.2.5 Select Option: Isotope

The fifth optional choice in the Select screen is Isotope, which gives the user the option of retaining all of the available isotopes of the given molecule or selecting individual isotopes to include in the output. In the following example, the user has previously selected ozone as at least one of the molecules. The Isotope box is clicked on the ozone box, and the following screen appears (O3 ISOTOPE SELECTION). In this example, one has chosen the odd assortment of the principal isotope and the pair with  $^{17}\text{O}$ . Thus, one can choose all of the isotopes for a molecule (a typical choice, therefore the default) or specific sets of isotopes, useful in some laboratory cell experiments. Of course, in the spectral range selected, there may not exist any data for some isotopes.

O3 ISOTOPE SELECTION	
ISOTOPE	ABUNDANCE
J. Phys. Chem. Ref. Data 13, 809-891 (1984)	
<input type="checkbox"/> ALL	
<input checked="" type="checkbox"/> $\text{O}_3$	0.992901
<input type="checkbox"/> $^{16}\text{O}^{16}\text{O}^{18}\text{O}$	0.00398194
<input type="checkbox"/> $^{16}\text{O}^{18}\text{O}^{16}\text{O}$	0.00199097
<input checked="" type="checkbox"/> $^{16}\text{O}^{16}\text{O}^{17}\text{O}$	0.0007475
<input checked="" type="checkbox"/> $^{16}\text{O}^{17}\text{O}^{16}\text{O}$	0.0003702

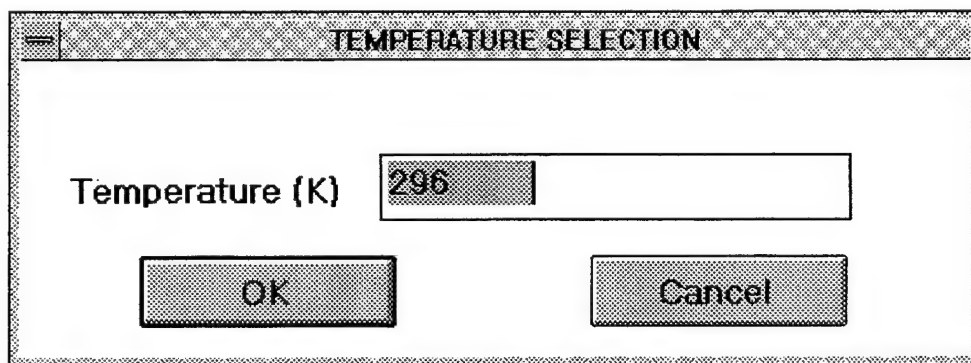
OK Cancel

Given in the second column in the isotope selection box are the actual values of isotopic abundances used in HITRAN. These values enable the user to re-normalize the intensities, for example, where the output is to correspond to a laboratory absorption experiment with enhanced isotopic mixtures.

### 3.2.6 Select Option: Temperature

The sixth optional choice is Temperature, which lets the user set the desired temperature for the chosen set of lines. The present allowable range of temperatures is 70K to 3000K. The parameters in a HITRAN transition that depend on temperature, namely the intensity of the line and the halfwidths, are given at a standard reference of 296K. Being an atmospheric database, many transitions that are appropriate for high temperatures are liable to be missing, a fact that the user should consider. This is particularly true in spectral regions where a molecule may have many "hot" bands originating from a low vibrational state. However, the temperature option is necessary for line files such as HITEMP, since the intensities in HITEMP line files are given at the standard 296K and must be converted through the temperature option to the required temperature.

Another caveat is that the partition sums used in SELECT necessary to perform the temperature conversion may have errors at the higher temperatures, noticeable in the case of species with many very low vibrational states such as  $\text{SF}_6$ . Nevertheless, we believe these errors are quite tolerable for most applications.



The image shows a graphical user interface window titled "TEMPERATURE SELECTION". Inside the window, there is a label "Temperature (K)" followed by a text input field containing the number "296". Below the input field, there are two buttons: "OK" on the left and "Cancel" on the right. The window has a standard Mac OS-style title bar with a small icon on the left.

### 3.2.7 Select Option: Band

The seventh optional choice in the Select screen is Band, which brings in the VIB LEVEL SELECTION screen, allowing the identification of vibrational levels for a specific molecule. This powerful feature allows the user to select individual vibrational bands from the input database file

by highlighting a quantum level from the UPPER LEVEL box and one from the LOWER LEVEL box. The user then depresses the **Add** button to include his selection. This procedure can be repeated to obtain a series of bands. In addition, one can choose ALL as either the upper or lower level. In this manner, it is possible to search the database for all transitions emanating from one particular lower level to ALL possible upper levels. If a transition was highlighted by mistake, a button is provided to **Delete** the choice from the UPPER-LOWER box. In this case one highlights the transition not to be considered in the search and clicks on the delete button. When the selection of bands is complete, the user clicks on OK. The default for the Band option is ALL transitions.

NOTE: The use of the Band option should be considered very carefully. It should only be employed by those users thoroughly familiar with the manipulation of various vibrational transitions for specific molecules.

VIB LEVEL SELECTION

☒ All

<input type="checkbox"/> H <sub>2</sub> O	<input type="checkbox"/> CO <sub>2</sub>	<input checked="" type="checkbox"/> O <sub>3</sub>	<input type="checkbox"/> N <sub>2</sub> O	<input type="checkbox"/> CO	<input type="checkbox"/> CH <sub>4</sub>	<input type="checkbox"/> O <sub>2</sub>	<input type="checkbox"/> NO
<input type="checkbox"/> SO <sub>2</sub>	<input type="checkbox"/> NO <sub>2</sub>	<input type="checkbox"/> NH <sub>3</sub>	<input type="checkbox"/> HNO <sub>3</sub>	<input type="checkbox"/> OH	<input type="checkbox"/> HF	<input type="checkbox"/> HCl	<input type="checkbox"/> HBr
<input type="checkbox"/> HI	<input type="checkbox"/> ClO	<input type="checkbox"/> OCS	<input type="checkbox"/> H <sub>2</sub> CO	<input type="checkbox"/> HCOCl	<input type="checkbox"/> N <sub>2</sub>	<input type="checkbox"/> HCN	<input type="checkbox"/> CH <sub>3</sub> Cl
<input type="checkbox"/> H <sub>2</sub> O <sub>2</sub>	<input type="checkbox"/> C <sub>2</sub> H <sub>2</sub>	<input type="checkbox"/> C <sub>2</sub> H <sub>6</sub>	<input type="checkbox"/> PH <sub>3</sub>	<input type="checkbox"/> CBF <sub>3</sub>	<input type="checkbox"/> SF <sub>6</sub>	<input type="checkbox"/> H <sub>2</sub> S	<input type="checkbox"/> HCOOH
<input type="checkbox"/> HD <sub>2</sub>	<input type="checkbox"/> O	<input type="checkbox"/> ClONO <sub>2</sub>					

OK Cancel

By clicking on a specific molecule (the following example is for O<sub>3</sub>) the Vibrational Selection for O<sub>3</sub> screen appears.

The user can now select upper level and lower level vibrational transitions for the given molecule. In the example below for O<sub>3</sub>, the transitions for  $\nu_1$  and  $\nu_3$  have been chosen.

UPPER LEVEL	LOWER LEVEL	UPPER- LOWER
ALL	ALL	001- 000
000	000	100- 000
010	010	
020	020	
100	100	
001	001	
030	030	
110	110	

Buttons: OK, Add, Delete, Cancel

After highlighting the upper and lower levels, the user presses the **Add** button. If a level has been incorrectly added, it can be highlighted and removed by pressing the **Delete** button.

### 3.2.8 Select Option: Cutoff

The eighth optional choice in the Select screen is the choice of Cutoff, which gives the user the option of eliminating lines below a specified intensity. To implement, one types in the threshold intensity in exponent notation. HAWKS will convert the exponent to a 3-digit value even if one number is typed in, *e.g.* 2.3E-9 becomes 2.3e-009. There are some transitions in HITRAN and many in HITEMP whose intensities (given at the standard 296K) are less than the single precision allowed by most compilers. In that case, Cutoff can be used to eliminate them from the selected output.

CUTOFF CRITERIA

Cutoff ( $\text{cm}^{-1}/(\text{molecule} * \text{cm}^{-2})$ ) 0

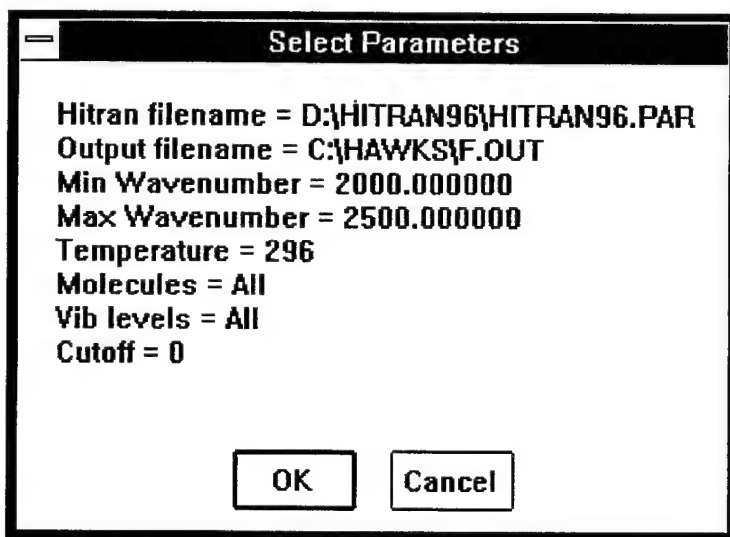
Buttons: OK, Cancel



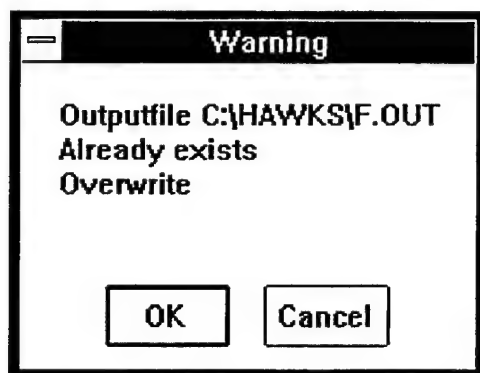
NOTE: This Cutoff option can be used to limit the dynamic range, but one generally does not know, a priori, what the overall effect on simulations that use the output file will be. Therefore, this option, as with the choice of Band, is probably only useful to very experienced users of the database. Since the plotting package (see Section 3.6) allows control of the minimum plotted intensity, this cutoff option does not need to be used for that purpose.

### 3.2.9 Select Option: RUN SELECT

The ninth optional choice in the Select option is RUN SELECT, which when activated, will produce an outline of the chosen case to run, as shown in the following example. This box is provided as a rough check for the user to verify his choices.



By clicking on the OK button the Select program will begin its operation. If however, the chosen named output file currently exists (\HAWKS\F.OUT in the example above) then the following overwrite confirmation screen will appear:



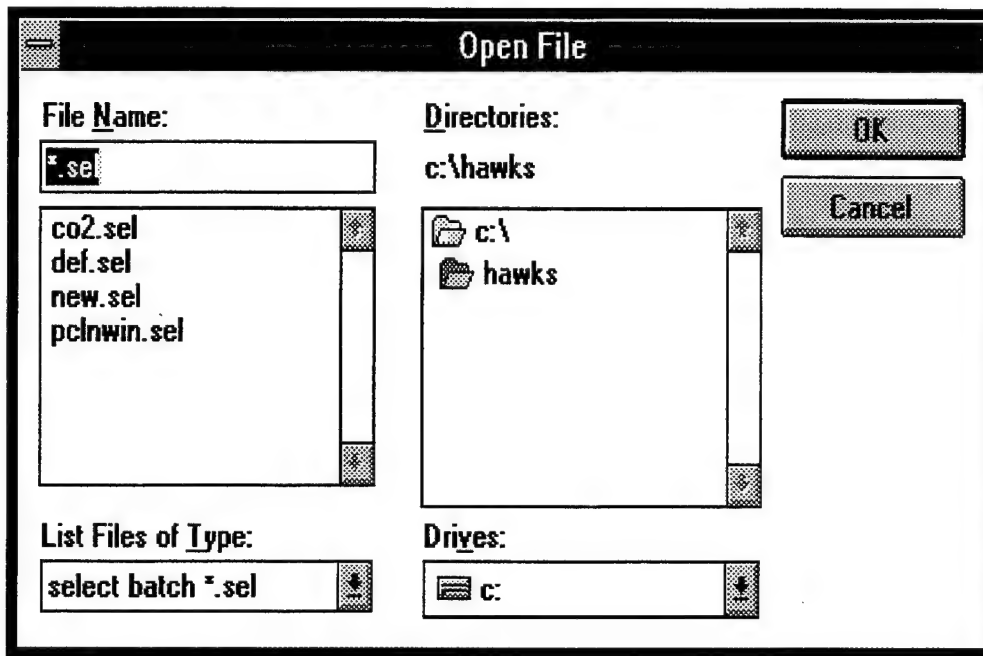
You may choose the overwrite option by depressing the OK button, or Cancel and return to the Select Option Output Filename, and rename the output file.

### 3.2.10 Select Option: RUN DESELECT

The RUN DESELECT option is provided to the user to perform the inverse operation on the HITRAN database to Select. The concept here is to allow an editing feature for subtracting old or unwanted bands from a database and leaving the skeleton database to which one subsequently may add new or replacement data. One proceeds with the same selection criteria as one would in a normal Select procedure. The only difference here is that the choice of spectral interval is ignored: the initial database being "deselected" is taken in full. One should note that ample disk space needs to be considered in the general case of deselecting a few bands of a molecule from the HITRAN database. The resulting database that is written will be almost the same size as the original.

### 3.2.11 Select Option: Open Batch

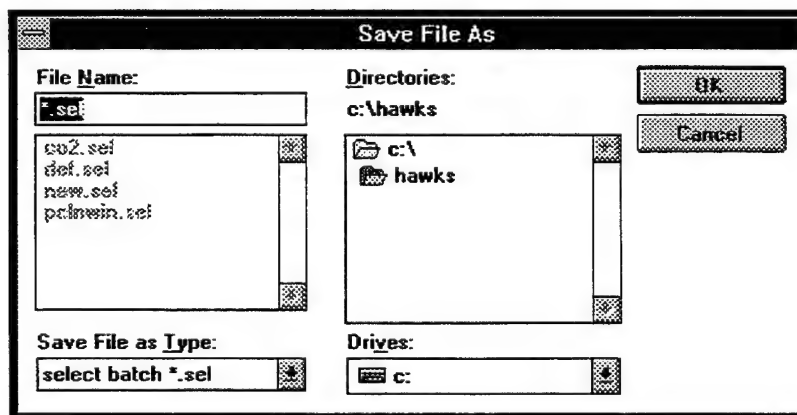
The eleventh optional choice in the Select option is Open Batch, which when activated, gives the user the ability to open a previously stored batch case for Select to operate on. See the Open Batch screen below:



NOTE: A default file setting up the Select choices is available as DEF.SEL.

### 3.2.12 Select Option: Save Batch

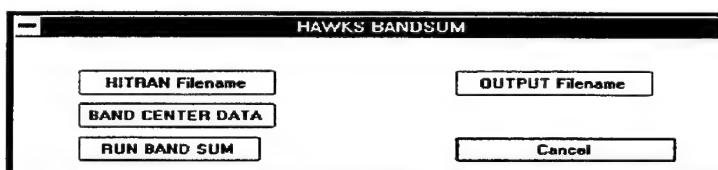
The twelfth choice in the Select option is Save Batch, which when activated, gives the user the option of saving the currently created operation under a user-defined file name (see example below). A stand-alone DOS program, PRTSEL.EXE, is provided to enable the user to print the batch file. This feature is useful for verifying elaborate selection criteria.



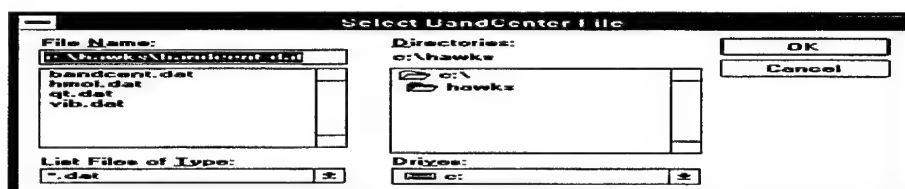
### 3.3 BandStat Option

The **BandStat** option runs the Bandsun program on a given file of data, or on the entire HITRAN96 database, for one or more molecules. The output gives: the number of lines for every band of each isotope; the minimum and maximum J values, wavenumber, line strengths; sum of the line strengths, and many additional spectroscopic parameters of use for in-depth analysis.

The program accessed by selecting the **BandStat** option from the main menu will give the following dialog box



The **HITRAN Filename**, and **OUTPUT Filename** options are used in the same way as described above in Sections 3.2.1, and 3.2.2 for the **Select Option**. Selecting the **Band Center Data** options brings up the dialog box:



which is used to select a file of band centers for each isotope of every molecule. The file must be an ASCII file of the following format:

```

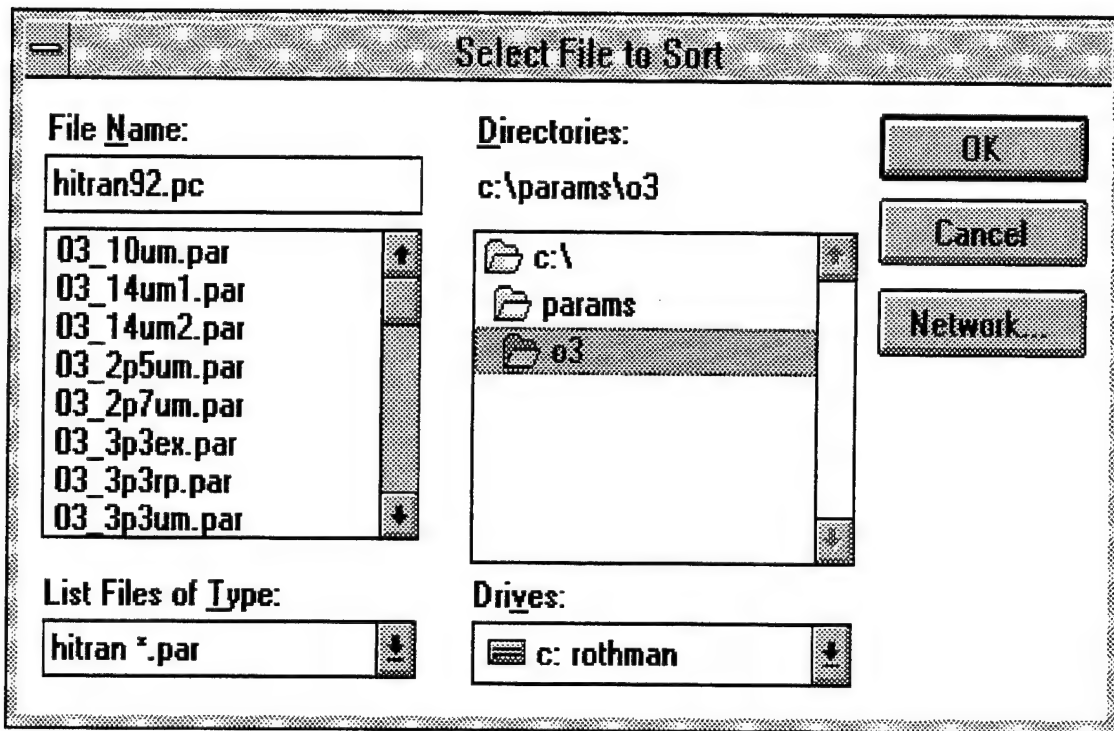
1  161  '      000'  '      000'
1  161  '      010'  '      010'
1  161  '      020'  '      020'
1  161  '      100'  '      100'

```

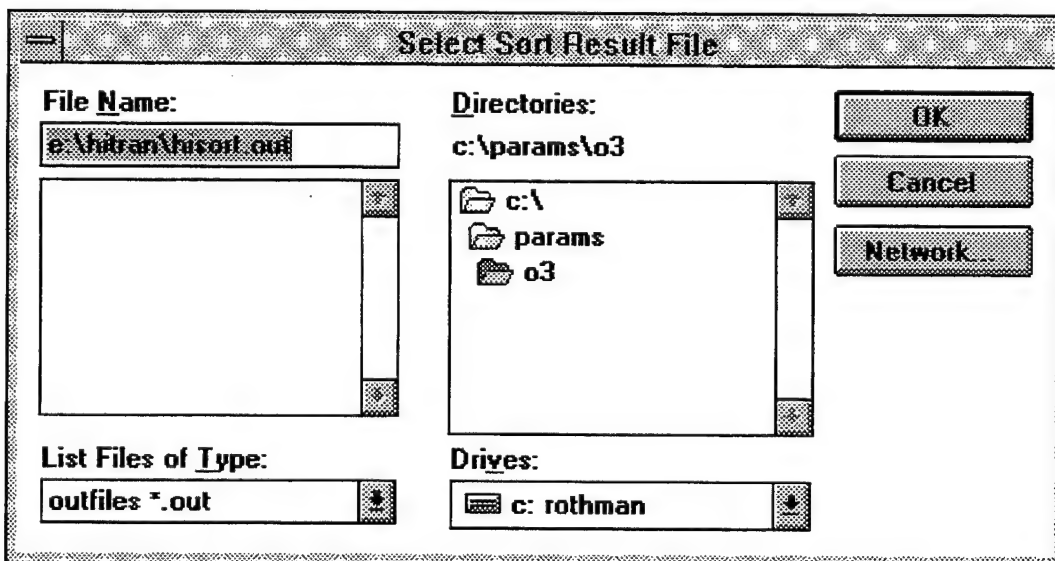
Users will probably employ the default file “Bandcent.dat” provided on the CD-ROM. Advanced users may want to edit this file to tailor it to specific molecules being investigated.

### 3.4 Sort Option

31



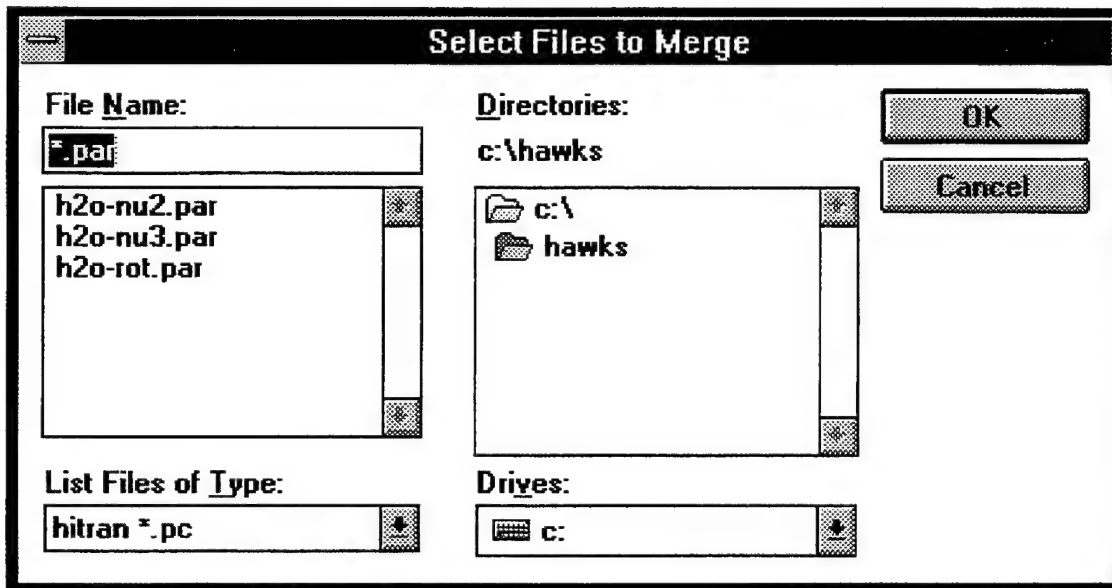
Next the user is asked to identify the name and location for the sorted result as shown in the next dialog box:



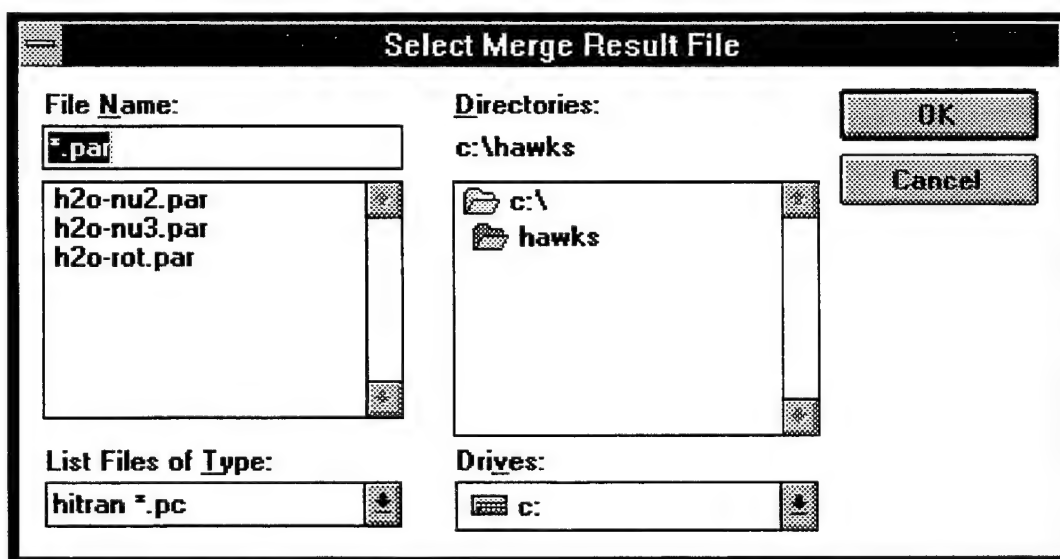
3.4.1

**Sort Option: Merge**

The second choice in the Sort pull down screen is Merge. The Merge option allows the user to merge two or more separate files into one file and gives the user the option of sending this merged file to whatever location is desired. The following screens will appear asking the user to identify files to be merged:



Click on the CANCEL button to end the selection of files being merged. A new dialog box will now appear directing the naming of the file containing the merged results.

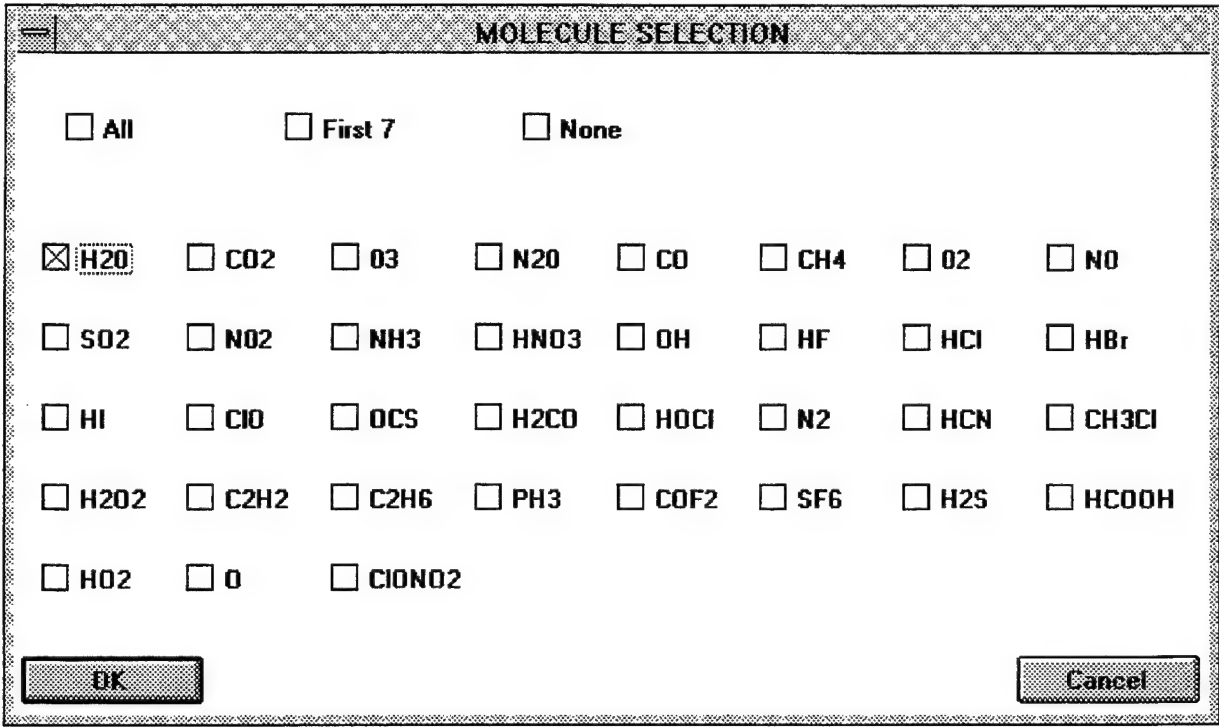


### 3.5 Reference Option

The next pull down screen is Reference and it contains three separate options: Molecule, Wavenumber, and Xsection, for obtaining information on references utilized in creating the database.

#### 3.5.1 Reference Option: Molecule

The first option, Molecule, allows the user to address the molecular reference table utilized by the HITRAN database for identifying the series of references for the line position, line intensity, and air-broadened halfwidth.

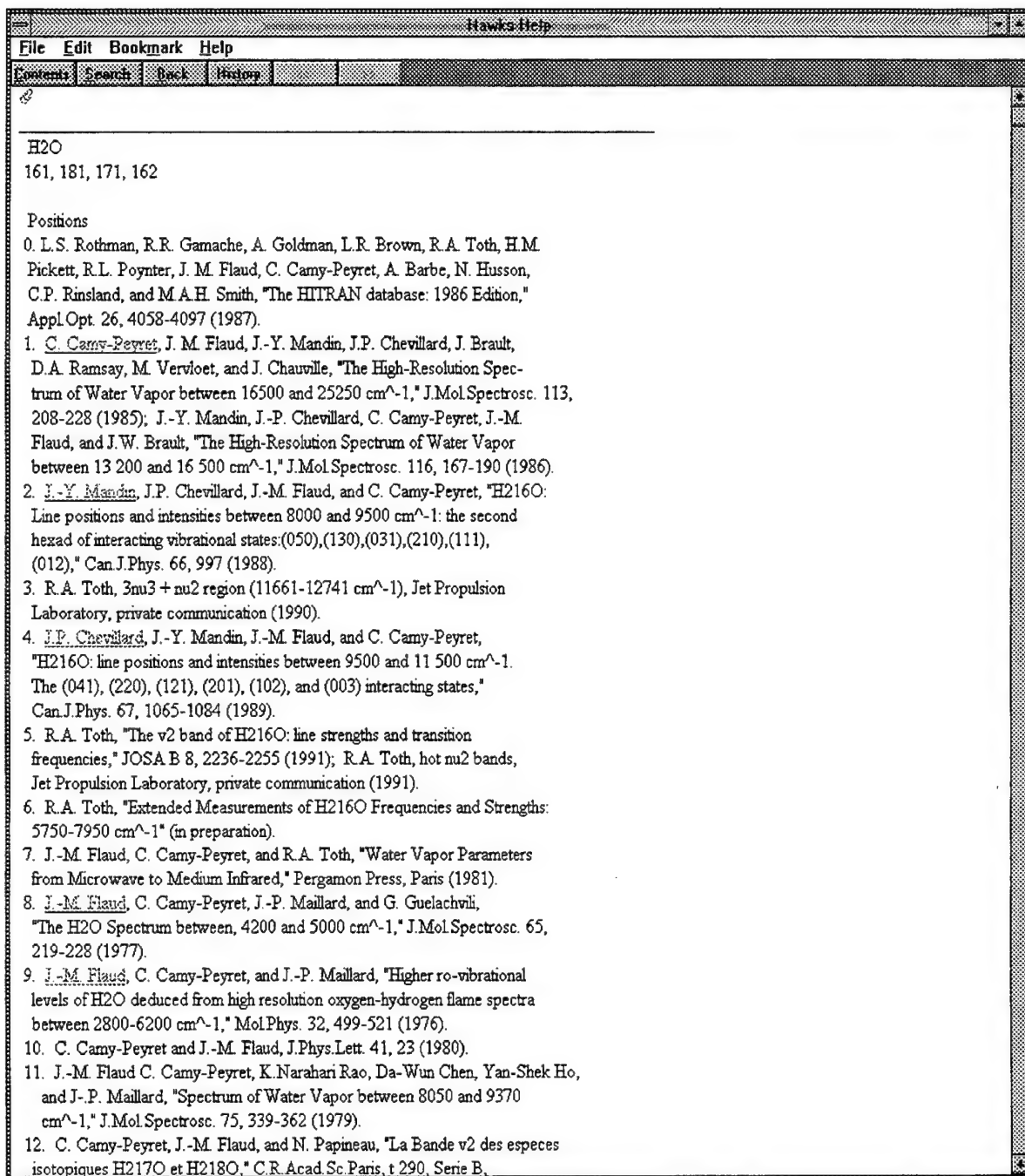


A dialog box titled "MOLECULE SELECTION" with a standard Windows-style border. At the top, there are three radio buttons: "All", "First 7", and "None". Below these, a grid of checkboxes lists various chemical species. The first checkbox, labeled "H2O", is checked. The other checkboxes are for CO2, O3, N2O, CO, CH4, O2, NO, SO2, NO2, NH3, HNO3, OH, HF, HCl, HBr, HI, ClO, OCS, H2CO, HOCl, N2, HCN, CH3Cl, H2O2, C2H2, C2H6, PH3, COF2, SF6, H2S, HCOOH, H02, O, and ClONO2. At the bottom left is an "OK" button and at the bottom right is a "Cancel" button.

MOLECULE SELECTION							
<input type="checkbox"/> All	<input type="checkbox"/> First 7	<input type="checkbox"/> None					
<input checked="" type="checkbox"/> H2O	<input type="checkbox"/> CO2	<input type="checkbox"/> O3	<input type="checkbox"/> N2O	<input type="checkbox"/> CO	<input type="checkbox"/> CH4	<input type="checkbox"/> O2	<input type="checkbox"/> NO
<input type="checkbox"/> SO2	<input type="checkbox"/> NO2	<input type="checkbox"/> NH3	<input type="checkbox"/> HNO3	<input type="checkbox"/> OH	<input type="checkbox"/> HF	<input type="checkbox"/> HCl	<input type="checkbox"/> HBr
<input type="checkbox"/> HI	<input type="checkbox"/> ClO	<input type="checkbox"/> OCS	<input type="checkbox"/> H2CO	<input type="checkbox"/> HOCl	<input type="checkbox"/> N2	<input type="checkbox"/> HCN	<input type="checkbox"/> CH3Cl
<input type="checkbox"/> H2O2	<input type="checkbox"/> C2H2	<input type="checkbox"/> C2H6	<input type="checkbox"/> PH3	<input type="checkbox"/> COF2	<input type="checkbox"/> SF6	<input type="checkbox"/> H2S	<input type="checkbox"/> HCOOH
<input type="checkbox"/> H02	<input type="checkbox"/> O	<input type="checkbox"/> ClONO2					
OK			Cancel				

By choosing a specific molecule, (the example shown below is for H<sub>2</sub>O) the listed references for line position, line intensity, and air-broadened halfwidth for that gas appears as a help file.





In this help file, some references have the lead author's name underlined and in green. By clicking on the author's name (e.g., C. Camy-Peyret), an abstract of that paper appears (see example below).

*The High-Resolution Spectrum of Water Vapor between 16500 and 25250 cm<sup>-1</sup>.*

*C. CAMY-PEYRET, J.-M. FLAUD, J.-Y. MANDIN, AND J.-P. CHEVILLARD*

*Laboratoire de Physique Moléculaire et d'Optique Atmosphérique Batiment 221 Campus d'Orsay  
91405 Orsay Cedex. France*

*J. BRAULT*

*Kitt Peak National Observatory Tucson. Arizona 85726*

*D. A. RAMSAY AND M. VERVLOET*

*Herzberg Institute of Astrophysics National Research Council of Canada Ottawa Ontario K1A 0R6,  
Canada*

*AND*

*J. CHAUVILLE*

*Observatoire de Meudon. 1, Place J Jansen. 92190 Meudon France*

*High-resolution spectra of water vapor have been recorded, with very good signal-to-noise ratios, between 16500 and 25250 cm<sup>-1</sup> using visible Fourier transform spectroscopy. Precise line positions have been derived, and 1174 vibration-rotation transitions belonging to 23 different bands of H<sub>2</sub>O have been assigned, leading to the determination of 539 vibration-rotation energy levels and greatly extending our knowledge of the highly excited vibrational states of the water molecule. The measurement of 630 line intensities with accuracies varying from 5 to 35%, depending on the strength of the line, has been performed.*

### **3.5.2 Reference Option: Wavenumber**

The second option in the REFERENCE pull down screen is WAVENUMBER. Here the listing of a specific frequency will identify the lines within the range of the requested frequency. In the example below, two lines are listed (the second line is at 2105.002817, the molecule is CO, the reference code used in the HITRAN database is 1 1 1 and the error code used is 5 6 5). This option allows the user to associate a particular line transition with its corresponding references (and error estimates as well).

**Hitran has 709409 lines and 102 header lines**

**Searching for 2105.000000**

**Line found between 539500 and 539509**

**K= 2104.9995 M= 03 kref= 1 sref= 1 wref= 2 kerr=0 serr=0 werr=2**

**K= 2105.002817 M= C0 kref= 1 sref= 1 wref= 1 kerr=5 serr=6 werr=5**

**Kref**, **sref**, **wref** all have hypertext link to the appropriate reference (they will be black, not green, on your screen), which is obtained by double clicking on the word. **Kerr**, **serr**, **werr** link to the error criteria definitions for the line position, line intensity, and air-broadened halfwidth. The criteria can be seen by double clicking on the word.

### 3.5.3 Reference Option: Xsection

The third option in the Reference pull down screen is Xsection. This choice will bring in a HELP-type screen describing the principal contributors to the cross-section database, identification of the specific heavy gases, and a list of the references to the research cited. The identifying labels (DU for example in the first reference below) are contained in the Headers to each array of cross-sections on the compilation.

#### *Cross Section Reference*

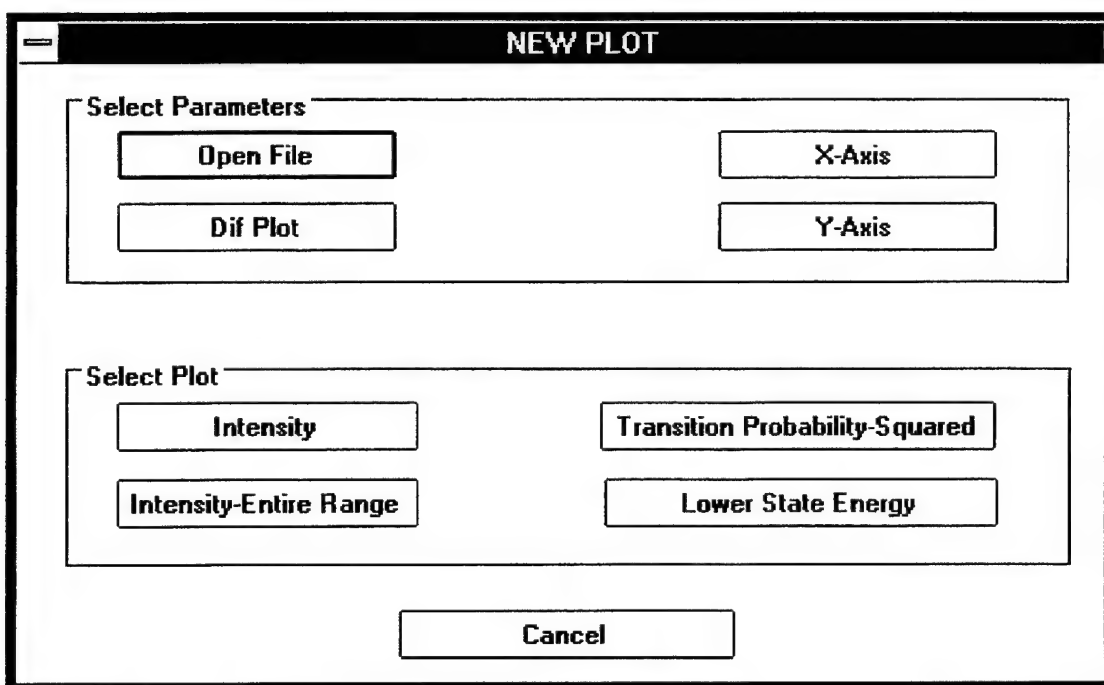
---

##### *Cross-section file:*

- DU = S.T. Massie, A. Goldman, D.G. Murcray, and J.C. Gille, "Approximate absorption cross sections of F12, F11, ClONO2, N2O5, HNO3, CCl4, CF4, F21, F113, F114, and HNO4," *Appl. Opt.* 24, 3426-3427 (1985).
- NCAR = A.H. McDaniel, C.A. Cantrell, J.A. Davidson, R.E. Shetter, and J.G. Calvert, "The Temperature Dependent, Infrared Absorption Cross Sections for the Chlorofluorocarbons: CFC-11, CFC-12, CFC-13, CFC-14, CFC-22, CFC-113, CFC-114, and CFC-115," *J. Atmos. Chem.* 12, 211-227 (1991); S.T. Massie, A. Goldman, A.H. McDaniel, C.A. Cantrell, J.A. Davidson, R.E. Shetter, and J.G. Calvert, "Temperature Dependent Infrared Cross Sections for CFC-11, CFC-12, CFC-13, CFC-14, CFC-22, CFC-113, CFC-114, and CFC-115," NCAR Technical Note/TN-358+STR (1991).
- NCAR-a = C.A. Cantrell, J.A. Davidson, A.H. McDaniel, R.E. Shetter, and J.G. Calvert, "Infrared Absorption Cross Sections for N2O5," *Chem. Phys. Lett.* 148, 358-363 (1988).
- RAL = J. Ballard, W.B. Johnston, M.R. Gunson, and P.T. Wassell, "Absolute Absorption Coefficients of ClONO2 Infrared Bands at Stratospheric Temperatures," *J. Geophys. Res.* 93, 1659-1665 (1988).
- ORPHAL-ORSAY = J. Orphal, M. Morillon-Chapey, and G. Guelachvili, "High-Resolution Absorption Cross Sections of Chlorine Nitrate in the  $\nu_2$  Band Region around 1292  $\text{cm}^{-1}$  at Stratospheric Temperatures," *J. Geophys. Res.* D (1994).
- N2O-SAO = K. Yoshino, D.E. Freeman, and W.H. Parkinson, "High Resolution Absorption Cross-Section Measurements of N2O at 295-299K in the Wavelength Region 170-222 nm," *Planet. Space Sci.* 32, 1219-1222 (1984).

### 3.6 Plot Option

The sixth optional screen is Plot. The HAWKS Plot screen has two selections: New Plot and Edit Plot. The latter, Edit Plot, is only operative if there is a plot on the screen. Selecting New Plot will give you the following screen:



The image shows a dialog box titled "NEW PLOT". It contains two main sections: "Select Parameters" and "Select Plot".

**Select Parameters**

Open File	X-Axis
Dif Plot	Y-Axis

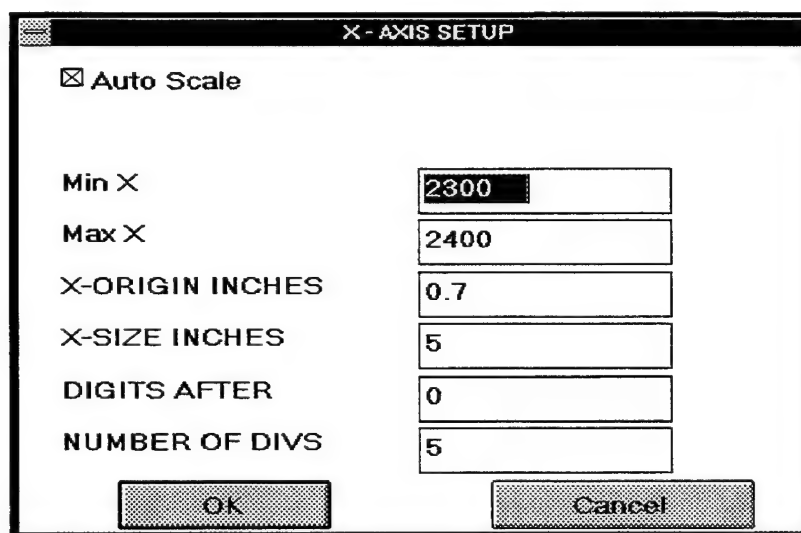
**Select Plot**

Intensity	Transition Probability-Squared
Intensity-Entire Range	Lower State Energy

At the bottom of the dialog box is a "Cancel" button.

This screen is divided into two parts. The upper section, Select Parameters, is used to open the file to be plotted, set the X- and Y-axes, make difference plots, and establish a width to the plotted lines. Difference plots is discussed below in Section 3.6.1. The lower section, Select Plot, determines what will be plotted, for example, the intensity of the lines (the most common usage) or the lower state energy. Both the X-axis and Y-axis have autoscaling, so that the user can immediately create a plot by selecting one of the options in the second section. The resulting plot will be a stick plot. In general, when there is a high density of lines in the spectral interval, the plot displayed on the screen will have blue and red lines. This is to indicate the maximum and minimum value in each channel. Typical computer monitors have approximately 512 horizontal and vertical pixels. However, the data may have many thousands of data points. Consequently, the data has been placed in bins corresponding to the number of display channels. The red and blue lines are used to indicate the maximum and minimum value in each display channel. One can easily expand the X-axis to see individual lines.

To manually adjust the X-axis, one clicks on the X-axis button and the following screen appears:



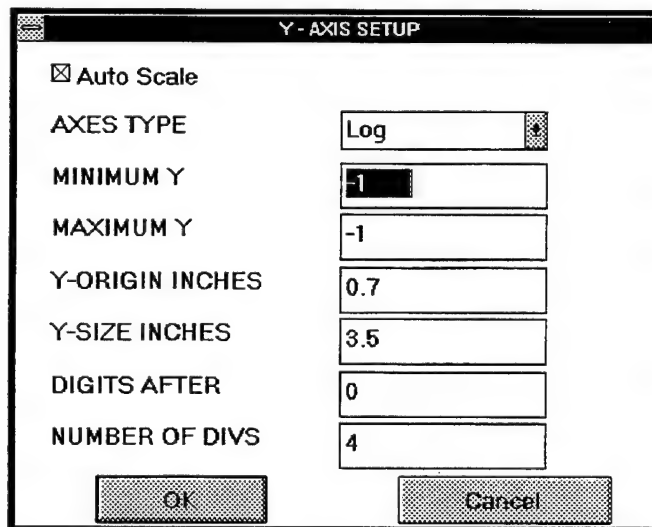
The image shows a dialog box titled "X-AXIS SETUP". It contains a checked checkbox labeled "Auto Scale". Below this are five input fields with labels to their left: "Min X" (value 2300), "Max X" (value 2400), "X-ORIGIN INCHES" (value 0.7), "X-SIZE INCHES" (value 5), and "DIGITS AFTER" (value 0). Below these fields is a label "NUMBER OF DIVS" with a value of 5. At the bottom of the dialog are two buttons: "OK" and "Cancel".

Label	Value
Min X	2300
Max X	2400
X-ORIGIN INCHES	0.7
X-SIZE INCHES	5
DIGITS AFTER	0
NUMBER OF DIVS	5

The user is provided different methods of defining the X axis for the given plot. If Auto Scale is

chosen, the program will control the setting of the maximum and minimum for the X Axis. When turning off the Auto Scale option, it is required to enter real numbers in the Min X and Max Y boxes. The X-ORIGIN allows one to set the distance from the bottom of the screen to the X axis. X-SIZE allows modification of the size of the X axis. These latter two options are very useful for those who have large display screens. DIGITS AFTER are the number of digits after the decimal point, and NUMBER OF DIVS is the number of divisions (marked off by tic marks) over the entire axis.

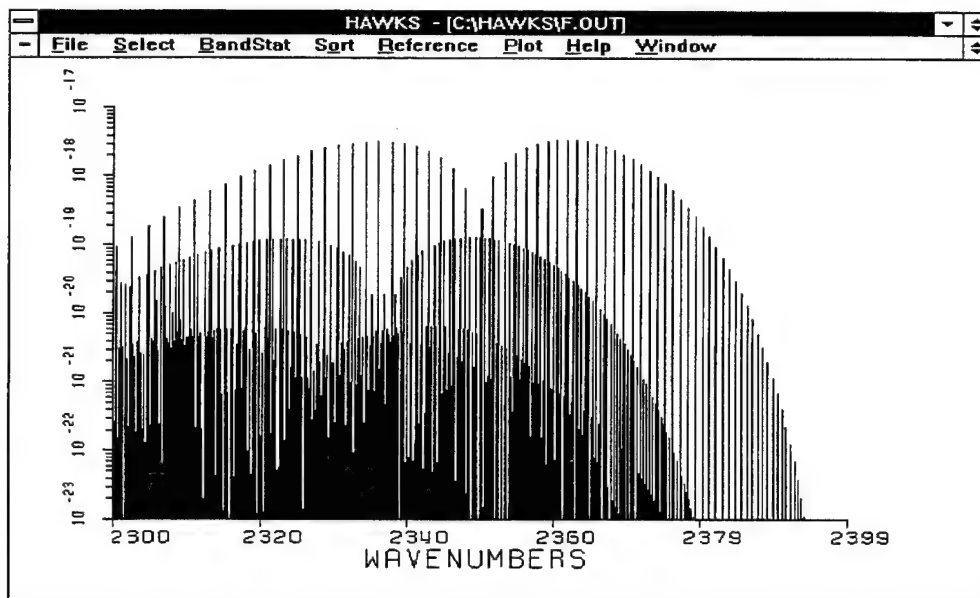
For the Y axis, the user is provided similar methods of defining the axis for the given plot, with one addition, Axes Type. Axes Type allows the user to plot the Y-values in either a linear or log scale. For log plots, one enters the value in exponential format, for example 1.5e-23 (remember to turn off Auto Scale first).



The image shows a dialog box titled "Y-AXIS SETUP". It contains several settings for the Y-axis. At the top, there is a checkbox labeled "Auto Scale" which is checked. Below this, there are labels for "AXES TYPE", "MINIMUM Y", "MAXIMUM Y", "Y-ORIGIN INCHES", "Y-SIZE INCHES", "DIGITS AFTER", and "NUMBER OF DIVS". Each label is followed by a text input field. The "AXES TYPE" field contains the word "Log". The "MINIMUM Y" field contains "-1". The "MAXIMUM Y" field contains "-1". The "Y-ORIGIN INCHES" field contains "0.7". The "Y-SIZE INCHES" field contains "3.5". The "DIGITS AFTER" field contains "0". The "NUMBER OF DIVS" field contains "4". At the bottom of the dialog box, there are two buttons: "OK" and "Cancel".

Setting	Value
Auto Scale	<input checked="" type="checkbox"/>
AXES TYPE	Log
MINIMUM Y	-1
MAXIMUM Y	-1
Y-ORIGIN INCHES	0.7
Y-SIZE INCHES	3.5
DIGITS AFTER	0
NUMBER OF DIVS	4

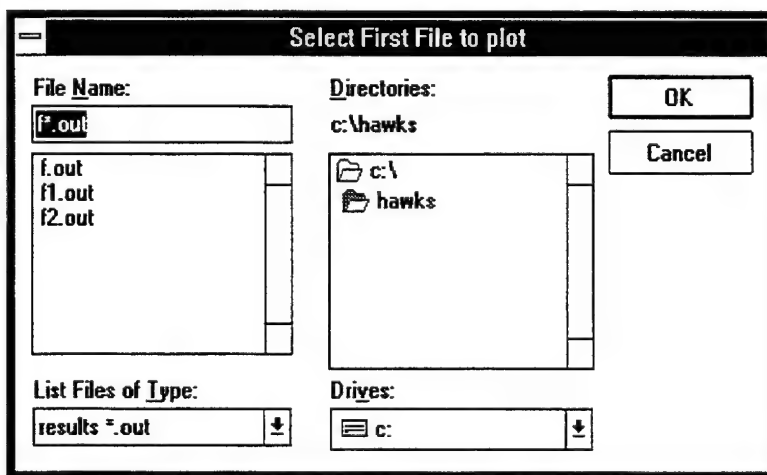
Proceeding clockwise, the first optional form of plotting the results is by Intensity vs frequency. The second optional form of plotting is by Transitional Probability-Squared vs frequency. The third optional form of plotting is the Lower State Energy. The final form of plotting is the Intensity-Entire Range of the applicable frequency. This latter choice overrules the X axis frequency selection and plots over the entire range of data in the opened file. A typical plot (Intensity vs wavenumber) is shown below.



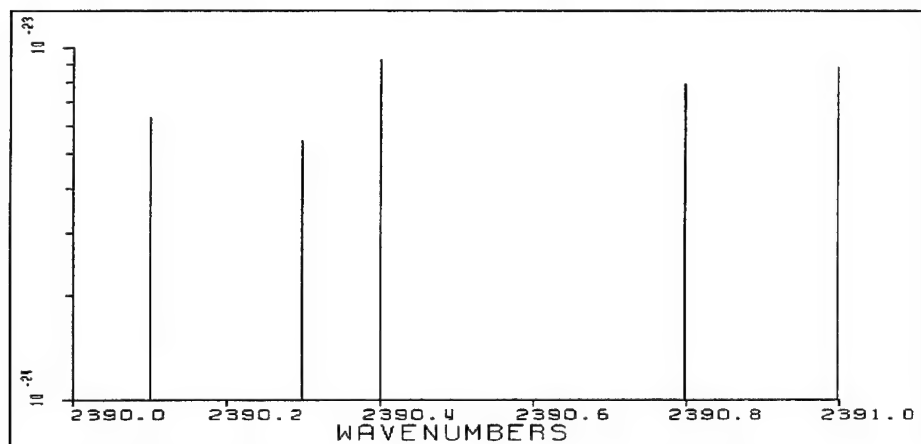
The figure above is a stick plot and is the usual use in examining parameters from HITRAN, HITEMP, or similar files.

### 3.6.1 Difference Plots (Dif file)

This option lets the user take the difference of two spectral plots. This can be a useful tool to determine small shifts in wavenumber (or line strength) between two files. The following screen is displayed when the **Dif file** option is selected:



The user is prompted to select two files (the second file is subtracted from the first). We will use f1.out and f2.out as an example to show how Dif file works. A stick plot of f1.out is shown below:

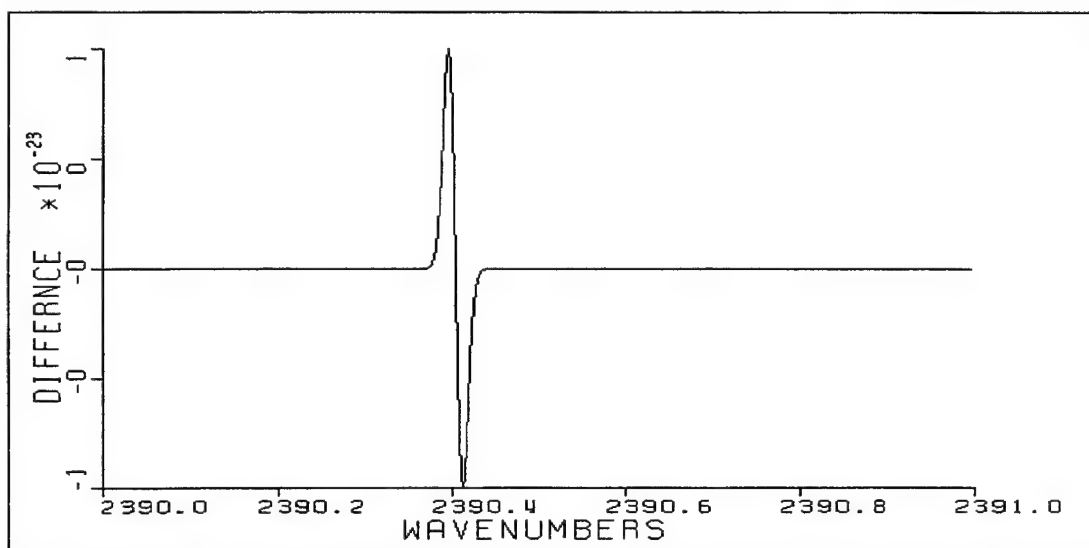


The spectrum contains five lines at 2390.1, .3, .4, .8 and 2391.0  $\text{cm}^{-1}$  respectively. The second file (f2.out) is identical to the first except that the line at 2390.4  $\text{cm}^{-1}$  has been shifted to 2390.41  $\text{cm}^{-1}$ . After the two files have been selected, the user is prompted to input a Doppler broadening coefficient. We have arbitrarily chosen a Doppler line shape to broaden the lines for subtraction. This is not an attempt to simulate a spectroscopic feature, but simply a means chosen to enable reasonable subtraction of lines.

A screenshot of a software dialog box titled 'LINE PARAMETERS'. It contains a label 'Dopler Temp.' followed by a text input field containing the number '5000'. Below the input field are two buttons: 'OK' and 'Cancel'.

We used 5000 in the current example with the resulting difference plot.





### 3.6.2 Edit Plot

The Edit Plot option allow the user to change the plot parameters without reopening the file. Selecting this option bring up the following dialog box:



The X-Axis, Y-Axis, and LINE PARAMS buttons have the same functions as described above. Selecting LINE PARAMS will give the LINE PARAMETERS dialog box shown at the bottom of the previous page.

### 3.7 Help Option

The seventh optional pull down screen is Help. This option gives the user informative help on all of the molecules stored in the database as well as pertinent information on the structure and uses of the HITRAN96 database. The first option in this pull down screen is HITRAN Help which will lead the user through a complete informative package of information on all of the molecules and isotopes available on the database.

HITRAN.HLX		
File Edit Bookmark Help		
Contents	Search	Back History
<p><b>HITRAN Database</b></p> <p>HITRAN96 is the latest version in a series of molecular spectroscopic databases gathered and released by the Air Force Phillips Laboratory. The following is a summary of molecular species present in HITRAN. For additional discussions of any molecules, or for summary tables of the bands and isotopes included in HITRAN, click on the molecule of interest:</p>		
Molecule	Isotopes	# Lines
<u>H2O</u>	4	49444
<u>CO2</u>	8	60802
<u>O3</u>	5	275133
<u>N2O</u>	5	26174
<u>CO</u>	6	4477
<u>CH4</u>	3	48032
<u>O2</u>	3	6292
<u>NO</u>	3	15331
<u>SO2</u>	2	38853
<u>NO2</u>	1	100680
<u>NH3</u>	2	11152
<u>HNO3</u>	1	165426
<u>OH</u>	3	8676
<u>HF</u>	1	107
<u>HCl</u>	2	533
<u>HBr</u>	2	576
<u>HI</u>	1	237
<u>ClO</u>	2	7230
<u>OCS</u>	4	858
<u>H2CO</u>	3	2702
<u>HOCl</u>	2	15565
<u>N2</u>	1	120
<u>HCN</u>	3	772
<u>CH3Cl</u>	2	9355
<u>H2O2</u>	1	5444
<u>C2H2</u>	2	1668
<u>C2H6</u>	1	4749
<u>PH3</u>	1	2886
<u>COF2</u>	1	54866
<u>SF6</u>	1	11520
<u>H2S</u>	3	7151
<u>HCOOH</u>	1	3388
<u>HO2</u>	1	26963

By

clicking

on any information in Green and underlined (hypertext) the user can jump to pertinent information on that particular subject. For example, by clicking on SO2 the following help screen appears:

---

*SO2 bands available (HITRAN96)*

*SO2 (sulfur dioxide) coverage in HITRAN96, includes 2 isotopes and 9 bands for a total of 34623 lines. This summary shows the band center, the transition, the spectral range of each band, the number of lines present in HITRAN96, the summed strength of the band, the minimum and maximum strengths of the lines present, and the highest J value for that band represented by a line in HITRAN96. You can use these summaries to get a feel for what spectral regions are impacted by the various transitions present. The bandcenter, Vmin, and Vmax are given in wavenumbers. The S values of intensity are given in units of (cm<sup>-1</sup>) / (molecule \* cm<sup>-1</sup>).*

*Note: if the table looks jumbled, simply use your mouse and increase the width of your display window that HELP is using. Due to the width of this table of values, the default width used by WinHelp may not be adequate to prevent wrapping of the value*

*SO2 MOLECULE: 34623 lines total*

*Total Number of lines for the 626 isotope is: 34336*

<i>Bandcenter</i>	<i>Trans</i>	<i>Vmin</i>	<i>Vmax</i>	<i>#lines</i>	<i>Sum S</i>	<i>Smin</i>	<i>Smax</i>	<i>Jmax</i>
	000 - 000	0 - 257		9622	2.583E-18	1.020E-28	6.190E-21	74
517.75	010 - 000	33 - 617		3326	3.899E-18	1.380E-24	7.080E-21	50
1151.7135	100 - 000	1043 - 1260		6835	3.519E-18	5.845E-24	5.841E-21	66
1362.0295	001 - 000	1311 - 1400		3618	3.080E-17	6.097E-23	6.094E-20	66
2492.4438	111 - 010	2463 - 2516		654	2.110E-20	1.018E-23	6.299E-23	45
2499.8701	101 - 000	2463 - 2527		1883	3.954E-19	1.030E-23	7.836E-22	59
000.0000	002 - 000	2599 - 2788		4742	3.966E-21	5.000E-26	1.030E-23	75
000.0000	003 - 000	3985 - 4093		3656	1.546E-21	5.000E-27	2.800E-24	76

*Total Number of lines for the 646 isotope is: 287*

<i>Bandcenter</i>	<i>Trans</i>	<i>Vmin</i>	<i>Vmax</i>	<i>#lines</i>	<i>Sum S</i>	<i>Smin</i>	<i>Smax</i>	<i>Jmax</i>
2475.8300	101 - 000	2463 - 2497		287	6.027E-21	9.736E-24	3.428E-23	40

---

### 3.7.1 Help Option: About

The second choice in the HELP section is About, which is a standard statement describing the construction of the HAWKS program for the HITRAN96 database.

### 3.8 Window Option

The last optional pull down screen is WINDOW, which is basically the same as the choice of the Window option in the Windows Program Manager. This includes commands to Cascade or Tile the available windows, Arrange Icons, and a command Close All, used to close all available windows. This pull down screen also includes a listing of all the available windows, with the active window checked (✓). Tiling can be useful to view a series of plots that have been constructed in HAWKS and Close All can be useful to purge a series of unwanted plots.

## 4. Accessing other databases

On the latest HAWKS compilation are three other sub-directories of HITRAN-like data. Within the directory **\SUPLEMNT** are three files, 36\_IR.PAR, 37\_ROT.PAR, 03\_NLTE.PAR, and under the **\UVLBL** path is 07\_SCHUM.PAR. These files can be manipulated with the SELECT or PLOT options just as the primary database HITRAN. Likewise for **\HITEMP**, one can process any of the three files: 01\_1500K.PAR, 02\_1000K.PAR, or 05\_HOT.PAR. The files in **\HITEMP** as stated previously, have their intensities tabulated at the nominal 296K. Nonetheless, they have been established using criteria for higher temperature applications, *e.g.* 1500K for the water vapor file and 1000K for the carbon dioxide file. The user should apply the temperature option of SELECT appropriately. Naturally if one selects, for example, 2000K for the CO<sub>2</sub> file, significant transitions or bands may be absent in some spectral intervals.

There is presently no software provided in HAWKS for the manipulation of the cross-sections, that is, the IR cross-sections of heavy molecular species such as exists in the directory **\IR\_XSECT** or the UV cross-sections in the path **\UVXSECT**. These cross-sections have been uniformly formatted according to the scheme presented in Ref. 4. They have been successfully manipulated by various familiar line-by-line transmission programs.

The aerosols in HAWKS represent a first for this compilation. There are presently nine data files in the directory **\AEROSOLS** each with the extension ".DAT". The files represent indices of refraction and are in tabular form. Some documentation of the files is provided in the file AEROSOL.DOC. It is hoped that the user community will provide feedback on this section of HAWKS, suggesting improvements and also a standardized format.

**5. Future Enhancements**

There is still much unfinished business concerning the future of HAWKS. The content of the compilation will see many improvements in the future, including extensions to the line-by-line portions, consideration of more parameters (issues like line-coupling and other foreign gas broadening for example), more species coverage with cross-sections for modeling, more extensive aerosol coverage, and extension of the hot-gas capabilities. The user-interface likewise will witness expansion: more operating systems (MAC), accessibility through the world-wide-web, and many more features. The goals of the compilation will also be broadened as we attempt to address the problems of DOE (ARM), NASA (in particular the remote sensing community of the Earth Orbiting System), defense, industry, academia, and the astrophysics community.

**6. Acknowledgments**

There have been many contributors to the spectroscopy of this effort; they are too numerous to cite here. We urge users of HAWKS to refer to the references now contained on all new transitions, and apologize for any omissions or oversights we may have made. In particular, we wish to express our appreciation for the efforts on behalf of the development of HITRAN to R.R. Gamache, R.B. Wattson, and R.L. Hawkins. The efforts as beta test sites by Drs. A. Goldman, J-M. Flaud, A. Perrin, C. Camy-Peyret, and P. Morris are gratefully recognized.

We wish to especially acknowledge the financial support of the Atmospheric Radiation Measurement (ARM) program, the Environmental Sciences Division of DOE, the Air Force Office of Scientific Research, and the AF Phillips Laboratory Geophysics Directorate.

## 7. References

1. R.A. McClatchey, W.S. Benedict, S.A. Clough, D.E. Burch, R.F. Calfee, K. Fox, L.S. Rothman, and J.S. Garing, "AFCRL Atmospheric Absorption Line Parameters Compilation," AFCRL-TR-73-0096 (1973), AD762904.
2. L.S. Rothman and R.A. McClatchey, "Updating the AFCRL Atmospheric Absorption Line Parameters Compilation," *Appl. Opt.* **15**, 2616 (1976); L.S. Rothman, "Update of the AFGL Atmospheric Absorption Line Parameters Compilation," *Appl. Opt.* **17**, 3517 (1978); L.S. Rothman, "AFGL Atmospheric Absorption Line Parameters Compilation: 1980 Version," *Appl. Opt.* **20**, 791 (1981); L.S. Rothman, R.R. Gamache, A. Goldman, J.R. Gillis, A. Barbe, L.R. Brown, R.A. Toth, J.-M. Flaud, and C. Camy-Peyret, "AFGL Atmospheric Absorption Line Parameters Compilation: 1982 Edition," *Appl. Opt.* **22**, 2247 (1983); L.S. Rothman, R.R. Gamache, A. Goldman, L.R. Brown, R.A. Toth, H.M. Pickett, R.L. Poynter, J.-M. Flaud, C. Camy-Peyret, A. Barbe, N. Husson, C.P. Rinsland, and M.A.H. Smith, "The HITRAN Database: 1986 Edition," *Appl. Opt.* **26**, 4058 (1987).
3. L.S. Rothman, S.A. Clough, R.A. McClatchey, L.G. Young, D.E. Snider, and A. Goldman, "AFGL Trace Gas Compilation," *Appl. Opt.* **17**, 507 (1978); L.S. Rothman, A. Goldman, J.R. Gillis, R.H. Tipping, L.R. Brown, J.S. Margolis, A.G. Maki, and L.D.G. Young, "AFGL Trace Gas Compilation: 1980 Version," *Appl. Opt.* **20**, 1323 (1981); L.S. Rothman, A. Goldman, J.R. Gillis, R.R. Gamache, H.M. Pickett, R.L. Poynter, N. Husson, and A. Chedin, "AFGL Trace Gas Compilation: 1982 Version," *Appl. Opt.* **22**, 1616 (1983).
4. L.S. Rothman, R.R. Gamache, R.H. Tipping, C.P. Rinsland, M.A.H. Smith, D.Chris Benner, V.Malathy Devi, J.-M. Flaud, C. Camy-Peyret, A. Perrin, A. Goldman, S.T. Massie, L.R. Brown, and R.A. Toth, "The HITRAN Molecular Database: Editions of 1991 and 1992," *J. Quant. Spectrosc. and Rad. Transfer* **48**, 469 (1992).

**APPENDIX A-1. Directories and Files on the CD-ROM**

The files on the HAWKS CD-ROM contained in the directories and sub-directories of Table 1 are listed below. The convention adopted for file type has been to use "DOC " for read me files, "PAR" for line-by-line files, "XSC" for cross-section files, "TXT" for ASCII text and tables, and "FOR" for FORTRAN source codes. In addition, for "PAR" files, the filename starts with a two-digit number corresponding to the arbitrary molecule numbers designated in HITRAN. The numbering of molecules has been chosen simply chronologically, that is, as they are appended to the database (see Appendix B for the numbering scheme).

There are several files and other software contained on the cd In addition to those described in this manual. They are briefly described below. The files in the sub-directory **\SOFTWARE\GENERIC** are provided for users not using MS WINDOWS or UNIX software utilities provided with the HAWKS compilation. These are provided, for example, for users employing other operating systems such as VMS. The important program provided here is an updated version of SELECT called SELECT96.C. This C-program performs the basic database selection criteria as required or specified by the user. The compiled version is SELECT96.exe. The program is similar to earlier versions of SELECT but has been made more rapid in its search algorithm. Two files are also provided to simplify compiling SELECT96.C. They are MAKEFILE.DOS and MAKEFILE.UNI which are used for DOS and UNIX respectively.

A library of programs has been provided for the correspondence of codes in the database and more readable or common notation, e.g., the program BD\_VIBS.FOR which relates the vibrational or "global" indices in the HITRAN database with the closest ASCII equivalent of quantum vibrational assignments. The library also contains the \*.CMN files that are necessary for some of the INCLUDE statements in general programs for HITRAN.

TABLE\_96.TXT is an ASCII file with the references used by HITRAN and also for the band centers. This table is slightly more current than the one accessed in WINDOWS through hypertext.

BSUMS\_96.TXT is a table of the band statistics in HITRAN96. This table also can be generated by using the BANDSTAT feature in the WINDOWS version of HAWKS. It contains, band-by-band for each molecule and isotope, the maximum and minimum of the parameters as well as the sums of the intensities of the lines in a band and the spectral extent of the band.

MOLPARAM.TXT provides a table of the isotopic abundances of the isotopomers present in HITRAN, the total partition function at 296K for each isotope, the spin-statistical weight, and the

molecular weights.

A program called TIPS.FOR is provided that enables the user to obtain the total internal partition sum for the species in HITRAN at temperatures from 70K to 3000K. The user should compile this program with the BD\_\*.FOR in this directory and also link with the \*.CMN files.

In the sub-directory **\HITRAN96\BY\_MOLEC** are contained individual files of the line-by-line HITRAN96 broken down by molecule. The files use the arbitrary molecule number as the first two characters of the file. The correspondence can be found in MOLPARAM.TXT, Appendix B of the Manual, or in the block data program BD\_MOL.FOR. For example, 01\_HIT96.PAR is the file for all the water line-by-line parameters in HITRAN96 (1 = H<sub>2</sub>O). When these files are combined and sorted, one obtains the full HITRAN96 database, given in the directory HITRAN96 (called HITRAN96.PAR).

In the directory **\SUPLEMNT** are deposited line-by-line data that have not met with sufficient validation for inclusion on the main database, HITRAN. The three files present in this supplemental section are: 03\_NLTE.PAR, 36\_HIT96.PAR, and 37\_HIT96.PAR. These files correspond respectively to high-vibrational ozone calculated parameters (useful for non-local thermodynamic equilibrium problems), NO<sup>+</sup> (the first ionized species to be placed in the HITRAN compilation), and HOBr IR parameters. Future releases of HAWKS/HITRAN will see files such as these incorporated into the main body of the database, while new supplemental files will most likely be deposited here.

In the directory **\IR\_XSECT** are placed files of IR cross-sections, described in previous articles on the database. In the current edition, several files have been added, for example the CFCs 11, 12, and 22 which now include the data at different pressures as well as temperature. This feature will hopefully enable the user to make more accurate atmospheric simulations. The files from earlier databases have been retained and are contained in the file XSECT92.XSC. The user should be aware that there are possibly some redundancies with the data, so caveat emptor. Each portion of the cross-section files, i.e., a panel with a temperature and pressure pair, contains a header that points to the reference for that observation.

In the directory **\HITEMP** one finds the first public edition of HITEMP, the high-temperature analog of HITRAN. The format of the line-by-line parameters is the same as for HITRAN. The user should be aware that the intensities have been scaled into the standard units of (cm<sup>-1</sup>/ (molecule•cm<sup>2</sup>) at 296K). Thus, FASCODE (a frequently-used line-by-line transmission/ radiance code) users, for example, should use the data as is. Their program will scale the parameters appropriately. The SELECT option provided in the WINDOWS and UNIX part of HAWKS will also



rescale the parameters to a desired temperature.

On this first version are three files. The file 01\_1500K.PAR contains water vapor parameters calculated using a criterion of 1500K. The criterion was chosen to include all bands and rotational levels appropriate at least to this temperature; above this temperature there may be missing transitions, depending on the spectral region chosen for one's problem. Owing to the re-scaling of the intensities to 296K, there will be some very low exponents of some of the intensity parameters. The water vapor data at this time only includes the principal isotope and covers the spectral range 500 to 5000  $\text{cm}^{-1}$ .

The 02\_1000K.PAR file is similarly carbon dioxide parameters. This file covers a spectral range of about 400 to 10000  $\text{cm}^{-1}$ , contains the three most abundant isotopes, and was calculated based on a criterion of 1000K. The same comments that were made for water vapor above apply here.

The file 05\_HOT.PAR contains data for carbon monoxide appropriate for very high temperatures. It is particularly useful for calculating solar lines.

It should be pointed out that the data in this directory are totally compatible with those in HITRAN, that is, transitions contained in both databases, for example transitions emanating from the ground state, have been made identical. This feature facilitates the use of the two databases simultaneously such as one might do when simulating the radiance of a hot source as seen through the intervening cooler atmosphere (where one would use HITRAN for the layers). In this example, use HITEMP for the hot source and HITRAN for the atmosphere; no line correlation problems will occur.

The subdirectory **\MODELS\MODTRAN\SOURCE** contains a version of the band-model code, MODTRAN3, that was current at the time of creating this edition of HAWKS. We have supplied the FORTRAN source code, MODTRAN3.F. The user must compile this program. All associated software is provided in various directories under **\MODELS\...**

We have also placed the MODTRAN technical manual in both MS-WORD form and Postscript form, MODTN\_WD.EXE and MODTN\_PS.EXE respectively in self-extracting form in the directory **\DOCUMENT**. Users should direct their technical and programmatic questions concerning MODTRAN to:

Ms. Gail Anderson, PL/GPOS, 29 Randolph Rd, Hanscom AFB, MA 01731-3010

Phone: (617) 377-2335; FAX: (617) 377-8900; E-mail: GAnderson@PLH.AF.MIL

For a PC-WINDOWS version of MODTRAN the user should contact the Ontar Corp. Attn:

Andrew McCann, 9 Village Way, North Andover, MA 01845-2000 USA

Phone: (USA)-508-689-9622, Fax: (USA)-508-681-4585

The directory **VAEROSOLS** contains the real and imaginary indices of refraction for many aerosols. Detailed information on these files is given in the AEROSOL.DOC file on the CD-ROM. Questions concerning the data should be addressed to Dr. Steven Massie at NCAR (303-497-1404, massie@ncar.ucar.edu).

The CD-ROM contains the following files and directories.

README	DOC	17,727	Directory of \HITEMP	
AEROSOLS	<DIR>			
DOCUMENT	<DIR>		HITEMP	DOC 2,308
HITEMP	<DIR>		01_1500K	PAR 119,748,918
HITRAN96	<DIR>		02_1000K	PAR 105,291,438
IR_XSECT	<DIR>		05_HOT	PAR 11,528,244
MODELS	<DIR>			
SOFTWARE	<DIR>		Directory of \HITRAN96	
SUPLEMNT	<DIR>			
UV	<DIR>		BY_MOLEC	<DIR>
			HITRAN96	PAR 101,935,026
Directory of \AEROSOLS				
AEROSOL	DOC	4,224		
DOWNING_	DAT	16,412	Directory of	
KOU_ETAL	DAT	30,046	\HITRAN96\BY_MOLEC	
PALMER_W	DAT	32,966		
REMSBERG	DAT	27,464	BY_MOLEC	DOC 601
SHETTLE	DAT	39,702	01_HIT96	PAR 5,043,288
STEELE_H	DAT	1,800	02_HIT96	PAR 6,201,804
TIMMERMA	DAT	12,154	03_HIT96	PAR 28,063,566
TOON_ETA	DAT	29,984	04_HIT96	PAR 2,669,748
WARREN	DAT	34,262	05_HIT96	PAR 456,654
Directory of \DOCUMENT			06_HIT96	PAR 4,899,264
HAWKS_WP	EXE		07_HIT96	PAR 641,784
HAWKS_PS	EXE		08_HIT96	PAR 1,563,762
MODTN_WD	EXE		09_HIT96	PAR 3,963,006
MODTN_PS	EXE		10_HIT96	PAR 10,269,360
			11_HIT96	PAR 1,137,504
			12_HIT96	PAR 16,873,452
			13_HIT96	PAR 884,952

## HAWKS Manual

## Appendix A-1

14_HIT96	PAR	10,914
15_HIT96	PAR	54,366
16_HIT96	PAR	58,752
17_HIT96	PAR	24,174
18_HIT96	PAR	737,460
19_HIT96	PAR	87,516
20_HIT96	PAR	275,604
21_HIT96	PAR	1,587,630
22_HIT96	PAR	12,240
23_HIT96	PAR	78,744
24_HIT96	PAR	954,210
25_HIT96	PAR	555,288
26_HIT96	PAR	170,136
27_HIT96	PAR	484,398
28_HIT96	PAR	294,372
29_HIT96	PAR	5,596,332
30_HIT96	PAR	1,175,040
31_HIT96	PAR	729,402
32_HIT96	PAR	345,576
33_HIT96	PAR	2,750,226
34_HIT96	PAR	204
35_HIT96	PAR	3,284,298

### Directory of \IR\_XSECT

IR_XSECT	DOC	765
CCL4	XSC	511,333
CFC11	XSC	6,287,689
CFC12	XSC	4,802,671
CFC22	XSC	696,866
CLONO2	XSC	73,899
SF6	XSC	214,201
XSECT92	XSC	5,376,625

### Directory of \MODELS\MODTRAN

CASE	<DIR>	
CHANGES	<DIR>	
DATABASE	<DIR>	
DOCS	<DIR>	
SOURCE	<DIR>	
README		12,884
MODELS	DOC	849

### Directory of \MODELS\MODTRAN\CASE

CASE1	TP5	388
CASE10	TP5	286
CASE11	TP5	286
CASE12	TP5	678
CASE13	TP5	289
CASE14	TP5	313
CASE2	TP5	287
CASE3	TP5	286
CASE4	TP5	286
CASE5	TP5	286
CASE6	TP5	287
CASE8	TP5	450
CASE9	TP5	317
MS1	TP5	386
MS2	TP5	386
CASE1	TP6	94,816
CASE10	TP6	49,122
CASE11	TP6	46,780
CASE12	TP6	11,846
CASE13	TP6	40,708
CASE14	TP6	44,636
CASE2	TP6	105,143
CASE3	TP6	44,673
CASE4	TP6	49,472
CASE5	TP6	54,234
CASE6	TP6	54,633
CASE8	TP6	37,470
CASE9	TP6	64,112
MS1	TP6	100,717
MS2	TP6	100,717

### Directory of \MODELS\MODTRAN\CHANGES

CODE-CHA 2	3,903
CODE-CHA 21	1,897
UPDATES1 21	1,725

### Directory of \MODELS\MODTRAN\DATABASE

REFBKG	5,181
--------	-------

## HAWKS Manual

SUN2		898,794
MAKEFILE	-BA	1,416
BMTP	ASC	8,648,416
UFTAPX	ASC	171,183
BCDDIR	F	4,725
BCDDIR	OUT	11,191

### Directory of \MODELS\MODTRAN\DOCS

LOWTRAN7	ASC	53,629
DISORT	DOC	34,398
LOWTRAN7	PS	306,595
LOWTRAN7	WP6	100,418

### Directory of \MODELS\MODTRAN\SOURCE

MAKEFILE		1,637
BMTRAN	F	7,324
D1MACH	F	9,895
DPDISORT	F	178,838
DPLINPAK	F	47,386
DRIVER	F	187,288
MODTRAN3	F	1,718,474
STDMDL	F	164,072
PARAMETE	LIS	375

### Directory of \SOFTWARE

GENERIC	<DIR>
UNIX	<DIR>
WINDOWS	<DIR>

### Directory of \SOFTWARE\GENERIC

BD-ISO	C	5,803
BD-MOL	C	1,145
BD-QT	C	1,865
BD-VIBS	C	18,968
QT	C	3,176
SELECT96	C	51,544
UTIL	C	5,953

## Appendix A-1

ISOTOPS	CMN	68
MOLEC	CMN	89
QOFT	CMN	111
SPECIES	CMN	43
VIBS	CMN	187
BANDCENT	DAT	64,479
QT	DAT	18,812
GENERIC	DOC	2,109
MAKEFILE	DOS	1,869
SELECT96	EXE	69,557
BD_ABUN	FOR	2,891
BD_ISO	FOR	3,406
BD_MOL	FOR	663
BD-QT	FOR	44,891
BD-VIBS	FOR	14,539
TIPS	FOR	3,398
ISOTOPS	H	164
MOLEC	H	138
QOFT	H	186
QT	H	178
SPECIES	H	128
UTIL	H	655
VIBS	H	220
BSUMS_96	TXT	286,602
TABLE_96	TXT	103,017
MAKEFILE	UNI	1,985

### Directory of \SOFTWARE\UNIX

hawks_SUNOS4.tar.Z	2,013,750
hawks_Solaris2.tar.Z	2,325,201

### Directory of \SOFTWARE\WINDOWS

HTLOGO2	BMP	287,682
ONTARLOG	BMP	16,502
PLGPLOGO	BMP	8,310
BANDCENT	DAT	64,479
ISO	DAT	1,271
QT	DAT	18,812
VIB	DAT	6,454
HAWKS	EXE	330,080
PRTSEL	EXE	31,758
SETUP	EXE	273,920
HAWKS	HLP	31,876

## HAWKS Manual

## Appendix A-1

HAWKS96	HLP	527,106
HITRAN	HLP	206,678
XSECTION	HLP	10,033
HAWKS	ICO	766
SETUP	INS	2,130
B	PIF	995
SETUP	PKG	281
DEF	SEL	2,598

### Directory of \SUPLEMNT

SUPLEMNT	DOC	699
03_NLTE	PAR	18,841,848
36_HIT96	PAR	123,013
37_HIT96	PAR	444,517

### Directory of \UV

LBL	<DIR>
XSECT	<DIR>

### Directory of \UV\LBL

07_SCHUM	DOC	3,224
07_SCHUM	PAR	1,124,040

### Directory of \UV\XSECT

N2O_ABS	DOC	1,057
SO2_ABS	DOC	1,209
N2O_SAO	XSC	143,308
SO2_SAO1	XSC	1,899,116
SO2_SAO2	XSC	408,080
SO2_SAO3	XSC	70,562

## APPENDIX B. HITRAN Molecules with Associated Indices

HITRAN Molecule Number	Molecule Chemical Symbol	Number of lines	HITRAN Molecule Number	Molecule Chemical Symbol	Number of lines
1	H <sub>2</sub> O	49444	21	HOCl	15565
2	CO <sub>2</sub>	60802	22	N <sub>2</sub>	120
3	O <sub>3</sub>	275133	23	HCN	772
4	N <sub>2</sub> O	26174	24	CH <sub>3</sub> Cl	9355
5	CO	4477	25	H <sub>2</sub> O <sub>2</sub>	5444
6	CH <sub>4</sub>	48032	26	C <sub>2</sub> H <sub>2</sub>	1668
7	O <sub>2</sub>	6292	27	C <sub>2</sub> H <sub>6</sub>	4749
8	NO	15331	28	PH <sub>3</sub>	2886
9	SO <sub>2</sub>	38853	29	COF <sub>2</sub>	54866
10	NO <sub>2</sub>	100680	30	SF <sub>6</sub>	11520
11	NH <sub>3</sub>	11152	31	H <sub>2</sub> S	7151
12	HNO <sub>3</sub>	165426	32	HCOOH	3388
13	OH	8676	33	HO <sub>2</sub>	26963
14	HF	107	34	O	2
15	HCl	533	35	ClONO <sub>2</sub>	32199
16	HBr	576	36	NO <sup>+</sup>	1206
17	HI	237	37	HOBr	4358
18	ClO	7230			
19	OCS	858			
20	H <sub>2</sub> CO	2702			

This table gives the HITRAN numbering scheme for the molecular species on various line-by-line portions of HAWKS. The first 35 molecules (including the oxygen atom, number 34) are contained in HITRAN. Molecules 36 (ionic species NO<sup>+</sup>) and 37 (HOBr) are contained in the Supplemental Directory.

**Index**

296K .....	6, 14, 16, 36, 39-41
aerosols .....	7, 36, 42
auto scale .....	29, 30
band .....	14, 15, 17, 20, 21, 27, 35, 39, 41
bandstat .....	8, 20, 39
bandsum .....	20
batch .....	18, 19
cancel .....	18, 23
cd-rom .....	1, 6, 21, 39, 42
climate assessment .....	5
copy .....	2, 9
cross-section .....	6, 27, 39, 40
cutoff .....	16, 17
directory .....	1, 2, 4, 5, 7, 36, 39-46
DOS .....	2, 3, 5, 7, 19, 39, 44
edit .....	2, 3, 5, 9, 21, 28, 33
exit .....	5, 9
FASCODE .....	40
hardware requirements .....	1
HAWKS .....	, 1-5, 7-9, 16, 17, 28, 35-37, 39-42, 44, 46,
help .....	2, 8, 24, 25, 27, 33-35
HITEMP .....	7, 14, 16, 31, 36, 40-42
hypertext .....	27, 34, 39
icon .....	2, 3, 8
infrared .....	6, 27
installation .....	1, 2, 5, 8
intensity .....	6, 14, 16, 17, 24, 27, 29, 30, 35, 41
isotope .....	13, 20, 35, 39, 41
laser .....	5
line-by-line .....	6, 7, 36, 37, 39, 40, 46
logo .....	9

## **HAWKS Manual**

## **Appendix A-1**

lower level .....	14, 15
lower state energy .....	29, 30
merge .....	21, 23
MODTRAN .....	7, 41, 43, 44
open .....	3, 9, 18, 21, 29
PIF .....	3-5, 44
print .....	9, 19
reference option .....	24, 26, 27
references .....	24-27, 37-39
run .....	1-3, 5, 17, 18, 21
save .....	5, 19
select .....	2-4, 7-20, 29, 32, 36, 39, 40
setup .....	1, 44
sort .....	8, 21, 23
species .....	6, 14, 36, 37, 40, 44, 46
spectral range .....	6, 11-13, 35, 41
temperature .....	7, 14, 27, 36, 40, 41
text editor .....	2, 3, 5
transmission .....	5, 36, 40
ultraviolet .....	6
UNIX .....	1, 2, 5, 7, 39, 40, 44
upper level .....	14, 15
wavelength .....	11
wavenumber .....	11, 20, 24, 26, 30, 31
WINDOWS .....	, 1, 3, 5, 7-10, 36, 39-41, 44,
xsection .....	24, 27, 44
x-axis .....	29, 33
y-axis .....	29, 33



**HITRAN HAWKS and HITEMP  
High-Temperature Molecular Database**

L. S. Rothman, Geophysics Directorate,  
Simulations Branch, Hanscom AFB, MA 01731-3010

R. B. Wattson, Stewart Radiance Laboratory, Utah State University, Bedford, MA  
01730

R. R. Gamache, Univ. of Mass at. Lowell, Lowell, MA 01854

J. Schroeder and A. McCann, Ontar, 9 Village Way, North Andover, MA 01845

**ABSTRACT**

The **HITRAN** database has been recognized for over 20 years as the international standard compilation of spectroscopic parameters for atmospheric gases. A new version is in beta testing and will be available for distribution within the next few months. Significant new additions have been made to the database to keep pace with the increasing requirements of the user community. One of these additions is a high temperature database (**HITEMP**) for CO<sub>2</sub>, H<sub>2</sub>O, and CO. These data will be of particular importance in remote sensing of high temperature sources such as flames, combustion processes, exhaust plumes and stellar atmospheres. This paper will describe the latest addition to HITRAN, the high-temperature database, and provide sample calculations using **PCLnWin**, a commercial implementation of the **FASCODE** atmospheric transmission/radiance code. Information is provided to obtain copies of the next HITRAN release. This work was sponsored with funds from the US Air Force, The Department of Energy and Ontar Internal IR&D funds.

**1. INTRODUCTION**

A comprehensive spectroscopic database of molecular parameters is required by all programs attempting to make line-by-line simulations. These simulations include both absorption and radiance calculations and generally are performed in moderately long atmospheric paths. The standard database, HITRAN, has existed for over 2 decades and is constantly being updated (expanded spectral coverage, more parameters per transition, weaker line inclusion, more species and isotopes, enhancement to meet the needs of a wide range of applications, especially remote sensing). A companion database, in the same format as HITRAN, has now been established; this database, HITEMP, is designed to fulfill the requirements of hot-source gaseous emission. The applications include target or plume detection, stellar atmospheres, pollution detection, etc.

The next HITRAN release will be under the **HAWKS** (HITRAN Atmospheric Work Station) umbrella. This new approach comes about because

of the expanded nature of the current database. It will include an updated version of the traditional HITRAN compilation of spectral parameters for atmospheric gases. However, also included will be supplemental data bases, greatly expanded cross-sections databases, UV (both line-by-line, and cross-sections) aerosols, and the aforementioned HITEMP. The "old faithful" Select FORTRAN source code is being superseded by DOS/WINDOWS and UNIX based executable code for data handling. The makeover of HITRAN, represented by HAWKS, is a significant enhancements designed to meet the changing needs of the user community. Tables 1 and 2 provide an overview of the file structure and molecular database for the next HITRAN release.

Directory	Sub-Directory	Megabytes
Software	<b>FORTRAN programs and Tables (ASCII)</b>	<b>~.6</b>
	<b>WINDOWS</b>	<b>~.2</b>
	<b>UNIX</b>	<b>~10</b>
<b>HITRAN</b>		<b>95</b>
<b>Supplemental</b>		<b>19</b>
<b>cross-sections</b>		<b>1.8</b>
<b>UV</b>	<b>Line-by-line</b>	<b>1.1</b>
	<b>Cross-sections</b>	<b>2.5</b>
<b>Aerosols</b>		<b>.2</b>
<b>HITEMP</b>		<b>236</b>

Table 1 File Structure for the next HITRAN release

HITRAN/HAWKS 1995				
Band Statistics for HITRAN'95		Band Stats for Supplementa		
1 H <sub>2</sub> O	49444	3 High-vib	184724	
2 CO <sub>2</sub>	60802	36 NO*	1206	
3 O <sub>3</sub>	232751	37 HOBr	4358	
4 N <sub>2</sub> O	26249 *			
5 CO	3877	Band Stats for HITEMP		
6 CH <sub>4</sub>	48032	1 H <sub>2</sub> O	1E+06	
7 O <sub>2</sub>	6227	2 CO <sub>2</sub>	1E+06	
8 NO	14732 *	5 CO	113022	
9 SO <sub>2</sub>	34623			
10 NO <sub>2</sub>	97813	Band Stats for UV		
11 NH <sub>3</sub>	10191	7 O <sub>2</sub>	11020	
12 HNO <sub>3</sub>	165426			
13 OH	8676			
14 HF	107			
15 HCl	533	Cross-section Sizes		
16 HBr	576	N <sub>2</sub> O -UV	143308 Bytes	
17 HI	237	SO <sub>2</sub> -UV	2E+06 Bytes	
18 ClO	7300	IR	2E+07 Bytes	
19 OCS	4295			
20 H <sub>2</sub> CO	2702	Aerosols		
21 HOCl	15565		229014 Bytes	
22 N <sub>2</sub>	120			
23 HCN	772			
24 CH <sub>3</sub> Cl	9355			
25 H <sub>2</sub> O <sub>2</sub>	5444			
26 C <sub>2</sub> H <sub>2</sub>	1745			
27 C <sub>2</sub> H <sub>6</sub>	4749			
28 PH <sub>3</sub>	2886			
29 COF <sub>2</sub>	54975			
30 SF <sub>6</sub>	11520			
31 H <sub>2</sub> S	5198			
32 HCOOH	3388			
33 HO <sub>2</sub>	26963			
34 O	2			
35 ClONO <sub>2</sub>	32199			
# lines =	949474	* = not final tally		

Table 2. Statistics of molecular data for the next HITRAN release

## 2. HITEMP

The high temperature datasets (HITEMP) for CO<sub>2</sub>, H<sub>2</sub>O and CO are a major addition and will be used in a variety of remote sensing applications ranging from exhaust gas monitoring to the investigation of stellar atmospheres. At elevated temperatures (>1000 K) many more molecular vibrational levels are populated compared to the number at atmospheric temperatures (~296 K). This results in thousands (even millions) of additional spectral lines. Traditionally, investigators have scaled the HITRAN database to estimate the absorption and emission spectra at elevated temperatures. Although the scaling from 296 K to higher temperatures is sufficiently accurate to estimate the line strength, etc. at the higher temperature, the “problem” is that the additional spectral lines were missing from the simulation. This approach often leads to significant underestimate of the source radiance. Examples of this problem are provided below.

Molecules	Spectral Coverage	# of Lines	Temperature of Calculation
CO <sub>2</sub>	158 - 9648 CM <sup>-1</sup> 1 - 63 μm	1,032,269 1st. three isotopes	DND <sup>1</sup> @ 1000 K
H <sub>2</sub> O	500 - 5000 CM <sup>-1</sup> 2 - 20 μm	1,174,009 principal isotope	DND @ 1500 K
CO	850 -- 6418 CM <sup>-1</sup> 1.6 - 12 μm	113,022 all significant isotopes	Solar Atlas

<sup>1</sup> Direct Numerical Diagonalization

**Table 3 Summary of the HITEMP Molecular Database**

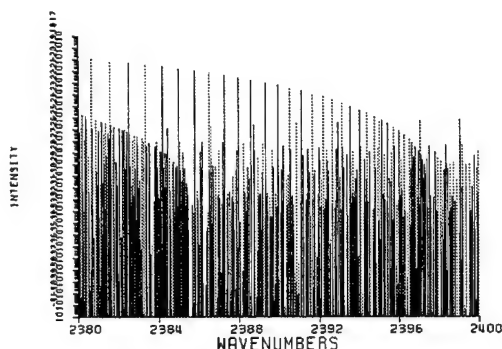


**Figure 1 CO<sub>2</sub> HITEMP**



**CO<sub>2</sub> HITRAN**

HITEMP remedies this HITRAN deficiency. The spectral range, number of spectral lines, and calculational temperature for the three gases included in the first HITEMP release are summarized below in Table 3.

Table 4 and Figure 1 illustrate some differences between HITRAN and HITEMP. For example, in the red and blue spike CO<sub>2</sub> spectral region (2100 - 2400 CM<sup>-1</sup>, 4.2 - 4.8 μm) HITRAN contains about 14,000 lines versus over 300,000 in HITEMP.

Molecules	Spectral Interval	HITRAN	HITEMP
CO <sub>2</sub>	2100 - 2400 CM <sup>-1</sup> 4.2 - 4.8 μm	13,804	300,581
CO <sub>2</sub>	3300 - 3800 CM <sup>-1</sup> 2.6 - 3.0 μm	11,113	186,483
H <sub>2</sub> O	3800 - 4100 CM <sup>-1</sup> 2.4 - 2.6 μm	6,068	60,120

**Table 4 Comparison of the HITEMP and HITRAN databases**

The line positions and intensities of water vapor were calculated from the Direct Numerical Diagonalization method <sup>1</sup>. For CO<sub>2</sub>, a table of spectroscopic constants, that is, distortion and higher order terms plus band intensities and Herman-Wallis factors was generated. However, very high weights were given to observed line positions from which lower-order constants were established via a least-squares method. The final parameters were then calculated using the standard formulae <sup>2</sup>. Halfwidths were applied to the parameters in the same fashion as HITRAN. The CO parameters were generated with the application from solar atlas <sup>3</sup>.

HITRAN/HITEMP will be used for numerous applications ranging from laboratory spectroscopic studies to input parametric data for computer codes. To make the data compatible with codes such as FASCODE, the data was scaled to a standard reference temperature of 296K for intensity and halfwidth. The exponents in the intensity field can thus be quite low, e.g. CO. (however the HAWKS software will reformat the data to desired temperature 70<T<3000 K). The dynamic range has also been limited by the choice of cutoff, for example limiting the total band intensities in the driver tables. Nonetheless, there should be more than ample range. Finally, the spectral data from HITRAN was merged into HITEMP to make the latter a stand alone database, that can be used for both atmospheric and high temperature applications

### 3. EXAMPLES: CO<sub>2</sub>, H<sub>2</sub>O

Several calculations are given below to illustrate the importance of using the HITEMP database in place of HITRAN for certain applications. The calculations were performed using PCLnWin, the Ontario commercial version of the US Air Force's FASCODE atmospheric transmission and radiance model. The calculations were made for a 5 meter source located 30 meters above the earth's surface at the temperature indicated on the figures. H<sub>2</sub>O and CO<sub>2</sub> concentrations were 200 and 250 PPM respectively while the 1976 US Standard concentrations were used for the remaining constituents.

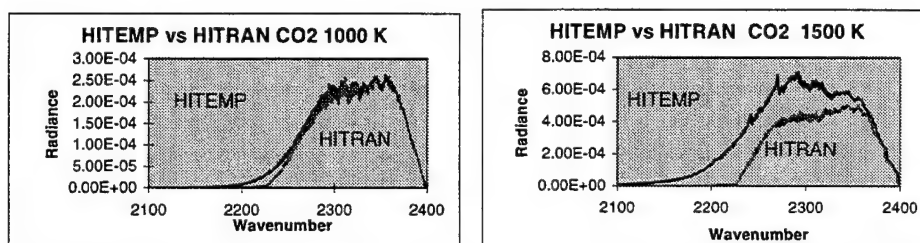


**Figure 2, HITEMP vs HITRAN for CO<sub>2</sub>  
at 1000 K and 1500 K between 2100 - 2400 CM<sup>-1</sup> (4.2 - 4.8 μm)**

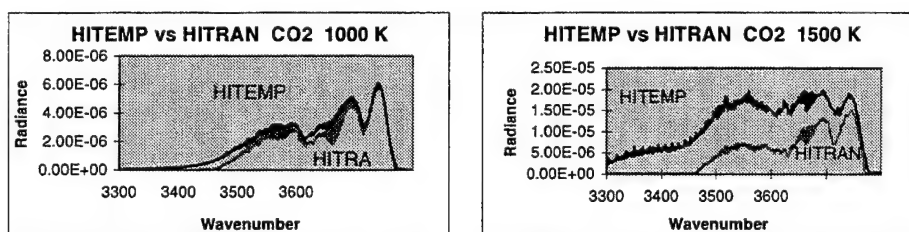


**Figure 3, HITEMP vs HITRAN for CO<sub>2</sub>  
at 1000 K and 1500 K between 3300 - 3800 CM<sup>-1</sup> (2.6 - 3.0 μm)**

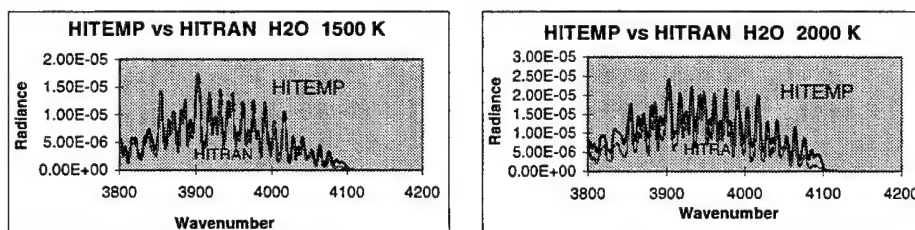


**Figure 4, HITEMP vs HITRAN for H<sub>2</sub>O  
at 1500 K and 2000 K between 3800 - 4100 CM<sup>-1</sup> (2.4 - 2.6 μm)**

Figures 2 and 3 indicate that there is not a significant difference for CO<sub>2</sub> at 1000 K except in the wings of the bands. However, at 1500 K there is a large difference across the entire band. The calculations shown in Figures 2, 3 and 4

were made at the full resolution of the database (i.e. line-by-line). They were degraded for display purposes to  $\sim 2 \text{ cm}^{-1}$  wavenumbers resolution by convolving the line-by-line results with a  $(\sin x/x)^2$  function.

For  $\text{H}_2\text{O}$  there appears to be little difference between HITRAN and HITEMP, even at 2000 K. However, care must be taken in interpreting the results for both  $\text{CO}_2$  and  $\text{H}_2\text{O}$ . This is illustrated in Figures 5 and 6 where the line-by-line data is shown as it would be observed by a sensor 5 Kilometers from the source.

Figure 5 is the atmospheric transmission for a 5 KM, horizontal path, using the 1976 US Standard model atmosphere. Figure 6 shows the radiance that is received at a sensor over this path for  $\text{H}_2\text{O}$  at 2000 K between 4015 and 4030  $\text{CM}^{-1}$  (2.48 - 2.49  $\mu\text{m}$ ). Figure 6 shows that the HITEMP lines (plot on the left) make a significant additional contribution over the HITRAN calculation (plot on the right) over this relatively narrow spectral region. The contribution will be quite large when integrated over a broad band. Consequently, HITEMP must be used for simulations at temperatures significantly above ambient.

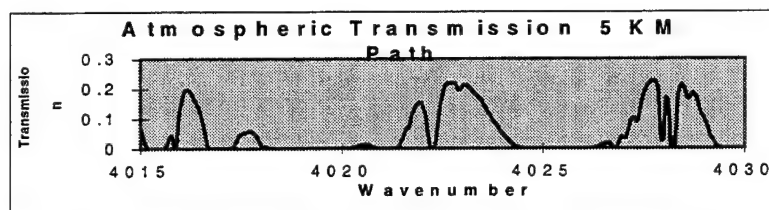


**Figure 5, Atmospheric Transmission for a 5 KM Path between 4015 and 4030  $\text{CM}^{-1}$  (2.48 - 2.49  $\mu\text{m}$ )**

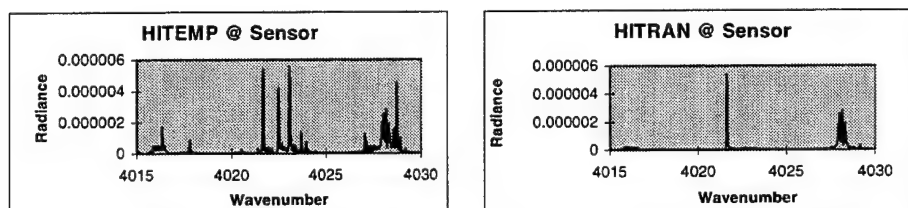


**Figure 6, HITEMP vs HITRAN for  $\text{H}_2\text{O}$  at 2000 K between 4015 and 4030  $\text{CM}^{-1}$  (2.48 - 2.49  $\mu\text{m}$ )**

#### 4. SUMMARY AND HAWKS/HITRAN DISTRIBUTION

This paper has described the HAWKS/HITRAN database. A new version will be available in the near future which contains significant enhancement over the 1992 edition. Of particular importance is the addition of the HITEMP (High-Temperature Molecular Database) for  $\text{CO}_2$ ,  $\text{H}_2\text{O}$  and  $\text{CO}$ . This paper has described the new database and shown calculations comparing the HITRAN and HITEMP datasets. HITEMP is a self-contained database and must be used for simulation at temperatures significantly above ambient.

The database is currently distributed on a single CD-ROM. Copies may be obtained by contacting:

**Dr. L. S. Rothman**

e-mail Rothman@PL9000.PLH.AF.MIL

e-mail LRothman@CfA.Harvard.edu

or

**The Ontar Corporation**

Tel (USA)-508-689-9622

Fax (USA)-508-681-4585

#### REFERENCES

1. R. B. Wattson and L. S. Rothman, "Direct Numerical Diagonalization: Wave of the Future," *JQSRT* **48**, 763 (1992).
2. L. S. Rothman, R. L. Hawkins, R. B. Wattson, and R. R. Gamache, "Energy Levels, Intensities, and Linewidths of Atmospheric Carbon Dioxide Bands," *JQSRT* **48**, 537 (1992).
3. R. Farrenq, G. Guelachvili, A. J. Sauval, N. Grevesse, and C. B. Farmer, "Improved Dunham Coefficients for CO from Infrared Solar Lines of High Rotational Excitation," *J.Mol.Spectrosc.* **149**, 375-390 (1991); D. Goorvitch, "Infrared CO Linelist for the  $^1\Sigma^+$  State," *Astrophys.J.Suppl.Ser.* **95**, 535-552 (1994).

01/11/96

**The MODTRAN 2/3 Report and LOWTRAN 7 MODEL**

F.X. Kneizys <sup>1</sup>	D.C. Robertson <sup>4</sup>
L.W. Abreu <sup>2</sup>	P. Acharya <sup>4</sup>
G.P. Anderson	L.S. Rothman
J.H. Chetwynd	J.E.A. Selby <sup>5</sup>
E.P. Shettle <sup>3</sup>	W.O. Gallery <sup>6</sup>
A. Berk <sup>4</sup>	S.A. Clough <sup>6</sup>
L.S. Bernstein <sup>4</sup>	

Edited By:

L.W. Abreu  
G.P. Anderson

1. Deceased
2. Currently at the Ontar Corporation
3. Currently at the Naval Research Laboratory
4. Currently at the Spectral Sciences, Inc.
5. Currently at the Northrop Corporation
6. Currently at the Atmospheric Environmental Research, Inc.

Prepared for:

Phillips Laboratory, Geophysics Directorate  
PL/GPOS  
29 Randolph Road  
Hanscom AFB, MA 01731-3010

**Contract F19628-91-C-0132**

**Ms. Gail Anderson, and Dr. Laurence S. Rothman, Technical Representatives**

Prepared by:

Ontar Corporation  
9 Village Way  
North Andover, MA 01845  
Tel: (USA)508-689-9622 Fax: (USA)508-681-4585



## Table of Contents

<b>1. INTRODUCTION</b>	<b>70</b>
<b>2. COMMON ELEMENTS</b>	<b>73</b>
<b>2.1 AIRMASS COMPUTATION (SPHERICAL REFRACTIVE GEOMETRY)</b>	<b>73</b>
2.1.1 Introduction	73
2.1.2 Definition of Equations	73
2.1.3 Atmospheric Refraction	76
2.1.4 Numerical Algorithm	78
2.1.5 Airmass Calculations	79
2.1.6 Index of Refraction	84
2.1.7 WATER VAPOR CONTINUUM	85
<b>2.2 MODEL ATMOSPHERES</b>	<b>88</b>
2.2.1. INTRODUCTION	88
2.2.2 . ATMOSPHERIC PROFILE DESCRIPTION	89
2.2.3. ERROR ESTIMATES and VARIABILITY	101
2.2.4. LIMITATIONS	101
<b>2.3 AEROSOL MODELS</b>	<b>102</b>
2.3.1 Introduction	102
2.3.2 Vertical Distribution in the Lower Atmosphere	103
2.3.3 Effects of Humidity Variations on Aerosol Properties	107
2.3.4 Vertical Distribution in the Stratosphere and Mesosphere	119
2.3.5 Use of the Aerosol Models	135
2.3.6. NAVY Maritime Aerosol Model	142
2.3.7 ARMY Vertical Structure Algorithm	147
<b>2.4 Particulate Extinction</b>	<b>155</b>
2.4.1. The Rain Model	155
2.4.2 Water Clouds	159
2.4.3 Ice Clouds	162
<b>3. THE MODTRAN MODEL</b>	<b>163</b>
<b>3.1 Introduction</b>	<b>163</b>
<b>3.2 MOLECULAR BAND MODEL PARAMETERS</b>	<b>166</b>
3.2.1 Line-Center Parameters	167
3.2.2 Line-Tail Parameters	169
3.2.3 Parameter Data File	170
<b>3.3 BAND-MODEL TRANSMITTANCE FORMULATION</b>	<b>171</b>
3.3.1 Line-Center Transmittance	171
3.3.2 Line-Wing Absorption	175
<b>3.4 Integration With LOWTRAN 7</b>	<b>176</b>
3.4.1 New Subroutines	176
3.4.2 Necessary Modifications to LOWTRAN 7	176

3.5 Upgraded Line-of-Sight Geometry	181
3.5.1 LOS Specification	181
3.5.2 Geometry Problems	182
3.5.3 Improved Numerical Accuracy	183
3.5.4 Slant Paths	183
<b>4. ATMOSPHERIC TRANSMITTANCE</b>	<b>186</b>
4.1 LOWTRAN 7 Molecular Transmittance Band Models	186
4.1.1 Introduction	186
4.1.2 The Transmittance Function	187
4.1.3 Model Development	189
4.1.4 Comparisons with Measurements	197
4.2 Nitric Acid	200
4.3 Nitrogen Continuum Absorption	201
4.4 Molecular Scattering	202
4.5 Ultra Violet Absorption	202
4.5.1 UV Oxygen Absorption	203
4.5.2 UV Ozone Absorption	207
4.6 Aerosol Transmittance	209
<b>5. ATMOSPHERIC RADIANCE</b>	<b>211</b>
5.1 Radiative Transfer Equations	211
5.2 Improved Solar Source Function	212
5.3 SOLAR/LUNAR SINGLE SCATTERING MODEL	214
5.3.1 Introduction	214
5.3.2 Radiative Transfer	215
5.3.3 Phase Functions for Scattering by Atmospheric Aerosols and Molecules	221
5.3.4 Recommendations of Usage	227
5.3.5 Directly-Transmitted Solar Irradiance	229
5.4 NEW MULTIPLE SCATTERING ALGORITHM	230
5.4.1 Introduction	230
5.4.2 Stream Approximation	231
5.4.3 Implementation in MODTRAN 2 and LOWTRAN 7	243
5.4.4 Comparison to Exact Calculations	256
<b>6. VALIDATION AND APPLICATIONS</b>	<b>259</b>
<b>7. DISCUSSION OF FUTURE MODIFICATIONS</b>	<b>264</b>
<b>REFERENCES</b>	<b>265</b>

<b>APPENDIX A MODTRAN 3 USER INSTRUCTIONS</b>	<b>295</b>
<b>A3. INSTRUCTIONS FOR USING MODTRAN 3</b>	<b>296</b>
<b>A3.1 Input Data and Formats</b>	<b>297</b>
<b>A3.2 Basic Instructions</b>	<b>299</b>
A3.2.1 CARD 1: LMODTRN, MODEL, ITYPE, IEMSCT, IMULT, M1, M2, M3,M4, M5, M6, MDEF, IM, NOPRT, TBOUND, SALB	299
A3.2.1B CARD 1A LDISORT, ISTRM, LSUN, ISUN, CO2MIX	302
A3.2.2 CARD 2: IHAZE, ISEASN, IVULCN, ICSTL, ICLD, IVSA, VIS, WSS, WHH, RAINRT, GNDALT	305
ASYM(N, I)= Aerosol or cloud asymmetry parameter A3.2.3 CARD 3: H1, H2, ANGLE, RANGE, BETA, RO, LEN	318
<b>A3.3 Non-Standard Conditions</b>	<b>327</b>
A3.3.1 ADDITIONAL ATMOSPHERIC MODEL (MODEL = 7)	328
A3.3.2 HORIZONTAL PATHS (MODEL = 0)	328
A3.3.3 USER INSERTED VALUES FOR ATMOSPHERIC GASES (MODEL 0 OR 7)	328
A3.3.4 USER INSERTED VALUES FOR AEROSOL VERTICAL DISTRIBUTION (MODEL = 0 OR 7)	328
A3.3.5 USER INSERTED VALUES FOR CLOUD AND OR RAIN RATES	329
A3.3.6 REPLACEMENT OF AEROSOL OR CLOUD ATTENUATION MODELS	329

# THE MODTRAN 2 / LOWTRAN 7 MODEL

## 1. INTRODUCTION

This report describes the inter-relationships of the MODTRAN (Ref 1) and LOWTRAN 7 (Ref. 2) models and the coordinated efforts in constructing a fully integrated computer code for predicting atmospheric radiance and transmittance. These models are extensions and upgrades to their predecessors: LOWTRAN 6 (Ref. 3), LOWTRAN 5 (Ref. 4), LOWTRAN 5B (Ref. 5), LOWTRAN 4 (Ref. 6), LOWTRAN 3B (Ref. 7), LOWTRAN 3 (Ref. 8) and LOWTRAN 2 (Ref. 9). All of the options and capabilities of the previous versions have been retained.

The first four sections of the report (Common Elements), contain information relevant to both models. Section 3 is specifically tailored to the MODTRAN 2 model. The remainder of the report is pertinent to both models.

The models calculate atmospheric transmittance, atmospheric background radiance, single-scattered solar and lunar radiance, direct solar and lunar irradiance and multiple-scattered solar and thermal radiance. The spectral resolution of LOWTRAN 7 is  $20\text{ cm}^{-1}$  FWHM (Full Width at Half-Maximum) in averaged steps of  $5\text{ cm}^{-1}$  in the spectral range of 0 to  $50,000\text{ cm}^{-1}$  or  $0.2\text{ }\mu\text{m}$  to infinity. The MODTRAN resolution is  $2\text{ cm}^{-1}$  FWHM in averaged steps of  $1\text{ cm}^{-1}$ . A single parameter band model (Pressure) is used for molecular line absorption in LOWTRAN 7, while MODTRAN utilizes (Pressure, Temperature and a line width). The effects of molecular continuum-type absorption; molecular scattering, aerosol and hydrometeor absorption and scattering are all included. Representative atmospheric aerosol, cloud and rain models are provided within the code with options to replace them with user-modeled or measured values. Spherical refraction and earth curvature (ray bending) are considered in the calculation of the atmospheric slant path and attenuation amounts along the path.

New atmospheric constituent profiles<sup>10</sup> containing separate molecular profiles (0 to 120 km) for thirteen (13) minor and trace gases are provided for use with both models. Six reference atmospheres, each defined by temperature, pressure, density and mixing ratios for  $\text{H}_2\text{O}$ ,  $\text{O}_3$ ,  $\text{CH}_4$ ,  $\text{CO}$  and  $\text{N}_2\text{O}$ , all as a function of altitude (selected from the U.S. Standard Supplements, 1966<sup>11</sup> and the U.S. Standard Atmosphere 1976<sup>12</sup>) allow a wide range of climatological choices.

For LOWTRAN 7, Pierluissi and Maragoudakis<sup>13</sup> have developed separate band models and band model parameters for the absorbing molecules:  $\text{H}_2\text{O}$ ,  $\text{O}_3$ ,  $\text{N}_2\text{O}$ ,  $\text{CH}_4$ ,

CO, O<sub>2</sub>, CO<sub>2</sub>, NO, NO<sub>2</sub>, NH<sub>3</sub> and SO<sub>2</sub> (see section 4.1). Analytic transmittance functions (double-exponential) replace numerical tables stored in previous LOWTRAN models. These band model parameters were developed with and based on degraded line-by-line spectra<sup>14</sup> and validated against laboratory measurements. Modifications to the water vapor continuum absorption at 1 and 10  $\mu\text{m}$  are included in both models. These corrections were based on a series of laboratory and field measurements<sup>15,16,17,18</sup>.

For MODTRAN 2, Anderson et al<sup>19</sup> have developed band model parameters from the HITRAN 1992<sup>20</sup> database with pressure and temperature dependence and a defined line width (see section 3). Besides its more recent and accurate derivation, the MODTRAN model also contains geometrical corrections to some long-standing problems with short and long horizontal-like paths<sup>21</sup>, errors currently existing in the older versions of LOWTRAN and FASCODE.

New ultraviolet absorption parameters for molecular oxygen (Schumann-Runge bands, Herzberg continuum) have been added to the codes<sup>22,23,24,25,26</sup>. The ozone absorption data in the ultraviolet (Hartley and Huggins bands) has been updated or improved based on more recent measurements<sup>27,28,29,30</sup>. These more recent additions also include temperature-dependent absorption coefficients.

An expanded, more precise extra-terrestrial solar source function is included in the models. The derivation of this solar source function is based on the work of Van Hoosier et al<sup>31,32</sup>, Neckel and Labs<sup>33</sup>, Werhli<sup>34</sup> and Thekeakara<sup>35</sup>. The spectral range of 0 to 57,470  $\text{cm}^{-1}$  is covered and is generally compatible with the resolution of the molecular absorption parameters of both models.

The models use an efficient and accurate multiple scattering parameterization<sup>36,37</sup> based on the two-stream approximation and an adding method for combining atmospheric layers. An interface scheme was developed utilizing a modified 3 term k-distribution method to match the multiple scattering approach to the LOWTRAN band model calculation of molecular gaseous absorption. This interface scheme is not needed in the MODTRAN model due to the more accurate 1  $\text{cm}^{-1}$  steps. An estimate of the errors due to the multiple scattering parameterization for solar and thermal radiance calculations is considered to be less than 10 percent.

All of the existing aerosol and rain models in previous versions were extended through the millimeter wavelength region. The Navy Maritime model was modified to improve its wind-speed dependence for the large particle component<sup>38</sup>. Water cloud models (cumulus, stratus, altostratus, strato-stratocumulus and nimbostratus) residing in RADTRAN<sup>39</sup> and FASCOD2<sup>40</sup> have been added to the models. A sub-visual cirrus

cloud model and a thin cirrus cloud model with realistic wavelength dependence and separate absorption, scattering and asymmetry parameters were developed for these radiative transfer models. A new aerosol model for desert-like conditions with wind speed dependence has also been added<sup>41,42</sup>. Both programs currently allow users to modify the aerosol profiles when operating in areas of elevated surfaces.

The stratospheric aerosols provide additional combinations of the wavelength dependent extinction coefficient models (background stratospheric, aged volcanic or fresh volcanic) and the vertical distribution profiles (background and moderate, high or extreme volcanic). The background stratospheric extinction model has been modified to utilize new refractive index data and size distribution measurements<sup>43</sup>.

## 2. COMMON ELEMENTS

### 2.1 AIRMASS COMPUTATION (SPHERICAL REFRACTIVE GEOMETRY)

The Airmass Computation description in this section is principally from Gallery<sup>44</sup> and the description contained in reference 3.

#### 2.1.1 Introduction

The transmittance and radiance along a path through the atmosphere is principally dependent on the total amount and the distribution of the absorbing or scattering species along the path. The integrated amount along a path is described by various names, including: column density, equivalent absorber amount, and "airmass". While the term "air mass" applies specifically to the total amount of gas along the path, it will be used here to refer loosely to the integrated amounts for all the different species relative to the amount for a vertical path. The calculation of air mass for realistic atmospheric paths requires that the earth's curvature and refraction be taken into account.

The model for calculating air mass has been greatly improved in MODTRAN 2. Previous models assumed that the index of refraction was constant between layer boundaries. The new model assumes a continuous profile for the refractive index, with an exponential profile between layer boundaries. It is more accurate than the previous models and works for all conceivable paths. All the options from the previous LOWTRAN models for specifying slant paths have been retained.

This section describes the model for calculating air mass and presents calculations of air mass for several representative atmospheric paths. For a detailed description of the method described here, see reference 44.

#### 2.1.2 Definition of Equations

The atmosphere is modeled as a set of spherically symmetric shells with boundaries at the altitudes  $Z_j$ ,  $j = 1, N$ . The temperature, pressure, and absorber (gas and aerosol) densities are specified at the layer boundaries. Between boundaries, the temperature profile is assumed to be linear, while the pressure and density profiles are assumed to follow exponential profiles. For example, the density  $\rho$  at an altitude  $z$  between  $z_j$  and  $z_{j+1}$  is given by:

$$\rho(z) = \rho_j \exp \left[ -\frac{(z - z_j)}{H_\rho} \right]$$

where the density scale height  $H_\rho$  is

$$H_\rho = \frac{(z_{j+1} - z_j)}{\ln(\rho_j / \rho_{j+1})}$$

The scale height varies with each layer and is different for pressure and density.

Consider an optical path through the atmosphere from point a to b as shown in Figure 1. The path is defined by the initial and final altitudes  $z_a$  and  $z_b$  and by the zenith angle  $\theta_0$  at a. The other path quantities are:  $s$ , the curved path length from a;  $\beta$ , the earth-centered angle;  $\phi$ , the zenith angle at b; and  $\psi$ , the total refractive bending along the path.

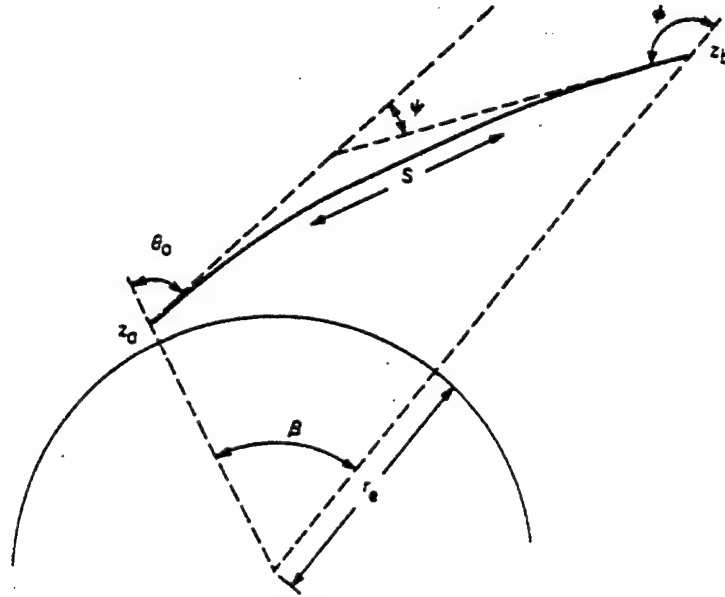


Figure 1. Slant Path Through the Atmosphere From Point a to Point b The integrated amount  $u$  of an absorber of density  $\rho(z)$  is given by:

$$u = \int_a^b \rho(z) ds \quad (1)$$

$$u = \int_a^b \rho(z) (ds/dz) dz \quad (2)$$

At any point along the path



$$\frac{ds}{dz} = (\cos \theta)^{-1} \quad (3)$$

where  $\theta$  is the local zenith angle.

Due to the curvature of the earth and to refraction,  $\theta$  varies along the path. However, if the zenith angle is less than about  $80^\circ$ , the variation of  $\theta$  along the path is negligible and Eq. (2) can be written as:

$$u = (\cos \theta_0)^{-1} \int_a^b \rho \, dz \quad (4)$$

Eq. (4) is called the secant approximation and is equivalent to assuming a plane-parallel atmosphere. The integral in Eq. (4) has a particularly simple form for an exponential density distribution:

$$\int_a^b \rho \, dz = H_\rho [\rho(z_a) - \rho(z_b)] \quad (5)$$

where  $H_\rho$  is the density scale height. If the path extends over several layers, each with a different scale height, then the integral in Eq. (5) must be broken into separate parts, one for each layer.

For the general case, curvature and refraction must be taken into account in Eq. (2). This is accomplished by a detailed numerical integration of Eq. (2) as follows. The interval from  $z_a$  to  $z_b$  is divided into a number of sub-intervals defined by  $z_1, z_2, \dots, z_N$ . The integral in Eq. (2) is approximated by the sum

$$u = \sum_{i=1}^{N-1} \bar{\rho}_i \Delta s_i \quad (6)$$

where

$$\bar{\rho}_i = \frac{1}{\Delta z_i} \int_{z_i}^{z_{i+1}} \rho(z) \, dz \quad (7)$$

$$\Delta s_i = \int_{z_i}^{z_{i+1}} (ds/dz) \, dz \quad (8)$$

Since the density is assumed to follow an exponential profile, the integral in Eq. (7) can be written analytically as

$$\bar{\rho}_i = \frac{H_\rho}{\Delta z_i} [\rho(z_i) - \rho(z_{i+1})] \quad (9)$$

where the scale height  $H_p$  is constant over the layer from  $z_a$  to  $z_b$ . The integral in Eq. (8) can be obtained numerically as shown in the next section.

The number and spacing of the intervals  $z_i$  are chosen so that Eq. (6) is a good approximation to Eq (2) as will also be shown. Again, if the path extends over several layers, with different scale heights in each, then the path integral must be performed separately for each layer. In the discussion that follows, it will be assumed that the path is confined to a single layer in which the scale heights are constant with altitude .

### 2.1.3 Atmospheric Refraction

The governing equation for a ray passing through the atmosphere is Snell's Law for a spherically symmetric medium, given by

$$n(r) r \sin \theta = C \quad , \quad (10)$$

where  $n$  is the index of refraction,  $r$  is the radius to a point along the ray,  $\theta$  is the zenith angle at that point, and  $C$  is a constant of the particular path. If the ray is horizontal at a point  $r_T$ ,  $\theta$  is equal to  $90^\circ$  at that point, and  $C$  equals  $n(r_T)r_T$ ; the altitude at that point is called the tangent height.

The index of refraction  $n$  is conveniently written as

$$n(r) = 1 + N(r) \quad , \quad (11)$$

where  $N(r)$  is called the refractivity (see Section 2.1.6 for a discussion of the index of refraction).  $N$  is wavenumber dependent and, in the visible and the infrared,  $N$  is also very nearly proportional to the total air density. At sea level, in the infrared,  $N$  is of the order of  $3 \times 10^{-4}$ . In these calculations, we assume that  $N$  follows an exponential profile with a scale height  $H_N$ .  $H_N$  is determined separately for each atmospheric layer.

The effect of refraction is to bend the path in the direction of increasing  $N$ . The radius of curvature  $K$  of the refracted ray can be shown to be:

$$K = -(n'/n) \sin \theta \quad (12)$$

where  $n' = dn/dr$ . It is useful to define the quantity  $R(r)$  as

$$R(r) = -\frac{r}{n/n'} \quad (13)$$

R is simply the ratio of  $r$  to the radius of curvature of a ray tangent at  $r$ . R is a property of the atmospheric profile and not the particular path and is a good measure of the importance of refraction at a particular altitude. For example, for the U. S. Standard Atmosphere, R is approximately 0.16 at sea level and decreases exponentially with altitude with a scale height of about 10 km.

To trace a ray through the atmosphere, consider the path shown in Figure 1:  $\theta_0$  is the zenith angle at  $Z_a$ ,  $\theta$  is the zenith angle at  $Z_b$ ,  $\beta$  is the earth-centered angle, and  $\psi$  is the bending along the path. Let  $s$  be the length of the path from point a. At any point the differential path quantities are given by

$$ds = \frac{1}{\cos \theta} dr \quad (14)$$

$$d\beta = \tan \theta \frac{1}{r} dr \quad , \quad (15)$$

where  $\theta$  is the zenith angle at the point. Substituting for  $\cos \theta$  from Eq. (10) into Eq. (14) gives:

$$ds = \left( 1 - \frac{C^2}{n^2 r^2} \right)^{-1/2} dr \quad (16)$$

Eq. (16) is the basic atmospheric ray trace equation. If the function  $n(r)$  is known, then Eq. (16) can be integrated numerically along the path.

However, the difficulty with integrating Eq. (16) is that it has a singularity at  $\theta = 90^\circ$ , that is, at the tangent height, where  $C = n(r_T) r_T$ . A simple change of variables will remove this singularity and also provide some insight into the importance of refraction. Define a new independent variable  $x$  as

$$x = r \cos \theta \quad . \quad (17)$$

( $x$  can be interpreted as the straight-line distance to the geometric tangent point).

Differentiating Eq. (17) gives

$$dx = [\cos \theta - r \sin \theta (d\theta/dr)] \quad (18)$$

Differentiating Eq. (10) and using Eq. (13) gives

$$d\theta/dr = -(1-r) \tan \theta / r \quad (19)$$

Substituting Eq. (19) into Eq. (18) gives

$$dx = (1 - R \sin^2 \theta) dr / \cos \theta \quad (20)$$

Comparing Eq. (20) with Eq (14) yields

$$ds = (1 - R \sin^2 \theta)^{-1} dx \quad (21)$$

In this form of the equation for  $ds$ , the right-hand side is a well-behaved function of  $r$  for all paths, including vertical and horizontal paths (except in the unusual case where  $R$  is  $\geq 1$  and the path curves back toward the earth, that is, looming). The intermediate variable  $x = r \cos \theta$ , is also well defined for all paths. In practice, the numerical integration of Eq. (21) is driven in steps of  $r$ , from  $r$  to  $r + \Delta r$ . The corresponding increment in  $x$  is calculated from Eq. (17). The integration of  $s$  from Eq. (21) is then straightforward.

#### 2.1.4 Numerical Algorithm

The numerical algorithm used to evaluate Eq. (6) is as follows:

1. Find the minimum and maximum altitude HMIN and HMAX along the path and the zenith angle  $\theta$  at HMIN. If the path goes through a tangent point, then solve Eq. (10) iteratively for the tangent height.
2. From the given atmospheric profile, construct a new profile at the layer boundaries from HMIN to HMAX, interpolating the pressure, temperature, and densities where necessary.
3. Starting with the lowest layer, trace the path through each layer: a. Divide the layer into sub-layers defined by the altitudes  $z_j$ , such that  $\Delta z_j = \tilde{\Delta s} \cos \theta_{j-1}$  where  $\tilde{\Delta s}$  is a nominal path length (5 km) and  $\theta_{j-1}$  is the zenith angle at  $z_{j-1}$ .

$$\Delta z_j = \tilde{\Delta s} \cos \theta_{j-1}$$

$$z_j = z_{j-1} + \Delta z_j$$

$$r_j = r_e + z_j \quad (r_e \text{ is radius of the earth})$$

$$n_j = 1 + N(z_j)$$

$$\sin \theta_j = \frac{C}{n_j r_j}$$

$$\cos \theta_j = (1 - \sin^2 \theta_j)^{1/2}$$

$$x_j = r_j \cos \theta_j$$

$$\Delta x_j = x_j - x_{j-1}$$

$$R_j = \frac{-r_j}{\left[ (dN/dr)_j / n_j \right]}$$

$$ds/dx|_j = (1 - R_j \sin^2 \theta_j)^{-1}$$

$$\Delta s_j = 1/2 (ds/dx|_{j-1} + ds/dx|_j) \Delta x_j$$

b. For each species, integrate the density  $\rho$ :

$$\rho_j = \rho(z_j)$$

$$\bar{\rho}_j = H_\rho (\rho_j - \rho_{j+1}) / \Delta z_j$$

$$u = \sum_{j=1}^{N-1} \bar{\rho}_j \Delta s_j$$

### 2.1.5 Airmass Calculations

This section will present plots of airmass values for three classes of slant paths. The term "airmass values" refers to the integrated amount of air along a path compared to the amount for a vertical path from ground to space. For example, the airmass value for

a path from the ground to space with the zenith angle at the ground of  $90^\circ$  is 38.1 for the U. S. Standard Atmosphere (one air mass equals  $2.15 \times 10^{25}$  molecules  $\text{cm}^{-2}$  or  $1.034 \times 10^3$  gm  $\text{cm}^{-2}$ ). These three paths are described by the initial altitude "H1" and the zenith angle "ANGLE" at H1. The other end of the path is the top of the atmosphere, here taken to be 100 km. The three classes of paths are: 1) H1 = 0 km for ANGLE varying from  $0$  to  $90^\circ$ ; 2) ANGLE =  $90^\circ$  for H1 varying from 0 to 50 km; 3) H1 = 30 km for ANGLE varying from  $85^\circ$  to  $95.1^\circ$  at which point the path intersects the earth. The wavenumber for these calculations was  $2000 \text{ cm}^{-1}$  ( $5 \mu\text{m}$ ). The dependence of air mass on wavenumber in the infrared is small.

In addition to the airmass value, the amounts of water vapor and of ozone relative to the amounts for a vertical path from ground to space are also shown. The relative amounts of these gases depend upon their vertical distribution; in these cases, the U. S. Standard Atmosphere density profiles are used. Since the distributions of these gases in the atmosphere are so variable, the relative amounts for other profiles could be significantly different. The values for water vapor and ozone shown here should be taken to be illustrative only.

Figure 2 (a and b) shows the airmass value, relative water vapor, and ozone amounts for path 1. Also shown in Figure 2(b) is the secant of the zenith angle. For a large zenith angle, the relative amount of water vapor is greater than the airmass value while the amount of ozone is less. This effect is due to the fact that for large zenith angles, the greater part of the path is near the ground. Water vapor is concentrated in the lower layers, so the relative amount of water vapor is large compared to the vertical path. Ozone, however, is concentrated in the stratosphere, which contains a relatively small part of the path. Note that the secant agrees to better than one percent with the airmass value up to  $72^\circ$ , up to  $80^\circ$  for water vapor, but only up to  $60^\circ$  for ozone. The discrepancy is due mainly to the effect of the earth's curvature and not refraction; by including curvature but neglecting refraction, the relative amounts can be calculated to better than one percent up to  $84^\circ$  for air,  $86^\circ$  for water vapor, and  $82^\circ$  for ozone.

Figure 3 shows the airmass values and relative amounts for path 2. These curves mimic the density profiles of air, water vapor, and ozone respectively, since the bulk of the gas is located within a few kilometers (vertically) of the observer altitude.

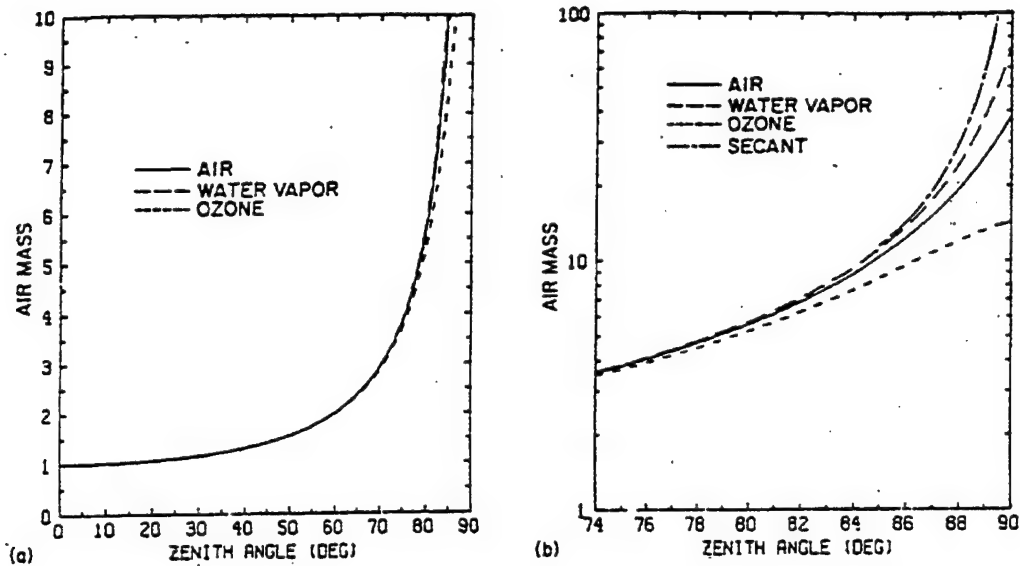


Figure 2. Relative Absorber Amounts vs Zenith Angle for Path 1. (a) 0 to 90° and (b) 74 to 90° (also shown is the secant of the zenith angle )

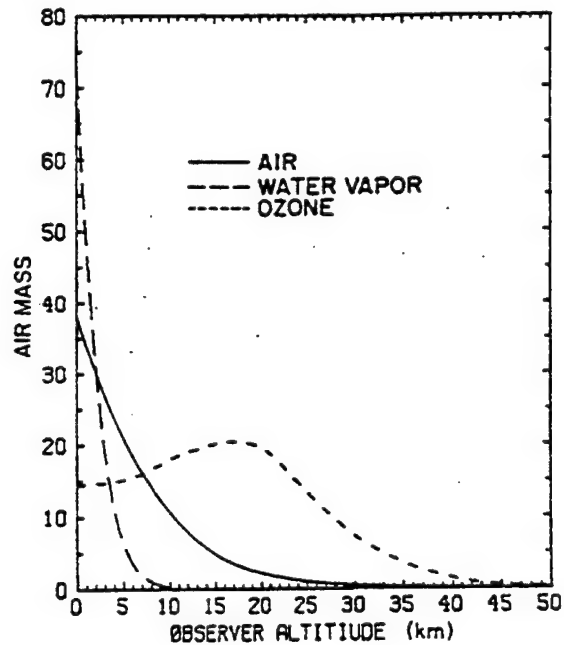


Figure 3 Relative Absorber Amounts vs Observer altitude (H1) for Path 2

The relative amounts shown in Figure 4 correspond to path 3, which is typical of a stratospheric balloon-borne experiment looking at the setting sun. Also shown on the

right-hand axis is the tangent height vs zenith angle and the angular diameter of the sun. If the sun is used as the source for a measurement, the airmass value to different points on the face of the sun can vary by a factor of 2 for large zenith angles. The variation in air mass due to this effect can be a major source of uncertainty in the measurement and must be considered carefully.

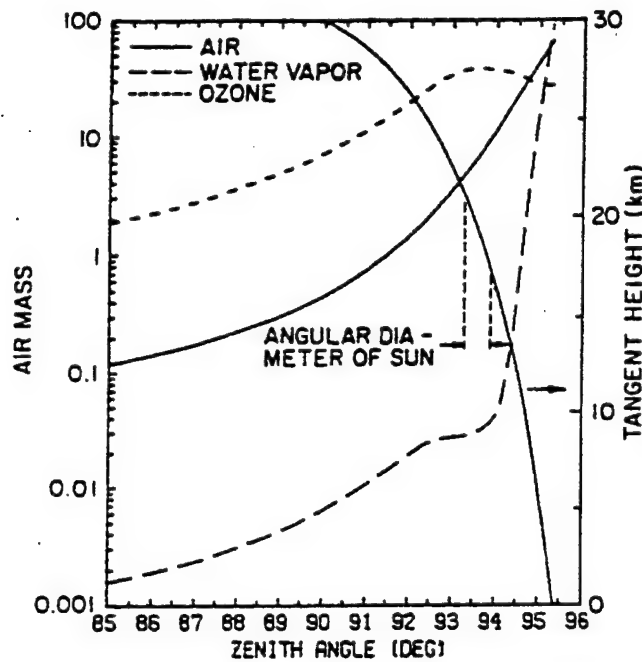


Figure 4. Relative Absorber Amounts vs Zenith Angle for Path 3. Also shown against the right-hand axis is the tangent height vs zenith angle and the angular diameter of the sun

Two other quantities of interest for atmospheric profiles are the tangent height and the refractive bending. The difference in tangent height between an un-refracted and a refracted ray coming in from space is shown as a function of the refracted tangent height in Figure 5 for three atmospheric profiles (the geometry is shown schematically in the inset). The total refractive bending for paths 1 and 2 are shown in Figures 6 and 7 for three atmospheric profiles. Note that the total bending for a path from the ground to space at  $90^\circ$  for the U.S. Standard Atmosphere and the Tropical Atmosphere is about  $0.5^\circ$ , which is the same as the solar diameter.



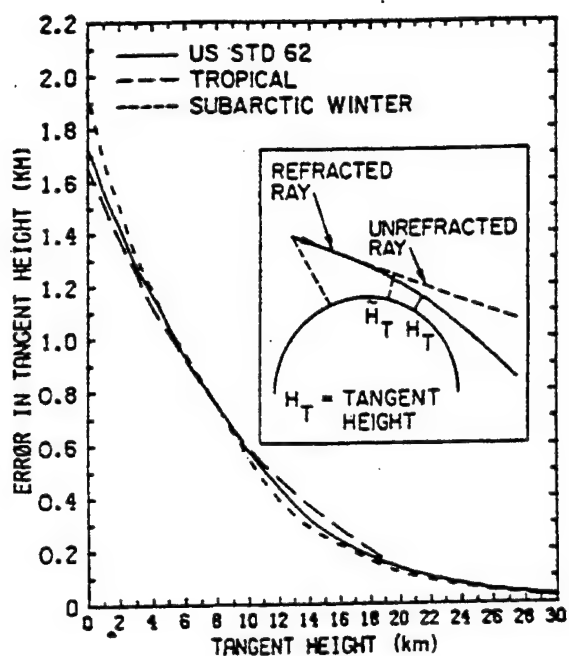


Figure 5. Un-refracted Tangent Height Minus Refracted Tangent Height vs Refracted Tangent Height for a Ray Coming in from Space for Three Atmospheric Profiles. The figure in the inset illustrates the paths

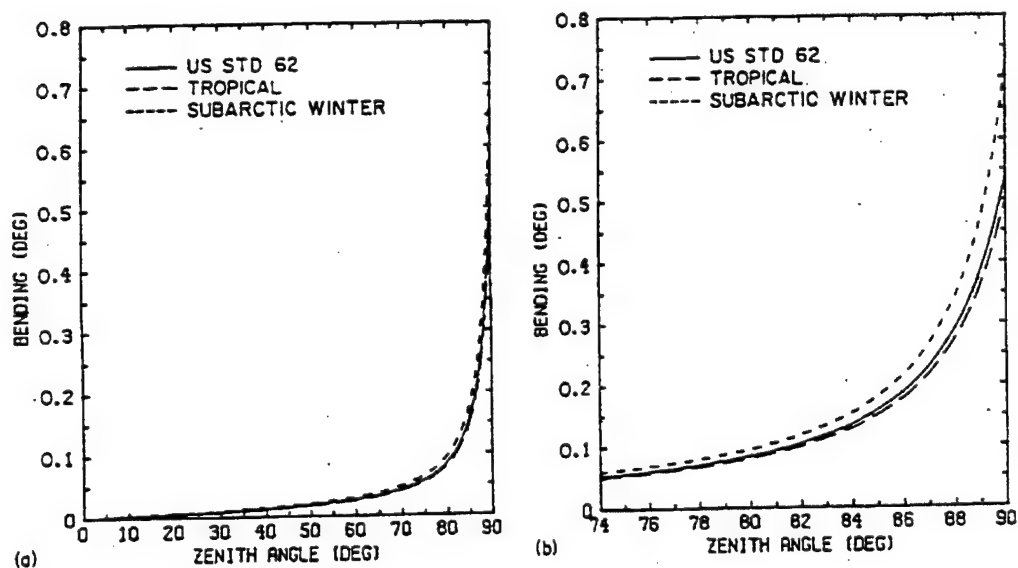


Figure 6. Refractive Bending vs Zenith Angle for Path 1, for Three Atmospheric Profiles. (a) 0 to 90° and (b) 74 to 90°

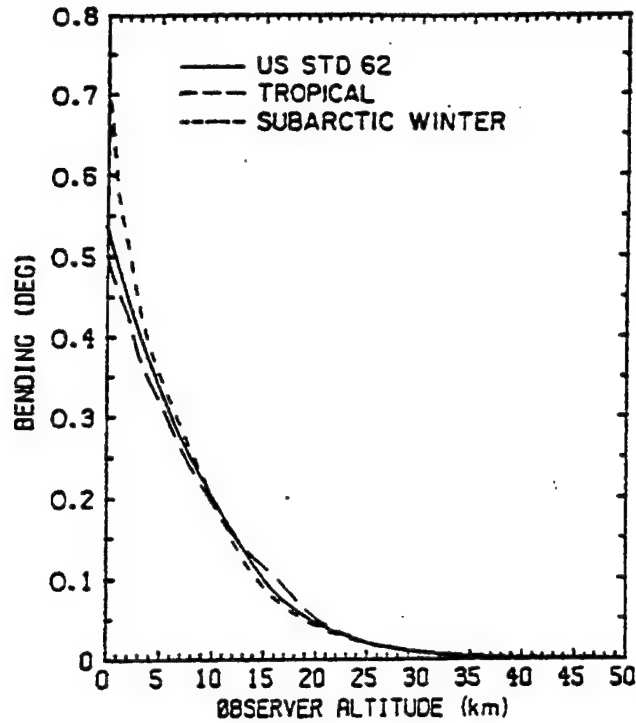


Figure 7. Refractive Bending vs Observer Altitude (H1) for Three Atmospheric Profiles

### 2.1.6 Index of Refraction

The equation for the index of refraction  $n$  is taken from Edlen<sup>45</sup> and is given by :

$$(n-1) \times 10^6 = \left[ a_0 + \frac{a_1}{1 - (\nu/b_1)^2} + \frac{a_2}{1 - (\nu/b_2)^2} \right] \cdot \frac{(P - P_w)}{P_0} \cdot \frac{296.15}{T} + \left[ c_0 - (\nu/c_1)^2 \right] \frac{P_w}{P_0} ,$$

where  $\nu$  is the wavenumber in  $\text{cm}^{-1}$ ,  $P$  is the total pressure in mb,  $P_w$  is the partial pressure of water vapor,  $P_0$  is 1013.25 mb,  $T$  is the temperature in Kelvin, and the constants  $a$ ,  $b$ , and  $c$  are:

$$a_0 = 83.43, \quad a_1 = 185.08, \quad a_2 = 4.11$$

$$b_1 = 1.140 \times 10^5, \quad b_2 = 6.24 \times 10^4$$

$$c_0 = 43.49, \quad c_1 = 1.70 \times 10^4$$

The formula used in previous versions of LOWTRAN was a simplified version of this expression.

### 2.1.7 WATER VAPOR CONTINUUM

An improved water vapor continuum model has been added to the models. This model for the continuum contribution from water vapor absorption was originally developed by Clough et al for use with the line-by-line transmittance and radiance atmospheric code, FASCOD2<sup>40</sup>.

For atmospheric applications it is advantageous to express the density dependence of the water vapor continuum absorption in terms of a self and foreign component. The continuum contribution to the absorption coefficient  $k_C(\nu)$ , is given by the expression:

$$k_C(\nu) = \rho_s \nu \tanh(hc\nu/2kT) \left[ \left( \frac{\rho_s}{\rho_0} \right) \mathcal{C}_s^0(\nu, T) + \left( \frac{\rho_f}{\rho_0} \right) \mathcal{C}_f^0(\nu, T) \right]$$

where  $T$  is the temperature ( $^{\circ}\text{K}$ ),  $\nu$  the wavenumber ( $\text{cm}^{-1}$ ),  $hc/k = 1.43879 \text{ } ^{\circ}\text{K}/\text{cm}^{-1}$ ,  $(\rho_s/\rho_0)$  and  $(\rho_f/\rho_0)$  are the number-density ratios for the self and foreign continuum; and  $\mathcal{C}_s^0$  and  $\mathcal{C}_f^0$  [ $(\text{cm}^{-1} \text{ mol}/\text{cm}^2)^{-1}$ ] are wavenumber-dependent continuum absorption parameters for the self and foreign components. The density  $\rho_s$  is the density of the water vapor and  $\rho_f$  is the density of all other molecular species; therefore,  $\rho_s + \rho_f$  represents the total density. The quantity,  $\rho_0$ , is the reference number density defined at 1013 mb and 296K. The present formulation in terms of density has the advantage that the continuum contribution to the absorption coefficient decreases with increasing temperature through the number-density ratio term. The quantities  $\mathcal{C}_s$  and  $\mathcal{C}_f$  for water vapor are stored in the program for the spectral range 0 to 20,000  $\text{cm}^{-1}$ .

The values for  $\mathcal{C}_s$  for water vapor at 296K are shown in Figure 8 together with the experimental values obtained by Burch et al.<sup>46-49</sup>. The strong temperature dependence of the self density-dependent water vapor continuum is treated by storing values of  $\mathcal{C}_s$  at 260K and 296K and linearly interpolating between the 260K and 296K values. The 260K result was obtained by extrapolating the fits to the 338K and 296K data of Burch et al.<sup>48</sup>. The results for 260K and 296K are shown in Figure 9.

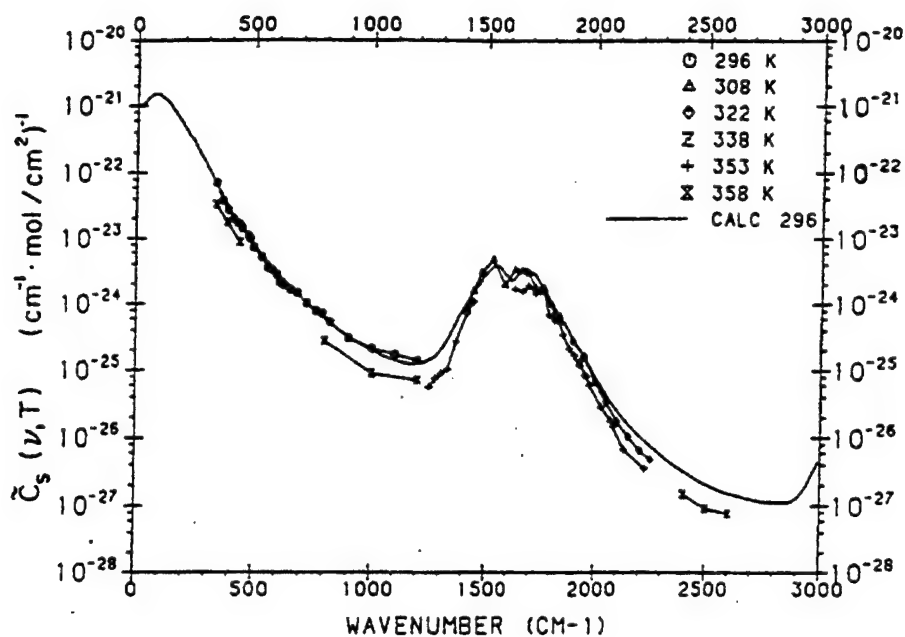


Figure 8. The Self Density-Dependent Continuum Values,  $C_s$ , for Water Vapor as a Function of Wavenumber. The experimental values are from Burch et al<sup>48</sup>

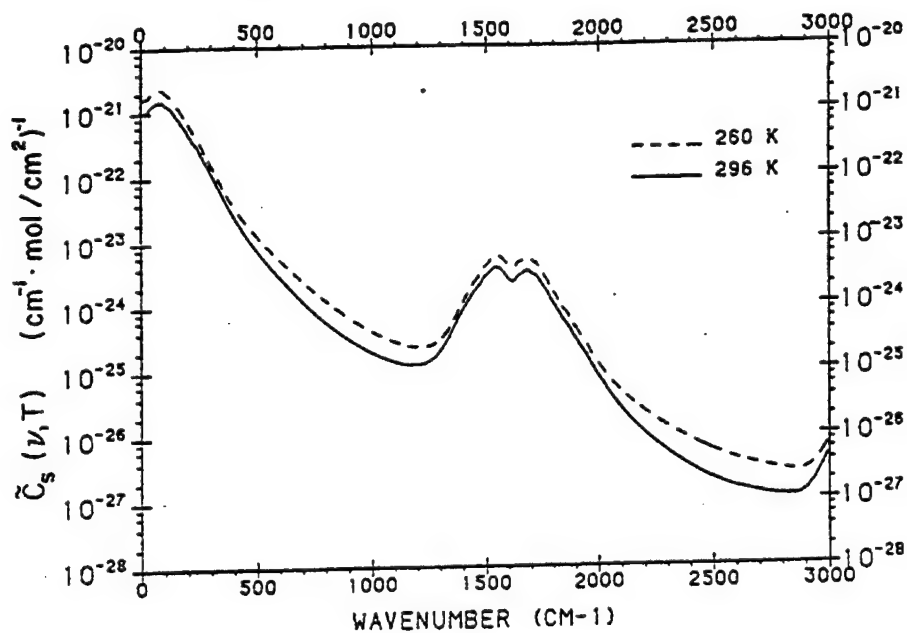


Figure 9. The Self Density-Dependent Continuum Values,  $C_s$ , for Water Vapor as a Fraction of Wavenumber at 260K and 296K. The values from 296K are fits to experimental results<sup>48</sup>; the 260K is extrapolated.

Only values near room temperature are available for the foreign dependence of the water vapor continuum. The continuum values  $\tilde{C}_f$  at 296K are shown in Figure 10 and have been obtained by a fit to the data of Burch<sup>46-49</sup>. There is still considerable uncertainty in the foreign values for the spectral window regions at 1000 and 2500  $\text{cm}^{-1}$ .

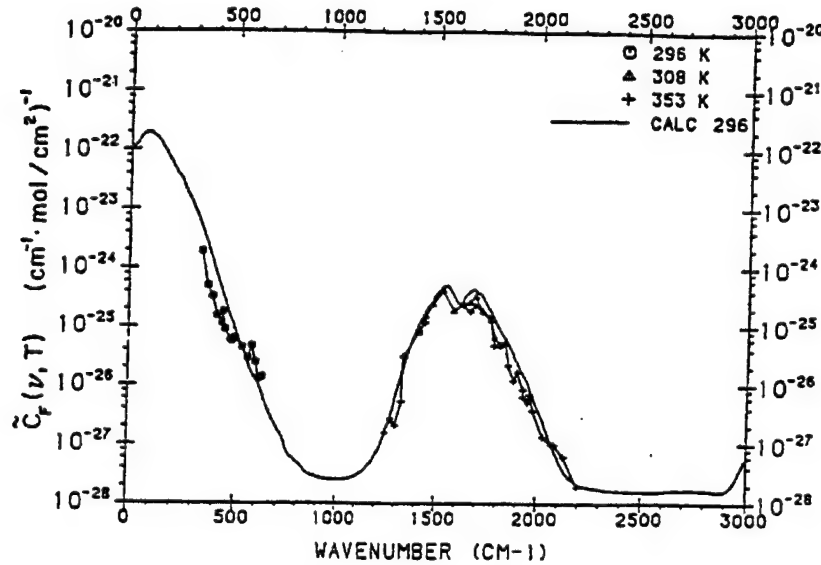


Figure 10. The Foreign Density Dependent Continuum Values,  $\tilde{C}_f$ , for Water Vapor as a Function of Wavenumber. The experimental values are from Burch, et al<sup>48</sup>

In the MODTRAN code, the total optical depth due to water vapor continuum absorption for an atmospheric slant path of N layers is given by:

$$\begin{aligned}
 \sum_{i=1}^N \int k_c(\nu) ds &= C_s(\nu, 296) \sum_{i=1}^N \int \left( \frac{\rho_s}{\rho_0} \right) \rho_s ds + \\
 &[C_s(\nu, 260) - C_s(\nu, 296)] \sum_{i=1}^N \left( \frac{296 - T_i}{296 - 260} \right) \int \left( \frac{\rho_s}{\rho_0} \right) \rho_s ds + \\
 &C_f(\nu, 296) \sum_{i=1}^N \int \left( \frac{\rho_f}{\rho_0} \right) \rho_s ds
 \end{aligned} \tag{23}$$

where  $ds$  is the incremental path length,  $T_i$  is the temperature of the  $i$ 'th layer,

and:

$$\begin{aligned}
 C_s(\nu, 296) &= \nu \tanh(hc\nu/2k(296)) \tilde{C}_s(\nu, 296) \\
 C_s(\nu, 260) &= \nu \tanh(hc\nu/2k(260)) \tilde{C}_s(\nu, 260) \\
 C_f(\nu, 296) &= \nu \tanh(hc\nu/2k(296)) \tilde{C}_f(\nu, 296)
 \end{aligned} \tag{24}$$

Calculations of atmospheric slant path transmittance using these modified water vapor continuum absorption coefficients will result in approximately the same attenuation as in the older LOWTRAN models for the atmospheric window regions from 8 to 12  $\mu\text{m}$  and 3.5 to 4.2  $\mu\text{m}$ . However, for other spectral regions, particularly from 4.5 to 5.0  $\mu\text{m}$ , significant improvement in atmospheric transmittance calculations has been made with the inclusion of the contribution of continuum absorption.

## 2.2 MODEL ATMOSPHERES

The description of the model atmospheres contained in this section is based directly on the AFGL report by Anderson<sup>10</sup> et al.

### 2.2.1. INTRODUCTION

Atmospheric radiance-transmittance spectral modeling requires an adequate description of the local thermal and constituent environment. A data base consisting of realistic vertical profiles for temperature and gas mixing ratios has been designed expressly for incorporation into such models. Its thermal structure is represented by a subset of the 1966 Atmospheric Supplements<sup>11</sup> (tropical (15N), middle latitude (45N) summer and winter, subarctic (60N) summer and winter) and the U.S. Standard Model Atmosphere, 1976<sup>12</sup>. The accompanying volume mixing ratio profiles rely as much as possible on current measurements and/or theoretical predictions.

More extensive literature reviews of atmospheric structure, variability, dynamics and chemistry are available (for example, Smith<sup>50</sup>, WMO<sup>51,52</sup>, and Brasseur and Solomon<sup>53</sup>).

This compilation includes only those gases currently part of the HITRAN 1992 database<sup>20</sup>. The range of tabulated atmospheric values for water vapor ( $\text{H}_2\text{O}$ ), ozone ( $\text{O}_3$ ), nitrous oxide ( $\text{N}_2\text{O}$ ), and methane ( $\text{CH}_4$ ) are primarily inferred from global satellite measurements<sup>54-56</sup>. The carbon monoxide ( $\text{CO}$ ) seasonal profiles, however, rely on the predictions of a photochemical-dynamic model<sup>57</sup>. The remaining individual

gas profiles have been derived from a variety of sources. All have been edited to produce the final tabulations; in most cases this consists of smoothing and interpolation to standard altitude levels. Some species, however, require additional extrapolation because of the unavailability of suitable data (particularly above the stratopause). In general, dayside estimates for diurnally-varying species ( $O_3$ ,  $NO$ , and  $NO_2$ , for example) have been adopted.

### 2.2.2 . ATMOSPHERIC PROFILE DESCRIPTION

The six reference atmospheres, each with associated volume-mixing ratio profiles for  $H_2O$ ,  $O_3$ ,  $N_2O$ ,  $CO$ , and  $CH_4$ , are presented in Table 1. Along with  $CO_2$ , these are the most radiatively active molecules. Sample profiles, appropriate for the U. S. Standard atmospheric conditions (MODEL 6), are shown in Figure 11. Because the mixing ratios of  $CO_2$  and  $O_2$  have been held seasonally invariant, they are listed in Table 2, as part of a set of single profiles numbered according to the HITRAN Database numbering system i.e.  $H_2O$  is 1,  $CO_2$  is 2, etc. The first seven molecules in Table 2 are the same as those in Figure 1 for the U.S. Standard Atmosphere. The 25 additional species, as identified on the HITRAN Database are:  $NO$ ,  $SO_2$ ,  $NO_2$ ,  $NH_3$ ,  $HNO_3$ ,  $OH$ ,  $HF$ ,  $HCl$ ,  $HBr$ ,  $HI$ ,  $ClO$ ,  $OCS$ ,  $H_2CO$ ,  $HOCl$ ,  $N_2$ ,  $HCN$ ,  $CH_3Cl$ ,  $H_2O_2$ ,  $C_2H_2$ ,  $C_2H_6$ ,  $PH_3$ ,  $COF_2$ ,  $SF_6$  and  $H_2S$ . See the Anderson<sup>10</sup> report for graphical representations for all the tabular data of these gases. (Note: although  $N_2$  is the dominant atmospheric gas, it appears as only a trace spectral contributor, whereas Argon is a major component of the atmosphere, but does not contribute to the opacity.)

#### Table 1. Reference Model Atmospheric Profiles

Model = 1 Tropical (15N Annual Average)  
 Model = 2 Mid-Latitude Summer (45N July)  
 Model = 3 Mid-Latitude Winter (45N Jan)  
 Model = 4 Sub-Arctic Summer (60N July)  
 Model = 5 Sub-Arctic Winter (60N Jan)  
 Model = 6 U. S. Standard (1976)

This tabular presentation includes: Altitude (km), Pressure (mb), Density ( $cm^{-3}$ ), and mixing ratios (ppmv) for  $H_2O$ ,  $O_3$ ,  $N_2O$ ,  $CO$ , and  $CH_4$ . Profiles for  $CO_2$  and  $O_2$  can be found in Table 2.

[(\*) indicates subsequent extrapolation adopted for that species]

#### Table Ia. Reference Atmospheric Model Profiles, Model 1. Tropical

MODEL = 1 TROPICAL

ALT	PRES	TEMP	DENSITY	$H_2O$	$O_3$	$N_2O$	$CO$	$CH_4$
-----	------	------	---------	--------	-------	--------	------	--------

## MODTRAN Report

## Appendix C

(KM)	(MB)	(K)	(CM <sup>-3</sup> )	(PPMV)	(PPMV)	(PPMV)	(PPMV)	(PPMV)
0.00	1.013E+03	299.7	2.450E+19	2.59E+04	2.87E-02	3.20E-01	1.50E-01	1.70E+00
1.00	9.040E+02	293.7	2.231E+19	1.95E+04	3.15E-02	3.20E-01	1.45E-01	1.70E+00
2.00	8.050E+02	287.7	2.028E+19	1.53E+04	3.34E-02	3.20E-01	1.40E-01	1.70E+00
3.00	7.150E+02	283.7	1.827E+19	8.60E+03	3.50E-02	3.20E-01	1.35E-01	1.70E+00
4.00	6.330E+02	277.0	1.656E+19	4.44E+03	3.56E-02	3.20E-01	1.31E-01	1.70E+00
5.00	5.590E+02	270.3	1.499E+19	3.35E+03	3.77E-02	3.20E-01	1.30E-01	1.70E+00
6.00	4.920E+02	263.6	1.353E+19	2.10E+03	3.99E-02	3.20E-01	1.29E-01	1.70E+00
7.00	4.320E+02	257.0	1.218E+19	1.29E+03	4.22E-02	3.20E-01	1.25E-01	1.70E+00
8.00	3.780E+02	250.3	1.095E+19	7.64E+02	4.47E-02	3.20E-01	1.19E-01	1.70E+00
9.00	3.290E+02	243.6	9.789E+18	4.10E+02	5.00E-02	3.20E-01	1.09E-01	1.69E+00
10.00	2.860E+02	237.0	8.747E+18	1.91E+02	5.60E-02	3.18E-01	9.96E-02	1.69E+00
11.00	2.470E+02	230.1	7.780E+18	7.31E+01	6.61E-02	3.14E-01	9.96E-02	1.68E+00
12.00	2.130E+02	223.6	6.904E+18	2.91E+01	7.82E-02	3.10E-01	7.81E-02	1.66E+00
13.00	1.820E+02	217.0	6.079E+18	9.90E+00	9.29E-02	3.05E-01	6.37E-02	1.65E+00
14.00	1.560E+02	210.3	5.377E+18	6.22E+00	1.05E-01	3.00E-01	5.03E-02	1.63E+00
15.00	1.320E+02	203.7	4.697E+18	4.00E+00	1.26E-01	2.94E-01	3.94E-02	1.61E+00
16.00	1.110E+02	197.0	4.084E+18	3.00E+00	1.44E-01	2.88E-01	3.07E-02	1.58E+00
17.00	9.370E+01	194.8	3.486E+18	2.90E+00	2.50E-01	2.78E-01	2.49E-02	1.55E+00
18.00	7.890E+01	198.8	2.877E+18	2.75E+00	5.00E-01	2.67E-01	1.97E-02	1.52E+00
19.00	6.660E 01	202.7	2.381E+18	2.60E+00	9.50E-01	2.53E-01	1.55E-02	1.48E+00
20.00	6.650E+01	206.7	1.981E+18	2.60E+00	1.40E+00	2.37E-01	1.33E-02	1.42E+00
21.00	4.800E+01	210.7	1.651E+18	2.65E+00	1.80E+00	2.19E-01	1.23E-02	1.36E+00
22.00	4.090E+01	214.6	1.381E+18	2.80E+00	2.40E+00	2.05E-01	1.23E-02	1.27E+00
23.00	3.500E+01	217.0	1.169E+18	2.90E+00	3.40E+00	1.97E-01	1.31E-02	1.19E+00
24.00	3.000E+01	219.2	9.920E 17	3.20E+00	4.30E+00	1.88E-01	1.40E-02	1.12E+00
25.00	2.570E+01	221.4	8.413E+17	3.25E+00	5.40E+00	1.76E-01	1.52E-02	1.06E+00
27.50	1.763E+01	227.0	5.629E+17	3.60E+00	7.80E+00	1.59E-01	1.72E-02	9.87E-01
30.00	1.220E+01	232.3	3.807E+17	4.00E+00	9.30E+00	1.42E-01	2.00E-02	9.14E-01
32.50	8.520E+00	237.7	2.598E+17	4.30E+00	9.85E+00	1.17E-01	2.27E-02	8.30E-01
35.00	6.000E+00	243.1	1.789E+17	4.60E+00	9.70E+00	9.28E-02	2.49E-02	7.46E-01
37.50	4.260E+00	248.5	1.243E+17	4.90E+00	8.80E+00	6.69E-02	2.74E-02	6.62E-01
40.00	3.050E+00	254.0	8.703E+16	5.20E+00	7.50E+00	4.51E-02	3.10E-02	5.64E-01
42.50	2.200E+00	259.4	6.147E+16	5.50E+00	5.90E+00	2.75E-02	3.51E-02	4.61E-01
45.00	1.590E+00	264.8	4.352E+16	5.70E+00	4.50E+00	1.59E-02	3.99E-02	3.63E-01
47.50	1.160E+00	269.6	3.119E+16	5.90E+00	3.45E+00	9.38E-03	4.48E-02	2.77E-01
50.00	8.540E-01	270.2	2.291E+16	6.00E+00	2.80E+00	4.75E-03*	5.09E-02	2.10E-01
55.00	4.560E-01	263.4	1.255E+16	6.00E+00	1.80E+00	3.00E-03	5.99E-02	1.65E-01
60.00	2.390E-01	253.1	6.844E+15	6.00E+00	1.10E+00	2.07E-03	6.96E-02	1.50E-01
65.00	1.210E-01	236.0	3.716E+15	5.40E+00	6.50E-01	1.51E-03	9.19E-02	1.50E-01
70.00	5.800E-02	218.9	1.920E+15	4.50E+00	3.00E-01	1.15E-03	1.94E-01	1.50E-01
75.00	2.600E-02	201.8	9.338E+14	3.30E+00	1.80E-01	8.89E-04	5.69E-01	1.50E-01
80.00	1.100E-02	184.8	4.314E+14	2.10E+00	3.30E-01	7.06E-04	1.55E+00	1.50E-01
85.00	4.400E-03	177.1	1.801E+14	1.30E+00	5.00E-01	5.72E-04	3.85E+01	1.50E-01
90.00	1.720E-03	177.0	7.043E+13	8.50E-01	5.20E-01	4.71E-04	6.59E+00	1.40E-01
95.00	6.880E-04	184.3	2.706E+13	5.40E-01	5.00E-01	3.93E-04	1.04E+01	1.30E-01
100.0	2.890E-04	190.7	1.098E+13	4.00E-01	4.00E-01	3.32E-04	1.71E+01	1.20E-01
105.0	1.300E-04	212.0	4.445E+12	3.40E-01	2.00E-01	2.84E-04	2.47E+01	1.10E-01
110.0	6.470E-05	241.6	1.941E+12	1.80E-01	5.00E-02	2.44E-04	3.36E+01	9.50E-02
115.0	3.600E-05	299.7	8.706E+11	2.40E-01	5.00E-03	2.12E-04	4.15E+01	6.00E-02
120.0	2.250E-05	380.0	4.225E+11	2.00E-01	5.00E-04	1.85E-04	5.00E+01	3.00E-02



Table Ib. Reference Atmospheric Model Profiles, Model 2. Midlatitude Summer

MODEL = 2 MIDLATITUDE SUMMER

ALT	PRES	TEMP	DENSITY	H <sub>2</sub> O	O <sub>3</sub>	N <sub>2</sub> O	CO	CH <sub>4</sub>
(KM)	(MB)	(K)	(CM <sup>-3</sup> )	(PPMV)	(PPMV)	(PPMV)	(PPMV)	(PPMV)
0.00	1.013E+03	294.2	2.496E+19	1.88E+04	3.02E-02	3.20E-01	1.50E-01	1.70E+00
1.00	9.020E+02	289.7	2.257E+19	1.38E+04	3.34E-02	3.20E-01	1.45E-01	1.70E+00
2.00	8.020E+02	285.2	2.038E+19	9.68E+03	3.69E-02	3.20E-01	1.40E-01	1.70E+00
3.00	7.100E+02	279.2	1.843E+19	5.98E+03	4.22E-02	3.20E-01	1.35E-01	1.70E+00
4.00	6.280E+02	273.2	1.666E+19	3.81E+03	4.82E-02	3.20E-01	1.31E-01	1.70E+00
5.00	5.540E+02	267.2	1.503E+19	2.23E+03	5.51E-02	3.20E-01	1.30E-01	1.69E+00
6.00	4.870E+02	261.2	1.351E+19	1.51E+03	6.41E-02	3.20E-01	1.29E-01	1.67E+00
7.00	4.260E+02	254.7	1.212E+19	1.02E+03	7.76E-02	3.20E-01	1.25E-01	1.65E+00
8.00	3.720E+02	248.2	1.086E+19	6.46E+02	9.13E-02	3.20E-01	1.19E-01	1.63E+00
9.00	3.240E+02	241.7	9.716E+18	4.13E+02	1.11E-01	3.16E-01	1.09E-01	1.62E+00
10.00	2.810E+02	235.3	8.656E+18	2.47E+02	1.30E-01	3.10E-01	9.96E-02	1.58E+00
11.00	2.430E+02	228.8	7.698E+18	9.56E+01	1.79E-01	2.99E-01	8.96E-02	1.54E+00
12.00	2.090E+02	222.3	6.814E+18	2.94E+01	2.23E-01	2.94E-01	7.81E-02	1.51E+00
13.00	1.790E+02	215.8	6.012E+18	8.00E+00	3.00E-01	2.86E-01	6.37E-02	1.48E+00
14.00	1.530E+02	215.7	5.141E+18	5.00E+00	4.40E-01	2.80E-01	5.03E-02	1.45E+00
15.00	1.300E+02	215.7	4.368E+18	3.40E+00	5.00E-01	2.72E-01	3.94E-02	1.42E+00
16.00	1.110E+02	215.7	3.730E+18	3.30E+00	6.00E-01	2.61E-01	3.07E-02	1.39E+00
17.00	9.500E+01	215.7	3.192E+18	3.20E+00	7.00E-01	2.42E-01	2.49E-02	1.36E+00
18.00	8.120E+01	216.8	2.715E+18	3.15E+00	1.00E+00	2.17E-01	1.97E-02	1.32E+00
19.00	6.950E+01	217.9	2.312E+18	3.20E+00	1.50E+00	1.84E-01	1.55E-02	1.28E+00
20.00	5.950E+01	219.2	1.967E+18	3.30E+00	2.00E+00	1.61E-01	1.33E-02	1.22E+00
21.00	5.100E+01	220.4	1.677E+18	3.45E+00	2.40E+00	1.32E-01	1.23E-02	1.15E+00
22.00	4.370E+01	221.6	1.429E+18	3.60E+00	2.90E+00	1.15E-01	1.23E-02	1.07E+00
23.00	3.760E+01	222.8	1.223E+18	3.85E+00	3.40E+00	1.04E-01	1.31E-02	9.73E-01
24.00	3.220E+01	223.9	1.042E+18	4.00E+00	4.00E+00	9.62E-02	1.40E-02	8.80E-01
25.00	2.770E+01	225.1	8.919E+17	4.20E+00	4.30E+00	8.96E-02	1.52E-02	7.89E-01
27.50	1.907E+01	228.5	6.050E+17	4.45E+00	6.00E+00	8.01E-02	1.72E-02	7.05E-01
30.00	1.320E+01	233.7	4.094E+17	4.70E+00	7.00E+00	6.70E-02	2.00E-02	6.32E-01
32.50	9.300E+00	239.0	2.820E+17	4.85E+00	8.10E+00	4.96E-02	2.27E-02	5.59E-01
35.00	6.520E+00	245.2	1.927E+17	4.95E+00	8.90E+00	3.70E-02	2.49E-02	5.01E-01
37.50	4.640E+00	251.3	1.338E+17	5.00E+00	8.70E+00	2.52E-02	2.72E-02	4.45E-01
40.00	3.330E+00	257.5	9.373E+16	5.10E+00	7.55E+00	1.74E-02	2.96E-02	3.92E-01
42.50	2.410E+00	263.7	6.624E+16	5.30E+00	5.90E+00	1.16E-02	3.14E-02	3.39E-01
45.00	1.760E+00	269.9	4.726E+16	5.45E+00	4.50E+00	7.67E-03	3.31E-02	2.87E-01
47.50	1.290E+00	275.2	3.398E+16	5.50E+00	3.50E+00	5.32E-03	3.49E-02	2.38E-01
50.00	9.510E-01	275.7	2.500E+16	5.50E+00	2.80E+00	3.22E-03	3.65E-02	1.94E-01
55.00	5.150E-01	269.3	1.386E+16	5.35E+00	1.80E+00	2.03E-03	3.92E-02	1.57E-01
60.00	2.720E-01	257.1	7.668E+15	5.00E+00	1.30E+00	1.40E-03	4.67E-02	1.50E-01
65.00	1.390E-01	240.1	4.196E+15	4.40E+00	8.00E-01	1.02E-03	6.40E-02	1.50E-01
70.00	6.700E-02	218.1	2.227E+15	3.70E+00	4.00E-01	7.77E-04	1.18E-01	1.50E-01
75.00	3.000E-02	196.1	1.109E+15	2.95E+00	1.90E-01	6.26E-04	2.94E-01	1.50E-01
80.00	1.200E-02	174.1	4.996E+14	2.10E+00	2.00E-01	5.17E-04	6.82E-01	1.50E-01
85.00	4.480E-03	165.1	1.967E+14	1.33E+00	5.70E-01	4.35E-04	1.47E+00	1.50E-01
90.00	1.640E-03	165.0	7.204E+13	8.50E-01	7.50E-01	3.73E-04	2.85E+00	1.40E-01
95.00	6.250E-04	178.3	2.541E+13	5.40E-01	7.00E-01	3.24E-04	5.17E+00	1.30E-01
100.0	2.580E-04	190.5	9.816E+12	4.00E-01	4.00E-01	2.84E-04	1.01E+01	1.20E-01
105.0	1.170E-04	222.2	3.816E+12	3.40E-01	2.00E-01	2.52E-04	1.87E+01	1.10E-01
110.0	6.110E-05	262.4	1.688E+12	2.80E-01	5.00E-02	2.26E-04	2.86E+01	9.50E-02
115.0	3.560E-05	316.8	8.145E+11	2.40E-01	5.00E-03	2.04E-04	3.89E+01	6.00E-02
120.0	2.270E-05	380.0	4.330E+11	2.00E-01	5.00E-04	1.85E-04	5.00E+01	3.00E-02

Table 1c. Reference Atmospheric Model Profiles, Model 3. Midlatitude Winter

MODEL = 3 MIDLATITUDE WINTER

ALT	PRES	TEMP	DENSITY	H <sub>2</sub> O	O <sub>3</sub>	N <sub>2</sub> O	CO	CH <sub>4</sub>
(KM)	(MB)	(K)	(CM <sup>-3</sup> )	(PPMV)	(PPMV)	(PPMV)	(PPMV)	(PPMV)
0.00	1.018E+03	272.2	2.711E+19	4.32E+03	2.78E-02	3.20E-01	1.50E-01	1.70E+00
1.00	8.973E+02	268.7	2.420E+19	3.45E+03	2.80E-02	3.20E-01	1.45E-01	1.70E+00
2.00	7.897E+02	265.2	2.158E+19	2.79E+03	2.85E-02	3.20E-01	1.40E-01	1.70E+00
3.00	6.938E+02	261.7	1.922E+19	2.09E+03	3.20E-02	3.20E-01	1.35E-01	1.70E+00
4.00	6.081E+02	255.7	1.724E+19	1.28E+03	3.57E-02	3.20E-01	1.31E-01	1.70E+00
5.00	5.313E+02	249.7	1.542E+19	8.24E+02	4.72E-02	3.20E-01	1.30E-01	1.69E+00
6.00	4.627E+02	243.7	1.376E+19	5.10E+02	5.84E-02	3.20E-01	1.29E-01	1.67E+00
7.00	4.016E+02	237.7	1.225E+19	2.32E+02	7.89E-02	3.20E-01	1.25E-01	1.65E+00
8.00	3.473E+02	231.7	1.086E+19	1.08E+02	1.04E-01	3.20E-01	1.19E-01	1.63E+00
9.00	2.993E+02	225.7	9.612E+18	5.57E+01	1.57E-01	3.16E-01	1.09E-01	1.62E+00
10.00	2.568E+02	219.7	8.472E+18	2.96E+01	2.37E-01	3.10E-01	9.96E-02	1.58E+00
11.00	2.199E+02	219.2	7.271E+18	1.00E+01	3.62E-01	2.99E-01	8.96E-02	1.54E+00
12.00	1.882E+02	218.7	6.237E+18	6.00E+00	5.23E-01	2.94E-01	7.81E-02	1.51E+00
13.00	1.611E+02	218.2	5.351E+18	5.00E+00	7.04E-01	2.86E-01	6.37E-02	1.48E+00
14.00	1.378E+02	217.7	4.588E+18	4.80E+00	8.00E-01	2.80E-01	5.03E-02	1.45E+00
15.00	1.178E+02	217.2	3.931E+18	4.70E+00	9.00E-01	2.72E-01	3.94E-02	1.42E+00
16.00	1.007E+02	216.7	3.368E+18	4.60E+00	1.10E+00	2.61E-01	3.07E-02	1.39E+00
17.00	8.610E+01	216.2	2.886E+18	4.50E+00	1.40E+00	2.42E-01	2.42E-02	1.36E+00
18.00	7.360E+01	215.7	2.473E+18	4.50E+00	1.80E+00	2.17E-01	1.97E-02	1.32E+00
19.00	6.280E+01	215.2	2.115E+18	4.50E+00	2.30E+00	1.84E-01	1.55E-02	1.28E+00
20.00	5.370E+01	215.2	1.809E+18	4.50E+00	2.90E+00	1.62E-01	1.33E-02	1.22E+00
21.00	4.580E+01	215.2	1.543E+18	4.50E+00	3.50E+00	1.36E-01	1.23E-02	1.15E+00
22.00	3.910E+01	215.2	1.317E+18	4.53E+00	3.90E+00	1.23E-01	1.23E-02	1.07E+00
23.00	3.340E+01	215.2	1.125E+18	4.55E+00	4.30E+00	1.12E-01	1.31E-02	9.73E-01
24.00	2.860E+01	215.2	9.633E+17	4.60E+00	4.70E+00	1.05E-01	1.40E-02	8.80E-01
25.00	2.440E+01	215.2	8.218E+17	4.65E+00	5.10E+00	9.66E-02	1.50E-02	7.93E-01
27.50	1.646E+01	215.5	5.536E+17	4.70E+00	5.60E+00	8.69E-02	1.60E-02	7.13E-01
30.00	1.110E+01	217.4	3.701E+17	4.75E+00	6.10E+00	7.52E-02	1.71E-02	6.44E-01
32.50	7.560E+00	220.4	2.486E+17	4.80E+00	6.80E+00	6.13E-02	1.85E-02	5.75E-01
35.00	5.180E+00	227.9	1.647E+17	4.85E+00	7.10E+00	5.12E-02	2.00E-02	5.05E-01
37.50	3.600E+00	235.5	1.108E+17	4.90E+00	7.20E+00	3.97E-02	2.15E-02	4.48E-01
40.00	2.530E+00	243.2	7.540E+16	4.95E+00	6.90E+00	3.00E-02	2.33E-02	3.93E-01
42.50	1.800E+00	250.8	5.202E+16	5.00E+00	5.90E+00	2.08E-02	2.62E-02	3.40E-01
45.00	1.290E+00	258.5	3.617E+16	5.00E+00	4.60E+00	1.31E-02	3.06E-02	2.88E-01
47.50	9.400E-01	265.1	2.570E+16	5.00E+00	3.70E+00	8.07E-03	3.80E-02	2.39E-01
50.00	6.830E-01	265.7	1.863E+16	4.95E+00	2.75E+00	4.16E-03*	6.25E-02	1.94E-01
55.00	3.620E-01	260.6	1.007E+16	4.85E+00	1.70E+00	2.63E-03	1.48E-01	1.57E-01
60.00	1.880E-01	250.8	5.433E+15	4.50E+00	1.00E+00	1.81E-03	2.93E-01	1.50E-01
65.00	9.500E-02	240.9	2.858E+15	4.00E+00	5.50E-01	1.32E-03	5.59E-01	1.50E-01
70.00	4.700E-02	230.7	1.477E+15	3.30E+00	3.20E-01	1.01E-03	1.08E+00	1.50E-01
75.00	2.220E-02	220.4	7.301E+14	2.70E+00	2.50E-01	7.88E-04	1.90E+00	1.50E-01
80.00	1.030E-02	210.1	3.553E+14	2.00E+00	2.30E-01	6.33E-04	2.96E+00	1.50E-01
85.00	4.560E-03	199.8	1.654E+14	1.33E+00	5.50E-01	5.19E-04	4.53E+00	1.50E-01
90.00	1.980E-03	199.5	7.194E+13	8.50E-01	8.00E-01	4.33E-04	6.86E+00	1.40E-01
95.00	8.770E-04	208.3	3.052E+13	5.40E-01	8.00E-01	3.67E-04	1.05E+01	1.30E-01
100.0	4.074E-04	218.6	1.351E+13	4.00E-01	4.00E-01	3.14E-04	1.71E+01	1.20E-01
105.0	2.000E-04	237.1	6.114E+12	3.40E-01	2.00E-01	2.72E-04	2.47E+01	1.10E-01
110.0	1.057E-04	259.5	2.952E+12	2.80E-01	5.00E-02	2.37E-04	3.36E+01	9.50E-02
115.0	5.980E-05	293.0	1.479E+12	2.40E-01	5.00E-03	2.09E-04	4.15E+01	6.00E-02
120.0	3.600E-05	333.0	7.836E+11	2.00E-01	5.00E-04	1.85E-04	5.00E+01	3.00E-02

Table 1d. Reference Atmospheric Model Profiles, Model 4. Subarctic Summer

MODEL = 4 SUBARCTIC SUMMER

ALT	PRES	TEMP	DENSITY	H <sub>2</sub> O	O <sub>3</sub>	N <sub>2</sub> O	CO	CH <sub>4</sub>
(KM)	(MB)	(K)	(CM <sup>-3</sup> )	(PPMV)	(PPMV)	(PPMV)	(PPMV)	(PPMV)
0.00	1.010E+03	287.2	2.549E+19	1.19E+04	2.41E-02	3.10E-01	1.50E-01	1.70E+00
1.00	8.960E+02	281.7	2.305E+19	8.70E+03	2.94E-02	3.10E-01	1.45E-01	1.70E+00
2.00	7.929E+02	276.3	2.080E+19	6.75E+03	3.38E-02	3.10E-01	1.40E-01	1.70E+00
3.00	7.000E+02	270.9	1.873E+19	4.82E+03	3.89E-02	3.10E-01	1.35E-01	1.70E+00
4.00	6.160E+02	265.5	1.682E+19	3.38E+03	4.48E-02	3.08E-01	1.31E-01	1.70E+00
5.00	5.410E+02	260.1	1.508E+19	2.22E+03	5.33E-02	3.02E-01	1.30E-01	1.69E+00
6.00	4.740E+02	253.1	1.357E+19	1.33E+03	6.56E-02	2.91E-01	1.29E-01	1.67E+00
7.00	4.130E+02	246.1	1.216E+19	7.97E+02	7.74E-02	2.82E-01	1.25E-01	1.65E+00
8.00	3.590E+02	239.2	1.088E+19	4.00E+02	9.11E-02	2.76E-01	1.19E-01	1.63E+00
9.00	3.108E+02	232.2	9.701E+18	1.30E+02	1.42E-01	2.70E-01	1.09E-01	1.62E+00
10.00	2.677E+02	225.2	8.616E+18	4.24E+01	1.89E-01	2.65E-01	9.96E-02	1.58E+00
11.00	2.300E+02	225.2	7.402E+18	1.33E+01	3.05E-01	2.60E-01	8.96E-02	1.54E+00
12.00	1.977E+02	225.2	6.363E+18	6.00E+00	4.10E-01	2.55E-01	7.81E-02	1.51E+00
13.00	1.700E+02	225.2	5.471E+18	4.45E+00	5.00E-01	2.49E-01	6.37E-02	1.47E+00
14.00	1.460E+02	225.2	4.699E+18	4.00E+00	6.00E-01	2.43E-01	5.03E-02	1.43E+00
15.00	1.260E+02	225.2	4.055E+18	4.00E+00	7.00E-01	2.36E-01	3.94E-02	1.39E+00
16.00	1.080E+02	225.2	3.476E+18	4.00E+00	8.50E-01	2.28E-01	3.07E-02	1.34E+00
17.00	9.280E+01	225.2	2.987E+18	4.05E+00	1.00E+00	2.18E-01	2.49E-02	1.29E+00
18.00	7.980E+01	225.2	2.568E+18	4.30E+00	1.30E+00	2.04E-01	1.97E-02	1.23E+00
19.00	6.860E+01	225.2	2.208E+18	4.50E+00	1.70E+00	1.82E-01	1.55E-02	1.16E+00
20.00	5.900E+01	225.2	1.899E+18	4.60E+00	2.10E+00	1.57E-01	1.33E-02	1.07E+00
21.00	5.070E+01	225.2	1.632E+18	4.70E+00	2.70E+00	1.35E-01	1.23E-02	9.90E-01
22.00	4.360E+01	225.2	1.403E+18	4.80E+00	3.30E+00	1.22E-01	1.23E-02	9.17E-01
23.00	3.750E+01	225.2	1.207E+18	4.83E+00	3.70E+00	1.10E-01	1.31E-02	8.57E-01
24.00	3.228E+01	226.6	1.033E+18	4.85E+00	4.20E+00	9.89E-02	1.40E-02	8.01E-01
25.00	2.780E+01	228.1	8.834E+17	4.90E+00	4.50E+00	8.78E-02	1.51E-02	7.48E-01
27.50	1.923E+01	231.0	6.034E+17	4.95E+00	5.30E+00	7.33E-02	1.65E-02	6.96E-01
30.00	1.340E+01	235.1	4.131E+17	5.00E+00	5.70E+00	5.94E-02	1.81E-02	6.44E-01
32.50	9.400E+00	240.0	2.839E+17	5.00E+00	6.90E+00	4.15E-02	2.00E-02	5.89E-01
35.00	6.610E+00	247.2	1.938E+17	5.00E+00	7.70E+00	3.03E-02	2.18E-02	5.24E-01
37.50	4.720E+00	254.6	1.344E+17	5.00E+00	7.80E+00	1.95E-02	2.34E-02	4.51E-01
40.00	3.400E+00	262.1	9.402E+16	5.00E+00	7.00E+00	1.27E-02	2.50E-02	3.71E-01
42.50	2.480E+00	269.5	6.670E+16	5.00E+00	5.40E+00	9.00E-03	2.65E-02	2.99E-01
45.00	1.820E+00	273.6	4.821E+16	5.00E+00	4.20E+00	6.29E-03	2.81E-02	2.45E-01
47.50	1.340E+00	276.2	3.516E+16	5.00E+00	3.20E+00	4.56E-03	3.00E-02	2.00E-01
50.00	9.870E-01	277.2	2.581E+16	4.95E+00	2.50E+00	2.80E-03	3.22E-02	1.66E-01
55.00	5.370E-01	274.0	1.421E+16	4.85E+00	1.70E+00	1.77E-03	3.65E-02	1.50E-01
60.00	2.880E-01	262.7	7.946E+15	4.50E+00	1.20E+00	1.21E-03	4.59E-02	1.50E-01
65.00	1.470E-01	239.7	4.445E+15	4.00E+00	8.00E-01	8.87E-04	6.38E-02	1.50E-01
70.00	7.100E-02	216.6	2.376E+15	3.30E+00	4.00E-01	6.76E-04	1.18E-01	1.50E-01
75.00	3.200E-02	193.6	1.198E+15	2.70E+00	2.00E-01	5.54E-04	3.03E-01	1.50E-01
80.00	1.250E-02	170.6	5.311E+14	2.00E+00	1.80E-01	4.65E-04	7.89E-01	1.50E-01
85.00	4.510E-03	161.7	2.022E+14	1.33E+00	6.50E-01	3.98E-04	1.82E+00	1.50E-01
90.00	1.610E-03	161.6	7.221E+13	8.50E-01	9.00E-01	3.46E-04	3.40E+00	1.40E-01
95.00	6.060E-04	176.8	2.484E+13	5.40E-01	8.00E-01	3.05E-04	5.92E+00	1.30E-01
100.0	2.480E-04	190.4	9.441E+12	4.00E-01	4.00E-01	2.71E-04	1.04E+01	1.20E-01
105.0	1.130E-04	226.0	3.624E+12	3.40E-01	2.00E-01	2.44E-04	1.88E+01	1.10E-01
110.0	6.000E-05	270.1	1.610E+12	2.80E-01	5.00E-02	2.21E-04	2.87E+01	9.50E-02
115.0	3.540E-05	322.7	7.951E+11	2.40E-01	5.00E-03	2.02E-04	3.89E+01	6.00E-02
120.0	2.260E-05	380.0	4.311E+11	2.00E-01	5.00E-04	1.85E-04	5.00E+01	3.00E-02

Table 1e. Reference Atmospheric Model Profiles, Model 5. Subarctic Winter

MODEL = 5 SUBARCTIC WINTER

ALT	PRES	TEMP	DENSITY	H <sub>2</sub> O	O <sub>3</sub>	N <sub>2</sub> O	CO	CH <sub>4</sub>
(KM)	(MB)	(K)	(CM <sup>-3</sup> )	(PPMV)	(PPMV)	(PPMV)	(PPMV)	(PPMV)
0.00	1.013E+03	257.2	2.855E+19	1.41E+03	1.80E-02	3.20E-01	1.50E-01	1.70E+00
1.00	8.878E+02	259.1	2.484E+19	1.62E+03	2.07E-02	3.20E-01	1.45E-01	1.70E+00
2.00	7.775E+02	255.9	2.202E+19	1.43E+03	2.34E-02	3.20E-01	1.40E-01	1.70E+00
3.00	6.798E+02	252.7	1.950E+19	1.17E+03	2.77E-02	3.20E-01	1.35E-01	1.70E+00
4.00	5.932E+02	247.7	1.736E+19	7.90E+02	3.25E-02	3.20E-01	1.31E-01	1.70E+00
5.00	5.158E+02	240.9	1.552E+19	4.31E+02	3.80E-02	3.20E-01	1.30E-01	1.69E+00
6.00	4.467E+02	234.1	1.383E+19	2.37E+02	4.45E-02	3.20E-01	1.29E-01	1.67E+00
7.00	3.853E+02	227.3	1.229E+19	1.47E+02	7.25E-02	3.20E-01	1.25E-01	1.65E+00
8.00	3.308E+02	220.6	1.087E+19	3.38E+01	1.04E-01	3.20E-01	1.19E-01	1.63E+00
9.00	2.829E+02	217.2	9.440E+18	2.98E+01	2.10E-01	3.16E-01	1.09E-01	1.62E+00
10.00	2.418E+02	217.2	8.069E+18	2.00E+01	3.00E-01	3.10E-01	9.96E-02	1.58E+00
11.00	2.067E+02	217.2	6.898E+18	1.00E+01	3.50E-01	2.99E-01	8.96E-02	1.54E+00
12.00	1.766E+02	217.2	5.893E+18	6.00E+00	4.00E-01	2.94E-01	7.81E-02	1.51E+00
13.00	1.510E+02	217.2	5.039E+18	4.45E+00	6.50E-01	2.86E-01	6.37E-02	1.47E+00
14.00	1.291E+02	217.2	4.308E+18	4.50E+00	9.00E-01	2.80E-01	5.03E-02	1.43E+00
15.00	1.103E+02	217.2	3.681E+18	4.55E+00	1.20E+00	2.72E-01	3.94E-02	1.39E+00
16.00	9.431E+01	216.6	3.156E+18	4.60E+00	1.50E+00	2.61E-01	3.07E-02	1.34E+00
17.00	8.058E+01	216.0	2.104E+18	4.65E+00	1.90E+00	2.42E-01	2.49E-02	1.29E+00
18.00	6.882E+01	215.4	2.316E+18	4.70E+00	2.45E+00	2.17E-01	1.97E-02	1.23E+00
19.00	5.875E+01	214.8	1.982E+18	4.75E+00	3.10E+00	1.84E-01	1.55E-02	1.16E+00
20.00	5.014E+01	214.2	1.697E+18	4.80E+00	3.70E+00	1.62E-01	1.33E-02	1.08E+00
21.00	4.277E+01	213.6	1.451E+18	4.85E+00	4.00E+00	1.36E-01	1.23E-02	1.01E+00
22.00	3.647E+01	213.0	1.241E+18	4.90E+00	4.20E+00	1.23E-01	1.23E-02	9.56E-01
23.00	3.109E+01	212.4	1.061E+18	4.95E+00	4.50E+00	1.12E-01	1.31E-02	9.01E-01
24.00	2.649E+01	211.8	9.065E+17	5.00E+00	4.60E+00	1.04E-01	1.40E-02	8.48E-01
25.00	2.256E+01	211.2	7.742E+17	5.00E+00	4.70E+00	9.57E-02	1.52E-02	7.96E-01
27.50	1.513E+01	213.6	5.134E+17	5.00E+00	4.90E+00	8.60E-02	1.72E-02	7.45E-01
30.00	1.020E+01	216.0	3.423E+17	5.00E+00	5.40E+00	7.31E-02	2.04E-02	6.94E-01
32.50	6.910E+00	218.5	2.292E+17	5.00E+00	5.90E+00	5.71E-02	2.49E-02	6.43E-01
35.00	4.701E+00	222.3	1.533E+17	5.00E+00	6.20E+00	4.67E-02	3.17E-02	5.88E-01
37.50	3.230E+00	228.5	1.025E+17	5.00E+00	6.25E+00	3.44E-02	4.43E-02	5.24E-01
40.00	2.243E+00	234.7	6.927E+16	5.00E+00	5.90E+00	2.47E-02	6.47E-02	4.51E-01
42.50	1.570E+00	240.8	4.726E+16	5.00E+00	5.10E+00	1.63E-02	1.04E-01	3.71E-01
45.00	1.113E+00	247.0	3.266E+16	5.00E+00	4.10E+00	1.07E-02	1.51E-01	3.00E-01
47.50	7.900E-01	253.2	2.261E+16	5.00E+00	3.00E+00	7.06E-03	2.16E-01	2.45E-01
50.00	5.719E-01	259.3	1.599E+16	4.95E+00	2.60E+00	3.97E-03	3.14E-01	1.98E-01
55.00	2.990E-01	259.1	8.364E+15	4.85E+00	1.60E+00	2.51E-03	4.84E-01	1.59E-01
60.00	1.550E-01	250.9	4.478E+15	4.50E+00	9.50E-01	1.73E-03	7.15E-01	1.50E-01
65.00	7.900E-02	248.4	2.305E+15	4.00E+00	6.50E-01	1.26E-03	1.07E+00	1.50E-01
70.00	4.000E-02	245.4	1.181E+15	3.30E+00	5.00E-01	9.60E-04	1.52E+00	1.50E-01
75.00	2.000E-02	234.7	6.176E+14	2.70E+00	3.30E-01	7.55E-04	2.17E+00	1.50E-01
80.00	9.660E-03	223.9	3.127E+14	2.00E+00	1.30E-01	6.10E-04	3.06E+00	1.50E-01
85.00	4.500E-03	213.1	1.531E+14	1.33E+00	7.50E-01	5.02E-04	4.56E+00	1.50E-01
90.00	2.022E-03	202.3	7.244E+13	8.50E-01	8.00E-01	4.21E-04	6.88E+00	1.40E-01
95.00	9.070E-04	211.0	3.116E+13	5.40E-01	8.00E-01	3.58E-04	1.06E+01	1.30E-01
100.0	4.230E-04	218.5	1.403E+13	4.00E-01	4.00E-01	3.08E-04	1.71E+01	1.20E-01
105.0	2.070E-04	234.0	6.412E+12	3.40E-01	2.00E-01	2.68E-04	2.47E+01	1.10E-01
110.0	1.080E-04	252.6	3.099E+12	2.80E-01	5.00E-02	2.35E-04	3.36E+01	9.50E-02
115.0	6.000E-05	288.5	1.507E+12	2.40E-01	5.00E-03	2.08E-04	4.15E+01	6.00E-02
120.0	3.590E-05	333.0	7.814E+11	2.00E-01	5.00E-04	1.85E-04	5.00E+01	3.00E-02

Table 1f Reference Atmospheric Model Profiles, Model 6. U. S. Standard

MODEL = 6 U. S. STANDARD, 1976

ALT	PRES	TEMP	DENSITY	H <sub>2</sub> O	O <sub>3</sub>	N <sub>2</sub> O	CO	CH <sub>4</sub>
(KM)	(MB)	(K)	(CM <sup>-3</sup> )	(PPMV)	(PPMV)	(PPMV)	(PPMV)	(PPMV)
0.00	1.013E+03	288.2	2.548E+19	7.75E+03	2.66E-02	3.20E-01	1.50E-01	1.70E+00
1.00	8.988E+02	281.7	2.313E+19	6.07E+03	2.93E-02	3.20E-01	1.45E-01	1.70E+00
2.00	7.950E+02	275.2	2.094E+19	4.63E+03	3.24E-02	3.20E-01	1.40E-01	1.70E+00
3.00	7.012E+02	268.7	1.891E+19	3.18E+03	3.32E-02	3.20E-01	1.35E-01	1.70E+00
4.00	6.166E+02	262.2	1.704E+19	2.16E+03	3.39E-02	3.20E-01	1.31E-01	1.70E+00
5.00	5.405E+02	255.7	1.532E+19	1.40E+03	3.77E-02	3.20E-01	1.30E-01	1.70E+00
6.00	4.722E+02	249.2	1.373E+19	9.25E+02	4.11E-02	3.20E-01	1.29E-01	1.70E+00
7.00	4.111E+02	242.7	1.228E+19	5.72E+02	5.01E-02	3.20E-01	1.25E-01	1.70E+00
8.00	3.565E+02	236.2	1.094E+19	3.67E+02	5.97E-02	3.20E-01	1.19E-01	1.70E+00
9.00	3.080E+02	229.7	9.719E+18	1.58E+02	9.17E-02	3.20E-01	1.09E-01	1.69E+00
10.00	2.650E+02	223.3	8.602E+18	7.00E+01	1.31E-01	3.18E-01	9.96E-02	1.69E+00
11.00	2.270E+02	216.8	7.589E+18	3.61E+01	2.15E-01	3.14E-01	8.96E-02	1.68E+00
12.00	1.940E+02	216.7	6.489E+18	1.91E+01	3.10E-01	3.10E-01	7.81E-02	1.66E+00
13.00	1.658E+02	216.7	5.546E+18	1.09E+01	3.85E-01	3.05E-01	6.37E-02	1.65E+00
14.00	1.417E+02	216.7	4.739E+18	5.93E+00	5.03E-01	3.00E-01	5.03E-02	1.63E+00
15.00	1.211E+02	216.7	4.050E+18	5.00E+00	6.51E-01	2.94E-01	3.94E-02	1.61E+00
16.00	1.035E+02	216.7	3.462E+18	3.95E+00	8.70E-01	2.88E-01	3.07E-02	1.58E+00
17.00	8.850E+01	216.7	2.960E+18	3.85E+00	1.19E+00	2.78E-01	2.49E-02	1.55E+00
18.00	7.565E+01	216.7	2.530E+18	3.83E+00	1.59E+00	2.67E-01	1.97E-02	1.52E+00
19.00	6.467E+01	216.7	2.163E+18	3.85E+00	2.03E+00	2.53E-01	1.55E-02	1.48E+00
20.00	5.529E+01	216.7	1.849E+18	3.90E+00	2.58E+00	2.37E-01	1.33E-02	1.42E+00
21.00	4.729E+01	217.6	1.575E+18	3.98E+00	3.03E+00	2.19E-01	1.23E-02	1.36E+00
22.00	4.047E+01	218.6	1.342E+18	4.07E+00	3.65E+00	2.05E-01	1.23E-02	1.27E+00
23.00	3.467E+01	219.6	1.144E+18	4.20E+00	4.17E+00	1.97E-01	1.31E-02	1.19E+00
24.00	2.972E+01	220.6	9.765E+17	4.30E+00	4.63E+00	1.88E-01	1.40E-02	1.12E+00
25.00	2.549E+01	221.6	8.337E+17	4.43E+00	5.12E+00	1.76E-01	1.50E-02	1.06E+00
27.50	1.743E+01	224.0	5.640E+17	4.58E+00	5.80E+00	1.59E-01	1.60E-02	9.87E-01
30.00	1.197E+01	226.5	3.830E+17	4.73E+00	6.55E+00	1.42E-01	1.71E-02	9.14E-01
32.50	8.010E+00	230.0	2.524E+17	4.83E+00	7.37E+00	1.17E-01	1.85E-02	8.30E-01
35.00	5.746E+00	236.5	1.761E+17	4.90E+00	7.84E+00	9.28E-02	2.01E-02	7.46E-01
37.50	4.150E+00	242.9	1.238E+17	4.95E+00	7.80E+00	6.69E-02	2.22E-02	6.62E-01
40.00	2.871E+00	250.4	8.310E+16	5.03E+00	7.30E+00	4.51E-02	2.50E-02	5.64E-01
42.50	2.060E+00	257.3	5.803E+16	5.15E+00	6.20E+00	2.75E-02	2.82E-02	4.61E-01
45.00	1.491E+00	264.2	4.090E+16	5.23E+00	5.25E+00	1.59E-02	3.24E-02	3.63E-01
47.50	1.090E+00	270.6	2.920E+16	5.25E+00	4.10E+00	9.38E-03	3.72E-02	2.77E-01
50.00	7.978E-01	270.7	2.136E+16	5.23E+00	3.10E+00	4.75E-03	4.60E-02	2.10E-01
55.00	4.250E-01	260.8	1.181E+16	5.10E+00	1.80E+00	3.00E-03	6.64E-02	1.65E-01
60.00	2.190E-01	247.0	6.426E+15	4.75E+00	1.10E+00	2.07E-03	1.07E-01	1.50E-01
65.00	1.090E-01	233.3	3.386E+15	4.20E+00	7.00E-01	1.51E-03	1.86E-01	1.50E-01
70.00	5.220E-02	219.6	1.723E+15	3.50E+00	3.00E-01	1.15E-03	3.06E-01	1.50E-01
75.00	2.400E-02	208.4	8.347E+14	2.83E+00	2.50E-01	8.89E-04	6.38E-01	1.50E-01
80.00	1.050E-02	198.6	3.832E+14	2.05E+00	3.00E-01	7.06E-04	1.50E+00	1.50E-01
85.00	4.460E-03	188.9	1.711E+14	1.33E+00	5.00E-01	5.72E-04	3.24E+00	1.50E-01
90.00	1.840E-03	186.9	7.136E+13	8.50E-01	7.00E-01	4.71E-04	5.84E+00	1.40E-01
95.00	7.600E-04	188.4	2.924E+13	5.40E-01	7.00E-01	3.93E-04	1.01E+01	1.30E-01
100.0	3.200E-04	195.1	1.189E+13	4.00E-01	4.00E-01	3.32E-04	1.69E+01	1.20E-01
105.0	1.450E-04	208.8	5.033E+12	3.40E-01	2.00E-01	2.84E-04	2.47E+01	1.10E-01
110.0	7.100E-05	240.0	2.144E+12	2.80E-01	5.00E-02	2.44E-04	3.36E+01	9.50E-02
115.0	4.010E-05	300.0	9.688E+11	2.40E-01	5.00E-03	2.12E-04	4.15E+01	6.00E-02
120.0	2.540E-05	360.0	5.114E+11	2.00E-01	5.00E-04	1.85E-04	5.00E+01	3.00E-02

## AFGL U.S. STANDARD. PROFILES

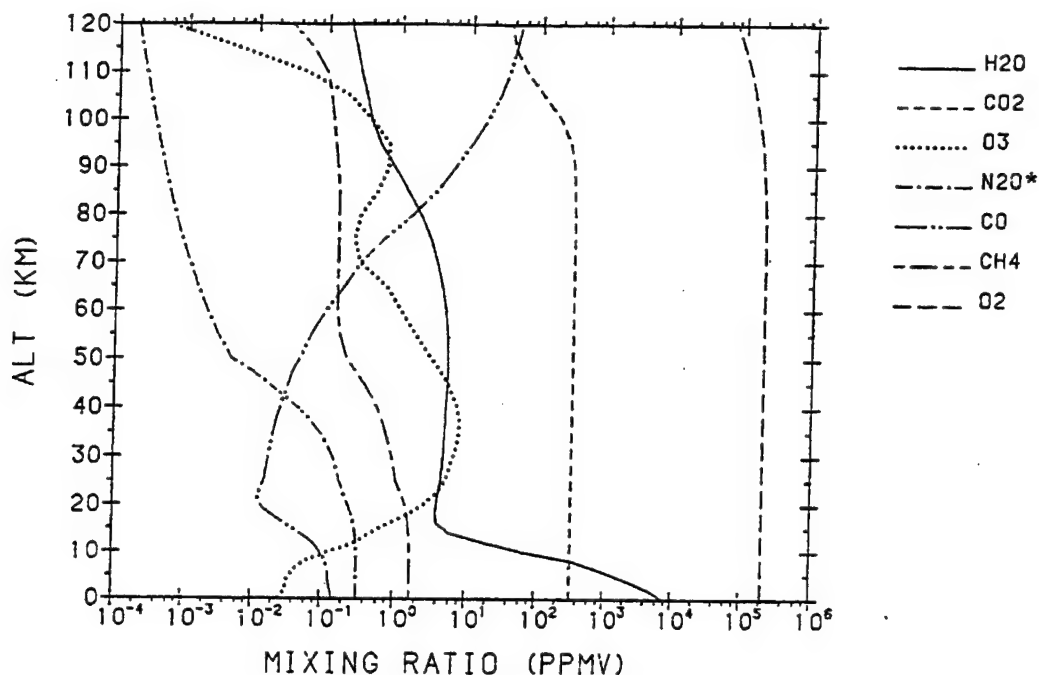


Figure 11. U.S. Standard Model Atmosphere Profiles for the mixing ratios of the major radiating atmospheric gases. This corresponds to Model 6 in Table 1; see text.

[(\*) indicates extrapolation adopted for that species; see tabular data]

**Table 2. Constituent Profiles (ppmv):**

Molecules 1-7 are Model 6 (U.S. Standard) compatible and are repeated here because they duplicate the numbering scheme utilized in the HITRAN 1992 data base. In addition, CO<sub>2</sub> and O<sub>2</sub> are only defined by a single profile so they have not been included in Table 1.

Molecules 8-28 are provided as single representative profiles. Their natural variability can be very different from the selected profile.

[(\*) indicates subsequent extrapolation adopted for that species]

Table 2a. Constituent Profiles (ppmv), H<sub>2</sub>O, CO<sub>2</sub>, O<sub>3</sub>, N<sub>2</sub>O, CO, CH<sub>4</sub>, O<sub>2</sub>

ALT (KM)	1 H <sub>2</sub> O (PPMV)	2 CO <sub>2</sub> (PPMV)	3 O <sub>3</sub> (PPMV)	4 N <sub>2</sub> O (PPMV)	5 CO (PPMV)	6 CH <sub>4</sub> (PPMV)	7 O <sub>2</sub> (PPMV)
0.0	7.75E+03	3.30E+02	2.66E-02	3.20E-01	1.50E-01	1.70E+00	2.09E+05
1.0	6.07E+03	3.30E+02	2.93E-02	3.20E-01	1.45E-01	1.70E+00	2.09E+05
2.0	4.63E+03	3.30E+02	3.24E-02	3.20E-01	1.40E-01	1.70E+00	2.09E+05
3.0	3.18E+03	3.30E+02	3.32E-02	3.20E-01	1.35E-01	1.70E+00	2.09E+05
4.0	2.16E+03	3.30E+02	3.39E-02	3.20E-01	1.31E-01	1.70E+00	2.09E+05
5.0	1.40E+03	3.30E+02	3.77E-02	3.20E-01	1.30E-01	1.70E+00	2.09E+05
6.0	9.25E+02	3.30E+02	4.11E-02	3.20E-01	1.29E-01	1.70E+00	2.09E+05
7.0	5.72E+02	3.30E+02	5.01E-02	3.20E-01	1.25E-01	1.70E+00	2.09E+05
8.0	3.67E+02	3.30E+02	5.97E-02	3.20E-01	1.19E-01	1.70E+00	2.09E+05
9.0	1.58E+02	3.30E+02	9.17E-02	3.20E-01	1.09E-01	1.69E+00	2.09E+05
10.0	7.00E+01	3.30E+02	1.31E-01	3.18E-01	9.96E-02	1.69E+00	2.09E+05
11.0	3.61E+01	3.30E+02	2.15E-01	3.14E-01	8.96E-02	1.68E+00	2.09E+05
12.0	1.91E+01	3.30E+02	3.10E-01	3.10E-01	7.81E-02	1.66E+00	2.09E+05
13.0	1.09E+01	3.30E+02	3.85E-01	3.05E-01	6.37E-02	1.65E+00	2.09E+05
14.0	5.93E+00	3.30E+02	5.03E-01	3.00E-01	5.03E-02	1.63E+00	2.09E+05
15.0	5.00E+00	3.30E+02	6.51E-01	2.94E-01	3.94E-02	1.61E+00	2.09E+05
16.0	3.95E+00	3.30E+02	8.70E-01	2.88E-01	3.07E-02	1.58E+00	2.09E+05
17.0	3.85E+00	3.30E+02	1.19E+00	2.78E-01	2.49E-02	1.55E+00	2.09E+05
18.0	3.83E+00	3.30E+02	1.59E+00	2.67E-01	1.97E-02	1.52E+00	2.09E+05
19.0	3.85E+00	3.30E+02	2.03E+00	2.53E-01	1.55E-02	1.48E+00	2.09E+05
20.0	3.90E+00	3.30E+02	2.58E+00	2.37E-01	1.33E-02	1.42E+00	2.09E+05
21.0	3.98E+00	3.30E+02	3.03E+00	2.19E-01	1.23E-02	1.36E+00	2.09E+05
22.0	4.07E+00	3.30E+02	3.65E+00	2.05E-01	1.23E-02	1.27E+00	2.09E+05
23.0	4.20E+00	3.30E+02	4.17E+00	1.97E-01	1.31E-02	1.19E+00	2.09E+05
24.0	4.30E+00	3.30E+02	4.63E+00	1.88E-01	1.40E-02	1.12E+00	2.09E+05
25.0	4.43E+00	3.30E+02	5.12E+00	1.76E-01	1.50E-02	1.06E+00	2.09E+05
27.5	4.58E+00	3.30E+02	5.80E+00	1.59E-01	1.60E-02	9.87E-01	2.09E+05
30.0	4.73E+00	3.30E+02	6.55E+00	1.42E-01	1.71E-02	9.14E-01	2.09E+05
32.5	4.83E+00	3.30E+02	7.37E+00	1.17E-01	1.85E-02	8.30E-01	2.09E+05
35.0	4.90E+00	3.30E+02	7.84E+00	9.28E-02	2.01E-02	7.46E-01	2.09E+05
37.5	4.95E+00	3.30E+02	7.80E+00	6.69E-02	2.22E-02	6.62E-01	2.09E+05
40.0	5.03E+00	3.30E+02	7.30E+00	4.51E-02	2.50E-02	5.64E-01	2.09E+05
42.5	5.15E+00	3.30E+02	6.20E+00	2.75E-02	2.82E-02	4.61E-01	2.09E+05
45.0	5.23E+00	3.30E+02	5.25E+00	1.59E-02	3.24E-02	3.63E-01	2.09E+05
47.5	5.25E+00	3.30E+02	4.10E+00	9.38E-03	3.72E-02	2.77E-01	2.09E+05
50.0	5.23E+00	3.30E+02	3.10E+00	4.75E-03*	4.60E-02	2.10E-01	2.09E+05
55.0	5.10E+00	3.30E+02	1.80E+00	3.00E-03	6.64E-02	1.65E-01	2.09E+05
60.0	4.75E+00	3.30E+02	1.10E+00	2.07E-03	1.07E-01	1.50E-01	2.09E+05
65.0	4.20E+00	3.30E+02	7.00E-01	1.51E-03	1.86E-01	1.50E-01	2.09E+05
70.0	3.50E+00	3.30E+02	3.00E-01	1.15E-03	3.06E-01	1.50E-01	2.09E+05
75.0	2.83E+00	3.30E+02	2.50E-01	8.89E-04	6.38E-01	1.50E-01	2.09E+05
80.0	2.05E+00	3.28E+02	3.00E-01	7.06E-04	1.50E+00	1.50E-01	2.09E+05
85.0	1.33E+00	3.20E+02	5.00E-01	5.72E-04	3.24E+00	1.50E-01	2.00E+05
90.0	8.50E-01	3.10E+02	7.00E-01	4.71E-04	5.84E+00	1.40E-01	1.90E+05
95.0	5.40E-01	2.70E+02	7.00E-01	3.93E-04	1.01E+01	1.30E-01	1.80E+05
100.0	4.00E-01	1.95E+02	4.00E-01	3.32E-04	1.69E+01	1.20E-01	1.60E+05
105.0	3.40E-01	1.10E+02	2.00E-01	2.84E-04	2.47E+01	1.10E-01	1.40E+05
110.0	2.80E-01	6.00E+01	5.00E-02	2.44E-04	3.36E+01	9.50E-02	1.20E+05
115.0	2.40E-01	4.00E+01	5.00E-03	2.12E-04	4.15E+01	6.00E-02	9.40E+04
120.0	2.00E-01	3.50E+01	5.00E-04	1.85E-04	5.00E+01	3.00E-02	7.25E+04



Table 2b. Constituent Profiles (ppmv), NO, SO<sub>2</sub>, NO<sub>2</sub>, NH<sub>3</sub>, HNO<sub>3</sub>, OH, HF

ALT (KM)	8 NO (PPMV)	9 SO <sub>2</sub> (PPMV)	10 NO <sub>2</sub> (PPMV)	11 NH <sub>3</sub> (PPMV)	12 HNO <sub>3</sub> (PPMV)	13 OH (PPMV)	14 HF (PPMV)
0.0	3.00E-04	3.00E-04	2.30E-05	5.00E-04	5.00E-05	4.40E-08	1.00E-08
1.0	3.00E-04	2.74E-04	2.30E-05	5.00E-04	5.96E-05	4.40E-08	1.00E-08
2.0	3.00E-04	2.36E-04	2.30E-05	4.63E-04	6.93E-05	4.40E-08	1.23E-08
3.0	3.00E-04	1.90E-04	2.30E-05	3.80E-04	7.91E-05	4.40E-08	1.97E-08
4.0	3.00E-04	1.46E-04	2.30E-05	2.88E-04	8.87E-05	4.40E-08	3.18E-08
5.0	3.00E-04	1.18E-04	2.30E-05	2.04E-04	9.75E-05	4.40E-08	5.63E-08
6.0	3.00E-04	9.71E-05	2.30E-05	1.46E-04	1.11E-04	4.40E-08	9.18E-08
7.0	3.00E-04	8.30E-05	2.30E-05	9.88E-05	1.26E-04	4.41E-08	1.53E-07
8.0	3.00E-04	7.21E-05	2.30E-05	6.48E-05	1.39E-04	4.45E-08	2.41E-07
9.0	3.00E-04	6.56E-05	2.32E-05	3.77E-05	1.53E-04	4.56E-08	4.04E-07
10.0	3.00E-04	6.08E-05	2.38E-05	2.03E-05	1.74E-04	4.68E-08	6.57E-07
11.0	3.00E-04	5.79E-05	2.62E-05	1.09E-05	2.02E-04	4.80E-08	1.20E-06
12.0	3.00E-04	5.60E-05	3.15E-05	6.30E-06	2.41E-04	4.94E-08	1.96E-06
13.0	2.99E-04	5.59E-05	4.45E-05	3.12E-06	2.76E-04	5.19E-08	3.12E-06
14.0	2.95E-04	5.64E-05	7.48E-05	1.11E-06	3.33E-04	5.65E-08	4.62E-06
15.0	2.83E-04	5.75E-05	1.71E-04	4.47E-07	4.52E-04	6.75E-08	7.09E-06
16.0	2.68E-04	5.75E-05	3.19E-04	2.11E-07	7.37E-04	8.25E-08	1.05E-05
17.0	2.52E-04	5.37E-05	5.19E-04	1.10E-07	1.31E-03	1.04E-07	1.69E-05
18.0	2.40E-04	4.78E-05	7.71E-04	6.70E-08	2.11E-03	1.30E-07	2.57E-05
19.0	2.44E-04	3.97E-05	1.06E-03	3.97E-08	3.17E-03	1.64E-07	4.02E-05
20.0	2.55E-04	3.19E-05	1.39E-03	2.41E-08	4.20E-03	2.16E-07	5.77E-05
21.0	2.77E-04	2.67E-05	1.76E-03	1.92E-08	4.94E-03	3.40E-07	7.77E-05
22.0	3.07E-04	2.28E-05	2.16E-03	1.72E-08	5.46E-03	5.09E-07	9.90E-05
23.0	3.60E-04	2.07E-05	2.58E-03	1.59E-08	5.74E-03	7.59E-07	1.23E-04
24.0	4.51E-04	1.90E-05	3.06E-03	1.44E-08	5.84E-03	1.16E-06	1.50E-04
25.0	6.85E-04	1.75E-05	3.74E-03	1.23E-08	5.61E-03	2.18E-06	1.82E-04
27.5	1.28E-03	1.54E-05	4.81E-03	9.37E-09	4.82E-03	5.00E-06	2.30E-04
30.0	2.45E-03	1.34E-05	6.16E-03	6.35E-09	3.74E-03	1.17E-05	2.83E-04
32.5	4.53E-03	1.21E-05	7.21E-03	3.68E-09	2.59E-03	3.40E-05	3.20E-04
35.0	7.14E-03	1.16E-05	7.28E-03	1.82E-09	1.64E-03	8.35E-05	3.48E-04
37.5	9.34E-03	1.21E-05	6.26E-03	9.26E-10	9.68E-04	1.70E-04	3.72E-04
40.0	1.12E-02	1.36E-05	4.03E-03	2.94E-10*	5.33E-04	2.85E-04	3.95E-04
42.5	1.19E-02	1.65E-05	2.17E-03	8.72E-11	2.52E-04	4.06E-04	4.10E-04
45.0	1.17E-02	2.10E-05	1.15E-03	2.98E-11	1.21E-04	5.11E-04	4.21E-04
47.5	1.10E-02	2.77E-05	6.66E-04	1.30E-11	7.70E-05	5.79E-04	4.24E-04
50.0	1.03E-02	3.56E-05	4.43E-04*	7.13E-12	5.55E-05*	6.75E-04	4.25E-04*
55.0	1.01E-02	4.59E-05	3.39E-04	4.80E-12	4.45E-05	9.53E-04	4.25E-04
60.0	1.01E-02	5.15E-05	2.85E-04	3.66E-12	3.84E-05	1.76E-03	4.25E-04
65.0	1.03E-02	5.11E-05	2.53E-04	3.00E-12	3.49E-05	3.74E-03	4.25E-04
70.0	1.15E-02	4.32E-05	2.31E-04	2.57E-12	3.27E-05	7.19E-03	4.25E-04
75.0	1.61E-02	2.83E-05	2.15E-04	2.27E-12	3.12E-05	1.12E-02	4.25E-04
80.0	2.68E-02	1.33E-05	2.02E-04	2.04E-12	3.01E-05	1.13E-02	4.25E-04
85.0	7.01E-02	5.56E-06	1.92E-04	1.85E-12	2.92E-05	6.10E-03	4.25E-04
90.0	2.13E-01	2.24E-06	1.83E-04	1.71E-12	2.84E-05	1.51E-03	4.25E-04
95.0	7.12E-01	8.96E-07	1.76E-04	1.59E-12	2.78E-05	2.42E-04	4.25E-04
100.0	2.08E+00	3.58E-07	1.70E-04	1.48E-12	2.73E-05	4.47E-05	4.25E-04
105.0	4.50E+00	1.43E-07	1.64E-04	1.40E-12	2.68E-05	1.77E-05	4.25E-04
110.0	7.98E+00	5.73E-08	1.59E-04	1.32E-12	2.64E-05	1.19E-05	4.25E-04
115.0	1.00E+01	2.29E-08	1.55E-04	1.25E-12	2.60E-05	1.35E-05	4.25E-04
120.0	1.00E+01	9.17E-09	1.51E-04	1.19E-12	2.57E-05	2.20E-05	4.25E-04



Table 2c. Constituent Profiles (ppmv), HCl, HBr, HI, ClO, OCS, H<sub>2</sub>CO, HOCl

ALT (KM)	15 HCL (PPMV)	16 HBR (PPMV)	17 HI (PPMV)	18 CLO (PPMV)	19 OCS (PPMV)	20 H <sub>2</sub> CO (PPMV)	21 HOCL (PPMV)
0.0	1.00E-03	1.70E-06	3.00E-06*	1.00E-08	6.00E-04	2.40E-03	7.70E-06
1.0	7.49E-04	1.70E-06	3.00E-06	1.00E-08	5.90E-04	1.07E-03	1.06E-05
2.0	5.61E-04	1.70E-06	3.00E-06	1.00E-08	5.80E-04	4.04E-04	1.22E-05
3.0	4.22E-04	1.70E-06	3.00E-06	1.00E-08	5.70E-04	2.27E-04	1.14E-05
4.0	3.19E-04	1.70E-06	3.00E-06	1.00E-08	5.62E-04	1.40E-04	9.80E-06
5.0	2.39E-04	1.70E-06	3.00E-06	1.00E-08	5.55E-04	1.00E-04	8.01E-06
6.0	1.79E-04	1.70E-06	3.00E-06	1.00E-08	5.48E-04	7.44E-05	6.42E-06
7.0	1.32E-04	1.70E-06	3.00E-06	1.00E-08	5.40E-04	6.04E-05	5.42E-06
8.0	9.96E-05	1.70E-06	3.00E-06	1.01E-08	5.32E-04	5.01E-05	4.70E-06
9.0	7.48E-05	1.70E-06	3.00E-06	1.05E-08	5.25E-04	4.22E-05	4.41E-06
10.0	5.68E-05	1.70E-06	3.00E-06	1.21E-08	5.18E-04	3.63E-05	4.34E-06
11.0	4.59E-05	1.70E-06	3.00E-06	1.87E-08	5.09E-04	3.43E-05	4.65E-06
12.0	4.36E-05	1.70E-06	3.00E-06	3.18E-08	4.98E-04	3.39E-05	5.01E-06
13.0	6.51E-05	1.70E-06	3.00E-06	5.61E-08	4.82E-04	3.50E-05	5.22E-06
14.0	1.01E-04	1.70E-06	3.00E-06	9.99E-08	4.60E-04	3.62E-05	5.60E-06
15.0	1.63E-04	1.70E-06	3.00E-06	1.78E-07	4.26E-04	3.62E-05	6.86E-06
16.0	2.37E-04	1.70E-06	3.00E-06	3.16E-07	3.88E-04	3.58E-05	8.77E-06
17.0	3.13E-04	1.70E-06	3.00E-06	5.65E-07	3.48E-04	3.50E-05	1.20E-05
18.0	3.85E-04	1.70E-06	3.00E-06	1.04E-06	3.09E-04	3.42E-05	1.63E-05
19.0	4.42E-04	1.70E-06	3.00E-06	2.04E-06	2.74E-04	3.39E-05	2.26E-05
20.0	4.89E-04	1.70E-06	3.00E-06	4.64E-06	2.41E-04	3.43E-05	3.07E-05
21.0	5.22E-04	1.70E-06	3.00E-06	8.15E-06	2.14E-04	3.68E-05	4.29E-05
22.0	5.49E-04	1.70E-06	3.00E-06	1.07E-05	1.88E-04	4.03E-05	5.76E-05
23.0	5.75E-04	1.70E-06	3.00E-06	1.52E-05	1.64E-04	4.50E-05	7.65E-05
24.0	6.04E-04	1.70E-06	3.00E-06	2.24E-05	1.37E-04	5.06E-05	9.92E-05
25.0	6.51E-04	1.71E-06	3.00E-06	3.97E-05	1.08E-04	5.82E-05	1.31E-04
27.5	7.51E-04	1.76E-06	3.00E-06	8.48E-05	6.70E-05	7.21E-05	1.84E-04
30.0	9.88E-04	1.90E-06	3.00E-06	1.85E-04	2.96E-05	8.73E-05	2.45E-04
32.5	1.28E-03	2.26E-06	3.00E-06	3.57E-04	1.21E-05	1.01E-04	2.96E-04
35.0	1.57E-03	2.82E-06	3.00E-06	5.08E-04	4.31E-06	1.11E-04	3.21E-04
37.5	1.69E-03	3.69E-06	3.00E-06	6.07E-04	1.60E-06	1.13E-04	3.04E-04
40.0	1.74E-03	4.91E-06	3.00E-06	5.95E-04	6.71E-07	1.03E-04	2.48E-04
42.5	1.76E-03	6.13E-06	3.00E-06	4.33E-04	4.35E-07	7.95E-05	1.64E-04
45.0	1.79E-03	6.85E-06	3.00E-06	2.51E-04	3.34E-07	4.82E-05	9.74E-05
47.5	1.80E-03	7.08E-06	3.00E-06	1.56E-04	2.80E-07	1.63E-05	4.92E-05
50.0	1.80E-03*	7.14E-06*	3.00E-06	1.04E-04*	2.47E-07*	5.10E-06*	2.53E-05*
55.0	1.80E-03	7.15E-06	3.00E-06	7.69E-05	2.28E-07	2.00E-06	1.50E-05
60.0	1.80E-03	7.15E-06	3.00E-06	6.30E-05	2.16E-07	1.05E-06	1.05E-05
65.0	1.80E-03	7.15E-06	3.00E-06	5.52E-05	2.08E-07	6.86E-07	8.34E-06
70.0	1.80E-03	7.15E-06	3.00E-06	5.04E-05	2.03E-07	5.14E-07	7.11E-06
75.0	1.80E-03	7.15E-06	3.00E-06	4.72E-05	1.98E-07	4.16E-07	6.33E-06
80.0	1.80E-03	7.15E-06	3.00E-06	4.49E-05	1.95E-07	3.53E-07	5.78E-06
85.0	1.80E-03	7.15E-06	3.00E-06	4.30E-05	1.92E-07	3.09E-07	5.37E-06
90.0	1.80E-03	7.15E-06	3.00E-06	4.16E-05	1.89E-07	2.76E-07	5.05E-06
95.0	1.80E-03	7.15E-06	3.00E-06	4.03E-05	1.87E-07	2.50E-07	4.78E-06
100.0	1.80E-03	7.15E-06	3.00E-06	3.93E-05	1.85E-07	2.30E-07	4.56E-06
105.0	1.80E-03	7.15E-06	3.00E-06	3.83E-05	1.83E-07	2.13E-07	4.37E-06
110.0	1.80E-03	7.15E-06	3.00E-06	3.75E-05	1.81E-07	1.98E-07	4.21E-06
115.0	1.80E-03	7.15E-06	3.00E-06	3.68E-05	1.80E-07	1.86E-07	4.06E-06
120.0	1.80E-03	7.15E-06	3.00E-06	3.61E-05	1.78E-07	1.75E-07	3.93E-06

Table 2d. Constituent Profiles (ppmv), N<sub>2</sub>, HCN, CH<sub>3</sub>Cl, H<sub>2</sub>O<sub>2</sub>, C<sub>2</sub>H<sub>2</sub>, C<sub>2</sub>H<sub>6</sub>, PH<sub>3</sub>

ALT (KM)	22 N <sub>2</sub> (PPMV)	23 HCN (PPMV)	24 CH <sub>3</sub> Cl (PPMV)	25 H <sub>2</sub> O <sub>2</sub> (PPMV)	26 C <sub>2</sub> H <sub>2</sub> (PPMV)	27 C <sub>2</sub> H <sub>6</sub> (PPMV)	28 PH <sub>3</sub> (PPMV)
0.0	7.81E+05	1.70E-04	7.00E-04	2.00E-04	3.00E-04	2.00E-03	1.00E-14*
1.0	7.81E+05	1.65E-04	6.70E-04	1.95E-04	1.72E-04	2.00E-03	1.00E-14
2.0	7.81E+05	1.63E-04	6.43E-04	1.92E-04	9.57E-05	2.00E-03	1.00E-14
3.0	7.81E+05	1.61E-04	6.22E-04	1.89E-04	6.74E-05	2.00E-03	1.00E-14
4.0	7.81E+05	1.60E-04	6.07E-04	1.84E-04	5.07E-05	1.98E-03	1.00E-14
5.0	7.81E+05	1.60E-04	6.02E-04	1.77E-04	3.99E-05	1.95E-03	1.00E-14
6.0	7.81E+05	1.60E-04	6.00E-04	1.66E-04	3.19E-05	1.90E-03	1.00E-14
7.0	7.81E+05	1.60E-04	6.00E-04	1.49E-04	2.80E-05	1.85E-03	1.00E-14
8.0	7.81E+05	1.60E-04	5.98E-04	1.23E-04	2.55E-05	1.79E-03	1.00E-14
9.0	7.81E+05	1.60E-04	5.94E-04	9.09E-05	2.40E-05	1.72E-03	1.00E-14
10.0	7.81E+05	1.60E-04	5.88E-04	5.79E-05	2.27E-05	1.58E-03	1.00E-14
11.0	7.81E+05	1.60E-04	5.79E-04	3.43E-05	2.08E-05	1.30E-03	1.00E-14
12.0	7.81E+05	1.60E-04	5.66E-04	1.95E-05	1.76E-05	9.86E-04	1.00E-14
13.0	7.81E+05	1.59E-04	5.48E-04	1.08E-05	1.23E-05	7.22E-04	1.00E-14
14.0	7.81E+05	1.57E-04	5.28E-04	6.59E-06	7.32E-06	4.96E-04	1.00E-14
15.0	7.81E+05	1.55E-04	5.03E-04	4.20E-06	4.52E-06	3.35E-04	1.00E-14
16.0	7.81E+05	1.52E-04	4.77E-04	2.94E-06	2.59E-06	2.14E-04	1.00E-14
17.0	7.81E+05	1.49E-04	4.49E-04	2.30E-06	1.55E-06	1.49E-04	1.00E-14
18.0	7.81E+05	1.45E-04	4.21E-04	2.24E-06	8.63E-07	1.05E-04	1.00E-14
19.0	7.81E+05	1.41E-04	3.95E-04	2.68E-06	5.30E-07	7.96E-05	1.00E-14
20.0	7.81E+05	1.37E-04	3.69E-04	3.68E-06	3.10E-07	6.01E-05	1.00E-14
21.0	7.81E+05	1.34E-04	3.43E-04	5.62E-06	1.89E-07	4.57E-05	1.00E-14
22.0	7.81E+05	1.30E-04	3.17E-04	1.03E-05	1.04E-07	3.40E-05	1.00E-14
23.0	7.81E+05	1.25E-04	2.86E-04	1.97E-05	5.75E-08	2.60E-05	1.00E-14
24.0	7.81E+05	1.19E-04	2.48E-04	3.70E-05	2.23E-08	1.89E-05	1.00E-14
25.0	7.81E+05	1.13E-04	1.91E-04	6.20E-05	8.51E-09	1.22E-05	1.00E-14
27.5	7.81E+05	1.05E-04	1.10E-04	1.03E-04	4.09E-09	5.74E-06	1.00E-14
30.0	7.81E+05	9.73E-05	4.72E-05	1.36E-04	2.52E-09	2.14E-06	1.00E-14
32.5	7.81E+05	9.04E-05	1.79E-05	1.36E-04	1.86E-09	8.49E-07	1.00E-14
35.0	7.81E+05	8.46E-05	7.35E-06	1.13E-04	1.52E-09	3.42E-07	1.00E-14
37.5	7.81E+05	8.02E-05	3.03E-06	8.51E-05	1.32E-09	1.34E-07	1.00E-14
40.0	7.81E+05	7.63E-05	1.32E-06	6.37E-05	1.18E-09	5.39E-08*	1.00E-14
42.5	7.81E+05	7.30E-05	8.69E-07	5.17E-05	1.08E-09	2.25E-08	1.00E-14
45.0	7.81E+05	7.00E-05	6.68E-07	4.44E-05	9.97E-10	1.04E-08	1.00E-14
47.5	7.81E+05	6.70E-05	5.60E-07	3.80E-05	9.34E-10	6.57E-09	1.00E-14
50.0	7.81E+05	6.43E-05*	4.94E-07*	3.48E-05	8.83E-10*	4.74E-09	1.00E-14
55.0	7.81E+05	6.21E-05	4.56E-07	3.62E-05	8.43E-10	3.79E-09	1.00E-14
60.0	7.81E+05	6.02E-05	4.32E-07	5.25E-05	8.10E-10	3.28E-09	1.00E-14
65.0	7.81E+05	5.88E-05	4.17E-07	1.26E-04	7.83E-10	2.98E-09	1.00E-14
70.0	7.81E+05	5.75E-05	4.05E-07	3.77E-04	7.60E-10	2.79E-09	1.00E-14
75.0	7.81E+05	5.62E-05	3.96E-07	1.12E-03	7.40E-10	2.66E-09	1.00E-14
80.0	7.81E+05	5.50E-05	3.89E-07	2.00E-03	7.23E-10	2.56E-09	1.00E-14
85.0	7.81E+05	5.37E-05	3.83E-07	1.68E-03	7.07E-10	2.49E-09	1.00E-14
90.0	7.80E+05	5.25E-05	3.78E-07	4.31E-04	6.94E-10	2.43E-09	1.00E-14
95.0	7.79E+05	5.12E-05	3.73E-07	4.98E-05	6.81E-10	2.37E-09	1.00E-14
100.0	7.77E+05	5.00E-05	3.69E-07	6.76E-06	6.70E-10	2.33E-09	1.00E-14
105.0	7.74E+05	4.87E-05	3.66E-07	8.38E-07	6.59E-10	2.29E-09	1.00E-14
110.0	7.70E+05	4.75E-05	3.62E-07	9.56E-08	6.49E-10	2.25E-09	1.00E-14
115.0	7.65E+05	4.62E-05	3.59E-07	1.00E-08	6.40E-10	2.22E-09	1.00E-14
120.0	7.60E+05	4.50E-05	3.56E-07	1.00E-09	6.32E-10	2.19E-09	1.00E-14

The altitude increments for both Table 1 and Table 2 are 1 km between 0 and 25 km, 2.5 km between 25 and 50 km, and 5 km between 50 and 120 km. These increments (and the subset of reference atmospheres themselves) have been chosen for their compatibility with existing profiles in other radiation models (particularly LOWTRAN 7), facilitating validation and inter-comparison tests. The units are: altitude in (km), temperature in (K), pressure in (mb), and mixing ratios in (ppmv). This profile set is available from PL/GPOS in computer-accessible formats, either as tables or FORTRAN data statements appropriate for direct incorporation into computer simulations (e.g. FASCOD3P).

A comprehensive bibliography on reference atmospheric constituent profiles appears in Appendix B of the Anderson report<sup>10</sup>.

### 2.2.3. ERROR ESTIMATES and VARIABILITY

The exactness of these tabulated values vary with species and altitude. At their best, they offer approximately 10-30% relative consistency for U.S. Standard Atmosphere conditions throughout the troposphere and stratosphere; exceptions include PH<sub>3</sub> which is unmeasured in the earth's atmosphere. The mesospheric and thermospheric profiles are much less certain and, in fact, are only defined for temperature, pressure, and the following constituents: H<sub>2</sub>O, CO<sub>2</sub>, O<sub>3</sub>, CO, CH<sub>4</sub>, O<sub>2</sub>, NO, SO<sub>2</sub>, OH, and H<sub>2</sub>O<sub>2</sub>. Mixing ratios for the remaining species have been extrapolated from measurements (usually near the stratopause) using a logarithmically decreasing mixing ratio scale height; the onset of such profile extrapolations is marked by asterisks (\*) in the tables and figures. This, of course, leads to unsupported estimates of abundance in the upper atmosphere. [The adopted logarithmic extrapolation scheme is a compromise between using either: (a) constant or, (b) constantly decreasing mixing ratios. The former introduces erroneous relative changes between extrapolated species. The latter, while obviously connoting the lack of data, introduces an abrupt discontinuity into the profiles.] The mixing ratios of all extrapolated species are, in any case, very small.

### 2.2.4. LIMITATIONS

Representative profiles do not necessarily resemble in situ environments, leading to constraints on their general applicability. WMO and COSPAR<sup>58</sup> have released new sets of standard temperature-density profiles in 1986 which provide significant enhancements to the NASA, 1966 Supplements and CIRA, 1972 Reference Atmospheres<sup>59</sup>. (A subset of the CIRA, 1972 profiles is available in this format.)

However, a more detailed climatology does not ensure adequate simulation of observed variability. Particularly in disturbed winter conditions, dynamic wave activity can bring about rapid changes in temperature and pressure, which can then propagate from the troposphere into and through the stratosphere.

In addition to any tropospheric meteorologically-driven changes in temperature, the water vapor and anthropogenic pollutants (CO, CO<sub>2</sub>, O<sub>3</sub>, nitrogen-oxygen compounds, etc.) exhibit factors of 100 or more local variability. Dynamic perturbations are less extreme in the stratosphere; however, horizontal gradients on local, latitudinal or seasonal scales often exceed factors of 2- 10. In the mesosphere and lower thermosphere, in addition to the extrapolated data, natural excursions brought on by responses to dynamic and solar influences can be substantial. Calculated radiances or transmittances which rely upon default choices represent only a reasonable set of possibilities; they do not replicate actual measurement conditions. When detailed comparisons between theoretical radiance/transmittance calculations and actual data are required, supporting sources (radiosondes, thermosondes, in situ measurements) are recommended.

## **2.3 AEROSOL MODELS**

### **2.3.1 Introduction**

The aerosol models built into MODTRAN 2 have been completely revised from the earlier versions of the LOWTRAN code. Earlier versions of LOWTRAN (before LOWTRAN 5) used the same model for aerosol composition and size distribution at all altitudes, simply changing the concentrations of the aerosols with height which means that the wavelength dependence of the aerosol extinction was independent of altitude.

The variation of the aerosol optical properties with altitude is now modeled by dividing the atmosphere into four height regions each having a different type of aerosol. These regions are the boundary or mixing layer (0 to 2 km), the upper troposphere (2 to 10 km), the lower stratosphere (10 to 30 km), and the upper atmosphere (30 to 100 km).

The earlier versions of LOWTRAN neglected changes in aerosol properties caused by variations in relative humidity. These aerosol models were representative of moderate relative humidities (around 80 percent). The models for the troposphere (rural, urban, maritime and tropospheric) which were previously used in earlier LOWTRAN models have been updated according to more recent measurements and also are now given as a function of the relative humidity. In addition, a wind-dependent

desert aerosol model, a new background stratospheric aerosol model and two new cirrus cloud models have been introduced into the program.

Only a brief description of the aerosol models and their experimental and theoretical bases will be presented in this report since they are described more fully elsewhere (see Shettle and Fenn<sup>60</sup>).

### 2.3.2 Vertical Distribution in the Lower Atmosphere

The range of conditions in the boundary layer (up to 2 km) is represented by four different aerosol models (rural, urban, maritime or desert) for each of several meteorological ranges\* between 2 and 50 km, and as a function of humidity. In the boundary layer the shape of the aerosol size distribution and the composition of the three surface models are assumed to be invariant with altitude. Therefore, only the total particle number is being varied. Although the total number density of air molecules decreases approximately exponentially with altitude, there is considerable experimental data which show that the aerosol concentration very often has a rather different vertical profile. One finds that, especially under moderate to low visibility conditions, the aerosols are concentrated in a uniformly mixed layer from the surface up to about 1 to 2 km altitude and that this haze layer has a rather sharp top, which appears to be associated with the height of the minimum temperature lapse rate<sup>63</sup>.

The vertical distribution for clear to very clear conditions, or meteorological ranges from 23 and 50 km, is taken to be exponential, similar to the profiles used in previous

\* The terms "meteorological range" and "visibility" are not always used correctly in the literature. Correctly <sup>61,62</sup> visibility is the greatest distance at which it is just possible to see and identify with the unaided eye: (a) in the daytime, a dark object against the horizon sky; and (b) at night, a known moderately intense light source. Meteorological range is defined quantitatively, eliminating the subjective nature of the observer and the distinction between day and night. Meteorological range  $V$  is defined by the Koschmieder formula

$$V = 1/\beta \ln 1/\epsilon = 3.912/\beta$$

where  $\beta$  is the extinction coefficient, and  $\epsilon$  is the threshold contrast, set equal to 0.02. As used in the MODTRAN computer code, the inputs are in terms of meteorological range, with  $\beta$ , the extinction coefficient, evaluated at 0.55  $\mu\text{m}$ . If only an observer visibility  $V_{\text{obs}}$  is available, the meteorological range can be estimated as  $V \approx (1.3 \pm 0.3) * V_{\text{obs}}$ .

versions of LOWTRAN. However, for the hazy conditions (10-, 5-, and 2-km meteorological ranges) the aerosol extinction is taken to be independent of height up to 1 km with a pronounced decrease above that height.

Above the boundary layer in the troposphere the distribution and nature of the atmospheric aerosols becomes less sensitive to geography and weather variations. Instead, the seasonal variations are considered to be the dominating factor. The aerosol concentration measurements of Blifford and Ringer<sup>64</sup> and Hoffman et al<sup>65</sup> indicate that there is an increase in the particulate concentration the upper troposphere during the spring and summer months. This is also supported by an analysis of searchlight data by Elterman et al.<sup>66</sup>

The vertical distribution of the aerosol concentrations for the different models is shown in Figure 12. Between 2 and 30 km, where a distinction on a seasonal basis is made, the spring-summer conditions are indicated with a solid line and fall-winter conditions are indicated by a dashed line.

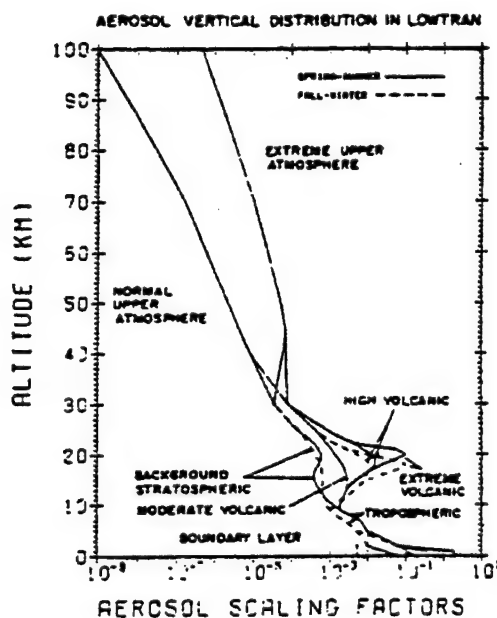


Figure 12a. Vertical Profiles of Aerosol Scaling Factors vs Altitude

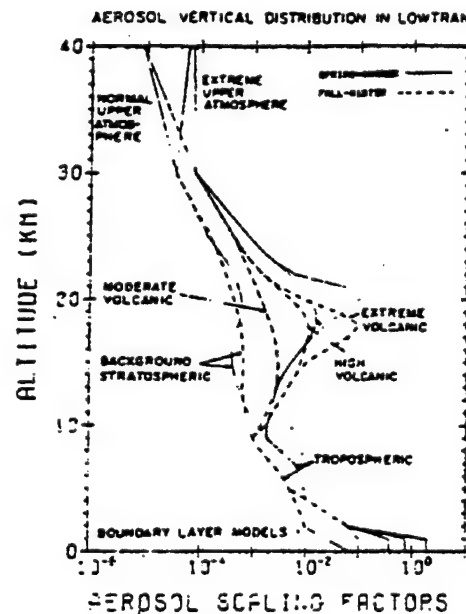


Figure 12b. Vertical Profiles of Aerosol Scaling Factors vs Altitude with the Region from 0 to 40 km Expanded

### 2.3.2.1 Use of Aerosol Vertical Profiles in MODTRAN

**Introduction:** The aerosol attenuation coefficients,  $\beta_{atn}(z, \lambda)$ , as a function of altitude,  $z$ , and wavelength,  $\lambda$ , in the MODTRAN/LOWTRAN/FASCODE propagation models are generated as a product of an altitude dependent aerosol concentration,  $s(z)$ , and a wavelength dependent aerosol attenuation,  $k_{atn}(\lambda)$ :

$$\beta_{atn}(z, \lambda) = s(z) \bullet k_{atn}(\lambda) \quad (25)$$

Where 'atn' represents 'ext' or 'abs' for the extinction or absorption respectively. [The codes calculate the scattering coefficients as the difference of the extinction and absorption coefficients,  $\beta_{scat}(z, \lambda) = \beta_{ext}(z, \lambda) - \beta_{abs}(z, \lambda)$ ]. The altitude-dependent scaling factor,  $s(z)$ , and the normalized attenuation coefficients,  $k_{atn}(\lambda)$ , in principle can be defined in any self-consistent way such that their product gives the attenuation coefficients,  $\beta_{atn}$ , with the correct units,  $[\text{km}^{-1}]$ . The way these are currently implemented in the propagation codes is discussed in the following sections.

**Altitude Dependent Scaling Factor:** As currently implemented in the codes, the scaling factor,  $s(z)$ , is the extinction coefficient at a wavelength of  $0.55 \mu\text{m}$ ,  $[\text{km}^{-1}]$ . It is calculated by Subroutine AERPRF using the data in Block Data PRFDTA. The data in PRFDTA is plotted as a function of altitude in Fig. 7 of the LOWTRAN 5 report<sup>4</sup> (pg 24) and Fig. 18-13 of the Handbook of Geophysics<sup>67</sup> (pg 18-14). The values are also tabulated in the Handbook in Table 18-10a (pg 18-18). The choice of values used depends on the Surface Meteorological Range, VIS (for  $z = 0$  to 5 km), the Season, ISEASN (for  $z = 2$  to 30 km), and the Volcanic Conditions, IVULCN (for  $z = 9$  to 40 km).

The value of  $s(z)$  at the surface,  $z = 0$ , is related to the meteorological range, VIS, by the Koschmieder formula (see the footnote on pg 26 of LOWTRAN 7):

$$IS = 3.912 / [s(z=0) + \beta_{Ray}] \quad (26)$$

where  $\beta_{Ray}$  is the Rayleigh scattering ( $\approx 0.012 \text{ km}^{-1}$ ) at the surface for a wavelength of  $0.55 \mu\text{m}$ . This leads to the following expression for  $s(0)$ :

$$s(0) = (3.912/VIS) - \beta_{Ray} \equiv \beta_{ext}(0, 0.55) \quad (27)$$



**Wavelength-Dependent Normalized Attenuation Coefficients:** The normalized extinction or absorption coefficients,  $k_{\text{ext}}(\lambda)$  or  $k_{\text{abs}}(\lambda)$ , are currently stored as the [unitless] ratios of the aerosol model dependent attenuation coefficients to the extinction coefficient at a wavelength of  $0.55 \mu\text{m}$  for that model:

$$k_{\text{ext}}(\lambda) = \text{Ext}(\lambda) / \text{Ext}(\lambda = 0.55 \mu\text{m}) \text{ and } k_{\text{abs}}(\lambda) = \text{Abs}(\lambda) / \text{Ext}(\lambda = 0.55 \mu\text{m}) \quad (28)$$

[Note with this definition,  $k_{\text{ext}}(\lambda=0.55\mu\text{m})=1.0$ ]. The appropriate values of  $k_{\text{ext}}(\lambda)$  and  $k_{\text{abs}}(\lambda)$  are chosen by Subroutine EXABIN, using the data in Block Data EXTDTA.

A different aerosol model, (with differing wavelength dependencies), is used for each of 4 altitude regions; the Boundary Layer, (0 to 2 km); the Free Troposphere, (2 to 9 km); the Lower Stratosphere, (9 to 30 km); and the Upper Atmosphere, (30 to 100 km {120 km in FASCODE}).

The choice, of which aerosol models are used within each of the 4 altitude regions, is controlled by IHAZE (within the 'Boundary Layer') and by IVULCN (within the 'Lower Stratosphere'). The Tropospheric Aerosol Model is always used within the 'Free Troposphere', (unless overridden by the user when specifying their own model atmosphere, by their choice for IHA 1, on Card 2C3). Similarly the Meteoric Dust Aerosol Model is always used within the 'Upper Atmosphere', (unless overridden by a user specified aerosol profile).

**Asymmetry Parameter and Phase Function:** The values used for the asymmetry parameter,  $g$ , and the phase function,  $P(\theta)$ , are determined by the choice of aerosol model for given altitude region and by the wavelength. They are independent of altitude within that altitude region.

**User Defined Aerosol Profiles And Attenuation Coefficients:** If the user specifies their own vertical distributions of aerosol concentration or their own aerosol attenuation coefficient models, they must do so consistently with the way these quantities are utilized by the propagation codes as discussed above. Thus the user specified values of AHAZE on 80-byte formatted record 2C3 (when MODEL = 7), should be the aerosol (or cloud) extinction at a wavelength of  $0.55 \mu\text{m}$ , with units of  $\text{km}^{-1}$ . If the user instead provides the equivalent liquid water content, EQLWCZ (in  $\text{gm}/\text{m}^3$ ), the codes internally compute the proper values for AHAZE. If the user provides their own aerosol attenuation model with 80-byte formatted records 2D, 2D1, and 2D2, the values of the normalized extinction and absorption coefficients, EXTC and ABSC, must follow the specification of Eq. (26), for  $k_{\text{ext}}(\lambda)$  and  $k_{\text{abs}}(\lambda)$ .



The one exception to this is if the user provides their own values for *both* the aerosol scaling factor,  $s(z)$ , with AHAZE, and the normalized attenuation coefficients,  $k_{atn}(\lambda)$ , with EXTC and ABSC. In this case, as long as AHAZE and both EXTC & ABSC are specified in a self-consistent manner so that their product, the aerosol attenuation coefficients,  $\beta_{atn}(z, \lambda)$ , as a function of altitude,  $z$ , and wavelength,  $\lambda$ , (as given by Eq. 25) has units of  $\text{km}^{-1}$ . So for example, the 'scaling factor',  $s(z)$ , *could be* given as the aerosol number density per volume or the aerosol mass per volume, with the 'normalized attenuation coefficient',  $k_{atn}(\lambda)$ , being the attenuation cross-section per aerosol particle or the attenuation cross-section per unit mass respectively.

### 2.3.3 Effects of Humidity Variations on Aerosol Properties

The basic effect of changes in the relative humidity on the aerosols, is that as the relative humidity increases, the water vapor condenses out of the atmosphere onto the existing atmospheric particulates. This condensed water increases the size of the aerosols, and changes their composition and their effective refractive index. The resulting effect of the aerosols on the absorption and scattering of light will correspondingly be modified. There have been a number of studies of the change of aerosol properties as a function of relative humidity<sup>60,68</sup>. The most comprehensive of these, especially in terms of the resulting effects on the aerosol properties is the work of Hanel<sup>68,69</sup>.

The growth of the particulates as a function of relative humidity, is based on the results tabulated by Hanel<sup>68</sup> for different types of aerosols. Once the wet aerosol particle size is determined, the complex refractive index is calculated as the volume-weighted average of the refractive indices of the dry aerosol substance and water<sup>70</sup>.

#### 2.3.3.1 Rural Aerosols

The "rural model" is intended to represent the aerosol conditions one finds in continental areas which are not directly influenced by urban and/or industrial aerosol sources. This continental, rural aerosol background is partly the product of reactions between various gases in the atmosphere and partly due to dust particles picked up from the surface. The particle concentration is largely dependent on the history of the air mass carrying the aerosol particles. In stagnating air masses, for example, under winter-type temperature inversions, the concentration may increase to values causing the surface layer visibilities to drop to a few kilometers.

The rural aerosols are assumed to be composed of a mixture of 70 percent of water-soluble substance (ammonium and calcium sulfate and also organic com-

pounds) and 30 percent dust-like aerosols. The refractive index for these components is based on the measurements of Volz.<sup>71,72</sup>

The rural aerosol size distribution is parameterized as the sum of two log-normal size distributions, to represent the multi-modal nature of the atmospheric aerosols that have been discussed in various studies. These parameters for rural model size distribution fall within what Whitby and Cantrell<sup>73</sup> give as a typical range of values for the accumulation (small) and coarse (large) particle modes.

To allow for the dependence of the humidity effects on the size of the dry aerosol, the growth of the aerosol was computed separately for the accumulation and coarse particle components. In computing the aerosol growth, changes in the width of the size distribution was assumed negligible so only the mode radius was modified by humidity changes. The effective refractive indices for the two size components are then computed as function of relative humidity.

Using Mie theory for scattering by spherical particles, the extinction and absorption coefficients for each of several different relative humidities were calculated. Figure 13

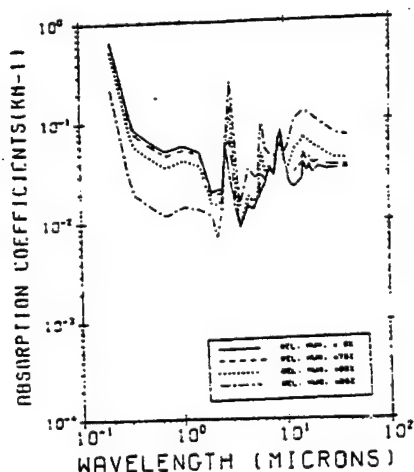


Figure 13a. Extinction Coefficients for the Rural Aerosol Model (Normalized to 1.0 at 0.55  $\mu\text{m}$ )

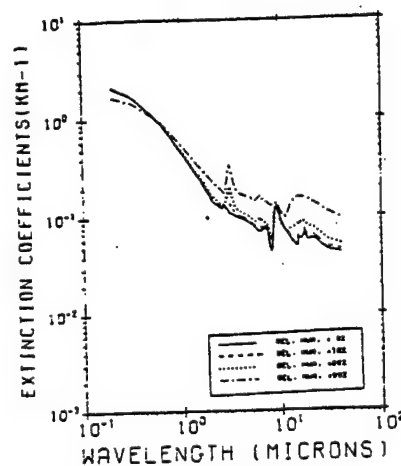


Figure 13b. Absorption Coefficients for the Rural Aerosol Model Corresponding to Figure 13a.

shows the resulting values for the different relative humidities which are stored in the MODTRAN code. The values have been normalized to an extinction coefficient of 1.0 at a wavelength of 0.55  $\mu\text{m}$ , which is the method used within the program.

### 2.3.3.2 Urban Aerosol Model

In urban areas the rural aerosol background gets modified by the addition of aerosols from combustion products and industrial sources. The urban aerosol

model therefore was taken to be a mixture of the rural aerosol with carbonaceous aerosols. The soot like aerosols are assumed to have the same size distribution as both components of the rural model. The proportions of the soot like aerosols and the rural type of aerosol mixture are assumed to be 20 percent and 80 percent respectively. The refractive index of the soot like aerosols was based on the soot data in Twitty and Weinman's<sup>74</sup> survey of the refractive index of carbonaceous materials.

Figure 14 shows the extinction and absorption coefficients for the urban models vs wavelength. As with the rural model the values are normalized so the extinction coefficient is 1.0, at a wavelength of 0.55  $\mu\text{m}$ .

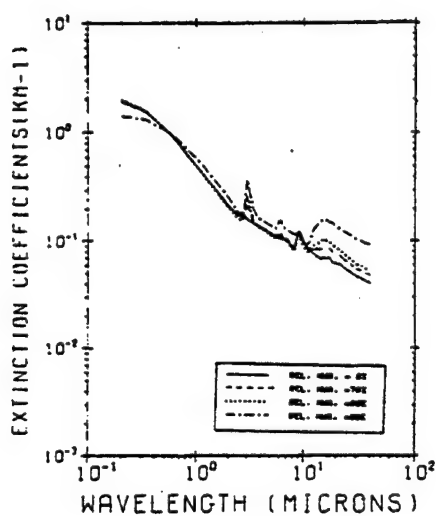


Figure 14a. Extinction Coefficients  
for the Urban Aerosol Model  
(Normalized to 1.0 at 0.55  $\mu\text{m}$ )

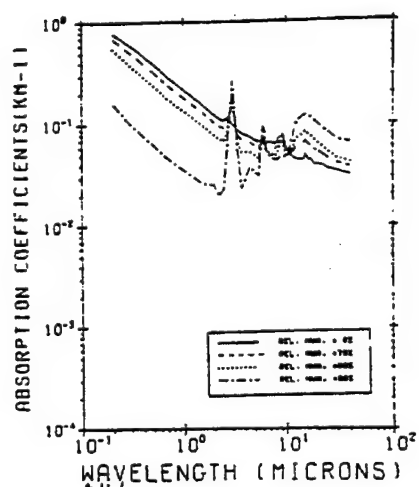


Figure 14b. Absorption Coefficients  
for the Urban Aerosol Model  
Corresponding to Figure 14a

### 2.3.3.3 Maritime Aerosol Model

The composition and distribution of aerosols of oceanic origin is significantly different from continental aerosol types. These aerosols are largely sea-salt particles which are produced by the evaporation of sea-spray droplets and then have continued growing due to accretion of water under high relative humidity conditions. Together with a background aerosol of more or less pronounced continental character, they form a fairly uniform maritime aerosol which is representative of the boundary layer in the lower 2 to 3 km of the atmosphere over

the oceans, but which also will occur over the continents in a maritime air mass. This maritime model should be distinguished from the direct sea-spray aerosol which exists in the lower 10 to 20 meters above the ocean surface and which is strongly dependent on wind speed .

Therefore, the maritime aerosol model has been composed of two components: one which developed from sea-spray; and a continental component which is assumed identical to the rural aerosol with the exception that the very large particles were eliminated, since they will eventually be lost due to fallout as the air masses move across the oceans. This model is similar to the one suggested by Junge<sup>75,76</sup> and is supported by a large body of experimental data.<sup>60</sup>

The refractive index is the same as that for a solution of sea salt in water, using a volume-weighted average of the refractive indices of water and sea salt. The

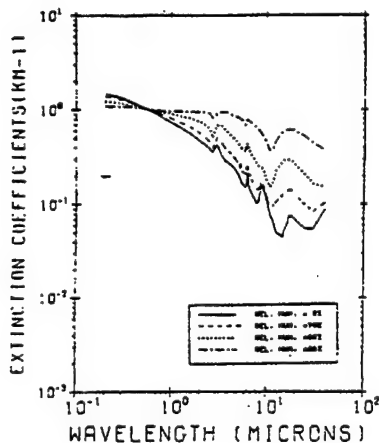


Figure 15a. Extinction Coefficients for the Maritime Aerosol Model (Normalized to 1.0 at 0.55 $\mu$ m)

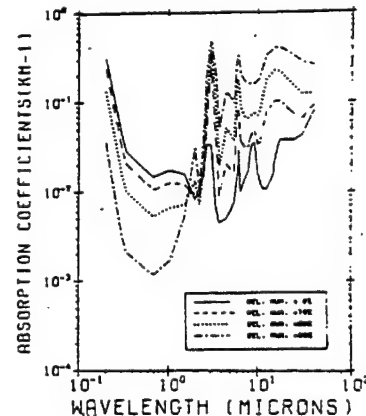


Figure 15b. Absorption Coefficients for the Maritime Aerosol Model Corresponding to Figure 15a.

refractive index of the sea salt is primarily taken from the measurements of Volz.<sup>77</sup> The normalized extinction and absorption coefficients vs wavelength for the maritime aerosols are shown in Figure 15 for several relative humidities.

#### 2.3.3.4 Tropospheric Aerosol Model

Above the boundary layer in the troposphere, the aerosol properties become more uniform and can be described by a general tropospheric aerosol model. The tropospheric model represents an extremely clear condition and can be represented by the rural model without the large particle component. Larger

aerosol particles will be depleted due to settling with time. This is consistent with the changes in aerosol size distribution with altitude suggested by Whitby and Cantrell.<sup>73</sup>

There is some indication from experimental data, that the tropospheric aerosol concentrations are somewhat higher during the spring-summer season than during the fall-winter period.<sup>64,65</sup> Different vertical distributions are given to represent these seasonal changes (see Section 2.3.2).

The dependence of the particle size on relative humidity is the same as for the small particle component of the rural model. The resulting normalized extinction and absorption coefficients are shown in Figure 16 for the different relative humidities.

### 2.3.3.5 Fog Models

When the air becomes nearly saturated with water vapor (relative humidity close to 100 percent), fog can form (assuming sufficient condensation nuclei are present). Saturation of the air can occur as the result of two different processes; the mixing of air masses with different temperatures and/or humidities (advection fogs), or by cooling of the air to the point where the temperature approaches the dew-point temperature (radiation fogs).<sup>78</sup>

To represent the range of the different types of fog, we chose two of the fog models presented by Silverman and Sprague,<sup>79</sup> following the work of Dyachenko.<sup>80</sup> These were chosen to represent the range of measured size distributions, and correspond to what Silverman and Sprague<sup>79</sup> identified as typical of radiation fogs and advection fogs. They also describe developing

and mature fogs, respectively. The normalized extinction and absorption coefficients for the two fog models are shown in Figure 17 as a function of wavelength.

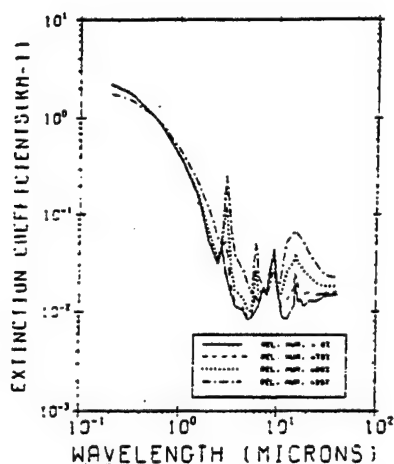


Figure 16a. Extinction Coefficients for the Tropospheric Aerosol Model (Normalized to 1.0 at 0.55 $\mu$ m)

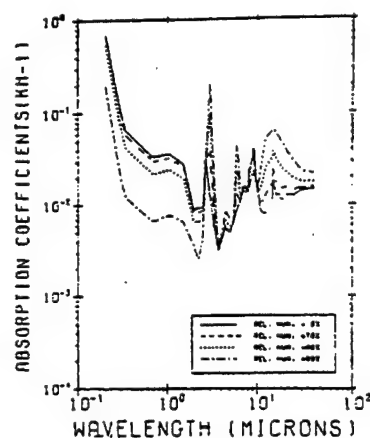


Figure 16b. Absorption Coefficients for the Tropospheric Aerosol Model Corresponding to Figure 16a

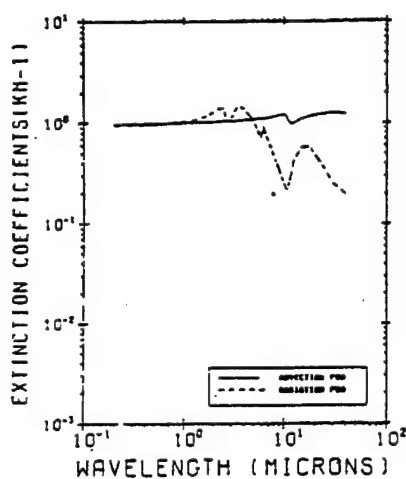


Figure 17a. Extinction Coefficients for the Fog Models (Normalized to 1.0 at 0.55 $\mu$ m)

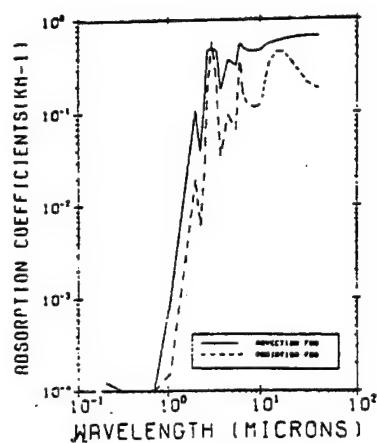


Figure 17b. Absorption Coefficients for the Fog Models Corresponding to Figure 17a

### 2.3.3.6 Wind Dependent Desert Aerosol Model

This synopsis of the wind dependent desert aerosol model is based on the Longtin, et al,<sup>81</sup> report. For a comprehensive description of the desert aerosol model please refer to that report.

Aerosols can be found throughout the atmosphere. They can have a role in cloud formation and precipitation processes and plus they can have an impact on the

radiation balance of the earth-atmosphere system. The radiative impact will depend on the size, shape and composition of the aerosols, as well as their spatial distribution in the atmosphere and the nature of the underlying surface.

Aerosols can be separated into a set of generic categories based primarily on their (spatial) location in the atmosphere. Each aerosol "type" has its own characteristic optical properties that distinguish it from other aerosols. For most aerosol types, a set of parameters exist for calculating aerosol radiative properties with reasonable accuracy.

An important aerosol type is the desert aerosol which is representative of arid and semi-arid regions. The desert aerosol model is included because about one-third of the earth's land surface area consists of arid and semi-arid terrain and because the radiative effects of desert aerosols are important during dust storm conditions. In addition, the source regions of desert aerosols have high solar insolation and strong convective processes that enable the particles to be lifted to altitudes where synoptic-scale air motions can transport the particles well beyond their source regions.

A tentative desert aerosol model was developed<sup>82</sup> for use in the Phillips Laboratory's Geophysics Directorate's atmospheric propagation models. This model was based primarily on recommendations from a meeting of experts conducted by the World Climate Research Programme<sup>83</sup>. The current desert aerosol model contains many improvements over the original Shettle model.

### PHYSICAL PROPERTIES OF DESERT AEROSOLS

The desert aerosol model that has been recommended by the World Climate Research Programme and utilized by Shettle is based on a limited data set. The formulation uses data that were obtained primarily in the Middle East, although measurements from other arid and desert locations have been included. Table 3 provides a partial listing of measurements<sup>84-94</sup> that relate to the physical properties of aerosols in arid or desert environments.

**Table 3. Summary of Aerosol Measurements for Arid or Semi-Arid Environments**

LOCATION	Period of Measurements	Measurement	Reference
		Type	

Central Sahara	Feb 1979-Feb 1982	SD	d'Almeida and Schutz <sup>84</sup>
Haswell, Colorado	Unknown	SD	Patterson and Gillette <sup>85</sup>
Plains, Texas	Unknown	SD	Patterson and Gillette <sup>85</sup>
Camp Derj and Sebha, Libya	Unknown	SD	Schutz and Jaenicke <sup>86</sup>
Mitzpe Ramon	Winter and Early Spring	SD, RAD	Levin and Lindberg <sup>87</sup>
Negev, Israel	1976	Comp	
Beer-Sheva, Israel	June 1977 - May 1978	Comp, TML	Kushelevsky et al. <sup>88</sup>
Arizona and Utah	June - July 1979	Comp, TML	Cahill et al. <sup>89</sup>
Namib Desert	Nov 1976 - April 1977	Comp	Annegarn et al. <sup>90</sup>
Tularosa Basin, NM	Aug 1984 - Aug 1985	Comp, SD	Pinnick et al. <sup>91</sup>
Mitzpe Ramon	Dust Storm on 6 June	SD, RAD	Levin et al. <sup>92</sup>
Negev, Israel	1977		
Grand Canyon, AZ	Dec 1979 - Nov 1981	TML, RAD	Malm and Johnson <sup>93</sup>
Iran and Pakistan	Unknown	RAD	Otterman et al. <sup>94</sup>

\* KEY: SD - Size Distributions, Comp - Composition, RAD - Radiative Measurements  
TML - Total Mass Loadings

### Source Regions and Transport Characteristics

Desert aerosols have been measured at great distances from their source regions. Saharan aerosols have been measured well into the tropical North Atlantic<sup>95,96</sup> and in Mediterranean countries<sup>97-99</sup>.

Desert aerosols originating from Asian deserts have been measured in the Hawaiian Islands<sup>100</sup>. The bulk aerosols in the lower few kilometers of the troposphere over the tropical North Atlantic consist primarily of sea-salt aerosols and mineral aerosols originating from the arid and semi-arid regions of West Africa<sup>95</sup>. These measurements indicate that the aerosols at a given location are not necessarily representative of the underlying soils. d'Almeida and Schutz<sup>84</sup> have shown from their data of soil samples and aerosol samples from across the Sahara desert that the aerosols are largely made up of crustal material that are representative of loose and finely grained soils. They state that flood plains near mountains offer probable production source areas for desert aerosols rather than dune-like deposits. These



results are consistent with those of Chester et al.<sup>99</sup> who performed an elemental analysis of aerosols from over the Tyrrhenian Sea. Their data indicated that the aerosols are characteristic of crystal material rather than from dune areas.

### Size Distributions

Aerosol size distributions are often modeled by the sum of two or three log normal distributions,

$$\frac{dN(r)}{d \log r} = \sum_{i=1}^{2,3} \frac{N_i}{(2\pi)^{1/2} \log \sigma_i} \exp \left( -\frac{[\log(r/R_i)]^2}{2(\log \sigma_i)^2} \right) \quad (29)$$

where  $N(r)$  is the particle concentration for particles greater than a given radius  $r$ ,  $N_i$  is the total number of particles for the distribution  $i$ ,  $\sigma_i$  is the geometric standard deviation and  $R_i$  is the geometric mean radius. The individual distributions are often meant to represent different size classifications that are representative of different production processes. Three size ranges; ( $10^{-7} < r < 10^{-5}$  cm;  $10^{-5} < r < 10^{-4}$  cm; and  $r > 10^{-4}$  cm) are typically used to describe aerosols in the atmosphere (see reference 83). The size ranges are referred to, respectively, as the Aitken or nucleation mode, the large or accumulation mode and the giant or coarse mode.

Based on an analysis of tropospheric aerosol measurements, Patterson and Gillette<sup>85</sup> characterized the distributions with three modes that they referred to respectively as, modes C, A, and B. Mode C represents particles centered at about 0.02 - 0.5  $\mu\text{m}$  and is representative of background aerosols. Mode A particles cover the radius range of 1 - 10  $\mu\text{m}$  and consist of particles produced from the parent soil by a sandblasting process. This component of the size distribution is determined by the lifting force of the local winds. Mode B particles peak at about 30  $\mu\text{m}$  radius and are primarily found when the wind speed is high and the dust loading is significant. Under heavy dust loading conditions, Patterson and Gillette found that only modes A and B were present as a result of soil erosion and sandblasting along with the subsequent injection of this material into the atmosphere. These results suggest that different size distribution formulations are needed to describe background desert and dust storm conditions.

The size distributions used in the tentative AFGL desert aerosol model, which were based on recommendations from the World Climate Research Programme, are shown in Table 4.

**Table 4. Parameters Used in the Background Desert and Desert Dust Storm Aerosol Models**

MODEL	i	N <sub>i</sub> (cm <sup>-3</sup> )	log (σ <sub>i</sub> )	R <sub>i</sub> (μm)
Background	1	997	0.328	0.0010
	2	842 4	0.505	0.0218
	3	7.10 * 10 <sup>-4</sup>	0.277	6.24
Dust Storm	1	726	0.247	0.0010
	2	1,140	0.770	0.0188
	3	1.78 * 10 <sup>-1</sup>	0.438	10.8

These values are based primarily on measurements<sup>95,101,102</sup> from the Sahara desert. For calm (or background) conditions, the parameters are similar to those for "remote continental aerosols." The parameters for the dust storm conditions are based on the work of Schutz and Jaenicke<sup>86</sup>, Jaenicke and Schutz<sup>101</sup> and d'Almeida and Jaenicke<sup>102</sup>. The major difference between the model for background and dust storm conditions is in the number of large particles in mode 3, the component associated with large particles that are injected by high winds. Therefore, the values for the dust storm model represent extreme values and should be linked to wind velocity.

### Composition

Compositional measurements indicate that desert aerosols are a mixture of different kinds of materials. Desert aerosols consist of a background component and a component representative of local soil sources. Depending upon location, desert aerosols can also have an anthropogenic component.

Simple visual examination of desert dust reveals many of the particles to have a light brown to tan appearance<sup>87</sup>, unlike urban aerosols that are generally gray or black. Elements commonly found in desert aerosols<sup>87-91</sup> include sodium, calcium, silicon, aluminum and sulfur. Silicon, presumably in the form of quartz and calcium, appear to be the most common elements in the desert aerosol<sup>87,88</sup>. The five most common

elements found by Kushelevsky et al.<sup>88</sup> were calcium, silicon, sulfur, iron and chlorine. Calcium, silicon and iron are primarily crustal in nature while sulfur and chlorine can have both crustal and industrial sources. Chlorine can also be derived from sea spray<sup>90</sup>.

Particles with radii less than about 0.4  $\mu\text{m}$  appear to have a large ammonium sulfate and ammonium bisulfate component while larger particles have quartz, clay components and other elements associated with soil or crustal sources<sup>89,90,91,99</sup>.

Generally speaking, desert aerosols are not hygroscopic. The only exception to this is a "well aged" desert aerosol in which the background component has acted as a condensation nuclei as a result of numerous trips up and down through the desert atmosphere.

Abundance's of the elements can vary from sample to sample as a function of wind speed (i.e., increased mass loading) and wind direction (i.e., source region). Cahill et al.<sup>89</sup> observed a seasonal variation in the amount of silicon particulate in samples collected in Arizona and Utah. Their results, which consisted of one year of data, indicated that for particles in the range 3.5 to 15  $\mu\text{m}$ , the silicon abundance increased to a maximum in the spring and then decreased to a minimum in the winter. Table 5, from Kushelevsky et al.<sup>88</sup> summarizes how the abundance's of these elements can vary on a day-to-day basis and when averaged over different meteorological conditions.

Carbon is generally found in very small abundance's in desert aerosols. However, due to its strong absorption, a small increase in the carbon amount, as little as 1%, can lead to a large increase in the total absorption properties of desert aerosols.

**Table 5.** Variation of Elemental Concentrations in Middle Eastern Desert Aerosols as (a) A Function of Source Region and (b) Averaged Over Meteorological Conditions. Measurements were made by Kushelevsky et al. at Beer-Sheva, Israel using Instrumental Neutron Activation Analysis and X-ray Fluorescence

(a)

WIND DIRECTION	MEAN WIND SPEED	TOTAL SUSPENDED PARTICULATE ~	NOTES	ELEMENTAL CONCENTRATIONS (%)				
	~( m s <sup>-1</sup> )	( g m <sup>-3</sup> )		Ca	Si	S	Fe	Cl
W-E	2.04	291		10	9	2	2	2
N-W	2.01	243		18	13	2	2	1

N-W	1.85	160		14	13	4	2	2
W-E	1.67	36	Rain	1	5	4	1	4
NW-E	2.29	104	Rain	9	11	3	2	2
W-SE	1.83	50	Rain	19	20	5	4	7
N-E	4.59	581	Dust Storm	18	21	1	3	0.4
W-SW	2.00	610	Dust Storm	17	18	1	2	1
W	2.73	1600	Dust Storm	22	17	0.3	2	0.1
N-E	2.25	613	Sharav	15	19	1	2	1
E-SE-E	2.87	412	Sharav	17	23	1	3	1
W Variable	3.16	5080	Sharav	16	18	0.2	3	0.2

(b)

METEOROLOGICAL	ELEMENTAL CONCENTRATIONS (%)				
CONDITIONS	Ca	Si	S	Fe	Cl
Normal	12.2	11.5	3.1	1.9	2.5
Rain	12.6	14.6	4.5	2.4	3.6
Dust Storm	16.8	18.0	0.6	2.4	0.5

Note: Sharav, or Khamsin, is a Dust Storm Characterized by Hot Winds from the North African Desert.

It Typically Occurs During the Period Between Easter and Pentecost

### Effects of Wind

Enormous amounts of clay and sand can be loaded into the desert atmosphere during windy conditions. During calm conditions the desert aerosol resembles aerosols other than that which would be produced from the underlying soil. In particular, Patterson and Gillette<sup>85</sup> have studied the composition of the desert aerosol in light, medium and heavy mass loading conditions and have found that particles having radii between 0.02 and 0.5  $\mu\text{m}$  were generally grey or black and represented the global background aerosol. Furthermore, these particles were always present in the same amount regardless of the amount of mass loading. Similar findings reported in the World Climate Programme study confirmed that under very calm conditions the composition of the desert aerosol resembles that of a remote continental aerosol.

Local wind conditions provide the mechanism to inject and transport aerosols. Wind also provides a mechanism for the generation of additional aerosols via a sandblasting process. The amount of aerosol injection and generation depends upon factors such as wind speed<sup>103,104</sup>, soil moisture, and the extent of vegetation<sup>105</sup>, soil texture and the amount of soil crusting<sup>106</sup>.

Soil movement as a result of aerodynamic forces occurs for wind speeds above a given threshold value. This wind speed threshold will vary as a function of soil condition and on the amounts of non-erodible elements, such as rocks and pebbles, on top of the soil. Utilizing a portable wind tunnel, Gillette<sup>104</sup> examined the threshold velocities for three different kinds of soils, two types of desert soil and one farmland soil. A relatively smooth desert soil had a threshold velocity of  $34.2 \text{ cm s}^{-1}$  while one with a pebble covering had a threshold velocity of  $121.9 \text{ cm s}^{-1}$ .

The size distribution of the aerosols that are injected into the air as a result of wind erosion has been found to be similar to that of the underlying soil<sup>105</sup>.

### Indices of Refraction

The index of refraction characterizes the optical properties of a particular material. It can be expressed as the complex number:

$$m = n + ik, \quad (30)$$

where  $n$  and  $k$  are related to the phase velocity and attenuation, respectively, of an electromagnetic wave as it passes through the material. In general, the index of refraction of a material will not be the same for all wavelengths of radiation.

#### 2.3.4 Vertical Distribution in the Stratosphere and Mesosphere

Measurement programs carried out over many years show that in the 10- to 30-km region there exists a background aerosol in the stratosphere which has a rather uniform global distribution. This background aerosol is considered to be mostly composed of sulfate particles formed by photochemical reactions.

These background levels are occasionally increased by factors of 100 or more due to the injection of dust from massive volcanic eruptions. Once such particles have been injected into the stratosphere they are spread out over large portions of the globe by the stratospheric circulation and diffusion processes, and it requires months or even years for them to become slowly removed from the stratosphere.<sup>107-109</sup>

There occurs also a seasonal and geographic variation of the stratospheric aerosol layer which is related to the height of the tropopause; a peak in the aerosol mixing ratio (that is, ratio of aerosol to air molecules) occurs several kilometers above the tropopause.<sup>65,110</sup>

The range of possible vertical distributions is represented by four different profiles (background stratospheric, moderate, high and extreme volcanic). Each of these

distributions is then modified according to the season. The different scaling factors for these vertical profiles are shown in Figure 11.

The vertical distribution in the upper atmosphere above 30 to 40 km is very uncertain because of the difficulty of obtaining reliable data. In situ measurements are limited to those obtained by rocket flights, and these altitudes are beyond the normal operational range of most lidar and searchlight systems which provide most of the remotely sensed data up to 30 or 40 km.

The most likely profile for this region is the one labeled as "Normal Upper Atmosphere" in Figure 11; it corresponds to a constant turbidity ratio of  $\approx 0.2$  above 40 km. This agrees with the aerosol extinction profile obtained by Cunnold et al<sup>111</sup> by inverting measurements of the horizon radiance from an X-15 aircraft. Measurements of the solar extinction through the atmospheric limb from the Apollo-Soyuz mission<sup>112</sup> tend to support this model.

Ivlev's<sup>113,114</sup> model for the upper atmosphere is shown as the curve labeled "Extreme Upper Atmosphere" in Figure 11. It is largely based on twilight observations<sup>115</sup> which neglected multiple-scattering effects. As a consequence, the model has to assume very high particulate concentrations in the upper atmosphere in order to be consistent with observations.

Nevertheless, extinction coefficients for the extreme upper-atmospheric model are consistent with the extreme values that have been observed in layers of a few kilometers thickness by lidar, <sup>116,117</sup> inferred from rocket observations of skylight,<sup>118,119</sup> and studies of noctilucent clouds.<sup>120</sup>

#### **2.3.4.1 Improved Background Stratospheric Aerosol Model**

##### **INTRODUCTION**

This is a synopsis of the Background Stratospheric Aerosol Model developed by Hummel et. al. <sup>43</sup>. This is an improved background stratospheric aerosol model in which temperature dependent indices of refraction for H<sub>2</sub>SO<sub>4</sub> have been used with a log normal size distribution. For a complete understanding of this modified model please refer to that document.

Aerosols commonly found at stratospheric altitudes, 10 - 30 km, are a result of photochemical formation involving sulfur compounds. These background aerosols are generally uniform over the globe. The concentrations of these stratospheric aerosols can be increased dramatically following massive volcanic eruptions. Additional sulfur based aerosols can be photochemically created from the sulfur gases in an eruption cloud. Volcanic ash and debris can also be injected into these altitudes.

Three stratospheric aerosol models<sup>601</sup> have been developed for use in the transmittance/radiance models MODTRAN 2 and FASCODE. The three models are for background stratospheric conditions, fresh volcanic aerosols, and aged volcanic aerosols. These models have also been adapted for use in the Standard Radiation Atmosphere (SRA)<sup>121</sup> models.

The background stratospheric aerosol consists of a 75 % solution of sulfuric acid in water. The wavelength dependent index of refraction for the solution is based on laboratory measurements at 300 K<sup>122,123,124</sup>. The indices of refraction for the volcanic ash are based on the measurements of Volz<sup>125</sup>. The size distributions for all three stratospheric aerosols are given by modified gamma distributions. Stratospheric temperatures are well below 300 K. Values of the index of refraction for H<sub>2</sub>SO<sub>4</sub> are now available at 250 K<sup>126</sup> and can be used to calculate temperature dependent indices of refraction for H<sub>2</sub>SO<sub>4</sub> for temperatures appropriate for stratospheric conditions. Also, recent measurements of the size distribution of stratospheric aerosols indicate that a log normal distribution may be more appropriate for stratospheric aerosols than a modified gamma distribution (see p. 30 of Ref <sup>83</sup>).

### Measurements of Stratospheric Aerosols

Two recent major volcanic eruptions have provided researchers with the opportunity to study stratospheric and volcanic aerosols in depth. The eruptions were Mt. St. Helens in 1980 and El Chichon in 1982. In both cases, the eruptions were intensely studied by ground and aircraft based lidars, balloons, aircraft and satellites.

### Lidar Studies

Lidar provides a tool to study particulate matter in the stratosphere. Lidars at various locations around the world have permitted researchers to study the distribution of volcanic materials injected into the stratosphere since the 1970's. The altitude resolution that can potentially be obtained from lidars allows researchers to study both the temporal and spatial details of volcanic eruption clouds. The worldwide network of lidars (e.g. References 127-132) provided extensive coverage of the eruption clouds from the Mount St. Helens and El Chichon eruptions. These lidars have also detected the presence of so-called "mystery clouds", clouds that cannot be traced to the eruption of known volcanoes.

The lidars used for probing the upper troposphere and stratosphere use the lidar backscattering ratio to identify layers of non-molecular scattering. The lidar backscattering ratio as a function of altitude,  $B(z)$ , is given as:

$$B(z) = 1 + f_A(z)/f_M(z) \quad (31)$$

where  $f_A(z)$  is the aerosol backscattering function and  $f_M(z)$  is the molecular backscattering function. A requirement for the use of (31) is the assumption that at some altitude the returned lidar signal is only from molecular scatters. This altitude, often called the matching altitude, is used to determine the atmospheric density profile required to give  $f_M(z)$ . Once this is known, any return greater than that produced by a pure molecular atmosphere is assumed to be from particulates. The matching altitude is generally taken to fall in the 30 km range, although Clemesha and Simonich<sup>129</sup> feel that the matching altitude should be taken at higher altitudes.

Table 6 summarizes results of several lidar studies<sup>128-131&133-137</sup> made under background and volcanic conditions. The studies indicate that a backscatter ratio of between 1.1 and 1.4 is representative of background stratospheric conditions. The backscatter ratio following an eruption is highly variable and depends on the force of the eruption, as measured by the amount of material injected and the height of the eruption cloud, as well as the sulfur content of the eruption cloud.

The lidar studies have detailed the layering of material following volcanic eruptions. The layers are highly dynamic and can change fairly quickly as a result of variations in the stratospheric circulation and as particles settle out.

**Table 6. Summary of Lidar Studies of Background and Volcanic Aerosol Conditions in the Stratosphere**

LOCATION	TIME PERIOD	WAVELENGTH ( $\mu\text{m}$ )	ALTITUDE REGION (km)	AVERAGE BACKSCATTER RATIO
Brazil <sup>131,135</sup> (23°S, 46°W)	July-August 1970	0.589	20	1.4
	1973	0.589	20	1.06 - 1.12
	August 1975	0.589	20	1.28
	April 1976	0.589	20	1.15
	1982	0.589	15 - 20	> 5.0 (Peak)
	May 1978-Apr 1979	0.694	16	1.052 $\pm$ 0.02



	May-June 1979	0.694	16	1.12 - 1.42
Japan	May 1978-Apr 1979	0.694	20	1.116 $\pm$ 0.05
(33°N, 130° E)	Nov 1979	0.532	21	1.05
(Ref 132,133,	Nov 1979	1.064	21	1.46 $\pm$ 0.19
136,137,138)	Dec 1979	0.532	21	1.2 (Peak)
	Dec 1979	1.064	21	2.0 (Peak)
	Apr 1982	0.532	24.5	400 (Peak)
Japan <sup>138</sup>	Apr-July 1982	0.694	24 - 26	44 (peak)
(35° N, 137°E)				
Italy <sup>130</sup>	Sept-Dec 1979	0.589	14 - 20	< 1.2
(42° N, 23° E)	June-July 1980	0.589	14- 20	2.0
Italy <sup>139</sup>	Mar Apr 1982	0.589	15 - 25	1.5 (Peak)
(42° N, 13° E)				

### Balloon Measurements

Hofmann and Rosen have made extensive measurements of background stratospheric<sup>138</sup> and volcanic aerosols<sup>139,140,141</sup> using balloon-borne instruments that can reach altitudes up to about 35 km. Their typical balloon package carries optical particle counters to measure condensation nuclei for particles with radii  $r \geq 0.01 \mu\text{m}$  and a dustsonde for particles with  $r \geq 0.15$  and  $r \geq 0.25 \mu\text{m}$ . A more recent version<sup>140</sup> also carries a large particle counter for  $r > 0.25, 0.95, 1.2$  and  $1.8 \mu\text{m}$ .

The particle size measurements provide integral values of the particle concentrations with sizes greater than or equal to the respective cut-off radii. By taking ratios of these concentrations, a set of size ratios can be obtained that can be related to size distribution.

The balloon packages have also been equipped with an intake heater that heats the air samples to around 150° C. This allows one to distinguish from volatile and nonvolatile aerosols. This technique has identified the volatile aerosols as having an average mixture of 75 %  $\text{H}_2\text{SO}_4$  and 25 %  $\text{H}_2\text{O}$ .

The balloon measurements of background conditions yielded average peak aerosol concentrations that would correspond to back scattering ratios of about 1.09 - 1.17 at  $0.6943 \mu\text{m}$ <sup>142</sup>. These results agree well with the lidar results summarized in Table 6.

Hofmann and Rosen conducted thirty six balloon flights from Laramie, Wyoming (41° N) to study the Mt. St. Helens eruption cloud during the year following the eruption<sup>139</sup>. The Mt. St. Helens eruption cloud was observed as four different layers at different altitudes over the 12 - 24 km region. The cloud was first observed at about 12

- 15 km in the vicinity of the jet stream. After about a week, a layer appeared in the 15 - 18 km range over Laramie. This layer became the main layer from the eruption. Material was also injected into the 18 - 24 km range where the summer stratospheric winds shift from westerlies to easterlies. The third layer was at 18 - 20 km where the winds were shifting and the fourth at 20 - 24 km where the winds were blowing from the east.

Hofmann and Rosen also studied the El Chichon cloud for eighteen months following its eruption<sup>140,141</sup>. Those flights were from Laramie and from locations in southern Texas (27° N - 29°N).

The flights discovered two major layers of aerosols separated by a very clean region. The first was around the tropopause and extended to about 21 km. The second layer was centered around 25 km and was generally about 5 km thick. The two layers may have resulted from two separate eruptions. The lower layer may have resulted from the initial 28 March 1982 eruption while the higher one may have come from the more violent 4 April 1982 eruption.

The upper layer was dominated by larger particles consisting of a mixture of about 80 % H<sub>2</sub>SO<sub>4</sub> and 20 % H<sub>2</sub>O while the lower layer consisted of an aerosol with a concentration of 60 - 65 % sulfuric acid. The difference in acid concentration was due to the warmer temperatures and lower water vapor abundance's in the upper layer.

Table 7 shows the peak aerosol concentrations measured above 20 km from the two locations as a function of time following the eruption. The data displayed only cover three of the size ranges measured. Data from a flight on February 5, 1982 are given as representative of pre-eruption values. The differences between the two locations result from the Texas flights penetrating denser regions of the eruption cloud.

The size distribution determined from balloon measurements taken 45 days after the eruption was bi-modal with mode radii of 0.02 and 0.7  $\mu\text{m}$ . After about June 1982, the production of condensation nuclei (e.g., the curve of  $r \geq 0.01 \mu\text{m}$ ) had essentially ceased and fallen back to pre-eruption values.

**Table 7.** Peak Aerosol Concentrations Above 20 km for Three Size Ranges As a Function of Time After the Eruption of El Chichon as Measured from Laramie, Wyoming and Southern Texas<sup>142</sup>. The data from 2/5/82 are given as representative of pre-eruption values

## PEAK AEROSOL CONCENTRATIONS

DAYS AFTER ERUPTION	$r \geq 0.01 \mu\text{m}$ (# $\text{cm}^{-3}$ )		$r \geq 0.15 \mu\text{m}$ (# $\text{cm}^{-3}$ )		$r \geq 0.25 \mu\text{m}$ (# $\text{cm}^{-3}$ )	
	Wyo	Texas	Wyo	Texas	Wyo	Texas
(2/5/82)	8		0.5		0.1	
2	25		0.8		0.1	
10	50		0.8		0.1	
20	48		0.7		0.1	
40	45		0.65		0.13	
45	700		22		16	
60	38	400	0.6	20	0.16	15
73	400		4.0		1.1	
80	200	160	4.2	16	2.0	13
95	45		8.0		6.0	
100	38	65	5.0	15	3.0	11
110	23		2.0		1.2	
120	24	30	4.0	12	2.8	10
125	24		5.2		4.0	
140	15	12	4.0	11	2.8	0.9
152	10		3.5		2.0	
160	13	13	5.0	11.5	4.0	0.85
178	10		1.8		0.8	
180	11	13.5	2.3	11	1.0	0.8
190	13		10.0		2.0	
200	12	14	7.0	10	2.5	0.7
215	11		4.0		3.0	
220	10		5.0		3.2	
240	10		7.1		5.2	

**Aircraft Measurements**

Extensive aircraft measurements of stratospheric aerosols were made of the Mt. St. Helens and El Chichon eruptions. Flight paths were often chosen to overlap other measurements such as the balloon measurements of Hofmann and Rosen.

**Size Distribution Measurements**

Oberbeck et al <sup>143</sup> collected particles from the Mt. St. Helens eruption cloud for a year using wire impactors flown upon the NASA U-2. The aircraft sampled the stratospheric aerosols at an altitude of 18.3 km, the height where the main aerosol layer eventually formed.

Table 8 shows the sampled aerosol particle concentrations for two size ranges,  $r < 0.15 \mu\text{m}$  and  $r > 0.15 \mu\text{m}$ , for the year following the eruption. In the six months after the

eruption, the total volume of aerosols with radii greater than  $0.03\ \mu\text{m}$  increased. The concentration of particles with radii less than  $0.15\ \mu\text{m}$  decreased while the concentration of particles with radii greater than  $0.15\ \mu\text{m}$  increased. This is consistent with the dispersal of an initially high concentration of small particles and the growth of aerosols by condensation. The aerosol levels returned to normal in about a year.

The El Chichon eruption was studied extensively by aircraft. One series of measurements involved measuring stratospheric size distributions with "Knollenberg" counters<sup>144</sup>. The measurements made prior to the eruption revealed relatively featureless size distributions. The data over the range  $0.1$  to  $1.0\ \mu\text{m}$  revealed particles that were largely  $\text{H}_2\text{SO}_4$ . Their number density varied with altitude from about  $20\ \text{cm}^{-3}$  at  $17\ \text{km}$  to about  $1\ \text{cm}^{-3}$  at  $20\ \text{km}$ .

Flights following the eruption suggested two dominant size modes. The first mode consisted of small particles ( $0.1 - 0.8\ \mu\text{m}$ ) that were primarily  $\text{H}_2\text{SO}_4$  and large particles ( $0.8 - 30\ \mu\text{m}$ ) that were primarily volcanic ash. Later flights indicated that particles up to  $2.0\ \mu\text{m}$  were largely  $\text{H}_2\text{SO}_4$  although some of the particles may have been coated with sulfuric acid.

**Table 8. Aerosol Concentrations From the Mt. St. Helens Eruption Cloud at 18.3 km in two Size Ranges as Measured by Wire Impactor<sup>143</sup>**

DATE	MONTHS AFTER ERUPTION	$r > 0.15\ \mu\text{m}$ ( $\text{cm}^{-3}$ )	$r < 0.15\ \mu\text{m}$ ( $\text{cm}^{-3}$ )
5/20/80	0	2.0	11.0
6/25/80	1	1.8	22.5
7/16/80	2	2.5	18.0
10/29/80	5	3.5	14.0
12/02/80	6.5	4.0	15.0
12/17/80	7	2.5	6.0
4/10/81	12	1.5	3.0

Oberbeck et al<sup>145</sup> also studied the El Chichon eruption cloud with the Ames Wire Impactor. Table 9 summarizes the total aerosol concentrations as measured at different altitudes. The size distribution measured prior to the eruption could be fitted with a log normal distribution with a total concentration of between  $3.4$  and  $4.3\ \text{cm}^{-3}$ , a mode radius of  $0.08\ \mu\text{m}$  and a standard deviation of about  $1.68$ . After the eruption, the

distribution was best represented with two log normal size distributions, an enhanced background of sulfuric acid particles with a larger mode radius and a sedimentation mode consisting of large silicates.

**Table 9. Total Aerosol Concentrations From the El Chichon Eruption Cloud at Various Altitudes as Measured by the Ames Wire Impactor<sup>145</sup>**

DATE	MONTHS AFTER ERUPTION	ALTITUDE (km)	N (cm <sup>-3</sup> )
10/16/81	—	18.3	6.3
5/5/82	1	20.7	3.9
7/23/82	3.5	20.7	7.8
9/23/82	5.5	19.8	13.68
11/4/82	7	20.7	6.2
11/5/82	7	20.7	5.4
12/13/82	8	20.7	7.9

Wilson et al<sup>146</sup> summarized many of the NASA U-2 measurements made at 20 km of aerosol particles less than 2.5  $\mu\text{m}$  in diameter, following the El Chichon eruption. Their results indicated that the background aerosols were dominated by particles with radii smaller than 0.05 or 0.03  $\mu\text{m}$ . Measurements in April and May 1982 indicated significant increases in the sub 0.1  $\mu\text{m}$  aerosol concentration that can only be explained by gas-phase reactions leading to the formation of secondary (non-eruption) aerosols. Measurements in the same size range made in late 1982 showed considerable depletion, suggesting coagulation of small particles to form larger ones.

#### Transmission Measurements

Witteborn et al<sup>147</sup> obtained infrared transmission spectra for the atmosphere above 11 km for latitudes between 2° S and 50° N. The measurements were made in December 1982 when the stratospheric aerosols were still considerably enhanced by the El Chichon eruption. The absorption was obtained by ratioing the transmission at 8.5  $\mu\text{m}$ , where the  $\text{H}_2\text{SO}_4$  absorption is strongest, to the transmission at 12  $\mu\text{m}$ , where the atmospheric transmission is nearly unity. The average absorption per unit air

mass was evaluated at 0.019, of which 0.010 was attributable to the presence of  $\text{H}_2\text{SO}_4$  aerosols. They also reported that the ratio of optical depth at  $8.5\ \mu\text{m}$  to that at  $0.5\ \mu\text{m}$ , obtained by Dutton and DeLuisi<sup>148</sup> was about 0.14 at  $20^\circ\text{N}$ .

### Composition Measurements

Woods and Chuan<sup>149</sup> sampled the El Chichon volcanic cloud using a quartz crystal micro balance (QCM) cascade impactor flown on the NASA U - 2. The QCM collected and classified particles into 10 size intervals from less than  $0.05\ \mu\text{m}$  to greater than  $25\ \mu\text{m}$  diameter. The collected aerosols were then analyzed for composition.

The compositional analysis indicated that the sub-micron particles were largely sulfuric acid droplets. This is contrasted with Mt. Agung in which the primary component was volcanic ash. Their measurements of the sulfuric acid aerosols indicated that they occurred in a relatively narrow size range with diameters from about  $0.08$  to  $0.45\ \mu\text{m}$ . Particles above this range were primarily lithic and magnetic materials from the volcano. Halite particles were also found and were believed to be from a salt dome that was located beneath El Chichon.

Patterson and co-workers have measured the optical properties of volcanic ash in visible wavelengths for ash from Mt. St. Helens<sup>150</sup> and El Chichon<sup>151</sup>. Their studies indicate that the imaginary component of the refractive index of the ash varies from volcano to volcano. The Mt. St. Helens ash had an imaginary component that decreased from about 0.01 at  $0.3\ \mu\text{m}$  to about 0.0015 at  $0.7\ \mu\text{m}$ . The corresponding values for the El Chichon ash were nearly constant at 0.001 over the same wavelength range.

### Parameters of the Background Stratospheric Aerosol Model

Figure 18 shows the extinction, scattering and absorption coefficients of the improved background stratospheric aerosol model. Table 10 lists the radiative parameters for the model at 215 K. Figures 19 (a) to (d) compare the respective parameters against those developed by Shettle and Fenn<sup>60</sup> and used in earlier versions of LOWTRAN and FASCODE.

The extinction coefficients for the model are smaller than those used by Shettle and Fenn. The differences are greatest for wavelengths longer than  $10\ \mu\text{m}$ . The differences are almost entirely due to changes in the absorption coefficient, as shown in Figure 19 (c). The differences in the scattering coefficients and asymmetry parameters are slight.

The changes seen in the new formulation are due almost entirely to the new indices of refraction. Figure 20 compares the extinction coefficients as a function of wavelength

of the new model, against those calculated using the proposed indices of refraction and the old modified gamma size distribution, and versus those calculated using the indices of refraction at 300 K and the proposed log normal size distribution. As shown, the change in indices of refraction is responsible for the majority of the differences.

**Table 10. Radiative Parameters for the Improved Background Stratospheric Aerosol Model at 215 K. The numbers in parentheses are powers of ten**

LAMBDA (μm)	INDEX OF REFRACTION		EXTINCTION (km <sup>-1</sup> )	SCATTERING (km <sup>-1</sup> )	ABSORPTION (km <sup>-1</sup> )	SINGLE	ASYMMETRY PARAMETER
	n <sub>r</sub>	n <sub>i</sub>				SCATTERING ALBEDO	
0.2000	1.526	0.0000	8.5042(-4)	8.5042(-4)	9.9774(-11)	1.000	0.6749
0.2500	1.512	0.0000	8.2526(-4)	8.2526(-4)	7.7618(-11)	1.000	0.6850
0.3000	1.496	0.0000	7.6454(-4)	7.6454(-4)	6.1260(-11)	1.000	0.6943
0.3371	1.484	0.0000	7.0676(-4)	7.0676(-4)	5.3356(-11)	1.000	0.6991
0.4000	1.464	0.0000	5.9964(-4)	5.9964(-4)	4.2364(-11)	1.000	0.7038
0.4880	1.456	0.0000	4.7910(-4)	4.7910(-4)	3.2920(-11)	1.000	0.6944
0.5145	1.454	0.0000	4.4694(-4)	4.4694(-4)	3.0642(-11)	1.000	0.6910
0.5500	1.454	0.0000	4.0980(-4)	4.0980(-4)	2.8160(-11)	1.000	0.6846
0.6328	1.452	0.0000	3.3318(-4)	3.3318(-4)	3.4244(-11)	1.000	0.6694
0.6943	1.452	0.0000	2.8750(-4)	2.8750(-4)	4.1196(-11)	1.000	0.6572
0.8600	1.448	0.0000	1.9352(-4)	1.9352(-4)	2.7574(-10)	1.000	0.6251
1.0600	1.443	0.0000	1.2364(-4)	1.2363(-4)	1.7375(-9)	1.000	0.5861
1.3000	1.432	0.0000	7.3706(-5)	7.3696(-5)	8.6378(-9)	1.000	0.5405
1.5360	1.425	-0.0001	4.6880(-5)	4.6786(-5)	9.4560(-8)	0.998	0.4965
1.8000	1.411	-0.0006	2.8732(-5)	2.8426(-5)	3.0578(-7)	0.989	0.4499
2.0000	1.405	-0.0013	2.0992(-5)	2.0382(-5)	6.1016(-7)	0.971	0.4164
2.2500	1.390	-0.0019	1.4050(-5)	1.3297(-5)	7.5308(-7)	0.946	0.3772
2.5000	1.362	-0.0040	9.6202(-6)	8.2414(-6)	1.3788(-6)	0.857	0.3385
2.7000	1.319	-0.0060	6.9164(-6)	4.9962(-6)	1.9202(-6)	0.722	0.3069
3.0000	1.288	-0.0875	2.7254(-5)	2.9016(-6)	2.4352(-5)	0.106	0.2599
3.2000	1.292	-0.1440	3.9576(-5)	2.6414(-6)	3.6936(-5)	0.067	0.2352

Table 10. (Continued)

LAMBDA ( $\mu\text{m}$ )	INDEX OF REFRACTION		EXTINCTION ( $\text{km}^{-1}$ )	SCATTERING ( $\text{km}^{-1}$ )	ABSORPTION ( $\text{km}^{-1}$ )	SINGLE SCATTERING ASYMMETRY	
	$n_r$	$n_i$				ALBEDO	PARAMETER
3.3923	1.366	-0.1780	4.4846(-5)	3.3360(-6)	4.1510(-5)	0.074	0.2234
3.5000	1.383	-0.1790	4.3322(-5)	3.2514(-6)	4.0072(-5)	0.075	0.2165
3.7500	1.420	-0.1650	3.6740(-5)	2.9738(-6)	3.3766(-5)	0.081	0.2028
4.0000	1.435	-0.1510	3.1134(-5)	2.5120(-6)	2.8622(-5)	0.081	0.1878
4.5000	1.427	-0.1560	2.7706(-5)	1.6342(-6)	2.6072(-5)	0.059	0.1554
5.0000	1.411	-0.1370	2.1660(-5)	1.0347(-6)	2.0624(-5)	0.048	0.1291
5.5000	1.376	-0.1950	2.7660(-5)	6.9628(-7)	2.6964(-5)	0.025	0.1057
6.0000	1.485	-0.1950	2.3758(-5)	7.4808(-7)	2.3010(-5)	0.031	0.0962
6.2000	1.485	-0.1470	1.7405(-5)	6.2782(-7)	1.6777(-5)	0.036	0.0909
6.5000	1.421	-0.0841	9.9074(-6)	3.8906(-7)	9.5182(-6)	0.039	0.0802
7.2000	1.235	-0.1660	1.8893(-5)	1.2362(-7)	1.8769(-5)	0.007	0.0595
7.9000	1.148	-0.4610	5.0566(-5)	2.5844(-7)	5.0306(-5)	0.005	0.0458
8.2000	1.220	-0.7090	7.2532(-5)	5.4006(-7)	7.1992(-5)	0.007	0.0413
8.5000	1.457	-0.8400	6.8040(-5)	6.9298(-7)	6.7348(-5)	0.010	0.0418
8.7000	1.753	-0.8170	5.0772(-5)	7.0854(-7)	5.0062(-5)	0.014	0.0479
9.0000	1.767	-0.6040	3.6972(-5)	4.7534(-7)	3.6496(-5)	0.013	0.0483
9.2000	1.704	-0.5570	3.5158(-5)	3.8212(-7)	3.4776(-5)	0.011	0.0451
9.5000	1.791	-0.7360	4.0840(-5)	4.6384(-7)	4.0378(-5)	0.011	0.0425
9.8000	2.128	-0.4650	1.9955(-5)	4.3004(-7)	1.9525(-5)	0.022	0.0525
10.0000	2.094	-0.3060	1.3457(-5)	3.5238(-7)	1.3105(-5)	0.026	0.0504
10.5910	1.805	-0.2100	1.0871(-5)	1.7696(-7)	1.0694(-6)	0.016	0.0379
11.0000	1.823	-0.4330	2.0778(-5)	1.8759(-7)	2.0590(-5)	0.009	0.0346
11.5000	2.024	-0.1990	7.9792(-6)	1.7553(-7)	7.8036(-6)	0.022	0.0365
12.5000	1.808	-0.1100	4.7986(-6)	8.6996(-8)	4.7116(-6)	0.018	0.0273
13.0000	1.790	-0.1120	4.7434(-6)	7.1830(-8)	4.6716(-6)	0.015	0.0250
14.0000	1.739	-0.1340	5.4362(-6)	4.8632(-8)	5.3876(-6)	0.009	0.0209
14.8000	1.663	-0.1630	6.6002(-6)	3.3622(-8)	6.5666(-6)	0.005	0.0180
15.0000	1.656	-0.1810	7.2602(-6)	3.1790(-8)	7.2284(-6)	0.004	0.0174
16.4000	1.692	-0.4630	1.6200(-5)	3.2838(-8)	1.6168(-5)	0.002	0.0144
17.2000	2.003	-0.6160	1.5554(-5)	4.4028(-8)	1.5510(-5)	0.003	0.0151
18.0000	2.207	-0.1660	3.5504(-6)	3.4570(-8)	3.5158(-6)	0.010	0.0163
18.5000	2.041	-0.0940	2.2486(-6)	2.5334(-8)	2.2232(-6)	0.011	0.0141
20.0000	1.895	-0.0558	1.3897(-6)	1.4947(-8)	1.3747(-6)	0.011	0.0111
21.3000	1.809	-0.1460	3.6235(-6)	1.0301(-8)	3.6128(-6)	0.003	0.0094
22.5000	1.942	-0.1870	3.9294(-6)	1.0351(-8)	3.9190(-6)	0.003	0.0090
25.0000	1.993	-0.0274	5.0360(-7)	7.0124(-9)	4.9658(-7)	0.014	0.0075
27.9000	1.916	-0.0221	3.8602(-7)	4.0356(-9)	3.8198(-7)	0.010	0.0058
30.0000	1.866	-0.0259	4.3630(-7)	2.7856(-9)	4.3352(-7)	0.006	0.0049
35.0000	1.856	-0.0315	4.5664(-7)	1.4768(-9)	4.5516(-7)	0.003	0.0036
40.0000	2.093	-0.1310	1.3585(-6)	1.2212(-9)	1.3573(-6)	0.001	0.0031
50.0000	2.163	-0.2380	1.8508(-6)	5.5384(-10)	1.8503(-6)	0.000	0.0020
60.0000	2.163	-0.2630	1.7005(-6)	2.6910(-10)	1.7002(-6)	0.000	0.0014
80.0000	2.156	-0.2760	1.3442(-6)	8.4884(-11)	1.3441(-6)	0.000	0.0008
100.0000	2.173	-0.2610	1.0032(-6)	3.5132(-11)	1.0032(-6)	0.000	0.0005
150.0000	2.183	-0.1720	4.3904(-7)	6.8248(-12)	4.3902(-7)	0.000	0.0002
200.0000	2.176	-0.1070	2.0646(-7)	2.1174(-12)	2.0646(-7)	0.000	0.0001
300.0000	2.179	-0.0386	4.9588(-8)	4.1658(-13)	4.9588(-8)	0.000	0.0001



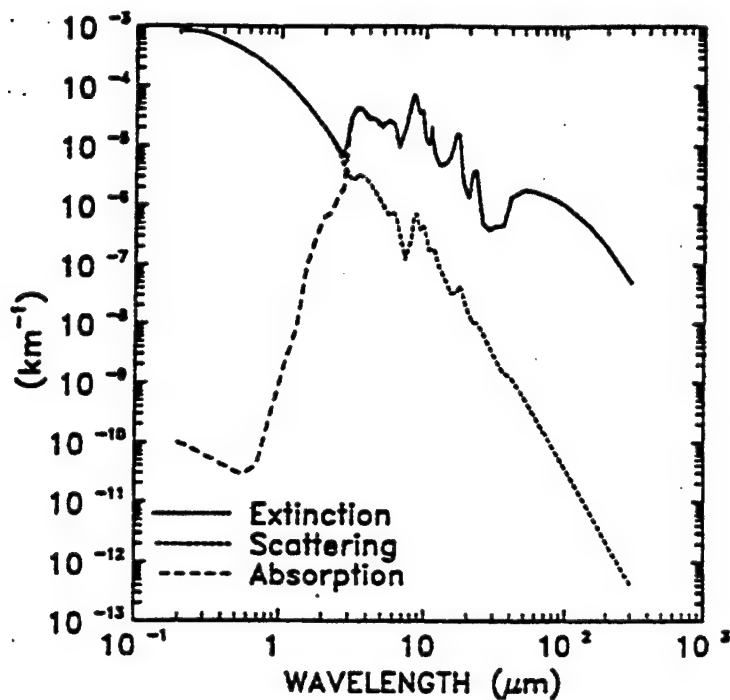


Figure 18. Extinction, Scattering and Absorption Coefficients as a Function of Wavelength for the Improved Background Stratospheric Aerosol Model

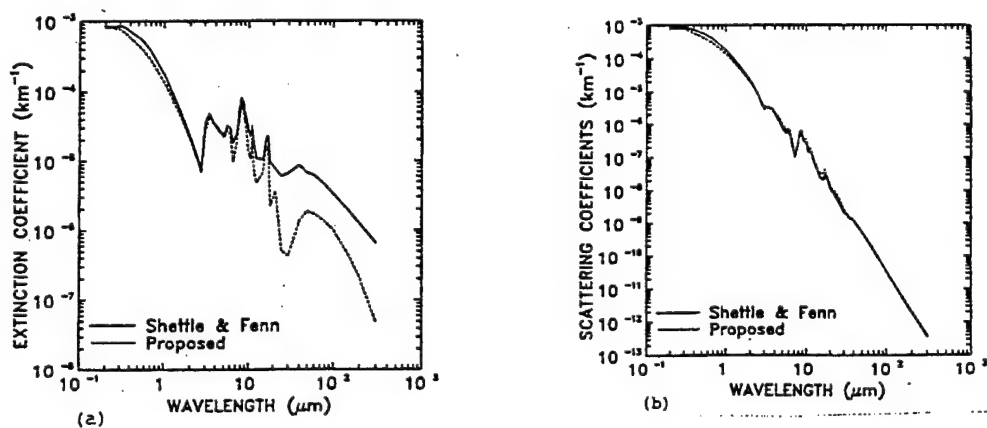


Figure 19. Comparison of the Improved Background Stratospheric Aerosol Model and that in Shettle and Fenn (a) Extinction Coefficients, (b) Scattering Coefficients, (c) Absorption Coefficients, and (d) Asymmetry Parameter

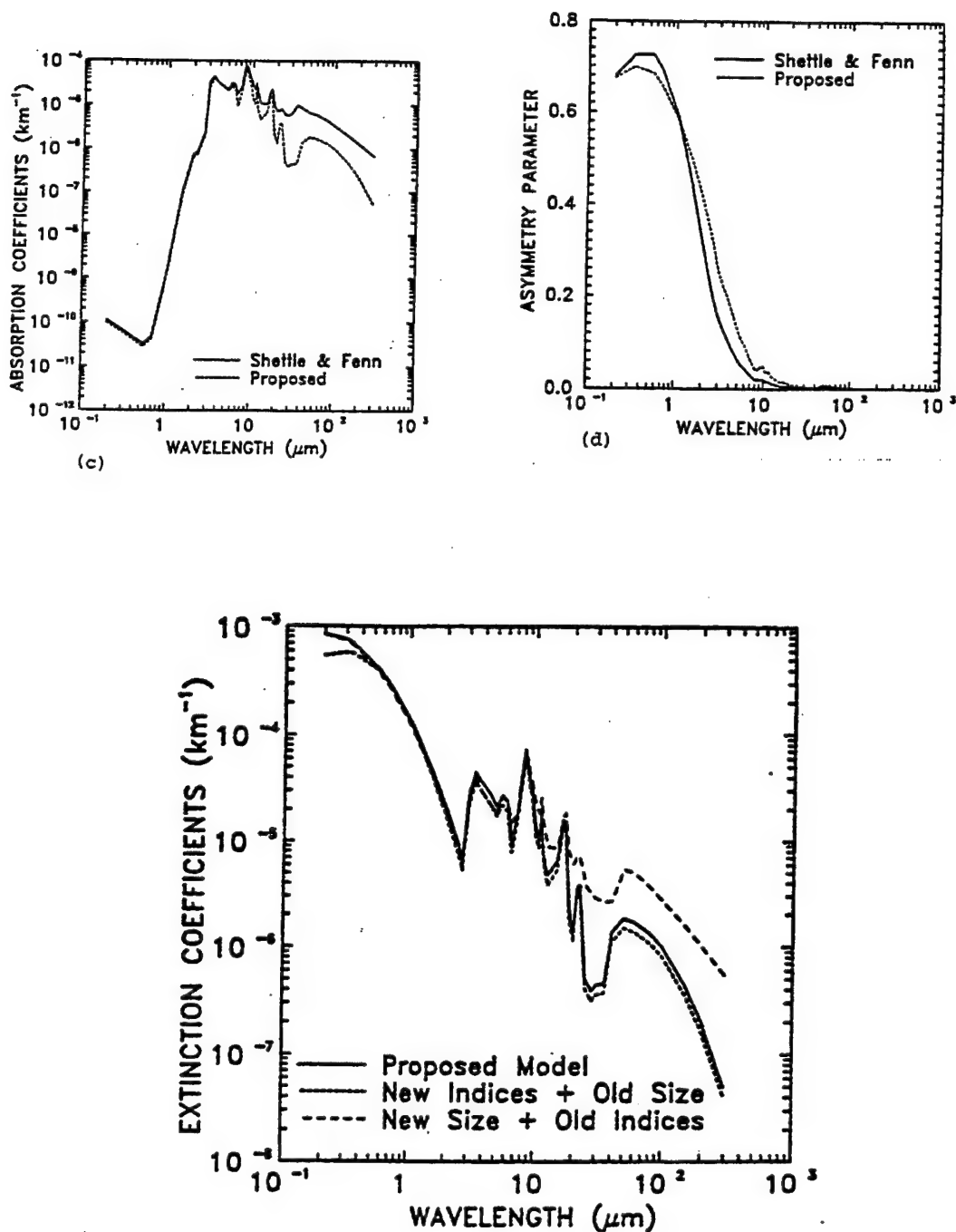


Figure 20. Extinction Coefficients as a Function of Wavelength for the Model (Solid Line), Calculated Using the New Indices of Refraction and the Modified Gamma Size Distribution (Dotted Line) and Calculated Using the Indices of Refraction at 300 K and the Proposed Log Normal Size Distribution

### 2.3.4.2 Volcanic Aerosol Models

There are two volcanic size distribution models: a "fresh volcanic model" which represents the size distribution of aerosols shortly after a volcanic eruption; and an "aged volcanic model" representing the aerosols about a year after an eruption. Both size distributions were chosen mainly on the basis of Mossop's<sup>152</sup> measurements following the eruption of Mt. Agung.

The refractive index for these models is based on the measurements of Volz<sup>72</sup>. The resulting normalized extinction and absorption coefficients for these two models are shown in Figure 21.

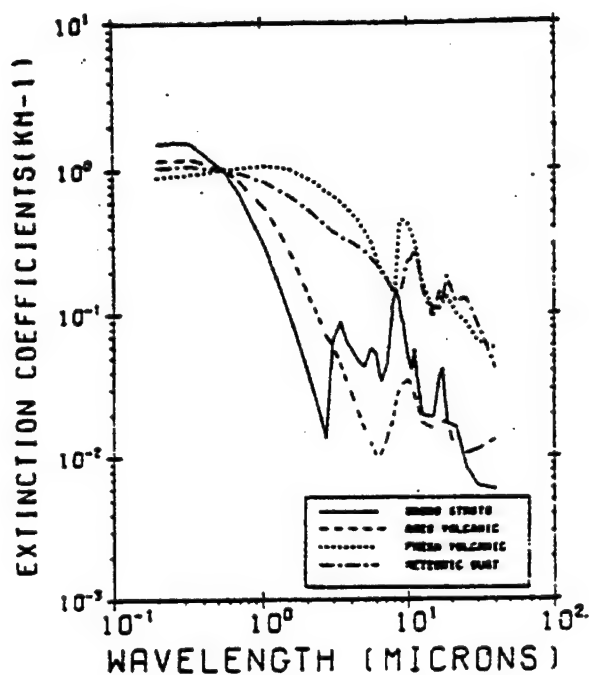


Figure 21a. Extinction Coefficients for the Upper Atmospheric Aerosol Models  
(Normalized to 1.0 at 0.55  $\mu\text{m}$ )

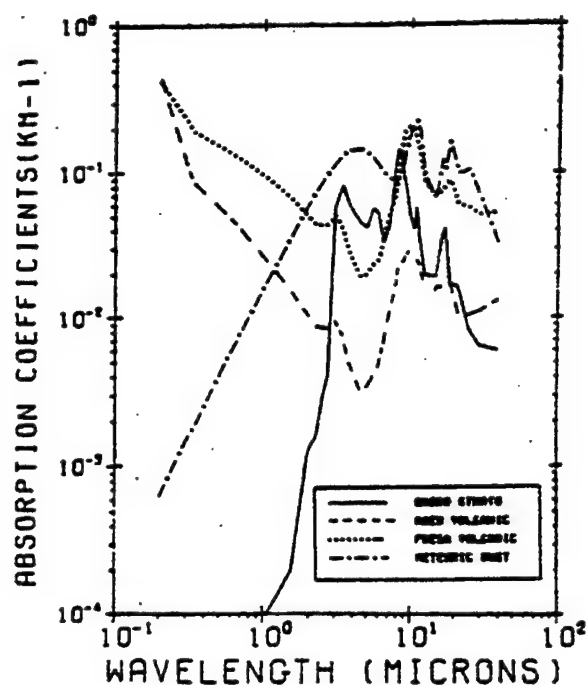


Figure 21b. Absorption Coefficients for the Upper Atmospheric Aerosol Models Corresponding to Figure 21a.

#### 2.3.4.3 Upper Atmosphere Aerosol Model

The major component of the normal upper-atmospheric aerosols is considered to be meteoric dust, which is consistent with the conclusions reached by Newkirk and Eddy<sup>153</sup> and later Rosen<sup>154</sup> in his review article. meteoric or cometary dust also form some of the layers occasionally observed in the upper atmosphere. Poultney<sup>117,155</sup> has related the lidar observations of layers in the upper atmosphere either to cometary sources of micro-meteoroid showers or noctilucent cloud observations. Divari et al<sup>156</sup> have related observations of increased brightness of the twilight sky to the Orinid meteor shower.

The refractive index of meteoric dust is based on the work of Shettle and Volz<sup>157</sup> who determined the complex refractive index for a mixture of chondrite dust which represents the major type of meteorite falling on the earth. <sup>158</sup>

The size distribution is similar in shape to the one developed by Farlow and Ferry<sup>159</sup> by applying Kornblum's<sup>160,161</sup> theoretical analysis (of the micro-meteoroid interaction with the atmosphere and their resulting concentration in the mesosphere) to the NASA<sup>162</sup> model of the meteoroid influx on the atmosphere. There are two important differences between the present size distribution model and Farlow and Ferry's.<sup>159</sup>

First, the present model has proportionately more smaller particles, and second, the number densities for all size ranges are several orders of magnitude larger than in Farlow and Ferry's <sup>159</sup> model. These differences are consistent with rocket observations in the upper atmosphere. <sup>159,163,164</sup>

The normalized extinction and absorption coefficients for this meteoric dust model for the aerosols of the upper atmosphere are shown in Figure 21 as a function of wavelength.

### **2.3.5 Use of the Aerosol Models**

The aerosol models defined in this report are representative of various general types of environments. Yet, the simple question: "Which model should be used for what location and weather situation?" is difficult to answer precisely. Some discussion on this point is necessary to give the user some guidance in choosing the appropriate model for a given condition.

#### **2.3.5.1 Boundary Layer Models**

For the boundary layer of the atmosphere up to 1 to 2 km above the surface, the composition of the aerosol particles is primarily controlled by sources (natural and man-made) at the earth's surface. The aerosol content of the atmosphere at a given location, will therefore depend on the trajectory of the local airmass during the preceding several days, and the meteorological history of the airmass. The amount of mixing in the atmosphere is controlled by the temperature profile and the winds. Precipitation will tend to wash the aerosols out of the atmosphere, although it should be noted that "frontal showers" often mark the boundary between two different air masses with generally different histories and correspondingly different aerosol contents.

The "rural" and the "urban" model are intended to distinguish between aerosol types of natural and man-made origin over a land area. Clearly, the man-made aerosol will be predominantly found in urban-industrial areas. However, it is quite likely that after the passage of a cold front, clear polar air also covers an urban area and that therefore the rural aerosol model, which is free of the component of industrial-carbonaceous aerosols, is more applicable. After a few days, as the clean airmass begins to accumulate local pollution, the urban model will once again become more representative.

Conversely, very often the pollution plume from major urban-industrial areas may, under stagnant weather conditions, diffuse over portions of a continent (for example, Central Europe, Northeastern United States), including its rural sections.

There is also a distinct difference between the composition of aerosols over the ocean and those over land areas due to the different surface-based sources. Aerosols in maritime environments have a very pronounced component of sea-salt particles from the sea water. Sea-salt particles are formed from sea spray from breaking waves. The larger particles fall out, but the smaller particles are transported up with the atmospheric mixing in the boundary layer. In coastal regions the relative proportions of particles of continental and oceanic origins will vary, depending on the strength and direction of the prevailing winds at time of observation.

While changes in visibility are often associated with changes in the relative humidity, (as the relative humidity approaches 100 percent the visibility tends to decrease), it is not possible to define a unique functional relationship between the visibility and relative humidity in the natural atmosphere. The reason for this is that any change in atmospheric moisture content is generally also associated with a change in the aerosol population itself due to change of the air mass. Only if the aerosol is contained in a closed system, where only the humidity changes, can such a unique relationship be developed. The measurements presented by Filippov and Mirumyants<sup>165</sup> clearly illustrate the difficulties in defining a simple unique expression relating visibility and relative humidity.

#### **2.3.5.2 Desert Aerosol Model**

The desert aerosol model has a sand component consisting of quartz particles and quartz particles contaminated with a 10% concentration of hematite. The  $0 \text{ ms}^{-1}$  wind speed is representative of background desert conditions, while a wind speed of  $30 \text{ ms}^{-1}$  would represent dust storm conditions. Wind speeds greater than 0 and less than  $30 \text{ ms}^{-1}$  are representative of conditions between these two extremes.

A number of important features of this model are worth commenting on. First there is selective absorption at visible wavelengths which becomes more pronounced as the wind speed increases. The selective absorption is due to the hematite in the sand component and will make the desert aerosol appear slightly reddish in color during dust storm conditions. The carbonaceous particles contribute very little to the total absorption of visible radiation primarily because their abundance is too small.

Another important consideration is the structure of the IR absorption. The peaks in the absorption near 3, 7 and  $9 \mu\text{m}$  for  $0 \text{ ms}^{-1}$  wind speed conditions are primarily due to the strong absorption bands of ammonium sulfate. For dust storm conditions however, the absorption in the IR is dominated by the sand component. Interestingly, there are minima in the absorption and maxima in the scattering near 8 and  $20 \mu\text{m}$ ,

which correspond to the centers of the strong crystal lattice absorption bands of quartz. It is believed that this phenomenon is a result of the quartz in the sand component acting as a reflector. To show this, consider an electromagnetic wave propagating in air as it encounters a plane boundary having a complex index of refraction,  $m = n + ik$ . For normal incidence, the reflectance is given by:

$$\text{Reflectance} = \frac{(n-1)^2 + k^2}{(n+1)^2 + k^2} \quad (31)$$

When  $n \ll 1$ ,  $n \gg 1$  or  $k \gg 1$  (as is the case for the absorption bands of quartz), the reflectance approaches 1.0. Thus the incident radiation is reflected and the absorption drops because the incident wave cannot penetrate the material to be absorbed.

Another point to consider is that the extinction is wavelength dependent for winds of  $0 \text{ ms}^{-1}$  but nearly constant at  $20$  and  $30 \text{ ms}^{-1}$ . These differences are driven by the relative contributions of the aerosol components. For winds of  $0 \text{ ms}^{-1}$ , only the smaller water soluble particles with respect to the wavelength dominate the extinction at visible and near IR wavelengths and, therefore, a wavelength dependence exists. On the other hand, in high wind speed conditions, the extinction is dominated by the much larger sand particles that approach the geometric optics regime.

The single scattering albedo at the UV and shorter visible wavelengths decrease significantly as the wind speed increases. This effect becomes less pronounced for the longer visible and near IR wavelengths. In the middle IR region, single scattering albedos for  $0$  and  $30 \text{ ms}^{-1}$  winds exhibit a high degree of structure. Specifically, sharp minima occur near  $3$ ,  $7$  and  $9 \mu\text{m}$ , which can be attributed to absorption by ammonium sulfate. For winds exceeding  $30 \text{ ms}^{-1}$ , large peaks occur near  $9$  and  $20 \mu\text{m}$  which is caused by excess scattering by the quartz in the sand component. Beyond  $40 \mu\text{m}$ , single scattering albedos for  $0 \text{ ms}^{-1}$  winds are much lower than those for winds of  $30 \text{ ms}^{-1}$ . This should not be interpreted as significant absorption, since the magnitude of the absorption is small beyond  $40 \mu\text{m}$  for lighter winds.

Generally speaking, the asymmetry parameter values as a function of wavelength are greater for dust storm conditions than those for background conditions throughout the  $0.2$  to  $300 \mu\text{m}$  region. This is not surprising because the scattering for dust storm conditions is dominated by the large sand particles (with respect to the wavelength of radiation) which have their scattering peaked in the forward direction.

### 2.3.5.3 Tropospheric Aerosol Model

The tropospheric aerosol model has been developed primarily for application in the troposphere, above the boundary layer, where the aerosols are not as sensitive to local surface sources. However, the tropospheric model should be used near ground level for particularly clear and calm conditions (in pollution free areas with visibilities greater than 30 to 40 km), where there has been little turbulent mixing for a period of 1 to 2 days, permitting the larger particles to have settled out of the atmosphere without being replaced by dust, blown into the air from the surface. (The sedimentation rate of a 10- $\mu\text{m}$  radius aerosol particle in the lower troposphere is approximately 1 km per day.)<sup>166</sup>

### 2.3.5.4 Fog Models

The fog models described in Section 2.3.3.5 were presented in terms of the atmospheric conditions leading to the development of the fog, so this provides a good basis for deciding which fog model to use. In more general terms, the visibilities will be less than 200 meters for thick fogs and the extinction will be virtually independent of wavelength. For these conditions the advection fog model should be used. For light to moderate fogs, the visibility will be 200 to 1000 meters and there will be a noticeable difference between the extinction for visible wavelengths and in the 8- to 12- $\mu\text{m}$  window. For these cases the radiation fog model should be used. For thin fog conditions where the visibility may be 1 to 2 km, the 99 percent relative humidity aerosol models may represent the wavelength dependence of the atmospheric extinction as well as any of the fog models.

### 2.3.5.5 Stratospheric and Upper Atmospheric Models

At irregular intervals (on the order of years) there are volcanic eruptions which inject significant amounts of aerosols into the stratosphere. For the first few months following such an eruption the fresh volcanic size distribution model would generally be the best one to use, and for the next year or so after that the aged volcanic size distribution model should be used. Under generally inactive volcanic periods, the background stratospheric model would be appropriate.

The choice of which vertical distribution profile to use would depend on the severity of the volcanic eruption and how long ago it was. The moderate volcanic profile is representative of the stratospheric conditions throughout the Northern Hemisphere during the mid and late 1960's following the eruption of Mt. Agung. It is also typical of conditions during late 1974 and 1975 after the Volcan de Fuego eruption. This profile is



also representative of conditions following the eruption of Mt. Pinatubo in June 1991 and continuing into mid 1993.

The high and extreme volcanic models are somewhat speculative as there have been no direct measurements of the vertical distribution of aerosol for such conditions. They are however consistent with the total optical thickness for aerosols inferred shortly after several major volcanic eruptions,<sup>108,109,167</sup> such as Katmai and Krakatoa, as well as the effects of Mt. Agung in the Southern Hemisphere.

### Enhanced Aerosols After a Volcanic Eruption

A volcanic eruption will increase the numbers and size distribution of sulfuric acid particles as a result of SO<sub>2</sub> injections into the stratosphere. The specific impact on aerosol loading in terms of size distribution and mixture of H<sub>2</sub>SO<sub>4</sub> and water will vary from eruption to eruption.

Figure 22 shows the extinction coefficients for stratospheric aerosols that have been "enhanced" by the chemical production and sedimentation of sulfuric acid particles. The calculations were based on the sum of two log normal size distributions based upon the work of Oberbeck et al.<sup>145</sup> following the eruption of El Chichon. The first distribution represents an enhanced background and has a particle density of 6 cm<sup>-3</sup>, mode radius of 0.14 μm and a standard deviation of 1.72. The second distribution results from the sedimentation of smaller particles and is represented by a particle density of 1.5 cm<sup>-3</sup>, a mode radius of 0.54 μm and a standard deviation of 1.22. The calculations were done with the proposed indices of refraction at 215 K and those at 300 K.

Both curves show a nearly flat response as a function of wavelength up to about 1.0 μm. Significant differences between the curves do not begin to appear until beyond 20 μm as a result of the differences in the imaginary component of the indices of refraction.

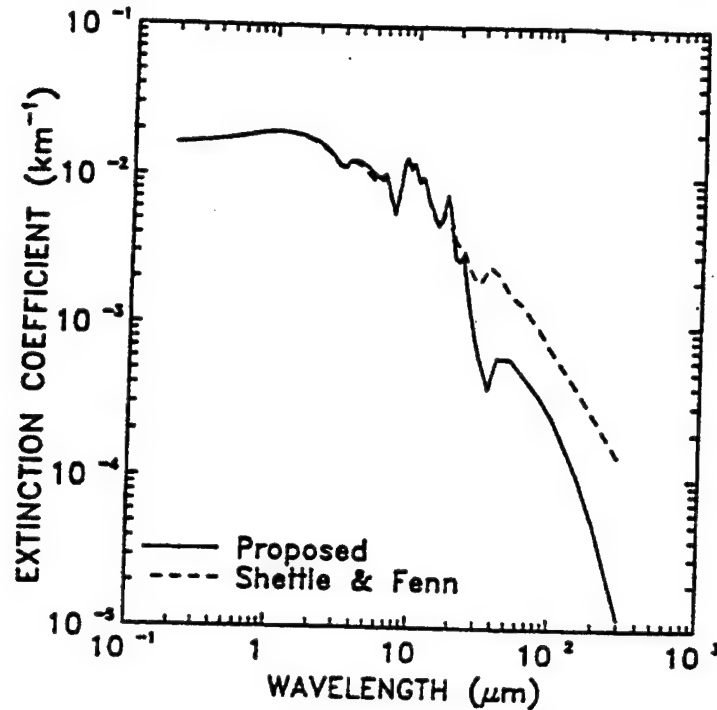


Figure 22. Extinction Coefficients as a Function of Wavelength for a Postulated Enhanced Stratospheric Aerosol Layer

#### 2.3.5.6 Seasonal and Latitude Dependence of Aerosol Vertical Distribution

In the mid-latitudes as the names suggest, the spring-summer aerosol vertical profiles are intended to be used during the spring and summer seasons and the fall-winter profiles used during the fall and winter seasons. However, the seasonal changes in aerosol distribution are partially a reflection of the changes in the tropopause height (especially for stratospheric aerosols). So in the tropical regions where the tropopause is generally higher, it is recommended that the spring-summer aerosol profile be used. Analogously, in the subarctic regions where the tropopause is lower, it is recommended that the fall-winter profile be used.

#### 2.3.5.7 Remarks on Applicability of the Aerosol Models

Typical conditions for which the different aerosol models apply as discussed in detail above are summarized in Table 11. However, it must be emphasized that these models only represent a simplified version of typical conditions. It is not practical to include all the details of natural aerosol distributions nor are existing experimental data sufficient to describe the frequency of occurrence of the different conditions. While these aerosol models were developed to be as representative as possible of different atmospheric

conditions, it should be kept in mind that the "rural" aerosol model does not necessarily exactly reproduce the optical properties in a given rural location at a specific time and date, any more than the mid-latitude summer model atmosphere would exactly reproduce the actual temperature and water vapor profiles for that same specific time and location.

**Table 11. Typical Conditions for Aerosol Model Applications**

1. Lower Atmospheric Models

1.1 Rural Model

- 1) Natural environment, midlatitude, overland.
- 2) Clean air in urban regions, following passage of a cold front.

1.2 Urban Model

- 1) Urban industrial aerosol.
- 2) Stagnant polluted air extending into rural regions.

1.3 Maritime Model

- 1) Mid-ocean (at least 300 km offshore) with moderate winds (above the first 10 to 20 meters).
- 2) Continental areas under strong prevailing wind from the ocean.

1.4 Tropospheric Model

- 1) Atmospheric region between top of boundary layer (approximately 2 km) and tropopause (8-18 km, depending on latitude and season).
- 2) Clean, calm air (meteorological range--40 km) in surface layer over land.

1.5 Fog Models

1.5.1 Advective Fog

- 1) Mixing of air masses of different moisture content and temperature, leading to saturation.
- 2) Lacking specific knowledge on the formation process, for mature fogs with meteorological range:  $V \leq 200$  meters.

1.5.2 Radiation Fog

- 1) Radiational cooling knowledge of the air to the dew point at night.
- 2) Lacking specific knowledge on the formation process, for developing fogs or meteorological ranges:  $200 \leq V \leq 1000$  meters

1.5.3 99 Percent Relative Humidity Aerosol Models

- 1) Light fogs ( $1 \leq V \leq 2$  km).

2. Stratospheric and Mesospheric Aerosol Models

2.1 Background Stratospheric Model

For time periods without any direct influence of volcanic dust contamination, for example, 1977 to 1980.

2.2 Moderate Volcanic Profile with Fresh Particle Size Distribution

For optical thickness approximately 0.03, up to a few years after eruption, for example, Northern Hemisphere, 1964 to 1968.

### 2.3 High Volcanic Profile and Fresh or Aged Particle Size Distribution

For optical thickness approximately 0. 1, up to a few months after eruption, for example, Southern Hemisphere. 1964-1965.

### 2.4 Extreme Volcanic Profile with Fresh Particle Size Distribution

For optical thickness approximately 0.3 or higher, up to a few weeks after a major eruption, for example, 1883 (Krakatoa) or 1912 (Katmai).

## 2.3.6. NAVY Maritime Aerosol Model

This chapter provides a brief description of the Navy maritime aerosol model and its implementation in MODTRAN. A complete discussion of the model is given by Gathman<sup>38</sup>. Since this model includes an explicit dependence on wind speed it is recommended that it be used instead of the maritime model, (developed for earlier versions of LOWTRAN) which assumed moderate wind speeds (see Shettle & Fenn)<sup>60</sup>. The latter model is retained in MODTRAN for comparison purposes.

### 2.3.6.1 Description of the Model

The aerosol population found over the world's ocean is significantly different in composition and distribution from that of a continental origin. These aerosol are largely derived from the sea. They are produced by the evaporation of sea spray and from jet and film droplets. Jet droplets are ejected into the air by the bursting of small air bubbles at the sea surface. The bursting of the bubble film leaves behind many smaller film droplets that may also be diffused into the air. These mechanisms are wind dependent and require white water phenomenon in order to produce aerosol.

Once the aerosol droplets are airborne, they undergo additional sorting and mixing processes. The marine boundary layer is usually capped by a temperature inversion and, within this boundary layer, the smaller marine aerosol together with any background aerosol form a fairly uniform aerosol spatial distribution. Once introduced into the atmosphere, the lifetime of an aerosol particle is dependent on the size of the particular aerosol particle. Those with very small sizes have a very long residence time in the boundary layer if there are no washout processes taking place. On the other hand, those with very large sizes have a short residence time and do not contribute to the stationary long-term aerosol population.

The Navy maritime aerosol model differentiates between these various types of aerosol by postulating that the marine atmosphere is composed of three distinct populations, each of which is described by a log normal size distribution. The parameters that describe the analytical form of the size distribution are then related to both recent meteorological history and current meteorological observations .

The smallest component of the model is a continental component. This is the background aerosol and although it apparently has little to do with current wind parameters, it is dependent on the elapsed time required for the air mass to traverse the sea from the continent to the point of observation. Quantification of this component in terms of routine meteorological measurements is difficult, but for convenience an integer from 1 to 10 is used to specify the ICSTL parameter, which gives a qualitative indication of the continental contribution: a value of 1 representing relatively pure maritime aerosol, and a value of ICSTL = 10 meaning a significant continental component.

The second component, the stationary component of the maritime aerosol, is the part of the maritime aerosol that depends on the current and past history of the wind and represents that portion of the spectra that are produced by the high wind and white water phenomenon but do not fall out rapidly. The amplitude of this component is related to the average wind speed over the past 24 hours, and is specified by the WHH parameter.

The third or "fresh" component of the Navy aerosol model is a log normal population of aerosol that is related to the current wind speed (specified in the program by the WSS parameter). The amplitude of this component is a function of the current wind speed and reflects the current action of the production of drops produced by white water as a result of wind wave actions.

The amplitudes of both the second and third components of the aerosol population reflect the necessity of wind speed being above a certain minimum value before white water phenomena are observed and thus, marine aerosol produced. This minimum value is 2.2 m/s.

The model is also responsive to the current relative humidity. It is well known that particles composed of sea salt are hygroscopic and change their composition and size as a function of the relative humidity. The model uses the "swelling factor" proposed by Fitzgerald<sup>168</sup>, which adjusts the mode radii of the three components of the model, but does not alter the total number of particles that are airborne. The model also adjusts the complex index of refraction of the aerosol based on the volume weighted method of Hänel<sup>169</sup>, using the refractive index of soluble aerosol (Volz)<sup>77</sup> for the dry component and that of pure water from Hale and Querry.<sup>70</sup>

#### **2.3.6.2 Use of the Navy Maritime Model**

As discussed in the preceding section, this model requires three parameters to be specified in addition to those used by the other aerosol models (that is visibility and

relative humidity). These additional parameters are: (1) ICSTL, which indicates the degree of continental influence, (2) WHH, the average wind speed over the past day, and (3) WSS, the current wind speed. The MODTRAN program will use default values for any unspecified parameter.

Three methods can be used to estimate ICSTL. The first is by plotting the airmass trajectory and determining the elapsed time,  $t$ , since the air parcel left land. This time is related to ICSTL by the following empirical equation:

$$ICSTL = INT(9 \exp[-t(days)/4] + 1) \quad , \quad (32)$$

where  $INT(x)$  truncates to the nearest integer less than  $x$ .

Secondly, if measurements of the current radon 222 concentrations in the atmosphere are available (Larson and Bressan)<sup>171</sup>, then the air mass parameter can be estimated by the formula:

$$ICSTL = INT(Rn/4) + \quad , \quad (33)$$

where  $Rn$  is the concentration of radon 222 in  $pCi/m^3$ . This relationship can be used because radon 222 is introduced into the atmosphere only by processes occurring over land. Therefore, since this radioactive substance has a half-life of 3.86 days, the concentration of radon 222 is then related to the time since the air parcel left the land.

A third method for determining ICSTL consists of subjectively choosing an integer between 1 and 10 to determine the "quality" of the air mass, with a value of "1" being for pure oceanic air and a value of "10" if the air has recently been ashore over a polluted industrial area. Values in between can be used to specify the various grey areas between these two extremes. If the user does not input a value for the parameter ICSTL, the LOWTRAN code will use a default value of  $ICSTL = 3$ .

The current wind speed, WSS, and the average wind speed over the past 24 hours, WHH, should be input in units of m/s. If the average wind speed is input as 0 or is given a negative value, a default value will be chosen that depends on the model atmosphere being used, (specified by the parameter MODEL). These default wind speeds are shown in Table 12. The default wind speeds are based on average values for observations made in the indicated region, except for the user-defined cases (MODEL = 0 or 7), which use a global mean value. If the current wind speed, WSS, is not specified, it is set equal to the average wind speed, WHH.

Table 12. Default Wind Speeds for Different Model Atmospheres

MODEL	Model Atmosphere	Default Wind Speed (m/s)
0	User-defined (Horizontal Path)	6.9
1	Tropical	4.1
2	Midlatitude summer	4.1
3	Midlatitude winter	10.29
4	Subarctic summer	6.69
5	Subarctic winter	12.35
6	U S. Standard	7.2
	User-defined	6.9

Visibility observations at sea are usually only estimates because of the lack of targets at fixed distances from the observer. Therefore, it is suggested in the use of this model that, unless visibility is measured accurately, the default visibility condition be used. This is important because user-specified visibility inputs adjust all of the extinction and absorption coefficients in the calculations in order to force the calculated extinction at  $0.55 \mu\text{m}$  to agree with the visibility and, if inaccurate, may introduce excessive error into the calculations.

The Navy model is designed to operate accurately within certain limits of input parameters. While parameter values outside of these limits are permitted by the overall MODTRAN 2 program, the accuracy of the predictions outside of these limits is reduced. The design limits of the model parameters are:

$$50 \text{ percent} \leq \text{Relative Humidity} \leq 98 \text{ percent}$$

$$0 \text{ m/s} \leq \text{WSS} \leq 20 \text{ m/s}$$

$$0 \text{ m/s} \leq \text{WHH} \leq 20 \text{ m/s, and}$$

$$0.8 \text{ km} \leq \text{VIS} \leq 80 \text{ km}.$$

For relative humidities or wind speeds outside these design limits the program will internally reset the value to the nearest limit, rather than try to extrapolate the aerosol properties.

### 2.3.6.3 Sample Calculations with the Navy Model

This section briefly presents some sample results of transmittance calculations using the Navy maritime aerosol model. Figure 23 shows the transmittance for a 10-km horizontal path at the surface, for each of the standard model atmospheres in MODTRAN. These calculations were all done using the default values for all the parameters. Thus, ICSTL was set to 3, the wind speed depended on the model atmosphere (see Table 12), and the maritime aerosol model calculated the visibility

based on the aerosol properties with these parameter values and the relative humidity for the model atmosphere. The values of the parameters for these different cases are summarized in Table 13.

The differences in the transmittances shown in Figure 23 are due both to variations in the aerosol properties for different atmospheric conditions and to the different amounts of water vapor in the various model atmospheres. The transmittance in the 3 through 5  $\mu\text{m}$  (2000 through 3300  $\text{cm}^{-1}$ ) window is more sensitive to changes in the aerosol properties and in the 8 through 13  $\mu\text{m}$  (750 through 1250  $\text{cm}^{-1}$ ) window, the transmittance is more sensitive to the variations in the water vapor.

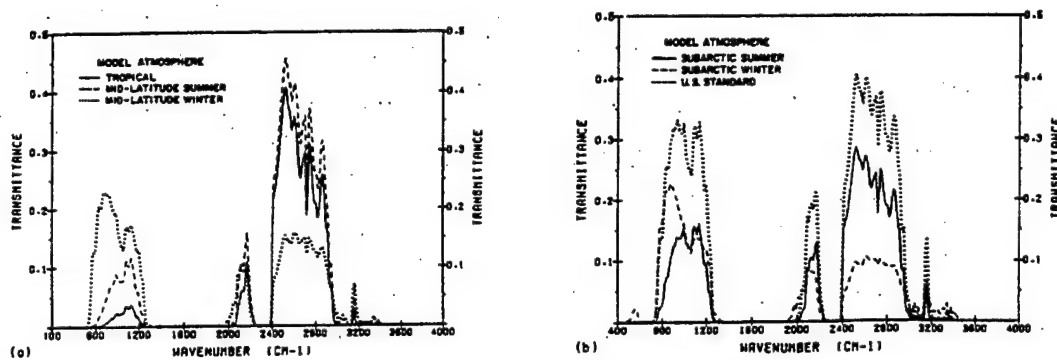


Figure 23. Atmospheric Transmittance for a 10-km Horizontal Path at the surface with the Navy Maritime Aerosol Model. (a) for the tropical, midlatitude summer, and midlatitude winter model atmospheres and (b) for the subarctic summer, subarctic winter, and U. S. Standard atmospheres.

**Table 13. Conditions for Sample Runs of the Navy Maritime Aerosol Model**

MODEL	Atmosphere	Wind (m/s)	Rel Hum (percent)	Vis (km)	$\rho\text{H}_2\text{O}$ ( $\text{gm}/\text{m}^3$ )
1	Tropical	4.10	73	49.4	19.0
2	Midlatitude summer	4.10	70	52.2	14.0
3	Midlatitude w inter	10.29	71	17.8	3.5
4	Subarctic summer	6.69	72	28.3	9.1
5	Subarctic winter	12.35	73	14.2	1.2
6	U. S. Standard	7.20	49	39.5	5.9



### 2.3.7 ARMY Vertical Structure Algorithm

#### 2.3.7.1 Introduction

An algorithm for modeling the vertical structure of aerosols has been added to the MODTRAN 2 code. It was developed initially to describe the vertical distribution of the atmospheric aerosols for conditions of limited visibility and beneath low-lying stratus cloud decks<sup>171</sup>. The formalism has been extended so it can also represent cases with no cloud ceiling and moderate to high visibility<sup>172</sup>. The algorithm will generate the vertical aerosol profile within the boundary layer from input parameters, such as surface visibility and the cloud ceiling height. This model is designed for use within the lowest 2 km of the atmosphere.

#### 2.3.7.2 The Vertical Profile Model

In low visibility situations, due either to haze or fog, increasing numbers of observations show that the measured visibility at the surface is not representative of conditions a few hundreds of meters, or even tens of meters, above the surface. Thus, the "slant path visibility" can be significantly different from the "horizontal visibility". In a significant fraction of the cases the visibility decreases as the height above the surface increases. These cases are of special concern here.

Detailed data on the vertical structure of fogs and hazes have been gathered in the Federal Republic of Germany on several different occasions.<sup>173,174</sup> Droplet size **distributions** in the 0.5- to 47- $\mu\text{m}$  range have been measured from a balloon-borne instrument, thus yielding vertical profiles.<sup>175</sup> Extinction coefficients at desired wavelengths or the liquid water content can be calculated from these measured droplet size distributions.

The vertical structure of these profiles has been examined previously by Duncan et al,<sup>176</sup> who characterized the vertical structure in the form

$$y = a'x + b' \quad , \quad (34)$$

where  $x = \log_{10} k(z)$ ,  $y = \log_{10} k(z + 20)$ ,  $a'$  and  $b'$  are coefficients that were chosen to fit the data, and  $k(z)$  is the value of the extinction coefficient at the altitude  $z$ ;  $k(z + 20)$  is then the value of this variable at an altitude of  $z + 20$  m. Thus, one can work stepwise from the surface up through the cloud boundary layer. Figure 24 shows the fit of Eq. (34) to the data. It should be noticed that there is a sharp change in slope at a

value of about  $7.1 \text{ km}^{-1}$  for the extinction. The physical significance of this inflection point is discussed below.

The point of intersection of the two line segments physically represents the changes in extinction due to changes in the state of particle growth as one moves from a sub-saturated environment (lower line segment), where relative humidities are less than 100 percent, to a super-saturated environment, (upper line segment). Thus, this point of intersection will be taken to represent the cloud base or lower cloud boundary.

Since  $x = \log_{10} k(z)$  in Eq. (34) and  $y$  is really just  $x + \Delta x$  over an altitude interval  $\Delta z$ , the relation for the extinction as a function of altitude can be expressed as<sup>171</sup>

$$k_e(0.55 \mu\text{m}) = A \exp[B \exp(Cz)] \quad (35)$$

where  $A$ ,  $B$ , and  $C$  are functions of preselected boundary values, the initial or starting value of extinction, and the cloud ceiling height. Note that since there are two straight line segments, the coefficients  $A$ ,  $B$ , and  $C$  have different values, depending on which part of the data curve (in Figure 24) is being followed.

The rate at which the extinction changes with altitude below the cloud base actually depends on the cloud ceiling height  $Z_c$ . The lower line segment in Figure 24 represents an average of several sets of data and therefore gives a single, average value for the

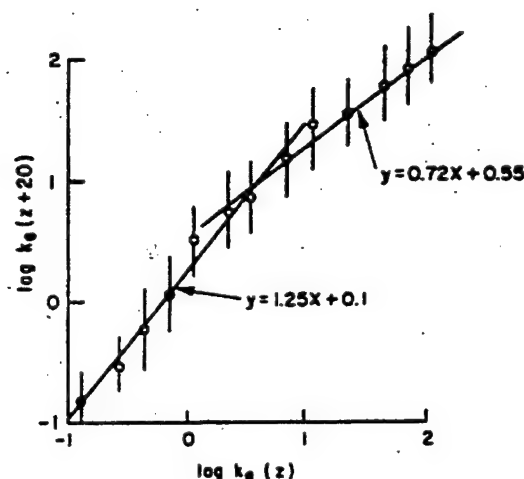


Figure 24. Relationship Between the Extinction Coefficient (at  $0.55 \mu\text{m}$ ) at Altitudes  $z$  and  $z + 20 \text{ m}$ . The vertical lines are the error bars for the data (after Duncan et al)<sup>176</sup>

coefficient  $C$  in Eq. (35). The explicit dependence of  $C$  on the cloud ceiling height can be incorporated by defining the coefficient  $C$  as

$$C = \frac{1}{z_c} \ln \left[ \frac{\ln(E/A)}{\ln(D/A)} \right] \quad (36)$$

where  $E$  is the value of the extinction at the cloud base,  $D$  is the observed value of extinction at the surface, and  $A$  is the same coefficient used in Eq. (35). In this case  $A$  is the lower limit to the extinction in the hazy/foggy region below the cloud. Figure 25 shows the visible extinction coefficient plotted as a function of altitude for the same initial surface value, but several different cloud ceiling heights. The solid line represents the (average) values from the line segments in Figure 24. The dashed vertical line represents the value of the extinction for the cloud base given by the intersection of the line segments in Figure 24. The solid line to the right of the dashed vertical line represents the extinction profile inside the cloud and can be appended to any one of the vertical profiles to the left.

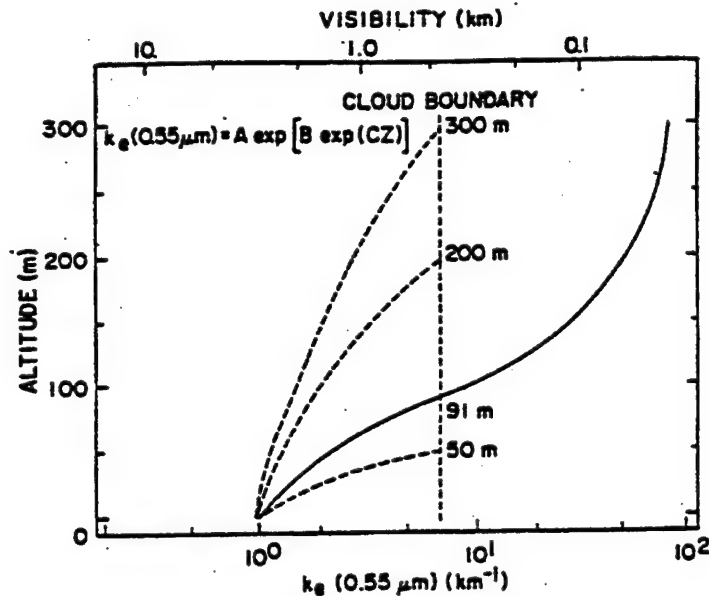


Figure 25. The Vertical Profile of the 0.55- $\mu\text{m}$  Extinction Coefficient for Various Cloud Ceiling Heights. The solid line shows the average profiles from Figure 24, the dashed vertical line represents the value at the cloud boundary

Initially the algorithm for the vertical structure of hazes, fogs, and clouds represented by Eq. (35) was developed for low visibility/low stratus conditions and is based on inputs of the surface meteorological range (extinction coefficient) and the cloud ceiling height. This algorithm has now been extended to cases where there may be no cloud ceiling and where the extinction coefficient decreases with increasing altitude.<sup>172</sup>

### 2.3.7.3 Applicability of the Vertical Structure Algorithm

Three initial visibility conditions are considered. The first condition is for stratus clouds and thick fogs (which in this instance may be treated as a cloud at the ground); the second condition is for hazes and fog; and the third condition is for the clear to hazy atmosphere. The vertical structure of visibility can be represented by four different types of curves as illustrated in Figure 26. Curves 1 and 2 represent the cases where the extinction coefficient increases (that is, visibility degrades) with increasing altitude; these cases are representative of the vertical structure of extinction for thick fogs or for low visibility/low stratus conditions. Curves 3 and 4 represent cases where the extinction coefficient decreases (that is, visibility improves) with increasing altitude. Each of these cases will now be briefly outlined.

Case 1: This curve is to be used for dense fogs at ground level or when one is at the cloud base or in the cloud. Physically this curve represents the increase in liquid water content (LWC), and consequently the increase in extinction coefficient and decrease in visibility, of a saturated parcel of air rising at the wet adiabatic lapse rate. This curve should be used only when the initial extinction coefficient (or meteorological range) is in the thick fog/cloud region, shown between the two dashed lines representing boundary values on the right-hand side of Figure 26.

Case 2: This curve is to be used for low visibility conditions beneath the clouds due to haze or fog when there is a low cloud ceiling present.

Case 3: This curve is to be used when there is a shallow radiation fog present or when a haze layer is capped by a distinct (low-lying) temperature inversion. A cloud ceiling is not present.

Case 4: This profile is to be used for cases where there is reasonable vertical homogeneity for visibility in a clear to slightly hazy atmosphere that may have a shallow haze layer near the surface. A cloud ceiling is not present.

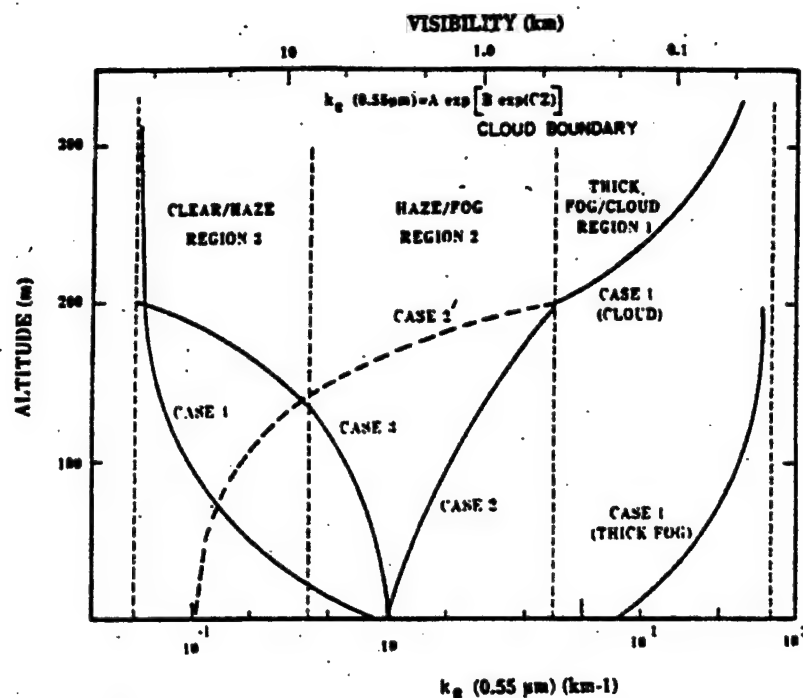


Figure 26. Four Different Cases Represented by the Vertical Structure Algorithm

Profiles of the 0.55- $\mu\text{m}$  extinction coefficient are shown in Figure 26 for these different cases. Two examples of representative profiles are shown for case 1. The first example is for a thick fog at the surface, which is represented by an extinction coefficient profile that increases with height. When the depth of the fog is not known (which is usually the case because the sky is obscured), a default depth of 200 m is recommended. The second example is for a low-lying stratus cloud; for illustration the cloud ceiling height is taken to be 200 m. This profile should only be used from the cloud base to the cloud top. Again, cloud thickness is usually not a measured quantity, and a default value of 200 m is recommended. The two examples shown here are actually the same profile, one starting at the surface for the thick fog and the other starting at the cloud base of a low-lying stratus cloud. Within region 1, thick fog/cloud, only profiles of the case 1 type should be used. For a dense, shallow radiation fog, use a profile for case 3 as described below.

A representative profile for the structure beneath a stratus cloud is shown for case 2. In this instance the visibility conditions at the surface are representative of region 2, haze/fog, and the cloud ceiling height is 200 m. The slope and shape of the vertical structure profile beneath the cloud deck are a function of the initial value of the

(surface) visibility and the cloud ceiling height. For haze/fog conditions, when a cloud ceiling height less than 2 km is present, a profile of the case 2 type should always be used.

Often a low-lying cloud cover is present when the surface visibility is clear to only slightly hazy. In this instance a vertical structure profile similar to case '2 is appropriate. This profile is denoted as case 2 ' and is shown in Figure 26 as an alternate profile for the instance of a 200-m cloud ceiling height. The only difference between case 2 and case 2 ' is the manner of choosing the value of the coefficient A, which in turn influences the shape of the vertical profile.

A shallow radiation fog or a haze layer bounded by a temperature inversion can be represented by a vertical structure profile as shown in Figure 26 for case 3. The boundary layer heights for such occurrences are often difficult to estimate. Temperature inversion heights can be obtained from acoustic sounders or radiosonde observations; often, visual sightings can be used to estimate depths of shallow fogs or haze layers. A nominal boundary layer height of 200 m has been selected for illustrative purposes. For radiation fogs where the depth is not known, a default value of 200 m is selected (a more realistic value for radiation fogs is about 50 m). To override the default value, read in the depth of the radiation fog as 50 m by setting ZINVSA to 0.05 km. For inversion layers where the height of the inversion or boundary layer is not known, a default value of 2 km is selected.

Case 4 is represented by a profile for the condition where the vertical structure is essentially constant with altitude, with the exception of the lowest hundred meters of the boundary layer. An appropriate default value is the nominal background value for the 0.55- $\mu\text{m}$  extinction coefficient for the fair weather case. Numerous observations have shown that the extinction coefficient is essentially constant within the planetary layer for well mixed conditions. Setting the coefficient C equal to zero in Eq. (35) will cause the algorithm to default to the observed surface value while providing a constant vertical profile.

Table 14 gives the tabular values of the 0.55- $\mu\text{m}$  extinction coefficients that are to be used as boundary values for the different cases in their respective regions of applicability.

Table 14. Summary of the Conditions and Parameter Values for Different VSA Cases  
 $k_e (0.55 \mu\text{m}) = A \exp [ B \exp ( C z ) ]$

	Case 1 (B < 0, C < 0)	Case 2 (B > 0, C > 0)	Case 2' (B > 0, C > 0)	Case 3 (B < 0, C > 0)	Case 4 (B > 0, C < 0)
Range of k	7.1 - 92 km <sup>-1</sup>	0.40 - 7.1 km <sup>-1</sup>	0.05 - 0.40 km <sup>-1</sup>	0.05 - 7.1 km <sup>-1</sup>	0.05 - 7.1 km <sup>-1</sup>
Region of applicability	thick fog/clouds (ceiling obscured)	haze/fog ceiling < 2000 m	clear/haze ceiling < 2000 m	no ceiling, or ceiling > 2000 m, distinct low-lying inversion or boundary layer	no ceiling, or ceiling > 2000 m, no inver- sion or bound- ary layer
Surface visibility (that is, meteorological range)	Visibility ≤ 0.5 km	Visibility ≈ 0.5-10 km	Visibility > 10 km	Visibility > 0.5 km	Visibility > 0.5 km
A	92 km <sup>-1</sup>	0.40 km <sup>-1</sup>	0.9 × D	1.1 × D	0.05 km <sup>-1</sup> *
B	ln (D/A)	ln (D/A)	ln (D/A)	ln (D/A)	ln (D/A)
C	-0.014 m <sup>-1</sup>	$\frac{1}{Z_c} \ln \left[ \frac{\ln(E/A)}{\ln(D/A)} \right]$	$\frac{1}{Z_c} \ln \left[ \frac{\ln(E/A)}{\ln(D/A)} \right]$	$\frac{1}{Z_b} \ln \left[ \frac{\ln(E/A)}{\ln(D/A)} \right]$	-0.015 m <sup>-1</sup> (default value)
D	initial value at surface or at cloud boundary (note D < A)	initial value at surface (note D > A)	initial value at surface (note D < 0.4 km <sup>-1</sup> )	initial value at surface (note D < A)	initial value at surface (note D > A)
E	(not used)	7.1 km <sup>-1</sup>	7.1 km <sup>-1</sup>	0.05 km <sup>-1</sup> *	(not used)
Z <sub>c</sub>	(not used)**	ceiling height (m)	ceiling height (m)	inversion or boundary layer height (m)	(not used)

\*A nominal background value for the lower troposphere.

\*\*When the fog or cloud depth is not known (usually the case), the algorithm should be used only up to 200 m above the surface or cloud boundary (a default value for the stratus cloud thickness).

#### 2.3.7.4 Activation of the Vertical Structure Algorithm

The operation of the Vertical Structure Algorithm (VSA) is controlled by three parameters, in addition to the Meteorological Range at the surface (VIS) and type of aerosol (IHAZE) for the boundary layer. These three additional parameters are: the cloud ceiling height (altitude of the cloud base), the thickness of the cloud or fog, and the height of the inversion or boundary layer, ZCVSA, ZTVSA, and ZINVSA respectively. The type of aerosol vertical profile generated depends on the values input for these parameters. The different cases or profile types selected are summarized in Table 15. Note that the value of ZINVSA will be ignored unless ZCVSA < 0.

The VSA defines the aerosol extinction at nine heights, from the ground to the top of the cloud (ZCVSA + ZTVSA) or the top of the boundary layer (ZINVSA). Ten meters above this cloud-top or boundary-layer level, the aerosol profile reverts to the standard MODTRAN aerosol vertical distribution (or the user-supplied profile for a MODEL = 7 case). For these nine heights the air pressure, temperature, and the ozone

concentration are found by interpolation from the model atmosphere indicated by the parameter MODEL (see the Users Guide to LOWTRAN 7<sup>2</sup> Section 10).

If the user is not utilizing MODTRAN's built-in cloud models (ICLD=1-10), the relative humidity for the MODTRAN model atmospheres does not consider the presence of clouds (that is, all the model atmospheres have  $RH \leq 80$  percent at all altitudes). The VSA model estimates the relative humidity as a function of the visible ( $\lambda = 0.55 \mu\text{m}$ ) extinction for the nine levels:

$$RH(z) = \begin{cases} \frac{86.407 + 6.953 \cdot \ln[k_e(z)]}{100\%}, & k_e < 7.064 \text{ km}^{-1} \\ 100\%, & k_e \geq 7.064 \text{ km}^{-1} \end{cases} \quad (37)$$

If the user inputs their own relative humidity profile (MODEL = 7), that will be used instead of Eq. (37).

**Table 15. Data Inputs and Default Values for the Different VSA Cases**

<u>Case</u>	<u>Selected by</u>	<u>Defaults</u> (Used if the indicated parameter = 0)
1. Fog	$VIS \leq 0.5 \text{ km}, ZCVSA \geq 0$	$ZCVSA = 0, ZTVSA = 0.2 \text{ km}$
2. Haze / light Fog Below Cloud	$0.5 < VIS \leq 10 \text{ km}, ZCVSA \geq 0$	$ZCVSA$ depends on $VIS$ $ZTVSA = 0.2 \text{ km}$
2'. Moderate / high Visibility Below Cloud	$VIS > 10 \text{ km}, ZCVSA \geq 0$	$ZCVSA = 1.8 \text{ km}$ $ZTVSA = 0.2 \text{ km}$
3. Radiation Fog / Haze Layer, No Low Cloud	$VIS > 0.5 \text{ km}, ZCVSA < 0,$ $ZINVSA \geq 0$	$ZINVSA = 0.2$ <u>RAD FOG</u> If ( $VIS < 2.0 \text{ km}$ or $IHAZE = 9$ ) $2.0$ <u>HAZE</u> If ( $VIS > 2.0 \text{ km}$ and $IHAZE \neq 9$ )
4. No Boundary Layer or Low Cloud	$VIS > 0.5 \text{ km}, ZCVSA < 0,$ $ZINVSA \geq 0$	



## 2.4 Particulate Extinction

### 2.4.1. The Rain Model

#### 2.4.1.1 Introduction

The rain model described in this section was chosen because it is able to relate the transmission over a given path to the most directly obtainable meteorological parameter. This parameter is the rain rate in mm/h, reported by worldwide weather stations on a six hourly basis.

The Marshall-Palmer (M-P)<sup>177</sup> raindrop size distribution was chosen because the two main components are rain rate and drop diameter, and the M-P raindrop size distribution is widely accepted in the research community. The M-P distribution is the same one being used in the millimeter region (Falcone et al)<sup>39</sup> by the FASCOD3P (Anderson et al)<sup>178</sup> high-resolution atmospheric transmittance/radiance modeling code.

#### 2.4.1.2 Formulation of the Model

The M-P drop size distribution is given in Eq. (38)

$$\frac{dN}{dD} = n(D) = N_o \exp(-\Lambda D) \quad , \quad (38)$$

where

$$N_o = 8,000. \text{ mm}^{-1} \text{ m}^{-3} \quad (39a)$$

$$\Lambda = 4.1 R^{-0.21} \quad (39b)$$

$R$  = rain rate ( $\text{mm hr}^{-1}$ )

$D$  = drop diameter (mm)

From Mie theory we can write the extinction coefficient,  $k_{\text{ext}}$ :

$$k_{\text{ext}} = \int_0^{\infty} \frac{\pi}{4} D^2 Q_{\text{ext}} [\pi D/\lambda, m(\lambda)] \frac{dN}{dD} dD \quad , \quad (40)$$

where  $Q_{\text{ext}}$  is the Mie Extinction Efficiency,  $\lambda$  is the wavelength, and  $m(\lambda)$  is the complex refractive index of water. Since for rain  $0.1 < D < 5$  mm, in the visible and infrared we have ( $D \gg \lambda$ ). Therefore,  $Q_{\text{ext}} \approx 2$ , independent of the wavelength. Using this assumption and Eq. (38) in Eq. (40) we have:

$$k_{\text{ext}} \approx \frac{\pi}{2} N_o \int_0^{\infty} D^2 \exp(-\Lambda D) dD \quad (41)$$

Carrying out the integration, this simplifies to:

$$k_{\text{ext}} \approx \pi N_o \Lambda^{-3} \quad (42)$$

Substituting Eq. (39) in Eq. (42) yields:

$$k_{\text{ext}} \approx 0.365 R^{0.63} (\text{km}^{-1}) \quad (43)$$

We should note here that this derivation shows that the extinction due to rain is independent of wavelength, assuming

$$\lambda \ll D \approx 0.1 \text{ to } 10 \text{ mm}.$$

In practice this assumption applies throughout the visible and the IR windows.

The transmittance over path length,  $s$ , in km, can be written as

$$\tau = \exp(-ks) \quad (44)$$

or using Eq. (43)

$$\tau = \exp(-0.365 R^{0.63} s) \quad (45)$$

It should be recognized that the extinction [Eq. (43)] or transmittance [Eq. (45)] measured by a transmissometer will, in general, have to be corrected for forward scattering effects. However, since this correction is a function of the receiver and source geometries it is beyond the scope of the current MODTRAN model. A discussion of this correction is given by Shettle et al<sup>179</sup>.

### 2.4.1.3 Other Raindrop-Size Distributions

Several researchers have attempted to relate the parameters in the exponential raindrop size distribution to the type of rainfall (for example, Joss and Waldvogel,<sup>180</sup> and Sekhon and Srivastava<sup>181</sup>). These different parameterizations lead to an expression similar to Eq. (43) for the extinction:

$$k_{ext} = A \bullet R^B \quad (46)$$

For the convenience of the MODTRAN users who may wish to modify SUBROUTINE TNRAIN, to implement one of these other models, the parameters for size distributions and extinction coefficients are summarized in Table 16.

**Table 16. Parameters Relating Size Distribution [Eq. (38)] Extinction**

Coefficient [Eq. (46)] to Rain Rate for Different Types of Rain

Type of Rain	$N_0$ ( $\text{mm}^{-1} \text{m}^{-3}$ )	$\Lambda$ ( $\text{mm}^{-1}$ )	A	B
Marshall-Palmer <sup>177</sup>	8, 000	4.1 $R^{-0.21}$	0.365	0.63
Drizzle (Joss and Waldvogel) <sup>180</sup>	30, 000	5.7 $R^{-0.21}$	0.509	0.63
Widespread (Joss and Waldvogel) <sup>180</sup>	7,000	4.1 $R^{-0.21}$	0.319	0.63
Thunderstorm (Joss and Waldvogel) <sup>180</sup>	1,400	3.0 $R^{-0.21}$	0.163	0.63
Thunderstorm (Sekhon and Srivastava) <sup>181</sup>	7,000 $R^{0.37}$	3.8 $R^{-0.14}$	0.401	0.79

The divergence between the two different thunderstorm models indicates the difficulty in making such parameterizations and the uncertainty in the parameter values given.

### 2.4.1.4 Sample Output of Typical Rain Cases

The atmospheric transmittance, using the M-P model with the MODTRAN code for rain rates varying from 1 to 100 mm/hr is shown in Figure 27 for 400 through 4000  $\text{cm}^{-1}$  and in Figure 28 for 4000 through 40000  $\text{cm}^{-1}$ ,

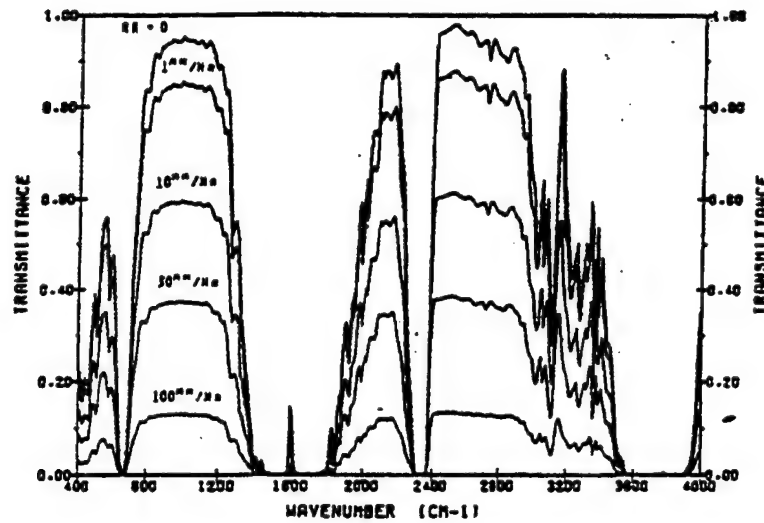


Figure 27. Atmospheric Transmittance for Different Rainrates (RR) and for Frequencies From 400 to 4000  $\text{cm}^{-1}$ . The measurement path is 300 m at the surface with  $T = T_{\text{dew}} = 10^\circ\text{C}$ , with a meteorological range of 23 km in the absence of rain.

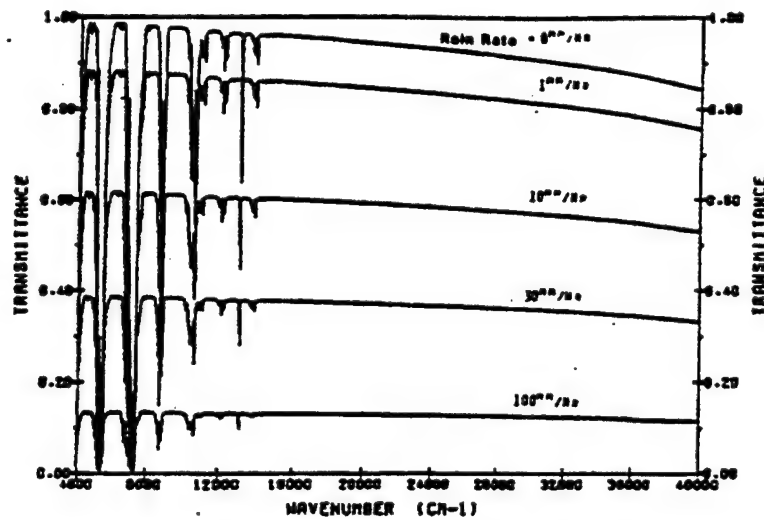


Figure 28. Atmospheric Transmittance for Different Rain rates (RR) and for Frequencies From 4000 to 40000  $\text{cm}^{-1}$ . The measurement path is 300 m at the surface with  $T = T_{\text{dew}} = 10^\circ\text{C}$ , with a meteorological range of 23 km in the absence of rain

## 2.4.2 Water Clouds

### 2.4.2.1 Introduction

Meteorologists classify clouds as low, middle or high according to the following rough estimates by Berry et al.<sup>182</sup>

low clouds	0-2000 meters
middle clouds	2000-6500 meters
high clouds	> 6500 meters

In addition, the vertical development of clouds should also be included. Table 17 relates the general classification of clouds to specific cloud type nomenclature.

**Table 17. Cloud Heights and Vertical Development**

Cloud Type	Cloud Symbol	Cloud Heights
Low clouds		
Stratus	St	0-2000 meters
Stratocumulus	Sc	
Nimbostratus	Ns	
Middle Clouds		2000-6500 meters
Altostratus	As	
Altostratus	Ac	
Vertically Developed Clouds		
Cumulus	Cu	700-8000 meters
Cumulonimbus	Cb	700-20000 meters

The water clouds covered in this section belong to the families of low and middle cloud classification. Specific references for various cloud types are Mason,<sup>183</sup> Borovikov,<sup>184</sup> Berry et al.,<sup>182</sup> Carrier,<sup>185</sup> Luke,<sup>186</sup> Diem,<sup>187</sup> Weickman and Aufra Kampe,<sup>188</sup> Durbin,<sup>189</sup> Gates and Shaw,<sup>190</sup> and Squires and Twomey.<sup>191</sup>

### 2.4.2.2 Choice of Cloud Models

The five water cloud models included in MODTRAN are; Stratus, Stratocumulus, Nimbostratus, Altostratus, and Cumulus. These models are based on a subset of the cloud models developed by Silverman and Sprague(1970),<sup>192</sup> and described in considerable detail by Falcone et al.<sup>39</sup>(1979). They were selected in part to encompass as wide a range as possible of the IR optical properties of the cloud models developed by Silverman and Sprague and to include typically recognizable cloud types.

The droplet size distributions for the models are represented by a modified gamma distribution, with  $\gamma = 1$  :

$$\frac{dN}{dr} = n(r) = a r^{\alpha} \exp(-b r^{\gamma}) \quad (47)$$

where  $a$ ,  $\alpha$ ,  $b$ , and  $\gamma$  are parameters defining the size distribution. The values of the parameters characterizing the fog and cloud droplet size distributions are summarized in Table 18.

#### 2.4.2.3 Structure of Cloud Models

Cloud water content is related to cloud droplet spectra. The values as originally proposed by Silverman and Sprague are for "typical" clouds. These "typical" clouds are not average values. For example, Silverman's Cloud Model 5 (our Cumulus, ICLD = 1) has a liquid water content of  $1\text{g/m}^3$  (Table 18). This type of cloud may have typical values of liquid water from  $0.5$  to  $1\text{g/m}^3$  with values as high as  $4\text{g/m}^3$  depending on geographical location (for example, New England vs. Florida). Liquid water content of clouds is very important because the cloud droplets are Rayleigh scatterers (see Figures 6-8 and Figure 13 in the Falcone et al.<sup>39</sup> report). Research has shown (Blau et al.<sup>193</sup>) that the liquid water content of non-precipitating clouds have values from  $0.1\text{g/m}^3$  to  $0.5\text{g/m}^3$  whereas precipitating clouds often have LWC greater than  $1.0\text{g/m}^3$

**Table 18. Parameters for Fog and Cloud Size Distribution Models Used**

Cloud Type	$\alpha$	$b$	$a$	$N_0^*$ ( $\text{cm}^{-3}$ )	$W^*$ ( $\text{g-m}^{-3}$ )	$R_N(\mu\text{m})$	$R_M(\mu\text{m})$	$\text{Ext}^*(\text{km}^{-1})$ $\lambda=0.55\ \mu\text{m}$
Heavy Advection Fog	3	0.3	0.027	20	0.37	10.0	20.0	28.74
Moderate Radiation Fog	6	3.0	607.5	200	0.02	2.0	3.0	8.672
Cumulus	3	0.5	2.604	250	1.00	6.0	12.0	130.8
Stratus	2	0.6	27.0	250	0.29	3.33	8.33	55.18
Stratus/Strato-Cumulus	2	0.75	52.734	250	0.15	2.67	6.67	35.65
Alto-Stratus	5	1.111	6.268	400	0.41	4.5	7.2	91.04

Nimbostratus	2	0.425	7.676	200	0.65	4.7	11.76	87.08
Cirrus	6	0.09375	2.21 ( $10^{-12}$ )	0.025	0.06405	64.0	96.0	1.011
Thin Cirrus	6	1.5	0.011865	0.5	3.128 ( $10^{-4}$ )	4.0	6.0	0.0831

\* Nominal values are shown for the number density, ( $N_0$ ), the liquid water (or ice) content ( $W$ ), and the visible extinction ( $Ext$ ); they can be specified by the user in running the code.  $R_N$ , and  $R_M$  denote the mode radii for the number and mass distribution respectively.

The structure of a typical modeled cloud with 3-8 mm/hr of rain is shown in Figure 29.

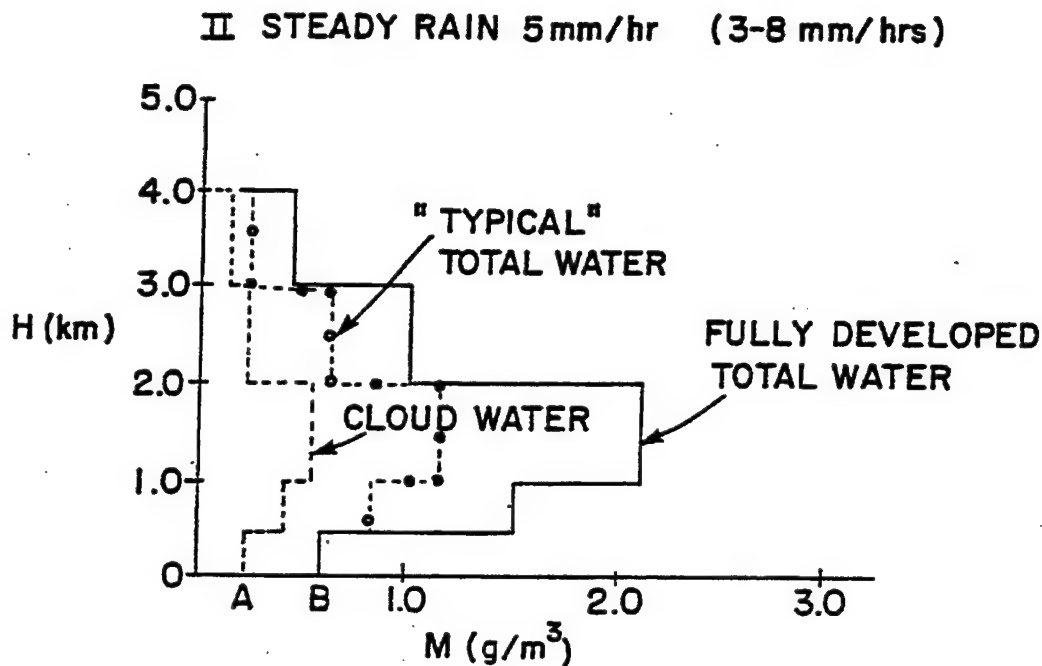


Figure 29. Model of a "typical" cloud with 5mm/hr steady rain

#### 2.4.2.4 Radiative Properties of Clouds

The radiative properties of the clouds were derived from complete Mie<sup>194</sup> scattering calculations using the refractive index of water from Hale and Querry (1973)<sup>70</sup> for wavelengths through 200  $\mu\text{m}$ , and for the longer wavelengths (in the mm region) the formulations of Ray (1972)<sup>195</sup> were utilized. The resulting extinction coefficients for the cloud models are displayed in Figure 30 as a function of wavelength.

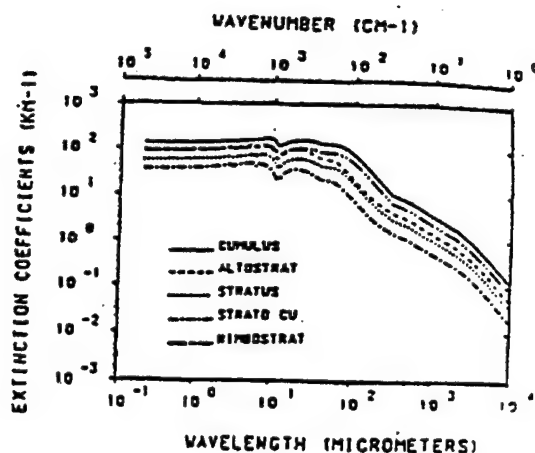


Figure 30. Spectral Dependence of the extinction coefficients for each water cloud model.

### 2.4.3 Ice Clouds

Three cirrus cloud models are retained in MODTRAN. The NOAA cirrus cloud model (next section) is aptly described by Hall et al. in chapter 7 of the LOWTRAN 6 report<sup>3</sup>. The NOAA model is retained for comparison with earlier LOWTRAN and FASCODE models. The regular cirrus model and the sub-visual cirrus model, described after the NOAA model, can be utilized in radiance calculations.

According to the International Cloud Atlas,<sup>196</sup> cirrus clouds are "composed almost exclusively of ice crystals". Since there is a scarcity of freezing nuclei active above  $-20^{\circ}\text{C}$  in the atmosphere, cirrus clouds are not often found at higher temperatures. In polar regions and in wintertime temperate zones near the Arctic or Antarctic, these low temperatures generally occur in the middle or upper troposphere.

#### 2.4.3.1 NOAA CIRRUS CLOUD MODEL

The NOAA empirically based cirrus cloud model developed for the calculation of transmittance through cirrus clouds should be considered valid from the ultraviolet  $0.317\text{ }\mu\text{m}$  to the  $10\text{ }\mu\text{m}$  window. The derivation of the model is based on numerous worldwide cirrus measurement programs and cirrus climatologies. This model does not separate the scattering and absorption and therefore cannot be used for radiance calculations.



### 3. THE MODTRAN MODEL

#### 3.1 Introduction

MODTRAN is a moderate resolution version of LOWTRAN 7 (Ref. 2). MODTRAN's spectral resolution is  $2\text{ cm}^{-1}$  (FWHM). Molecular absorption is calculated in  $1\text{ cm}^{-1}$  spectral bins, while the other parts of the calculation remain unchanged. The molecular species affected are :

water vapor, carbon dioxide, ozone, nitrous oxide, carbon monoxide, methane, oxygen, nitric oxide, sulfur dioxide, nitrogen dioxide, ammonia and nitric acid.

Their absorption properties (the band model parameters) are calculated from the HITRAN 1992 line atlas<sup>20</sup>, which contains all lines in the  $0 - 22,600\text{ cm}^{-1}$  spectral region that have significant absorption for atmospheric paths. The increased resolution of MODTRAN spans the same spectral region as LOWTRAN. Calculations at larger wavenumbers, the visible and ultraviolet spectral regions ( $> 22600\text{ cm}^{-1}$ ), are performed at the lower spectral resolution of LOWTRAN,  $20\text{ cm}^{-1}$ .

A new set of band models for calculating transmittance has been developed for the MODTRAN code. The increased spectral resolution is achieved using an approach developed earlier for a  $5\text{ cm}^{-1}$  option to LOWTRAN 5 (Ref. 5). In that earlier approach, band model parameters were calculated from the existing (1980) HITRAN database and used to determine the equivalent width of the absorbing molecular gases in  $5\text{ cm}^{-1}$  spectral intervals. The MODTRAN 2 band model parameters are calculated in  $1\text{ cm}^{-1}$  intervals.

The molecular transmittance calculation for each bin has three elements. First, the Voigt lineshape of an "Average" line is integrated over the  $1\text{ cm}^{-1}$  interval; when a bin contains more than one line of a given species, the lines are assumed to be randomly distributed with statistical overlap; finally, the contribution from lines whose centers are in nearby bins is calculated as a molecular "continuum" component. The other LOWTRAN components, which have insignificant spectral structure at  $1\text{ cm}^{-1}$ , are calculated at their  $5\text{ cm}^{-1}$  increments and interpolated to arrive at the total transmittance for each interval. The calculational grid consists of non-overlapping  $1\text{ cm}^{-1}$  bins, which are degraded to the desired spectral resolution with an internal triangular slit function. Since these bins are square and non-overlapping, the nominal spectral resolution of MODTRAN is reported as  $2\text{ cm}^{-1}$  (FWHM).

The comparison of MODTRAN and LOWTRAN 7 calculations shown in Figure 35 illustrates the increased spectral resolution. The figure shows the transmittance calculated at 2 and 20  $\text{cm}^{-1}$  resolution for a low altitude slant path through the US Standard Atmosphere. The 2  $\text{cm}^{-1}$  curve results from the internal triangular slit function ( $IFWHM=2$ ), and the 20  $\text{cm}^{-1}$  curve is the regular LOWTRAN 7 result interpolated to 5  $\text{cm}^{-1}$  intervals. The MODTRAN calculation resolves line structure below 2180  $\text{cm}^{-1}$  (primarily water), the band center of the  $\text{N}_2\text{O}$  fundamental at 2220  $\text{cm}^{-1}$ , and the  $\text{CO}_2$  band center at 2284  $\text{cm}^{-1}$ .

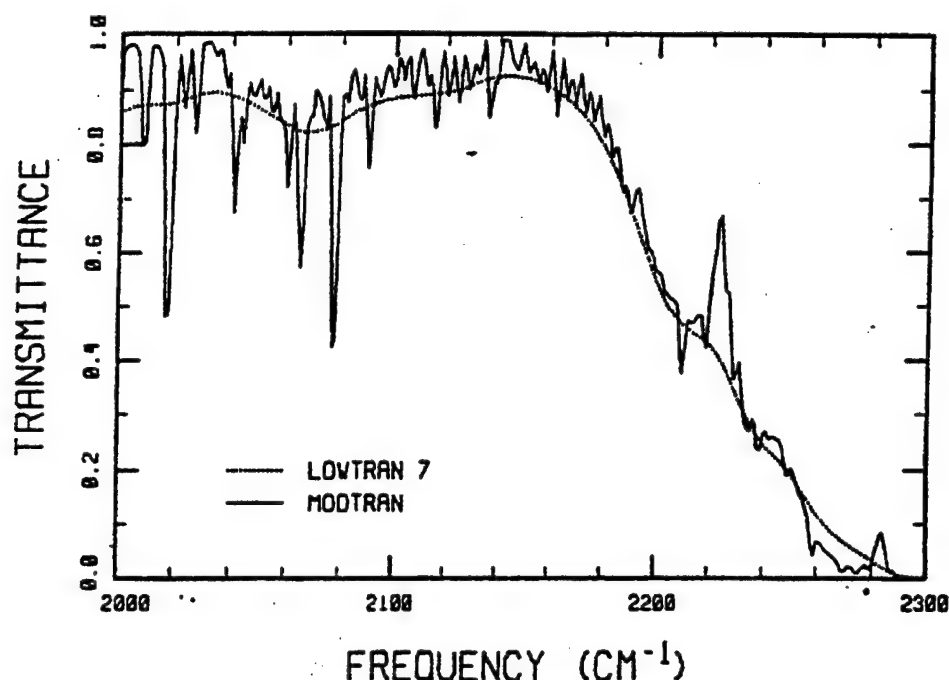


Figure 35. Atmospheric Transmittance for a Slant Path from 5 to 10 km at 15° from Zenith and Through the US Standard Atmosphere with no Haze. The Solid Curve was Calculated with MODTRAN at 2  $\text{cm}^{-1}$  Spectral Resolution, and the Dotted Curve with LOWTRAN 7 at 20  $\text{cm}^{-1}$  Resolution.

The input data sequence for MODTRAN is identical to that of LOWTRAN 7 except for two additional parameters on Cards 1 and 4. A logical parameter, MODTRN, has been added to the front end of CARD 1,

```
READ(IRD,'(L1,I4,12I5,F8.3,F7.2)')MODTRN,MODEL,ITYPE,IEMSCT,
1 IMULT,M1,M2,M3,M4,M5,M6,MDEF,IM,NOPRT,TB0UND,SALB
```

and the input to CARD 4 has been changed to integer format with a resolution parameter, *IFWHM*, added

```
READ(IRD,'(4I10)')IV1,IV2,IDV,IFWHM.
```

*MODTRN* is simply a switch which when set to F (false) permits the running of LOWTRAN 7 and when set to T (true) activates MODTRAN. The parameter *IFWHM*, which is only read if *MODTRN* is true, specifies the full width at half maximum, FWHM, of an internal triangular slit function.

MODTRAN and LOWTRAN 7 differ in their approaches to calculating molecular transmittance. For several different spectral intervals LOWTRAN 7 uses a one-parameter band model (absorption coefficient) plus molecular density scaling functions. The MODTRAN band model uses three temperature-dependent parameters, an absorption coefficient, a line-density parameter and an average linewidth. The spectral region is partitioned into  $1\text{ cm}^{-1}$  bins for each molecule. Within each bin, contributions from transitions whose line centers fall within the bin are modeled separately from nearby lines centered outside of that bin (see Figure 36). The absorption due to lines within the bin is calculated by integrating over a Voigt line shape. The Curtis-Godson approximation (discussed below in 3.3.1.1), is accurate for the moderate temperature variations found in the earth's atmosphere, is used to replace multi-layered paths by an equivalent homogeneous one.

The *k*-distribution method, which is used in the multiple scattering treatment of LOWTRAN 7 to correct for averaging over large spectral intervals, is not necessary in the MODTRAN model. This is true because three (monochromatic) *k* values are used for the  $5\text{ cm}^{-1}$  steps of LOWTRAN 7, while the  $1\text{ cm}^{-1}$  MODTRAN steps provide an equivalent accuracy for the multiple scattering option.

MODTRAN is better suited than LOWTRAN for atmospheric paths which lie completely above 30 km. This is due to the integration over the Voigt lineshape combined with the explicit temperature and pressure dependencies of the band model parameters. The Voigt lineshape is necessary at these altitudes because the Doppler

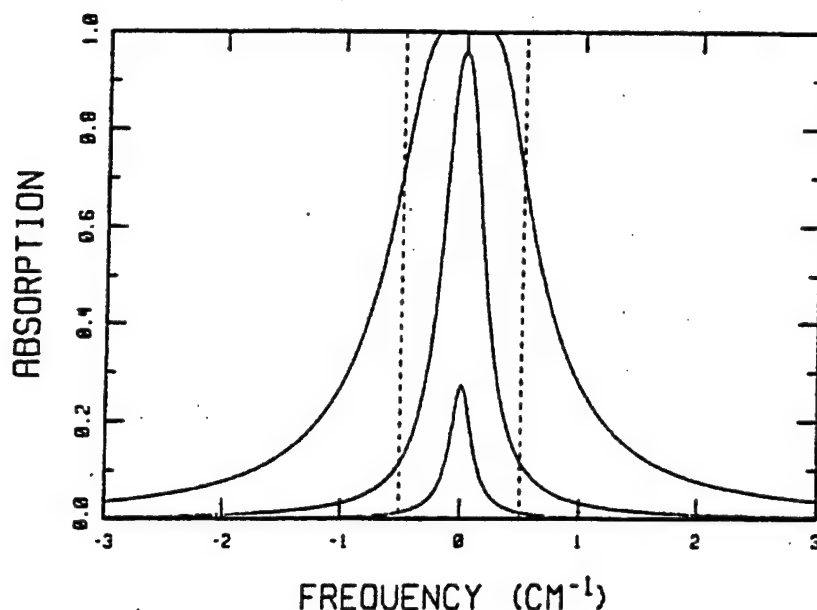


Figure 36. Absorption from Lorentzian Lines with Optical Depths of 0.1, 1, and 10. Halfwidth was Set to  $0.1 \text{ cm}^{-1}$ . In the Band Model Transmittance Formulation, Absorption from Line Centers (Segment of Curves Falling Within the Spectral Bin Denoted by the Dashed Lines) is Modeled Separately from Absorption due to Line Tails (Outside the Dashed Lines).

linewidth is greater than the Lorentz. The  $20 \text{ cm}^{-1}$  versions of LOWTRAN suffer because they use a single set of band model parameters (nominally sea level at 296 K) coupled with spectrally independent scaling functions for the molecular densities. It is also worth mentioning that, for paths which lie completely above 60 km, another problem arises: many of the molecules are no longer in local thermodynamic equilibrium (LTE). This means that the strengths of some molecular bands can no longer be determined from the ambient temperature. MODTRAN gives reasonable results for those bands which are in LTE; the problem is identifying those spectral regions which are not in LTE.

### 3.2 MOLECULAR BAND MODEL PARAMETERS

The basic idea behind band model techniques<sup>5</sup> is to determine a set of parameters from which transmittance over finite frequency intervals can be calculated. In MODTRAN, three band model parameters are used, an absorption coefficient, a line

density and a line width. The absorption coefficient measures the total strength of lines in an interval. The line density is a line-strength weighted average for the number of lines in the interval, and the line-width parameter is a line-strength weighted average line width.

MODTRAN uses a bin width of one wavenumber,  $\Delta\nu = 1 \text{ cm}^{-1}$ . Line data from the HITRAN 1992 database<sup>20</sup> is used to calculate the band model parameters. The compilation contains data on molecular lines in the frequency range 0 to  $22600 \text{ cm}^{-1}$ . For each molecule with lines whose centers fall within a given spectral bin, the temperature-dependent absorption coefficients and line densities along with the line-width parameter are stored for subsequent use in calculating molecular absorption; a single temperature-dependent absorption coefficient parameter is used to determine the tail contributions to each spectral bin from lines centered in nearby bins.

### 3.2.1 Line-Center Parameters

Each frequency bin corresponds to a  $1 \text{ cm}^{-1}$  interval and contains parameters for molecules with lines in that interval. Line center data are derived from the HITRAN database<sup>20,197</sup>, and band model parameters have been determined for the following molecules<sup>198-219</sup>:

H<sub>2</sub>O, CO<sub>2</sub>, O<sub>3</sub>, N<sub>2</sub>O, CO, CH<sub>4</sub>, O<sub>2</sub>, NO, SO<sub>2</sub>, NO<sub>2</sub>, NH<sub>3</sub> &  
HNO<sub>3</sub>

The molecular absorption coefficients ( $S/d$ ) ( $\text{cm}^{-1} \text{ amagats}^{-1}$ ) are calculated at 5 reference temperatures:

$$T = 200, 225, 250, 275 \text{ \& } 300 \text{ K} \quad (48)$$

Linear interpolation is used to calculate absorption coefficients at temperatures between 200 and 300 K. For temperatures below 200 and above 300 K, the extreme values, ( $S/d$ ) ( $T=200\text{K}$ ) and ( $S/d$ ) ( $T=300\text{K}$ ), respectively, are used. The absorption band model parameters are calculated from the individual line strengths,

$$(S/d) = \frac{1}{\Delta\nu} \sum_j S_j(T) \quad (49)$$

Here  $S_j(T)$  is the integrated line strength at temperature  $T$  of the  $j$ 'th line of molecule  $m$  in bin  $i$ . The line strength at an arbitrary temperature is scaled from the HITRAN line strength at its standard temperature,  $T_s = 296$  K, by:

$$S_j(T) = \frac{Q_r(T_s)Q_v(T_s)}{Q_r(T)Q_v(T)} \frac{1 - \exp(-hc\nu_j/kT)}{1 - \exp(-hc\nu_j/kT_s)} \exp\left(\frac{E_j}{k} \frac{T - T_s}{T T_s}\right) S_j(T_s) \quad (50)$$

where  $Q_r$  and  $Q_v$  are the rotational and vibrational partition functions,  $E_j$  is the energy of the lower transition state, and  $\nu_j$  is the transition frequency. The constants are the speed of light ( $c$ ), the Boltzman constant ( $k$ ), and the Planck constant ( $h$ ).

A collision-broadened or Lorentz line-width parameter  $\gamma_c^\circ$  is defined at STP ( $T_0 = 273.15$  K,  $P_0 = 1013.25$  mb). A single value can be stored because the pressure and temperature dependence of the Lorentz line width is easily modeled,

$$\gamma_c(T, P) = \gamma_c^\circ \frac{P}{P_0} (T_0/T)^x \quad (51)$$

where the exponent  $x$  has been set to  $1/2$  for all molecules except  $\text{CO}_2$ , for which  $x$  has been taken as  $3/4$ . The  $\gamma_c^\circ$  band model parameter is calculated as a line-strength weighted average over the tabulated Lorentz line widths  $\gamma_{c,j}(T_s)$ :

$$\gamma_c^\circ = (T_s/T_0)^x \left[ \sum_j \gamma_{c,j}(T_s) S_j(T_s) \right] / \left[ \sum_j S_j(T_s) \right] \quad (52)$$

Like the absorption coefficients, the line-density band-model parameters ( $1/d$ ) (cm) are calculated at the five reference temperatures and interpolated when used by the band model subroutines. The line density is defined by:

$$(1/d) = \frac{1}{\Delta\nu} \left( \sum_{j=1}^N S_j \right)^2 / \sum_{j=1}^N S_j^2 \quad (53)$$

This definition for the line spacing, which is derived in the appendix of the Berk report,<sup>1</sup> produces a smaller value than the usual definition involving a sum over the square root

of the line strengths.<sup>223,224</sup> The new form results when account is taken of finite bin widths. The absorption of a line within a finite bin is less than its total line strength: this is consistent with a decreased value for  $(1/d)$ .

### 3.2.2 Line-Tail Parameters

The line-tail parameters consist of line contributions from lines located outside of a given bin but within  $\pm 25 \text{ cm}^{-1}$ . The line-tail absorption coefficient band-model parameters  $C \text{ (cm}^{-1} \text{ amagat}^{-1})$  are determined by integrating the Lorentz line shape over this interval:

$$C = \frac{1}{\pi \Delta \nu} \sum_{k=i-25}^{i+25} (1 - \delta_{ki}) \left\{ \frac{[(S/d) \gamma_c]_k}{(k-i)^2 + 1/4} f[(k-i) \Delta \nu] \right. \\ \left. + \frac{[(S/d) \gamma_c]_k}{(k+i)^2 + 1/4} f[(k+i) \Delta \nu] \right\}, \quad (54)$$

where the delta function serves to exclude the  $k=i$  term from the sum (i.e., the line center contribution), and  $f[\Delta \nu]$  is a lineshape form factor. The form factor is 1.0 within  $25 \text{ cm}^{-1}$  of the line centers. Except for  $\text{H}_2\text{O}$  and  $\text{CO}_2$ , tail contributions beyond  $25 \text{ cm}^{-1}$  are assumed negligible and are not included. The usual LOWTRAN 7 water continuum consists of tail contributions from lines located beyond  $25 \text{ cm}^{-1}$  plus extrapolated (flat) values of this contribution within  $25 \text{ cm}^{-1}$  (for smoothness). For  $\text{CO}_2$ , the continuum from FASCOD2<sup>40</sup> has been added to the parameter  $C$  to account for the tail contributions from lines beyond  $25 \text{ cm}^{-1}$ :

$$C \rightarrow C + \nu_i \tanh\left(\frac{hc \nu_i}{2kT}\right) \frac{T_s}{T} \tilde{C}(\nu_i) \quad (55)$$

Here,  $\tilde{C}(\nu_i)$  is the frequency interpolated value from the FASCOD2 block data */FCO2/*. For both  $\text{H}_2\text{O}$  and  $\text{CO}_2$ , the value of  $C$  has also been reduced by an amount equal to its value at  $25 \text{ cm}^{-1}$  from the line center since this contribution is already included in the continuum data. The constant  $C$  is proportional to pressure (which arises from the Lorentz line width, Equation (51)):

$$C(P) = \frac{P}{P_0} C(P_0) \quad (56)$$

### 3.2.3 Parameter Data File

Because of the large amount of data, the band-model parameters are stored in an external file that is written in binary format; this allows for quicker access during the calculation. Each entry corresponds to a  $1\text{ cm}^{-1}$  interval and contains a molecular parameter set. Since no data for molecules without lines in a given interval are stored, a parameter identifying the active species is included.

The first entry of a parameter set is the bin number,  $i$ . From the bin number, the midpoint of the interval is calculated

$$\nu_i = i \Delta\nu \quad , \quad (57)$$

and all lines whose centers fall in the half-opened interval  $[\nu_i - \Delta\nu/2, \nu_i + \Delta\nu/2]$  contribute to bin  $i$ .

The molecular parameter set is identified by the parameter  $m$ . The HITRAN database<sup>20</sup> convention is used for this labeling

$m$	1	2	3	4	5	6	7	8	9	10	11	12
molecule	H <sub>2</sub> O	CO <sub>2</sub>	O <sub>3</sub>	N <sub>2</sub> O	CO	CH <sub>4</sub>	O <sub>2</sub>	NO	SO <sub>2</sub>	NO <sub>2</sub>	NH <sub>3</sub>	HNO <sub>3</sub>

The next entries in the parameter set are the molecular absorption coefficients ( $S/d$ ) ( $\text{cm}^{-1}\text{ amagats}^{-1}$ ) calculated at the five reference temperatures. These entries are followed by the STP Lorentz half width,  $\gamma^\circ_{\text{C}}$ , multiplied by  $10^4$  and stored as an integer. Line-spacing parameters ( $1/d$ ) for the five reference temperatures complete the line-center parameter sets.

For line tails, each line contains data on one or two molecules. These line-tail parameter sets use the same format as the line-center parameter sets. Again, the first entry is the bin number  $i$  and the second entry is the molecule designation  $m$ . To recognize that these parameter sets denote line-tail contributions, their molecule labels are offset by 12.

$m$	13	14	15	16	17	18	19	20	21	22	23	24
molecule	H <sub>2</sub> O	CO <sub>2</sub>	O <sub>3</sub>	N <sub>2</sub> O	CO	CH <sub>4</sub>	O <sub>2</sub>	NO	SO <sub>2</sub>	NO <sub>2</sub>	NH <sub>3</sub>	HNO <sub>3</sub>



The continuum parameters, C, are stored in place of the (S/d). Unless all tail contributions have been defined for frequency bin i, the molecular designation and continuum parameters for a second molecule follow the first on the same parameter set.

A sample of the formatted data for frequency bins 2294 and 2295 is shown below:

2294 1	2.561E-07 9.816E-07 3.157E-06 8.694E-06 2.083E-05	592	1.814E+00 2.645E+00 3.273E+00 3.359E+00 3.182E+00
2294 2	1.384E+00 1.436E+00 1.598E+00 1.904E+00 2.377E+00	730	1.138E+00 1.375E+00 1.837E+00 2.486E+00 3.021E+00
2294 4	1.961E-03 2.842E-03 3.769E-03 4.683E-03 5.540E-03	757	2.227E+00 2.385E+00 2.517E+00 2.627E+00 2.720E+00
2294 13	1.681E-08 6.871E-08 2.090E-07 5.126E-07 1.071E-06	14	8.325E-02 7.507E-02 7.245E-02 7.535E-02 8.356E-02
2294 15	5.052E-09 5.037E-09 4.896E-09 4.678E-09 4.116E-09	16	3.339E-04 4.363E-04 5.346E-04 6.230E-04 6.978E-04
2294 18	3.393E-06 3.291E-06 3.529E-06 4.055E-06 1.816E-06	0	0.000E+00 0.000E+00 0.000E+00 0.000E+00 0.000E+00
2295 2	3.195E-02 7.865E-02 1.678E-01 3.166E-01 5.403E-01	688	2.986E+00 2.537E+00 2.305E+00 2.217E+00 2.211E+00
2295 4	2.653E-03 3.804E-03 5.003E-03 6.174E-03 7.261E-03	766	2.729E+00 2.966E+00 3.161E+00 3.320E+00 3.449E+00
2295 6	1.511E-06 1.603E-06 1.659E-06 1.687E-06 1.691E-06	725	1.824E+00 1.898E+00 1.946E+00 1.975E+00 1.991E+00
2295 13	2.796E-08 1.118E-07 3.432E-07 8.628E-07 1.860E-06	14	1.309E-01 1.257E-01 1.302E-01 1.444E-01 1.675E-01
2295 16	3.903E-04 4.882E-04 5.769E-04 6.524E-04 7.129E-04	18	2.271E-06 3.894E-06 6.420E-06 9.811E-06 1.393E-05

In bin 2294, there are H<sub>2</sub>O, CO<sub>2</sub> and N<sub>2</sub>O line center parameter sets and tail data for H<sub>2</sub>O, CO<sub>2</sub>, O<sub>3</sub>, N<sub>2</sub>O and CH<sub>4</sub>. In bin 2295, there is no line center data for H<sub>2</sub>O, but lines do exist for CH<sub>4</sub>. Also, bin 2295 does not contain any O<sub>3</sub> continuum data.

### 3.3 BAND-MODEL TRANSMITTANCE FORMULATION

#### 3.3.1 Line-Center Transmittance

The band-model transmittance formulation<sup>5</sup> developed for the 5 cm<sup>-1</sup> option to LOWTRAN 5 (Ref. 4) was used to create a moderate resolution option for LOWTRAN 7. The expression used to calculate molecular transmittance is based on a statistical model for a finite number of lines within a spectral interval, and is given by:

$$\tau = (1 - \langle W_{sl} \rangle / \Delta \nu)^{\langle n \rangle} \quad (58)$$

where  $\tau$  is the transmittance,  $\langle W_{sl} \rangle$  is the Voigt single-line equivalent width for the line-strength distribution in a spectral interval, and  $\langle n \rangle$  is the path-averaged effective number of lines in the bin:

$$\langle n \rangle = \Delta \nu \langle 1/d \rangle \quad (59)$$

$\langle 1/d \rangle$  is the path-averaged line spacing.

For large  $\langle n \rangle$  [(S/d) and  $\Delta \nu$  fixed], the transmittance simplifies to the more recognizable exponential form, Beer's Law, given by:

$$\tau \rightarrow \exp(-\langle W_{sl} \rangle \langle 1/d \rangle) \quad (60)$$

for the relatively low temperatures encountered in the earth's atmosphere, the number of lines in a bin from a single molecular species is usually small so that the power law transmittance formulation is preferred.

There are many approximations available for calculating the equivalent width of a Voigt line shape; different ones are valid for different regimes, Doppler or collision broadening, weak line or strong line, etc. However, no single approximation is adequate for the range of pressures and optical path lengths encountered in atmospheric transmission calculations. Rather than incorporating different approximations, a direct evaluation of the exact expression for the equivalent width of a single line in a finite spectral interval;  $\langle W_{sl} \rangle$  is given by:

$$\langle W_{sl} \rangle = \frac{\Delta \nu}{X_m} \int_0^{X_m} 1 - \exp\left\{-[Su/d] \sqrt{\ln 2/\pi} F(X,Y)/\langle \gamma_d/d \rangle\right\} dx \quad (61)$$

$$F(X,Y) = \frac{Y}{\pi} \int_{-\infty}^{\infty} \frac{\exp(-T^2) dT}{Y^2 + (X-T)^2}, \quad (62)$$

$$X_m = \frac{1}{2} \sqrt{\ln 2} \langle n \rangle / \langle \gamma_d/d \rangle, \quad (63)$$

$$Y = \sqrt{\ln 2} \langle \gamma_c/d \rangle / \langle \gamma_d/d \rangle, \quad (64)$$

where  $F(X,Y)$  is the Voigt line shape function,  $[Su/d]$  is the total optical depth, and  $\langle \gamma_d/d \rangle$  and  $\langle \gamma_c/d \rangle$  are the path averaged Doppler and collision broadened line shape band model parameters, respectively. To accurately calculate  $\langle W_{sl} \rangle$ , we separate its contributions as shown:

$$\langle W_{sl} \rangle = \langle W_{sl}^0 \rangle - \langle W_{sl}^1 \rangle \quad (65)$$

$$\langle W_{sl}^0 \rangle = \frac{\Delta \nu}{X_m} \int_0^{\infty} 1 - \exp\left\{-[Su/d] \sqrt{\ln 2/\pi} F(X,Y)/\langle \gamma_d/d \rangle\right\} dx \quad (66)$$

$$\langle W_{sl}^1 \rangle = \frac{\Delta \nu}{X_m} \int_{X_m}^{\infty} 1 - \exp \left\{ -[Su/d] \sqrt{\ln 2/\pi} F(X, Y) / \langle \gamma_d / d \rangle \right\} dx \quad (67)$$

The tail contribution,  $\langle W_{sl}^1 \rangle$  can easily be evaluated in terms of the error function since  $X_m \gg Y$  for cases calculated with MODTRAN:

$$\langle W_{sl}^1 \rangle \approx \exp(-z^2) + \sqrt{\pi} z \operatorname{erf}(z) - \quad , \quad (68)$$

$$z \equiv \frac{2}{\langle n \rangle} \sqrt{[Su/d] \langle \gamma_c / d \rangle / \pi} \quad . \quad (69)$$

To determine  $\langle W_{sl}^0 \rangle$ , an interpolation between the Lorentz and Doppler limits is used. Based on an interpolation formula developed by Ludwig et. al. [Equations (5-25) and (5-26)],<sup>220</sup> the Lorentz and Doppler equivalent widths are given by:

$$L \equiv \frac{4}{4 + [Su/d] / \langle \gamma_c / d \rangle} \quad , \quad (70)$$

$$D \equiv \frac{2}{\ln 2} \frac{\langle \gamma_d / d \rangle^2}{[Su/d]^2} \ln \left( 1 + \frac{\ln 2}{2} \frac{[Su/d]^2}{\langle \gamma_d / d \rangle^2} \right) \quad , \quad (71)$$

$\langle W_{sl}^0 \rangle$  is determined from the following interpolation formula which is more numerically stable:

$$\langle W_{sl}^0 \rangle^2 = \frac{[Su/d]^2}{\langle 1/d \rangle^2} \left\{ 1 - (1-L)(1-D) / \sqrt{1 - LD(2-L)(2-D)} \right\} \quad 72)$$

Figure 37 shows a comparison of Equation (72) to exact calculations for the equivalent width of a single, isolated spectral line with a Voigt lineshape. The lowest curve is the pure Doppler limit and the highest curve is the Lorentz limit. The exact values are taken from Penner.<sup>225</sup> The predictions of Equation (72) are shown as solid lines for the same values of the parameter  $Y$  in Equation (64). The overall agreement between the two families of curves illustrates the quality of the interpolation formula.

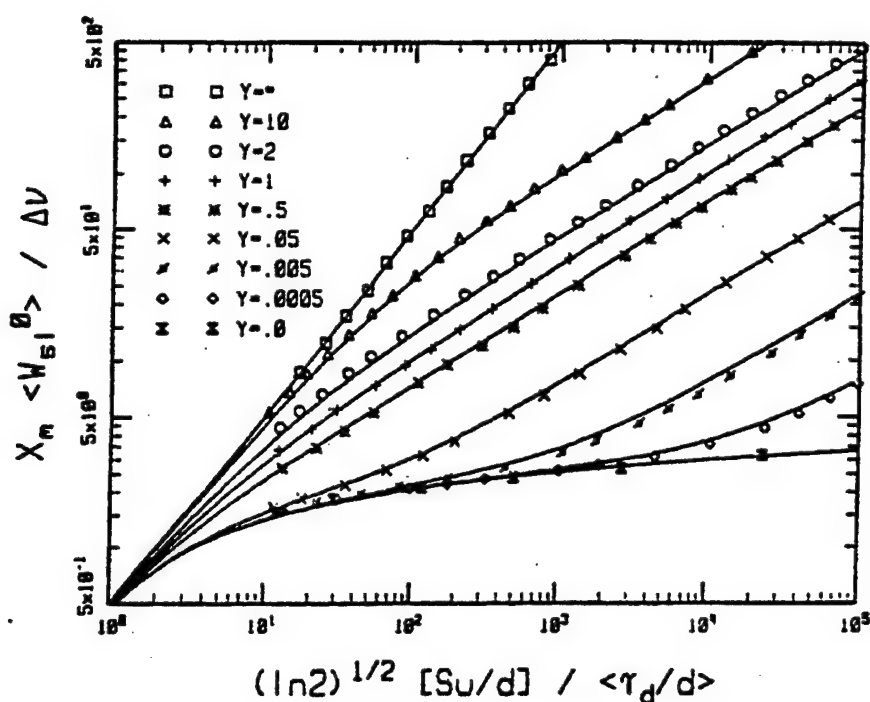


Figure 37. Curves of Growth for Spectral Lines with Combined Doppler and Lorentz Line Broadening. The Exact Calculations<sup>225</sup> are Presented as Individual Values. The NASA Formula,<sup>220</sup> Equation (72), is Shown as Solid Lines. The Values of Y From Bottom to Top are: 0, 0.0005, 0.005, 0.05, 0.5, 1.0, 2, 10, and  $\infty$ .

### 3.3.1.1 Curtis-Godson Approximation

Path averages are calculated with the Curtis-Godson approximation.<sup>220-222</sup> This approximation replaces an inhomogeneous path with a homogeneous one by using average values for the various band-model parameters. The Curtis-Godson approximation is very accurate for paths where the temperature and concentration gradients are not particularly steep. This is the case for atmospheric paths where the temperature variations for arbitrary paths fall within the range of 200 to 300 K. The total optical depth is a sum over contributions from the individual layers and is given by:

$$[Su/d] = \sum_l (S/d)_l (\Delta u)_l \quad (73)$$

where  $(\Delta u)_l$  is the incremental absorber amount from layer  $l$  and  $(S/d)_l$  is the absorption coefficient band-model parameter at the temperature of the layer  $l$ . Note, frequency and species indices are implicitly assumed for this and subsequent equations.

The optical depth is used as the weighting function in calculating the path averages:

$$\langle 1/d \rangle = \frac{1}{[Su/d]} \sum_i (1/d)_i (S/d)_i (\Delta u)_i \quad (74)$$

$$\langle \gamma_c/d \rangle = \frac{1}{[Su/d]} \sum_i (\gamma_c)_i (1/d)_i (S/d)_i (\Delta u)_i \quad (75)$$

$$\langle \gamma_d/d \rangle = \frac{1}{[Su/d]} \sum_i (\gamma_d)_i (1/d)_i (S/d)_i (\Delta u)_i \quad (76)$$

The band model parameters were defined in the previous section, and  $(\gamma_d)_i$  is the usual Doppler width in  $(\text{cm}^{-1})$ :

$$(\gamma_d)_i = \frac{v_i}{c} \sqrt{2(\ln 2) NkT/M} \quad (77)$$

where M is equal to the molecular mass (g/mole) of the molecule and N is Avogadro's number.

### 3.3.2 Line-Wing Absorption

The power-law transmittance, Equation (58), considers only lines which originate within a given spectral interval, and for these lines, only that fraction of the line profile which falls within the interval is included in the computation of the equivalent width. This approximation is reasonable in the strongly absorbing region of a band; however, because the absorptivity is expressed in terms of the local line strength distribution, it becomes a poor approximation in regions where the tail contributions from nearby lines dominate the contributions from weak or non-existent lines within a given interval (bin). This typically occurs in the center and far wings of a band (i.e., past the band head), and also in spectral intervals containing no lines which are in the vicinity of strong lines. For these situations, the local absorption is dominated by the accumulated tails of the stronger lines located outside the interval. The effect of line wing absorption is included in the transmittance by adjoining an exponential term:

$$\tau = (1 - \langle W_{sl} \rangle / \Delta \nu)^{\langle n \rangle} e^{-[Cu]} \quad (78)$$

where  $[Cu]$  is the total continuum optical depth:

$$[Cu] = \sum_l (C)_l (\Delta u)_l \quad (79)$$

The layer subscript  $\ell$  on  $C$ , labels both the pressure Equation (56) and temperature (interpolated) dependencies.

### 3.4 Integration With LOWTRAN 7

Integration of the MODTRAN subroutines into LOWTRAN 7 was accomplished with minimal changes to the original code. In subroutine TRANS, a single call to subroutine BMDATA reads the first necessary wavenumber block of band model parameters and calculates wavenumber independent quantities. For each wavenumber, calls to subroutine BMOD are made once for initialization and then additionally in the loop over atmospheric layers that calculates the molecular transmittance. In MSRAD, the call to FLXADD is replaced by a call to BMFLUX for the moderate-resolution option.

#### 3.4.1 New Subroutines

The new MODTRAN subroutines are listed in this section. For a detailed description of the functions of each subroutine refer to References 1 and 21.

The principal subroutines added for the basic MODTRAN band model are; BMDATA, BMOD, BMLOAD, BMTRAN, BMERFU, BMFLUX, and DRIVER. Many additional routines have been added for the Upgraded Line-of-Sight Geometry<sup>21</sup> (section 3.5).

#### 3.4.2 Necessary Modifications to LOWTRAN 7

Modifications to LOWTRAN 7 have been kept to a minimum. As mentioned earlier, the switch MODTRN has been added to /CARD 1/. Only if MODTRN is .TRUE. are any of these changes activated.

Most of the routines from LOWTRAN 7 remain unchanged. A number of routines have been modified only in that the blank common along with the labeled commons /CARD1/, /CARD4/, /SOLS/ and /TRAN/ have been changed. These routines are ABCDTA, AEREXT, AERNM, CIRR18, CIRRUS, CLDPRF, DESATT, EQUWLC, EXABIN, FLXADD, LAYVSA, PHASEF, RDLXA, RDNSM, RFPATH, SSRAD and VSANM.

A number of routines have undergone minor modifications. Routines GEO and SSGEO were altered in order to make the following changes/additions:

- (1) The matrices WPATH (WPATHS) and WPMS (WPMSS) have been combined into the single matrix WPATH (WPATHS),
- (2) Layer pressures and temperatures are stored for use by the band model routines, and
- (3) Curtis-Godson averaged pressures and temperatures are determined for solar paths.

STDMDL calculates actual rather than scaled molecular column densities when MODTRN is .TRUE.. Finally, routine MSRAD computes molecular optical thicknesses and calls routine BMFLUX.

Significant changes were made to the MAIN program routine. It has been split into two routines. The new MAIN consists of almost 1000 lines of introductory comments and a single call to the new subroutine DRIVER. DRIVER is the driving routine for MODTRAN and it contains all the executable statements from the MAIN program of LOWTRAN 7. In addition, it defines a pointer array called KPOINT that maps the HITRAN molecular labels (1-12) into the LOWTRAN 7 labels. Also, DRIVER checks the spectral inputs. For moderate resolution, the variables *IVI*, *IV2* and *IDV* need not be multiples of 5, and the additional variable *IFWHM* must be read.

Considerable modifications were required for the subroutine TRANS. This routine is currently divided into three separate subroutines: TRANS, LOOP and BMDATA. When MODTRN is .TRUE., TRANS:

- (1) sets the internal frequency step size to  $1\text{ cm}^{-1}$ ,
- (2) calls the MODTRAN subroutines to calculate molecular transmittance,
- (3) interpolates transmittances calculated at  $5\text{ cm}^{-1}$  intervals for the aerosols and molecular continua, and employs a discretized triangular slit function with FWHM set to *IFWHM* to automatically degrade the  $1\text{ cm}^{-1}$  bin results to the requested spectral resolution.

Note that the discretized triangular slit function when *IFWHM* is set to  $1\text{ cm}^{-1}$  is a  $1\text{ cm}^{-1}$  rectangular slit function, as shown in Figure 38. The figure also demonstrates

that, when the printing step-size parameter  $IDV$  ( $=2$  here) is larger than  $IFWHM$ , the frequency range is under-sampled.

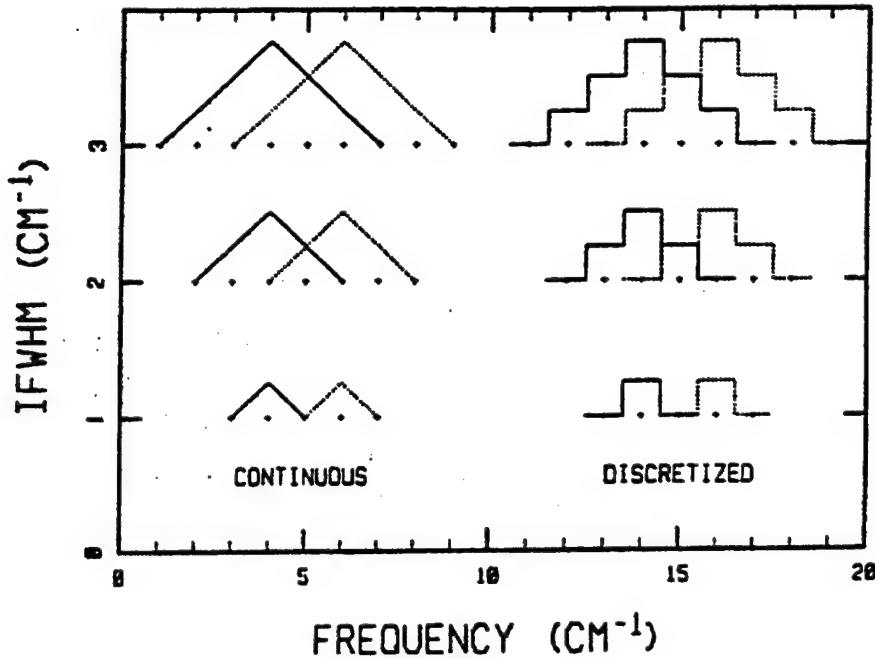


Figure 38. Comparison of Continuous and Discretized Triangular Slit Functions. FASCODE Uses the Weighting from the Continuous Function, but MODTRAN Uses the Discretized Approximation. For this Example,  $IDV = 2$  and the Curves are Shown for  $IFWHM = 1, 2$ , and  $3$ .

LOWTRAN 7 and MODTRAN also differ in their approaches to handling molecular transmittance. Since the LOWTRAN model has been optimized for 296 K, low level paths, LOWTRAN should not be used for atmospheric paths completely above 30 km. MODTRAN, on the other hand, uses a Voigt lineshape, which is applicable at higher altitudes. Figures 39-41 demonstrate MODTRAN's high altitude capabilities. First, Figure 39 shows that LOWTRAN 7 and MODTRAN do indeed predict vastly different radiances at higher altitudes. Radiation levels from  $H_2O$  rotations along a 60 km limb path are shown. The LOWTRAN spectral radiances are much too low at these altitudes. To demonstrate that MODTRAN calculations are correct, validations have been performed against SHARC 2,<sup>226</sup> the Strategic High Altitude Radiation Code. SHARC performs NLTE (non-local thermodynamic equilibrium) calculations from 60 to 300 km altitude. However, at 60 km, vibration state populations are essentially LTE and  $H_2O$



rotations are always treated as LTE in SHARC, so comparisons between MODTRAN and SHARC should produce similar results. With a 60 km limb path, the two codes predict similar spectral radiances for H<sub>2</sub>O rotations (Figure 40) and for the 15  $\mu$ m CO<sub>2</sub> band (Figure 41), which is mostly LTE. The SHARC calculations were done at a spectral resolution of 0.5 cm<sup>-1</sup> and degraded to 1 cm<sup>-1</sup> (FWHM).

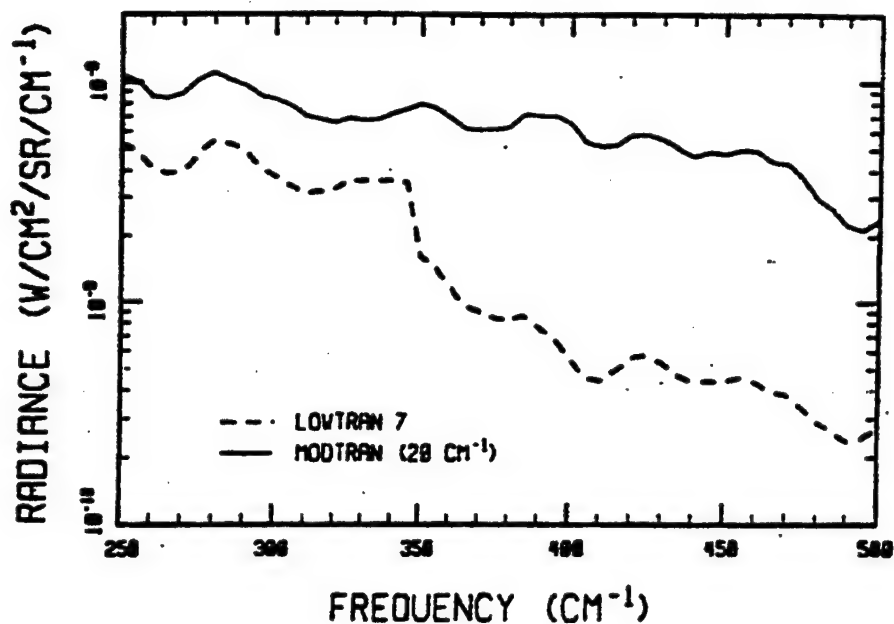


Figure 39. LOWTRAN 7 and MODTRAN Predictions for Radiation from the H<sub>2</sub>O Rotational Band for a 60 km Limb Path. At These Altitudes, LOWTRAN Under Predicts the Radiance.

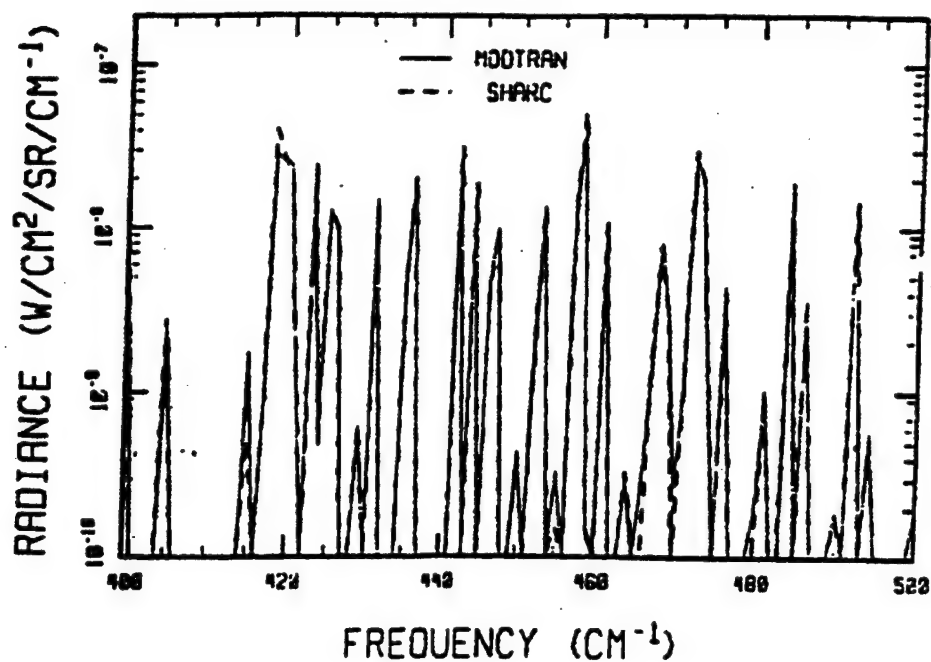


Figure 40. MODTRAN and SHARC Predictions of H<sub>2</sub>O Rotations for 60 km Limb.

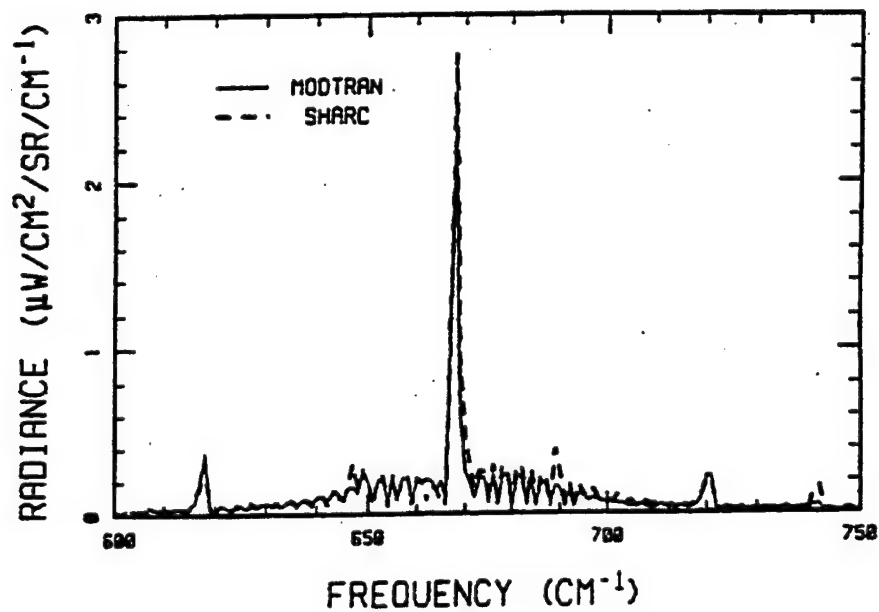


Figure 41. MODTRAN and SHARC Predictions of the 15  $\mu\text{m}$  CO<sub>2</sub> Band for 60 km Limb.

### 3.5 Upgraded Line-of-Sight Geometry

The geometry package in MODTRAN allows the user several different options for unambiguously specifying the line-of-sight (LOS). For a detailed description of the possible choices refer to the Users Guide To LOWTRAN 7 (Ref. 2). The routines are capable of calculating some unspecified parameters and creating a "complete set" of LOS parameters. However, for some particular paths, the output parameters are often different from the chosen inputs. This is particularly noticeable for slant paths specified by range and zenith angle, especially those paths which are near-horizontal, and for many input sets where the LOS is only a few kilometers or less. These problems have been corrected by upgrading the geometry package.

#### 3.5.1 LOS Specification

The input parameters for characterizing a general LOS path are listed in Table 20. It should be noted that HMIN is also the tangent altitude for long limb viewing paths, which reach a minimum altitude (tangent point) and then increase in altitude. The three generic path types recognized by MODTRAN are listed in Table 21. The type is selected by assigning the appropriate value to the input variable ITYPE. The ITYPE = 3 path is a special case of ITYPE = 2 where H2 is space, that is, the outer boundary of the highest atmospheric layer (100 km).

**Table 20. The LOS Parameters**

H1	sensor or observer altitude
H2	final altitude
ANGLE	zenith angle at H1
BETA	earth-center angle
RANGE	distance along the LOS between H1 and H2
HMIN	minimum altitude of the LOS

**Table 21. Path Types in MODTRAN**

<u>ITYPE</u>	<u>PATH DESCRIPTION</u>
1	horizontal homogeneous path with constant temperature, pressure and concentrations
2	vertical or slant path between H1 and H2

## 3 vertical or slant path to space from H1

For slant paths, one of four parameter sets are used to specify a path. They are H1 and two additional parameters. Table 22 lists the four possibilities, each identified by a case label: 2A, 2B, 2C or 2D. These case designations are internal to the MODTRAN code. Some of these input schemes are converted into other equivalent schemes for subsequent calculations. The most convenient parameter set for tracing a ray through the atmosphere is CASE 2A, so all paths are eventually converted to this case. CASE 2B is converted to 2A by determining H2. CASE 2C is converted to 2D by determining BETA, and finally both 2C and 2D are converted to 2A by determining ANGLE. Potential accuracy problems generated in any one case can then carry over into other cases.

**Table 22. Parameter Sets for ITYPE = 2 Paths.**

<u>CASE LABEL</u>	<u>SPECIFIED PARAMETERS</u>
2A	H1, H2, ANGLE
2B	H1, ANGLE, RANGE
2C	H1, H2, RANGE
2D	H1, H2, BETA

### 3.5.2 Geometry Problems

The mismatch between the input and output LOS parameters are confined to some slant paths specified by ITYPE = 2 and 3. The following is a listing of the specific problems in these mismatches:

- (1) Simple numerical precision problems;
- (2) Calculation of H2 without refraction effects for CASE 2B;
- (3) Failure to converge when determining ANGLE for CASES 2C and 2D; and
- (4) Short slant paths.

Since ITYPE = 3 is a special case of ITYPE = 2 and utilizes the same routines, the ITYPE = 2 LOS upgrades automatically carry over to the ITYPE = 3 cases. The following approach was taken:

- (1) Improved numerical accuracy of some specific algorithms;
- (2) For slant paths exceeding 2 km, solve refraction and convergence problems; and
- (3) Ignore refraction for short slant paths.

### 3.5.3 Improved Numerical Accuracy

Some FORTRAN statements were replaced by identical equivalent statements that are numerically stable. As an example, the expression:

$$R_1^2 + R_2^2 - 2R_1R_2\cos\beta \quad (80)$$

where  $R_i = R_e + H_i$ ,  $i = 1, 2$  and  $R_e$  = earth radius, is replaced by:

$$(H_1 - H_2)^2 + 4R_1R_2 \sin^2(\beta/2) \quad (81)$$

In the first expression, the third term nearly equals the sum of the first two terms for small values of  $\beta$ . The inclusion of  $R_e^2$  in all terms means that, for small  $\beta$ , a large number is subtracted from another number of comparable magnitude. This leads to a significant loss in accuracy. The second expression is more accurate because some  $R_e$ 's have been eliminated.

A Taylor series expansion is also used for improving the numerical accuracy of small beta cases:

$$(H_1 - H_2)^2 - R_1R_2 \left\{ -(\beta^6/135) + (\beta^4/12) - \beta^2 \right\} \quad (82)$$

The sextic term is first in this expansion, because in summing up a series of terms in a computer, it is more accurate to start with the smaller terms. A number of FORTRAN variables were changed from single to double precision.

The resulting improved numerical accuracy was sufficient to obtain agreement among input and output parameters for CASE 2A and for many input sets of CASE 2C. However, these improvements did not solve all of the CASE 2C problems.

Table 23 compares the MODTRAN and MODTRAN2 output ranges for various input schemes of CASE 2C. For some small input ranges, MODTRAN output ranges differ greatly from the input values. For input ranges of 2.0, 6.0 and 20.0 km, MODTRAN's calculation of ANGLE failed to converge, thereby yielding no output ranges.

### 3.5.4 Slant Paths

Consistency for the CASE 2B input cases is obtained by determining  $H_2$  by a refractive calculation when converting to 2A. A modified iterative procedure for determining BETA produces accurate convergence for the 2D cases.

CASE 2B (H1, ANGLE, RANGE)**Table 23. Examples for CASE 2C with H1=5 and H2=5 km.**

<u>INPUT</u>	<u>RANGE (km)</u>	
	<u>MODTRAN</u>	<u>MODTRAN2</u>
2.01	-----	2.00
4.70	5.31	4.72
6.00	-----	6.01
8.0	7.51	8.01
9.0	7.51	9.01
10.0	9.20	10.02
20.0	-----	20.01
50.0	50.51	50.02
100.0	100.52	100.01
200.0	199.96	200.01
300.0	300.13	300.01

The LOS path for this case is converted to CASE 2A by computing H2, but without refraction. Once H2 is calculated, CASE 2A proceeds by including atmospheric refraction effects. A new set of routines includes refraction in the initial H2 calculation. As a result, the input and output parameters are now in general agreement as shown in Table 24. Since refraction tends to bend the rays towards the earth, the H2 values calculated with refraction (MODTRAN2) are consistently less than those calculated via straight line geometry (MODTRAN).

**Table 24. Examples for CASE 2B with H1 = 5 km and ANGLE = 92°.**

<u>INPUT</u>	<u>RANGE (km)</u>		<u>H2 (km)</u>	
	<u>MODTRAN</u>	<u>MODTRAN2</u>	<u>MODTRAN</u>	<u>MODTRAN2</u>
10	10	10	4.66	4.66
50	49	50	3.45	3.43
100	96	100	2.29	2.20
150	136	150	1.53	1.30
200	162	200	1.16	0.74
250	358	250	1.18	0.52
300	385	300	1.59	0.64
350	427	350	2.39	1.11

The value of H2 with refraction is calculated by summing the differential elements of range,  $ds$ , along the LOS from H1 to H2. The most convenient variable of integration is the radial distance,  $r$ , of a point on the ray from the center of the earth. Thus H2 is the altitude at which the integrated path length equals the input RANGE. This method of determining H2 is non-iterative and rapid.

#### CASE 2D (H1, H2, BETA)

For this case MODTRAN computes ANGLE iteratively. Initially, an educated guess of ANGLE based on straight line geometry is made, and the corresponding BETA is computed by including refraction. If this calculated BETA does not agree with the input, a new guess of ANGLE is made, and the process is repeated until convergence occurs. If the iteration does not converge, the calculations are skipped. A new iterative algorithm based on a Newton-Raphson scheme was adopted to consistently produce acceptable convergence. In this scheme, ANGLE is incremented by an amount based on its derivative with respect to BETA. The examples shown in Table 23 for which MODTRAN did not yield any output ranges were caused by convergence problems with CASE 2D (to which all CASE 2C inputs were converted to). As can be seen, MODTRAN2 yields very accurate output ranges for these input scenarios.

##### **3.5.4.1 Short Slant Paths**

Short slant paths are defined as paths whose lengths are less than 2 kilometers. These are treated differently than the general slant paths, because even in double precision the refractive calculations were numerically unstable.

Since refraction is insignificant at these short ranges, it is ignored. All short slant paths are converted into CASE 2A. A DATA statement in the DRIVER subroutine governs the value of the switch (currently 2 km) for short slant paths. The MODTRAN2 results for ranges slightly less than 2 km and slightly greater than 2 km have a smooth convergence. However, the user should be aware of this controlling switch when performing detailed studies centered on this range.

## 4. ATMOSPHERIC TRANSMITTANCE

### 4.1 LOWTRAN 7 Molecular Transmittance Band Models

The molecular transmittance band models described here is summarized from the Pierluissi and Maragoudakis report.<sup>13</sup>

#### 4.1.1 Introduction

The calculation of the molecular transmittance band models for LOWTRAN 7 is best summarized by referring to Tables 25 and 26. Table 25 shows that the older versions of LOWTRAN had modeled water vapor from 350 to 14520  $\text{cm}^{-1}$ , with two gaps in between for which calculations were not advisable. Ozone had extended continuously from 575 to 3270  $\text{cm}^{-1}$  in the infrared region. Likewise, the single model for all the uniformly mixed gases had extended from 500 to 13245  $\text{cm}^{-1}$ , with a wide spectral gap in between. Table 26 shows that the water vapor model had been extended continuously from 0 to 17860  $\text{cm}^{-1}$ , while ozone has been corrected by eliminating some spectral regions for which calculations were unnecessary. The five individual models for the uniformly-mixed gases allow for the use of different combinations of absorber concentrations, and extended the spectral coverage from 0 to 15955  $\text{cm}^{-1}$ . Finally, Table 26 shows the addition of the four trace gases which were added to LOWTRAN 7.

**Table 25. Summary of the Molecular Absorption Band Models In LOWTRAN 6.**

<u>ABSORBER</u>	<u>SPECTRAL RANGE</u> ( $\text{cm}^{-1}$ )
Water Vapor ( $\text{H}_2\text{O}$ )	350-9195, 9878-12795, 13400-14520
Ozone ( $\text{O}_3$ )	575-3270, 13000-24200, 27500-50000
Uniformly-Mixed Gases ( $\text{CH}_4$ , $\text{N}_2\text{O}$ , $\text{O}_2$ , $\text{CO}$ , $\text{CO}_2$ )	500-8070, 12950-13245



Table 26. Summary of the Molecular Absorption Band Models in LOWTRAN 7

<u>ABSORBER</u>	<u>SPECTRAL RANGE (cm<sup>-1</sup>)</u>
WATER Vapor (H <sub>2</sub> O)	0-17860
Ozone (O <sub>3</sub> )	0-200, 515-1275, 1630-2295, 2670-3260, 13000-24200, 27500-50000
<u>Uniformly-Mixed Gases:</u>	
Methane (CH <sub>4</sub> )	1065-1775, 2345-3230, 4110-4690, 5865-6135
Nitrous Oxide (N <sub>2</sub> O)	0-120, 490-775, 865-995, 1065-1385, 1545-2040, 2090-2655, 2705-2865, 3245-3925, 4260-4470, 4540-4785, 4910-5165
Oxygen (O <sub>2</sub> )	0-265, 7650-8080, 9235-9490, 12850-13220, 14300-14600, 15695-15955
Carbon Monoxide (CO)	0-175, 1940-2285, 4040-4370
Carbon Dioxide (CO <sub>2</sub> )	425-1440, 1805-2855, 3070-4065, 4530-5380, 5905-7025, 7395-7785, 8030-8335, 9340-9670
<u>Trace Gases:</u>	
Nitric Oxide (NO)	1700-2005
Nitrogen Dioxide (NO <sub>2</sub> )	580-925, 1515-1695, 2800-2970
Ammonia (NH <sub>3</sub> )	0-2150
Sulfur Dioxide (SO <sub>2</sub> )	0-185, 400-650, 950-1460, 2415-2580

#### 4.1.2 The Transmittance Function

The molecular transmittance  $\tau$  averaged over a spectral interval  $\Delta\nu$  with a triangular instrument response function of 20 cm<sup>-1</sup> full-width at half intensity, was approximated by the exponential function<sup>227</sup>

$$\tau = \exp \{-(CW)^a\} \quad (83)$$

where

$$= (P/P_o)^n (T_o/T)^m U \quad (84)$$

$$C = 10C' \quad (85)$$

$$= 0.7732 \cdot 10^{-4} M \rho_a Z \quad \text{for all absorbers except H}_2\text{O}. \quad (86)$$

$$= 0.1 \rho_w Z \quad \text{for H}_2\text{O} \quad (87)$$

In these equations  $P(\text{atm})$ ,  $T(\text{K})$ ,  $M(\text{ppmv})$ ,  $\rho_w (\text{g/m}^3)$ , and  $\rho_a (\text{g/m}^3)$  are vertical profiles of pressure, temperature, volume-mixing ratio, water vapor density, and air density, respectively. In Eq. (86),  $U (\text{atm cm})$  is the absorber amount, while  $U (\text{g/cm}^2)$  is the absorber amount in Eq. (87). The path length is  $Z(\text{km})$ , and the subscript "o" denotes conditions at a standard temperature and pressure (viz. one atm and 273.15 K, respectively). The band model is further defined by the absorber parameters set ( $a$ ,  $n$ , and  $m$ ), and by a set of  $C'$  values at  $5 \text{ cm}^{-1}$  spectral intervals. In Eq. (85),  $C$  is redefined in terms of  $C'$  for computational convenience. The complete parameter set  $a$ ,  $n$ ,  $m$ , and  $C'$ ,  $i = 1, 2, \dots, I$ , for  $I$  spectral intervals, was obtained from the equation

$$\varepsilon = \sum_i \sum_j \{ \tau(i, j) - \tau_m(i, j) \}^2 \quad (88)$$

where  $\varepsilon$  is the least-squares error, minimized using the conjugate gradient descent,  $j = 1, 2, \dots, J$  is an index for the data values,  $\tau$  is a transmittance datum, and  $\tau_m$  is the band model in Eq. (83).

Equation (83) is useful as a transmittance function because it is analytically simple and asymptotic to one and zero, respectively, as the argument ranges from zero to infinity. It was used with an earlier version of LOWTRAN<sup>228</sup> for curve-fitting to the empirical transmission tables in LOWTRAN 3B for water vapor, the uniformly-mixed gases, and ozone. Although not much physical significance may be attributed to this function, Pierluissi and Gomez<sup>229</sup> have shown that in some cases empirical approximations have out-performed theoretically-based band models such as the Elsasser<sup>230</sup> model and the Goody<sup>231</sup> random model. It does not approach the functional form of any such classical models in either the limiting weak-line or strong-line conditions (i.e.,  $U/P$  very small or

very large, respectively). Pierluissi, et al.<sup>227</sup> reported that it leads to a transmittance polynomial proposed by Smith<sup>232</sup> for use with water vapor and carbon dioxide, which in turn, originated as an approximation to the strong-line limit to the random model. These earlier classical models were derived mostly for homogeneous paths, specific absorption-line configurations, and Lorentzian-broadening conditions. Equation (83) is used here along in-homogenous paths, for non-specific absorption-line configurations and for combinations of Lorentzian and Doppler broadening conditions.

The transmittance data used in connection with Eq. (88) in the determination of the complete set of the model parameters, consisted primarily of a combination of laboratory measurements and averaged line-by-line spectra. The line-by-line spectra were generated through calculations with FASCOD1C<sup>14</sup> which in turn used standard atmospheric profiles<sup>233</sup> and with the AFGL line parameter compilation<sup>234,235</sup>. The modeling of H<sub>2</sub>O involved laboratory measurements<sup>236,237</sup> which were not considered in earlier versions of LOWTRAN. Table 27 summarizes the range of all of the transmittance-data parameters adopted for the LOWTRAN 7 band model.

The absorber vertical concentrations for each one of the gases modeled consisted of the profiles proposed by Smith<sup>50</sup>, extrapolated so as to match the 33 altitude increments historically used in the LOWTRAN models. These vertical absorption concentrations were then updated with the Anderson<sup>10</sup> atmospheric constituent profiles.

#### 4.1.3 Model Development

The numerical procedures discussed briefly in a previous section, were used with the available data to determine the parameters  $a$ ,  $n$ ,  $m$ , and  $C'$  for the 11 absorbers. In Eqs. (83) through (85) the parameters  $a$ ,  $n$  and  $m$  are normally expected to be spectrally independent for a given absorber. The parameter  $C'$  is, then, expected to assume all the spectral variability of the band absorption. Although this was the case in general for all the gases having a small number of bands, a few required the use of different sets of parameters throughout the absorption spectrum. Table 28 summarizes the results derived from the modeling efforts. The criterion used for deciding on the number of bands to be modeled with a single-parameter set was that the RMS transmittance deviation between the model and the modeling data remained below 2 percent.

**TABLE 27. Range of Calculated and Measured Transmittance Data Used in the Validation of the Band Models for Molecular Absorption****RANGE OF MODEL DATA**

ABSORBER	SPECTRAL RANGE (cm <sup>-1</sup> )	PRESSURE		TEMP- PERATURE		ABSORBER Amount		REFERENCES
		(ATM) MEAS.	CALC.	(K) MEAS.	CALC.	(ATM CM) MEAS.	CALC.	
Ammonia (NH <sub>3</sub> )	0-2150	0.163E+0	0.102E+0		217	0.935E-2	0.962E-2	
		to	to	300	to	to	to	238
		0.824E+0	1.000E+0		300	0.308E+0	0.316E-1	
Carbon Dioxide (CO <sub>2</sub> )	425-1440							
	1805-2855							
	3070-4065	0.100E-1	0.117E-1	216	217	0.804E-1	0.856E-2	
	4530-5380	to	to	to	to	to	to	236,241,242,243
	5905-7025	1.000E+0	1.000E+0	300	288	0.235E+5	0.300E+5	
	7395-7785							
	8030-8335							
	9340-9670							
Carbon Monoxide (CO)	0-175	0.304E+0	0.102E+0		230	0.730E-1	0.350E-1	
	1940-2285	to	to	300	to	to	to	236
	4040-4370	1.000E+0	1.000E+0		300	0.143E+3	0.275E+3	
Methane (CH <sub>4</sub> )	1065-1775	0.100E+0	0.102E+0	302	217	0.922E-1	0.997E-1	
	2345-3230	to	to	to	to	to	to	236
	4110-4690	1.000E+0	1.000E+0	310	300	1.375E-1	1.359E+2	
	5865-6135							
Nitric Oxide (NO)	1700-2005	0.136E-1	0.546E-1		217	0.722E-1	0.619E-3	
		to	to	300	to	to	to	239
		0.966E+0	1.000E+0		288	0.310E+0	0.310E+0	

**TABLE 27. (Continued) Range of Calculated and Measured Transmittance Data Used in the Validation of the Band Models for Molecular Absorption**

**RANGE OF MODEL DATA**

ABSORBER	SPECTRAL RANGE (cm <sup>-1</sup> )	PRESSURE		TEMP- PERATURE (K)		ABSORBER Amount (ATM CM)		REFERENCES
		(ATM) MEAS.	CALC.	MEAS.	CALC.	MEAS.	CALC.	
Nitrogen Dioxide (NO <sub>2</sub> )	580-925	0.663E-1	0.551E-1	298	217	0.823E-2	0.948E-3	
	1515-1695	to	to	to	to	to	to	237
	2800-2970	1.000E+0	1.000E+0	328	288	0.919E+0	0.119E+0	
Nitrous Oxide (N <sub>2</sub> O)	0-120							
	490-775							
	865-995							
	1065-1385	0.515E-4	0.102E+0	296	217	0.686E-3	0.962E-3	
	1545-2040	to	to	to	to	to	to	236
	2090-2655	0.484E+0	1.000E+0	301	300	0.387E+3	0.829E+2	
	2705-2865							
	3245-3925							
	4260-4470							
	4540-4785							
Oxygen (O <sub>2</sub> )	4910-5165							
	0-265	0.940E+0	0.102E+0		217	0.237E+4	0.489E+3	
	7650-8080		to	300	to	to	to	240
	9235-9490		1.000E+0		300	0.219E+6	0.256E+9	
	12850-13220							
	14300-14600							
	15695-15955							
Ozone (O <sub>3</sub> )	0-200		0.102E+0		217		0.992E-3	
	515-1275		to	300	to		to	
	1630-2295		1.000E+0		288		0.992E+1	
	2670-3560							

**TABLE 27. (CONTINUED) Range of Calculated and Measured Transmittance Data Used in the Validation of the Band Models for Molecular Absorption**

**RANGE OF MODEL DATA**

ABSORBER	SPECTRAL RANGE (cm <sup>-1</sup> )	PRESSURE		TEMP- PERATURE		ABSORBER Amount		REFERENCES
		(ATM) MEAS.	CALC.	(K) MEAS.	CALC.	(ATM CM) MEAS.	CALC.	
Sulfur Dioxide (SO <sub>2</sub> )	0-185	0.500E-1	0.102E+0	296	217	0.186E-1	0.987E-2	
	400-650	to	to	to	to	to	to	244
	950-1460	1.000E+0	1.000E+0	298	300	0.584E+1	0.290E+2	
	2415-2580							
Water Vapor (H <sub>2</sub> O)			0.102E+0		217		0.964E-3	
	0-1000		to		to		to	
			1.000E+0		288		0.483E+4	
	1005-16045		0.102E+0		217		0.254E+3	
	16340-17860		to		to		to	237
			1.000E+0		288		0.255E+6	

The resulting spectral parameters  $C'$  at 5 cm<sup>-1</sup> intervals are tabulated in Appendix A of the Pierluissi report,<sup>13</sup>

It is worth noting at this point that in the process of determining the band-model parameters in the region from zero to 20 cm<sup>-1</sup>, it was necessary to mimic the lines in this region from zero to 20 cm<sup>-1</sup>. This allowed for the calculation of mean transmittances at 5 cm<sup>-1</sup> intervals using a triangular scanning function of 20 cm<sup>-1</sup> full-width at half intensity on the monochromatic transmittance spectra.

Plots of the transmission functions (i.e.  $\tau$  versus CW) for each absorber are also of interest when comparing the relative behavior of the different absorbers. Figures (42) through (45) depict the composite transmission functions for the uniformly-mixed gases, the trace gases, water vapor, and ozone. Plots of the spectral parameter  $C'$  for each absorber are included in Appendix B and individual transmission curves for each model are included in Appendix C of the Pierluissi report.<sup>13</sup>

Table 28. Summary of the Absorber Parameters for the Band Models Developed.

Absorber	Spectral Range (cm <sup>-1</sup> )	Absorber A	Model N	Parameters M	RMS Error (%)
Ammonia (NH <sub>3</sub> )	0-385	0.4704	0.8023	-0.9111	1.41
	390-2150	0.6035	0.6968	0.3377	0.76
Carbon Dioxide (CO <sub>2</sub> )	425-835	0.6176	0.6705	-2.2560	1.84
	840-1440	0.6810	0.7038	-5.0768	2.18
	1805-2855	0.6033	0.7258	-1.6740	2.27
	3070-3755	0.6146	0.6982	-1.8107	1.95
	3760-4065	0.6513	0.8867	-0.5327	2.49
	4530-5380	0.6050	0.7883	-1.3244	3.33
	5905-7025	0.6160	0.6899	-0.8152	1.28
	7395-7785	0.7070	0.6035	0.6026	0.30
	8030-8335	0.7070	0.6035	0.6026	0.30
	9340-9670	0.7070	0.6035	0.6026	0.30
Carbon Monoxide (CO)	0-175	0.6397	0.7589	0.6911	0.28
	1940-2285	0.6133	0.9267	0.1716	0.71
	4040-4370	0.6133	0.9267	0.1716	0.71
Methane (CH <sub>4</sub> )	1065-1775	0.5844	0.7139	-0.4185	1.56
	2345-3230	0.5844	0.7139	-0.4185	1.56
	4110-4690	0.5844	0.7139	-0.4185	1.56
	5865-6135	0.5844	0.7139	-0.4185	1.56
Nitric Oxide (NO)	1700-2005	0.6613	0.5265	-0.4702	0.31
Nitrogen Dioxide (NO <sub>2</sub> )	580-925	0.7249	0.3956	-0.0545	1.49
	1515-1695	0.7249	0.3956	-0.0545	1.49
	2800-2970	0.7249	0.3956	-0.0545	1.49
Nitrous Oxide (N <sub>2</sub> O)	0-120	0.8997	0.3783	0.9399	0.24
	490-775	0.7201	0.7203	0.1836	1.49
	865-995	0.7201	0.7203	0.1836	1.49
	1065-1385	0.7201	0.7203	0.1836	1.49
	1545-2040	0.7201	0.7203	0.1836	1.49
	2090-2655	0.7201	0.7203	0.1836	1.49
	2705-2865	0.6933	0.7764	1.1931	1.23
	3245-3925	0.6933	0.7764	1.1931	1.23
	4260-4470	0.6933	0.7764	1.1931	1.23
	4540-4785	0.6933	0.7764	1.1931	1.23
	4910-5165	0.6933	0.7764	1.1931	1.23

**Table 28. (Continued) Summary of the Absorber Parameters for the Band Models Developed.**

Absorber	Spectral Absorber		Model		Parameters		RMS
	Range (cm <sup>-1</sup> )	A	N	M			Error (%)
Oxygen	0-265	0.6011	1.1879	2.97381			1.42
(O <sub>2</sub> )	7650-8080	0.5641	0.9353	0.1936			0.96
	9235-9490	0.5641	0.9353	0.1936			0.96
	12850-13220	0.5641	0.9353	0.1936			0.96
	14300-14600	0.5641	0.9353	0.1936			0.96
	15695-15955	0.5641	0.9353	0.1936			0.96
Ozone	0-200	0.8559	0.4200	1.3909			1.34
(O <sub>3</sub> )	515-1275	0.7593	0.4221	0.7678			2.25
	1630-2295	0.7819	0.3739	0.1225			1.13
	2670-2845	0.9175	0.1770	0.9827			0.30
	2850-3260	0.7703	0.3921	0.1942			0.25
Sulfur	0-185	0.8907	0.2943	1.2316			1.24
Dioxide	400-650	0.8466	0.2135	0.0733			2.38
(SO <sub>2</sub> )	950-1460	0.8466	0.2135	0.0733			2.38
	2415-2580	0.8466	0.2135	0.0733			2.38
Water	0-345	0.5274	0.9810	0.3324			1.99
Vapor	350-1000	0.5299	1.1406	-2.6343			1.26
(H <sub>2</sub> O)	1005-1640	0.5416	0.9834	-2.5294			0.85
	1645-2530	0.5479	1.0043	-2.4359			1.08
	2535-3420	0.5495	0.9681	-1.9537			2.74
	3425-4310	0.5464	0.9555	-1.5378			1.54
	4315-6150	0.5454	0.9362	-1.6338			2.37
	6155-8000	0.5474	0.9233	-0.9398			1.97
	8005-9615	0.5579	0.8658	-0.1034			1.29
	9620-11540	0.5621	0.8874	-0.2576			1.52
	11545-13070	0.5847	0.7982	0.0588			0.93
	13075-14860	0.6076	0.8088	0.2816			1.23
	14865-16045	0.6508	0.6642	0.2764			0.59
	16340-17860	0.6570	0.6656	0.5061			0.77



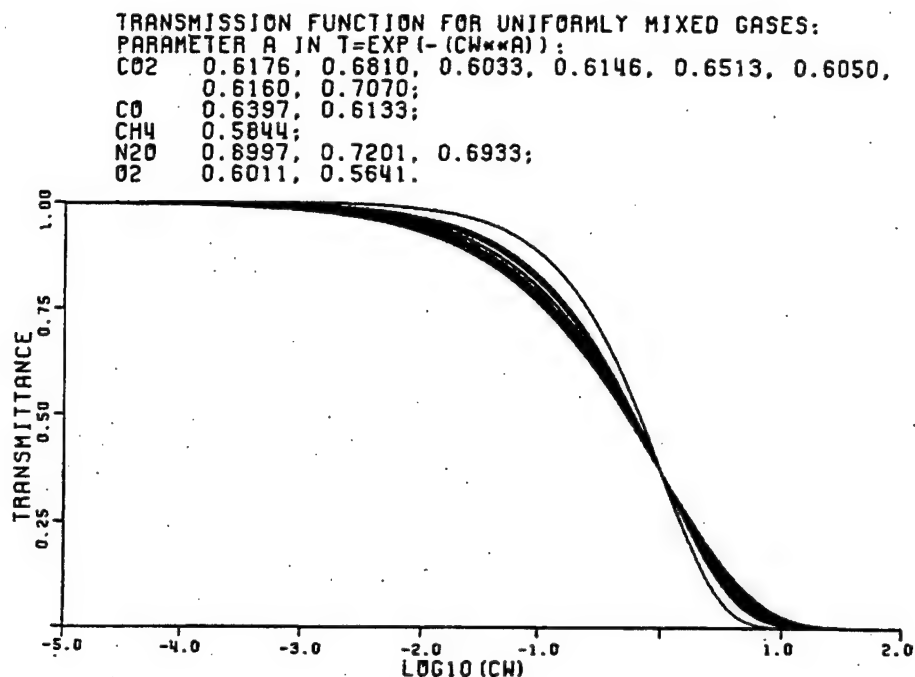


Figure 42. Composite Plot of the Transmission Functions (Eq. 83) for the Uniformly-Mixed Gases.

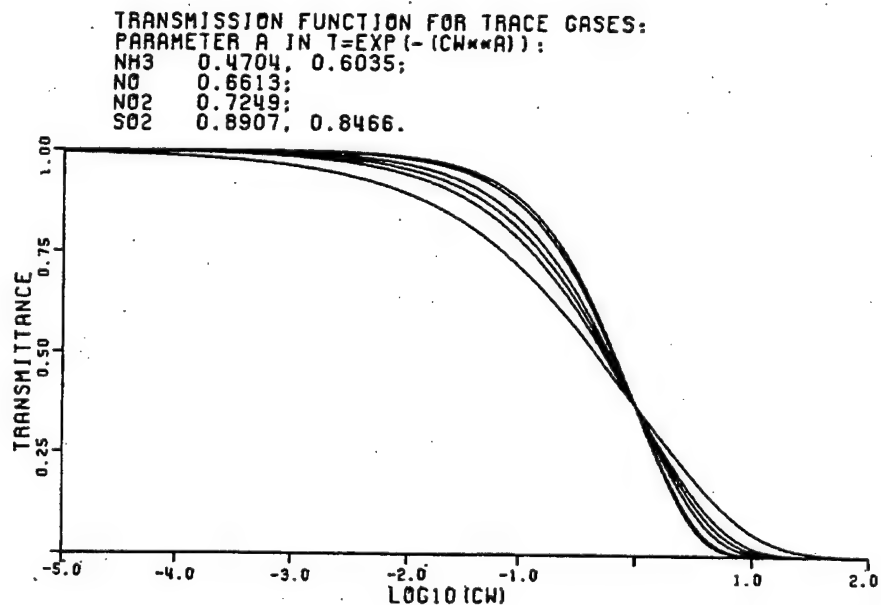


Figure 43. Composite Plot of the Transmission Functions (Eq. 83) for the Trace Gases.

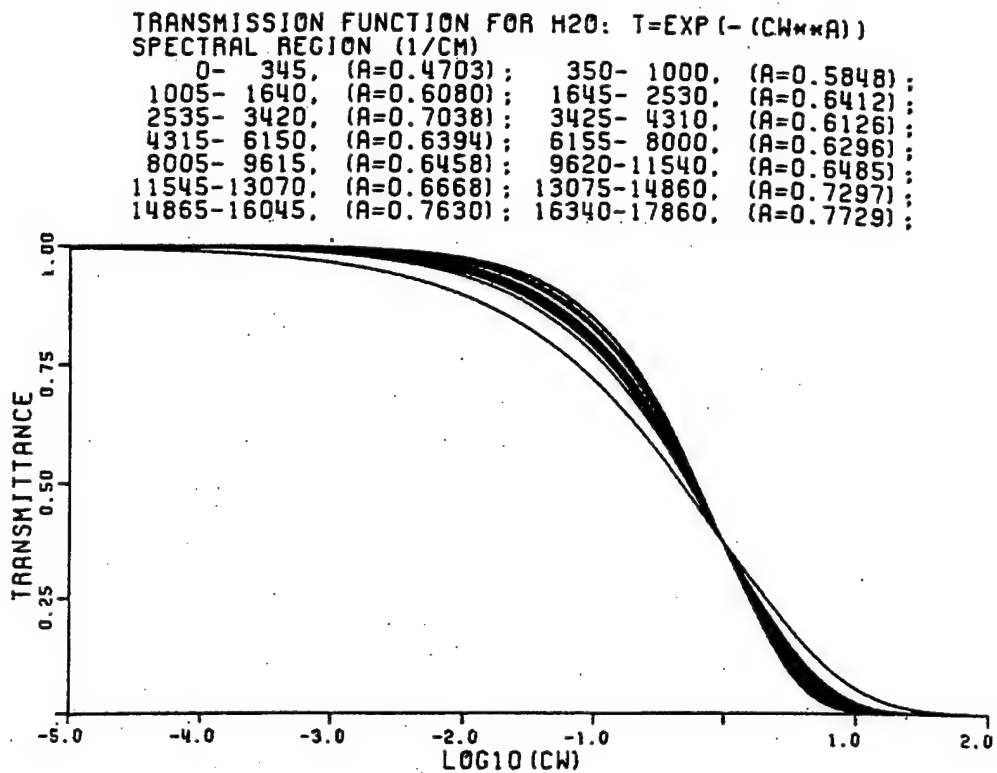


Figure 44. Composite Plot of the Transmission Functions (Eq. 83) for Water Vapor.

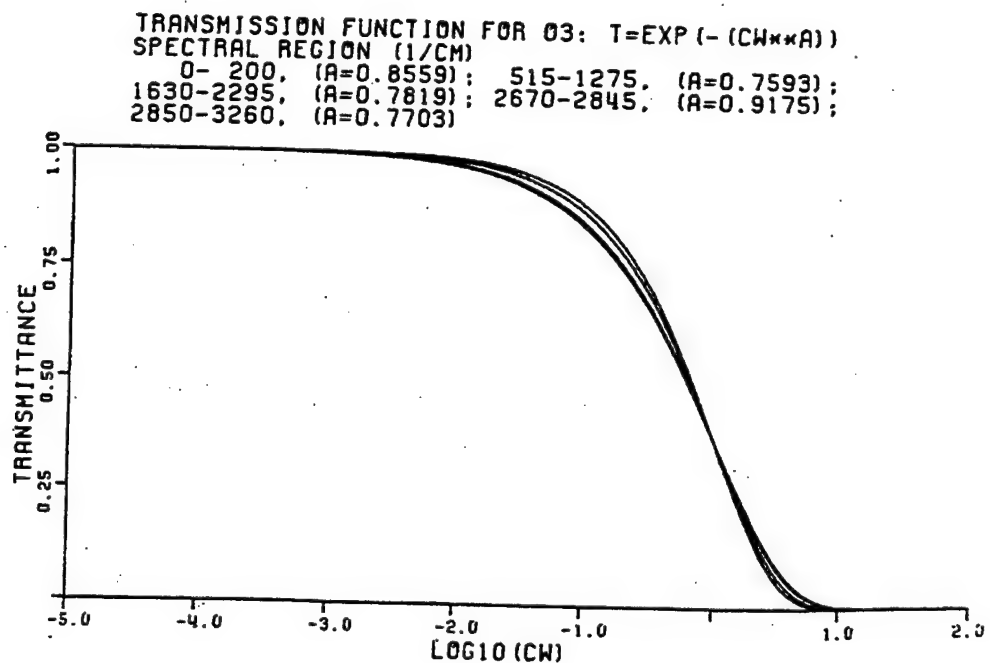


Figure 45. Composite Plot of the Transmission Functions (Eq. 83) for Ozone.

#### 4.1.4 Comparisons with Measurements

Prior to the determination of the model parameters, the line-by-line data were compared with available measurements. Magnetic tapes containing measured spectra for CO<sub>2</sub>, CH<sub>4</sub>, NO<sub>2</sub>, N<sub>2</sub>O, SO<sub>2</sub>, and H<sub>2</sub>O were used. Only graphical data were available for NH<sub>3</sub>, CO, NO, O<sub>2</sub>, and O<sub>3</sub>. Graphical comparisons of ozone spectra were made only over a narrow spectral region and, hence, are not worthy of further discussion. However, H<sub>2</sub>O comparisons were made over nearly the entire infrared region and were included in two separate reports. Appendix D of the Pierluissi report <sup>13</sup> shows some representative plots of both the nearly monochromatic spectra and of the corresponding degraded values.

Once the spectral comparisons were completed and the band-model parameters determined, comparisons were then made between the degraded line-by-line and model-calculated transmittances. Appendix E (Ref. 13) shows typical comparisons for H<sub>2</sub>O and O<sub>3</sub>, while similar comparisons for the remaining gases may be found in an earlier report by Pierluissi.<sup>245</sup> Special calculations were made for several bands for the remaining gases. Such cases included bands in the spectral region from 0 to 350 cm<sup>-1</sup> of NH<sub>3</sub>, CO, N<sub>2</sub>O, O<sub>2</sub>, O<sub>3</sub>, SO<sub>2</sub>, and H<sub>2</sub>O, as well as several others, primarily in the infrared region. Sample comparisons between the degraded line-by-line and band-model calculations for the gases absorbing in the region from 0 to 350 cm<sup>-1</sup> are shown separately in Appendix F of the Pierluissi report. <sup>13</sup>

Upon completion of the modeling of all the absorbing species, the resulting band models were incorporated into LOWTRAN 7. Figures (46) through (48) show the spectral differences between the transmittances from LOWTRAN 6 and those calculated with the LOWTRAN 7 band models for the combined uniformly-mixed gases, water vapor and ozone, respectively. They are for a path tangent to the earth's surface, extending from one end of the U.S. Standard Atmosphere to the other. They indicate that, in general, transmittance was over-estimated in LOWTRAN 6. This difference may be attributed to inaccuracies in the band models, as well as to absorption bands not modeled in the original LOWTRAN development. More examples of these types of comparisons are shown in Appendix G (Ref. 13). Additional transmittance plots for those paths using the proposed band models are included in Appendix H (Ref. 13).

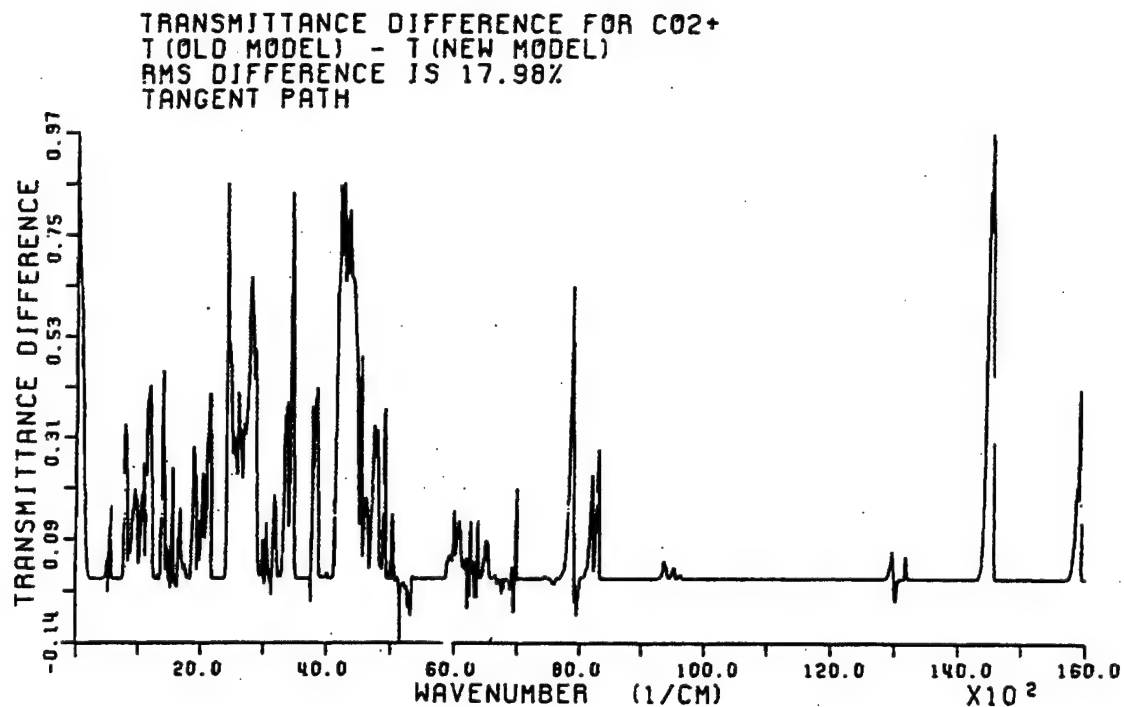


Figure 46. Transmittance Difference Between LOWTRAN 6 Calculations and the LOWTRAN 7 Model for the Uniformly-Mixed Gases Along a Path Tangent to the Earth's Surface in the U.S. Standard Atmosphere.

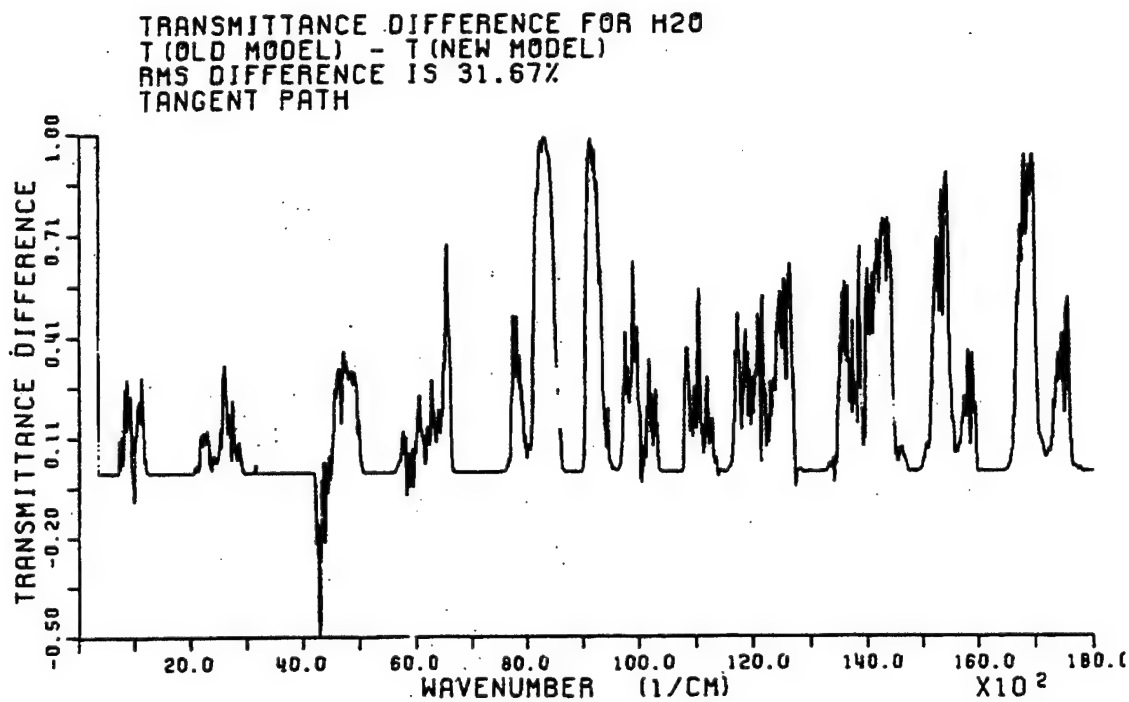


Figure 47. Transmittance Difference Between LOWTRAN 6 Calculations and the

LOWTRAN 7 Model for Water Vapor Along a Path Tangent to the Earth's Surface in the U.S. Standard Atmosphere.

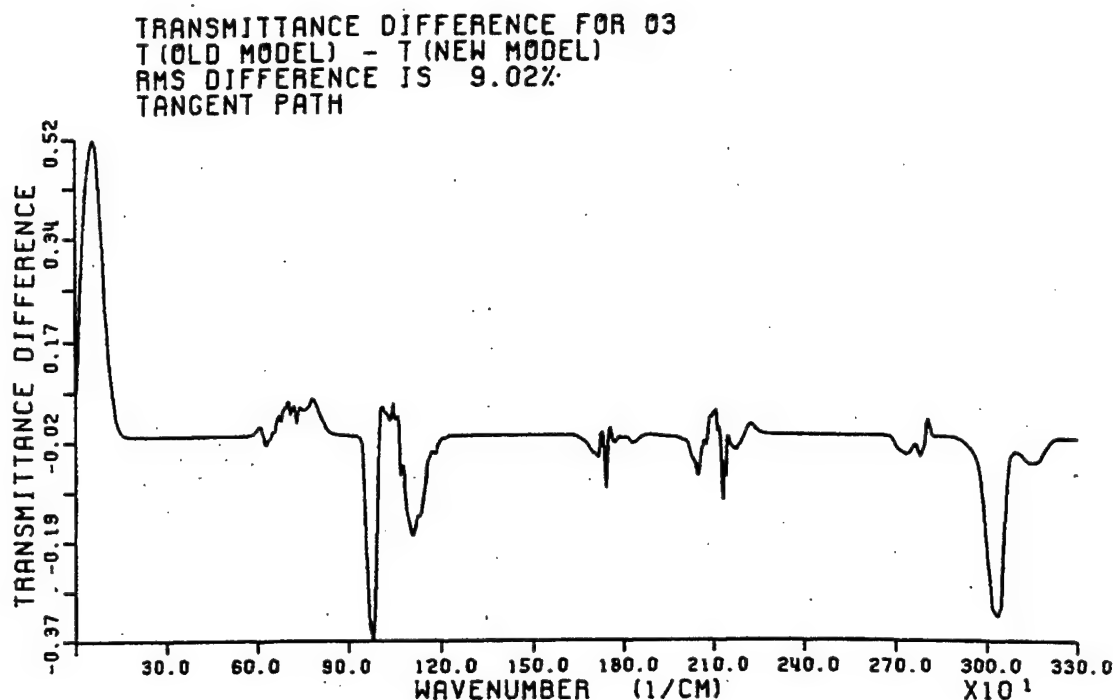


Figure 48. Transmittance Difference Between LOWTRAN 6 Calculations and the LOWTRAN 7 Model for Ozone Along a Path Tangent to the Earth's Surface in the U.S. Standard Atmosphere.

The band models were designed for  $20 \text{ cm}^{-1}$  intervals and the spectral parameters repeated at  $5 \text{ cm}^{-1}$  steps for easy incorporation into upgraded versions of LOWTRAN. The transmission function consisted of an exponential, defined by one spectral and three absorber parameters, representing a simple power relation between the pressure, temperature, and absorber amount along a slant atmospheric path. The determination of the parameters was accomplished through the use of non-linear numerical techniques.

Initially, the available measured data for  $\text{CO}_2$ ,  $\text{CH}_4$ ,  $\text{NO}_2$ ,  $\text{N}_2\text{O}$ ,  $\text{SO}_2$ , and  $\text{H}_2\text{O}$  were compared for accuracy with line-by-line calculations using FASCOD1C. Graphical data in the form of spectral curves were available for comparison for  $\text{NH}_3$ ,  $\text{CO}$ ,  $\text{NO}$ ,  $\text{O}_2$ , and  $\text{O}_3$ . Following this form of validation, the line-by-line data, and in some cases the transmittance measurements, were used in the determination of all the band-model parameters for all the gases of interest. Comparisons were then made between the

degraded measurements, the degraded transmittance calculations, and the recalculated transmittances using the resulting band models.

As a result of all the transmittance comparisons made in the process of the development and validation of the band models for molecular absorption, the following conclusions may be made:

1. The high-resolution transmittance measurements available in magnetic tape form for CO<sub>2</sub>, CH<sub>4</sub>, NO<sub>2</sub>, N<sub>2</sub>O, SO, and H<sub>2</sub>O, and in graphical form for NH<sub>3</sub>, CO, NO, O<sub>2</sub>, and O<sub>3</sub>, agreed reasonably well with line-by-line calculations using FASCOD1C.
2. Calculations using the band-model parameters, agreed within a mean (over all wavenumbers and gases) RMS transmittance difference of 2.0% with the degraded line-by-line data used in their determination.
3. Calculations using these LOWTRAN 7 band models with the corresponding transmittances computed with LOWTRAN 6 agreed within 2.85% for the uniformly-mixed gases, 16.36% for H<sub>2</sub>O and 1.84% for O<sub>3</sub>, along a vertical path from sea level to the top of the U.S. Standard Atmosphere.

#### 4.2 Nitric Acid

The transmittance due to HNO<sub>3</sub> has been assumed to lie in the weak-line or linear region. Absorption coefficients digitized at 5 cm<sup>-1</sup> intervals for the 5.9-μm, 7.5-μm, and 11.3-μm bands of HNO<sub>3</sub> are in the LOWTRAN model. These coefficients were obtained by Goldman, Kyle and Bonomo<sup>246</sup> by fitting their experimental results with the statistical band-model approximation, and these results are displayed in Figure 49.

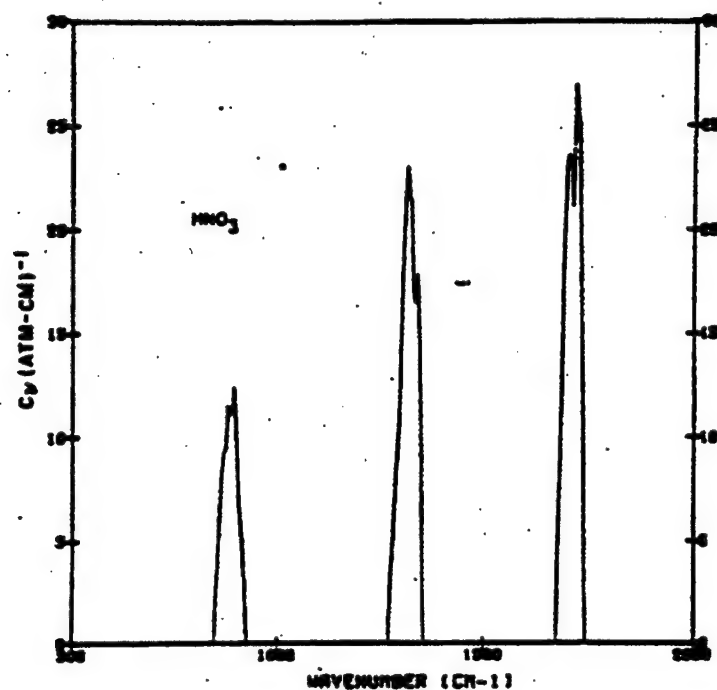


Figure 49. Absorption Coefficient  $C_v$  for Nitric Acid, from 500 to 2000  $\text{cm}^{-1}$ .

### 4.3 Nitrogen Continuum Absorption

The continuum due to collision-induced absorption by nitrogen in the 4- $\mu\text{m}$  region, is included in the LOWTRAN model based on the measurements of Reddy and Cho<sup>247</sup> and Shapiro and Gush<sup>248</sup> (see also McClatchey et al<sup>249</sup>). The nitrogen continuum absorption is displayed in Figure 50. The transmittance due to continuum absorption is assumed to follow a simple exponential law.

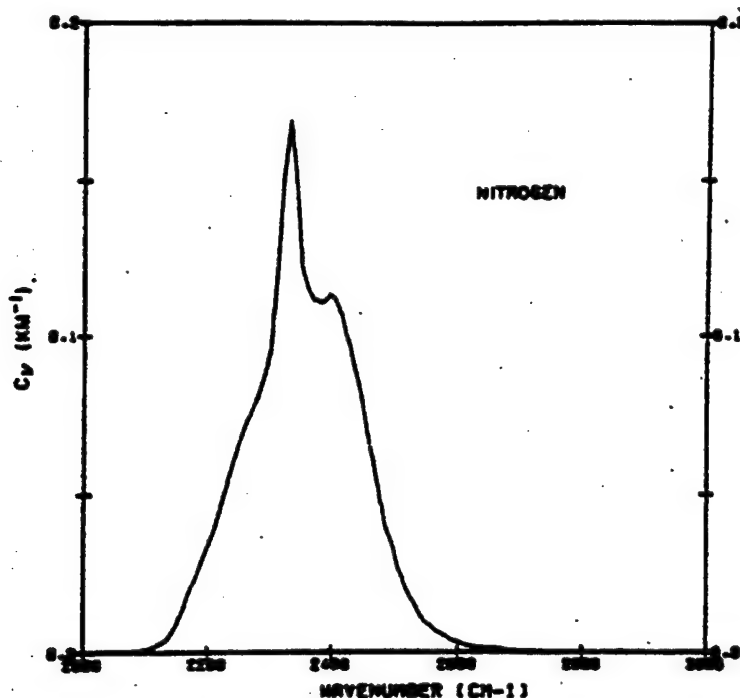


Figure 50. Absorption Coefficient  $C_v$  for the Nitrogen Continuum, from 2000 to 3000  $\text{cm}^{-1}$ .

#### 4.4 Molecular Scattering

The attenuation coefficient ( $\text{km}^{-1}$ ) due to molecular scattering, (stored in the variable  $ABS(6)$ ), is introduced into MODTRAN via the following expression:

$$ABS(6) = \nu^4 / (9.26799 \cdot 10^{18} - 1.07123 \cdot 10^9 \cdot \nu^2) \quad (89)$$

where  $\nu$  is in wavenumbers ( $\text{cm}^{-1}$ ). The above expression was obtained from a least square fit to molecular scattering coefficients. This function improves the fit in the ultraviolet region.

#### 4.5 Ultra Violet Absorption

Spectroscopic data describing the ultraviolet absorption properties of molecular oxygen and ozone have been collected for incorporation into the FASCODE and MODTRAN models. This data includes the  $\text{O}_2$  Herzberg continuum and Schumann-Runge bands as well as the  $\text{O}_3$  Hartley and Huggins bands. These systems result in the dissociation of the parent molecule and the creation of atomic oxygen<sup>250-254</sup>.



#### 4.5.1 UV Oxygen Absorption

The dissociation of oxygen allotropes is of paramount importance to the chemical makeup of the earth's atmosphere. The strongly absorbing  $O_2$  Schumann-Runge and weaker Herzberg systems influence differing altitude regimes in the atmosphere because of the relative strengths of their respective transition probabilities. Figure 51 (after Watanabe<sup>255</sup>) shows the approximate depth of penetration of solar irradiance throughout the UV spectral range. In general, solar radiation in the 0.175 to 2.0  $\mu m$  spectral region is completely absorbed by the Schumann-Runge system at altitudes above 40 km. At longer wavelengths (greater than 0.2  $\mu m$ ) absorption by ozone begins to compete with the residual Schumann-Runge and Herzberg absorption; the combination does not allow solar energy at wavelengths less than 0.3  $\mu m$  to penetrate to the surface. In addition to this shielding of high energy solar radiation, the UV absorption properties of ozone provide the dominant source of stratospheric heating.

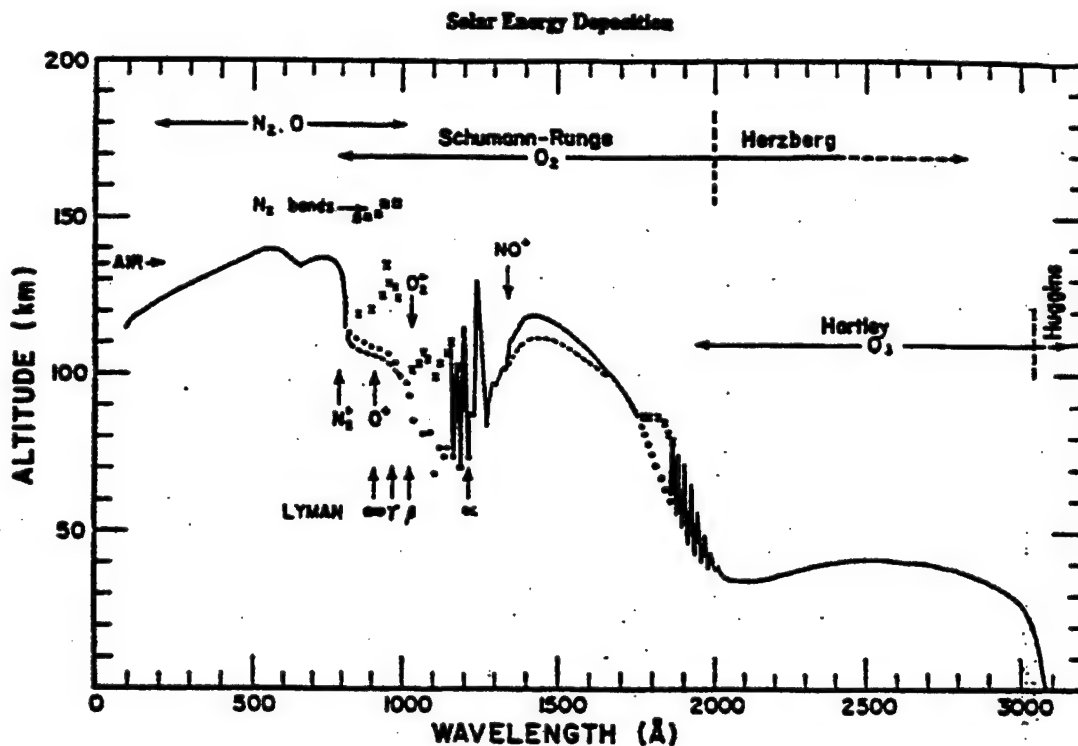


Figure 51. The Approximate Altitude at Which  $1/e^{\text{th}}$  of the Solar Irradiance is Deposited; after Watanabe.<sup>255</sup> In the UV Wavelength Spectral Range, MODTRAN Includes the Effects of the Ozone Hartley and Huggins Bands Plus Portions of the Molecular Oxygen Schumann-Runge and Herzberg Systems.

## HERZBERG CONTINUUM

While the Herzberg continuum absorption is small relative to both the Schumann-Runge and ozone contributions, it is extremely important to the maintenance of the stratospheric photochemical balance. Until recently the Herzberg continuum was believed to be almost 40% stronger than the currently accepted estimate. Since it lacks any detailed spectral structure, the absorption properties are readily described by an analytic function proposed by Johnson et. al.<sup>23</sup> After fitting the combined measurements of U.S. and French laboratories<sup>22</sup> to a function of this form, the cross section can be expressed as:

$$\sigma(0, \mu m) = 6.88E-24 R \exp[-69.7374 \{\ln(R)\}^2] \quad (96)$$

where:  $R = 0.20487/(\mu)$

and  $\mu$  = wavelength in  $\mu m$ .

The longevity of the erroneously large Herzberg values can be traced to their pressure dependence, related to dimer formation. The cross sections are so small that laboratory determinations have to rely on high pressure techniques to create the necessary opacities. Historically, extrapolation to zero pressure was attempted, but with little success. In fact, long-path, low pressure stratospheric measurements of attenuation of solar irradiance provided the first verification that the laboratory estimates were seriously in error.<sup>256,257</sup>

Accurate determination of the pressure dependence of  $O_2$  within an  $O_2$  environment is an important part of any laboratory measurement of the cross section. Yoshino et.al.<sup>22</sup> provide an equation of the form:

$$\sigma(p, \mu m) = \sigma(0, \mu m) (1 + (\Gamma(\mu m)/\sigma(0, \mu m)) \cdot P_{O_2}(Torr)) \quad (97)$$

where  $\Gamma(\mu m)$  represents the pressure dependent term. However, because of coding considerations the MODTRAN formulations replace the spectrally dependent  $\Gamma$  with a proportionality constant,

$$\Gamma(\mu m)/\sigma(0, \mu m) \approx 1.81E-3 \quad (98)$$

that is consistent to within 10% for most of the Herzberg spectral range (between 0.20 and 0.23  $\mu m$ ); see Fig. 52. The errors gradually increase to 30% at 0.24  $\mu m$ . The magnitude of this wavelength-dependent error is generally tolerable because the

pressure contribution is often a fractionally small portion of the diminishing O<sub>2</sub> cross section which is overwhelmed by the ozone cross section. However, near the surface (high pressures and low ozone mixing ratios) the errors can become significant.

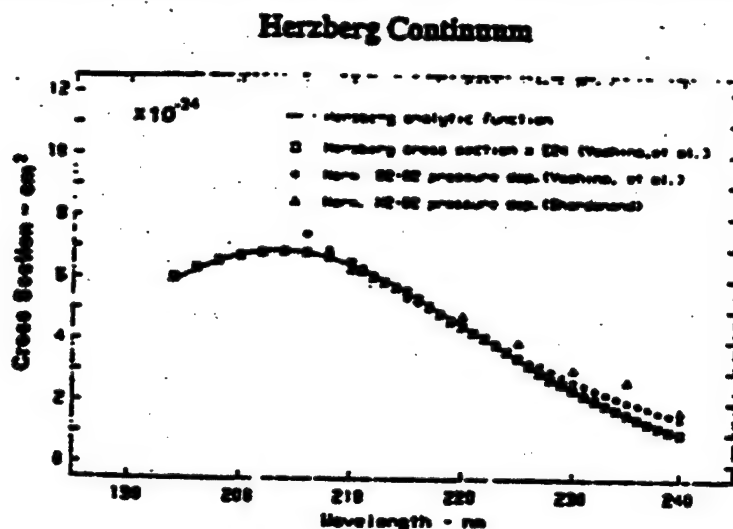


Figure 52. The Form of the Analytic Function Used to Express the Herzberg Continuum

Within MODTRAN 2, Plus the Supporting Measurements for that Continuum and its Normalized Pressure-Dependent Terms.

Atmospheric pressure dependence is also governed by interaction with Nitrogen (O<sub>2</sub> - N<sub>2</sub> dimer formation). Shardanand<sup>24</sup> has provided an estimate of this effect, N<sub>2</sub> being approximately 45% as efficient as pure O<sub>2</sub>. Figure 52 shows the degree of spectral similarity between the N<sub>2</sub> dimer effect and the pure Herzberg absorption,  $\sigma(o, \mu m)$ , hence it has similarly been scaled to  $\sigma(o, \mu m)$ . The pressure dependence of the Herzberg continuum for a combination of 21% oxygen and 78% nitrogen, including the 45% efficiency factor is then:

$$\sigma(p, \mu m) = \sigma(o, \mu m) (1 + 0.83(P/P_o)(T_o/T)) \quad (99)$$

The total pressure has been replaced by a normalized density function with  $P_o$  and  $T_o$  at STP.

As mentioned above, the Herzberg bands are not included explicitly in MODTRAN. While they would not contribute to the photochemical production of odd oxygen, there is some contribution in the calculation of total transmittance.<sup>259</sup> This has been approximated in MODTRAN by extending the Herzberg analytic equation to longer wavelengths (0.277  $\mu m$  or 36000  $cm^{-1}$ ) with a linearly smooth damping to zero

absorption at that arbitrary cutoff. The errors introduced by this approximation are potentially serious for transmittance calculations for ozone-poor lines of sight (such as solar-blind calculations at the surface<sup>260</sup>). However, for most general cases the effect of the omission is not discernible. A more correct band model approximation is planned for an upgraded version of MODTRAN.

### SCHUMANN-RUNGE BANDS

The O<sub>2</sub> Schumann-Runge band analysis has been addressed in two ways: (1) a line-by-line spectroscopic atlas, similar in format to the HITRAN database<sup>20</sup>, has been calculated from published energy levels; and (2) a one parameter 20 cm<sup>-1</sup> resolution band model has been generated for incorporation into LOWTRAN and MODTRAN. Using the new atlas, line-by-line syntheses of the Schumann-Runge cross sections, including temperature-dependence of the vibronic population levels, have been created using FASCOD3P. It is important to note, that while the Schumann-Runge system exhibits very rich spectral structure, including rotational splitting at fractions of a wavenumber separation, the half widths of the lines are sufficiently broadened by pre-dissociation to be independent of pressure and temperature. Figure 53 shows a portion of the new database, with line positions and relative strengths at line center; the triplet structure is not depicted. Individual band groupings are easily identified.

The 20 cm<sup>-1</sup> band model for the Schumann-Runge system (as currently available in MODTRAN) was developed from a similar line-by-line formulation<sup>25</sup> with additional laboratory measurements.<sup>261</sup> The band model is inadequate for detailed spectroscopic calculations because it does not correctly simulate the strong temperature-dependence of the O<sub>2</sub> cross sections due to the change in population of the first excited state ( $v'' = 1$ ). This effect is strongest in the spectral regions away from the  $v'' = 0$  band heads (i.e. in the window regions). Solar energy penetrates deepest into the atmosphere in just these window regions, so an improved formulation is mandatory if it is needed for photochemical calculations.

Given these stated inaccuracies, the band model does show reasonable agreement with in situ measurements of the depleted solar irradiance. In Figure 54 data from the 1983 balloon flight of a single dispersion half-meter Ebert-Fastie spectrometer<sup>262</sup> is compared to simulated data using the new Schumann-Runge band model. These calculations also include other major portions of the LOWTRAN 7 algorithm, specifically the Herzberg continuum and ozone cross sections. The only exception to LOWTRAN 7

compatibility is the solar irradiance; the lack of solar spectral signature can be seen near  $0.199 \mu\text{m}$  ( $199 \text{ nm}$ ) in the simulated data. This band model algorithm is patterned on

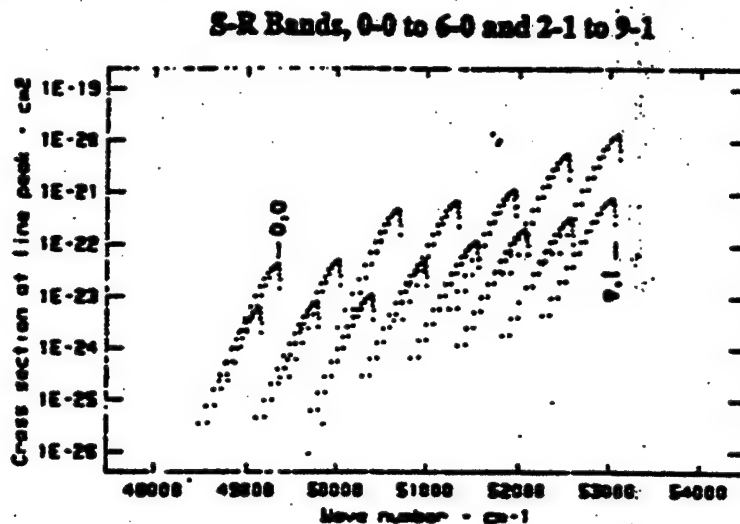


Figure 53. Calculated Line Positions and Strengths for a Portion of the Schumann-Runge Band system. MODTRAN Directly Accesses Only those Bands with Frequencies Less than  $50,000 \text{ cm}^{-1}$ , Although Coding for the Entire Depicted Range is Included.

the one principally developed for the IR by Pierluissi and Maragoudakis,<sup>13</sup> including the use of the Pierluissi fitting parameters for  $\text{O}_2$ . A single spectral function  $[C(\mu\text{m})]$  has been calculated for the wavelength range from  $0.1875$  to  $0.203 \mu\text{m}$ . With a more sensitive band model, the wavelength range of MODTRAN can be extended to include the entire Schumann-Runge system. The expectation is that this new band model will separate the  $v'' = 0$  from the  $v'' = 1$  bands, with the treatment of the ground state transitions remaining as described above. [ **NOTE:** while the preliminary band model parameters are available within the MODTRAN 2 coding, they are not directly accessible for wavelengths smaller than  $0.2 \mu\text{m}$ . This limitation is currently imposed by an "IF TEST" related only to the non-availability of the aerosol functions for these wavelengths. The solar irradiance, Rayleigh scattering coefficients and an estimated Herzberg continuum are all provided.]

#### 4.5.2 UV Ozone Absorption

Absorption by ozone, the remaining UV-active oxygen allotrope, is described in both MODTRAN and FASCODE by a temperature-dependent (quadratic) continuum. This continuum includes two major bands, the spectrally overlapping Huggins and Hartley systems. [NOTE: Steinfeld, et.al.<sup>263</sup> present an excellent review.] The Hartley band is

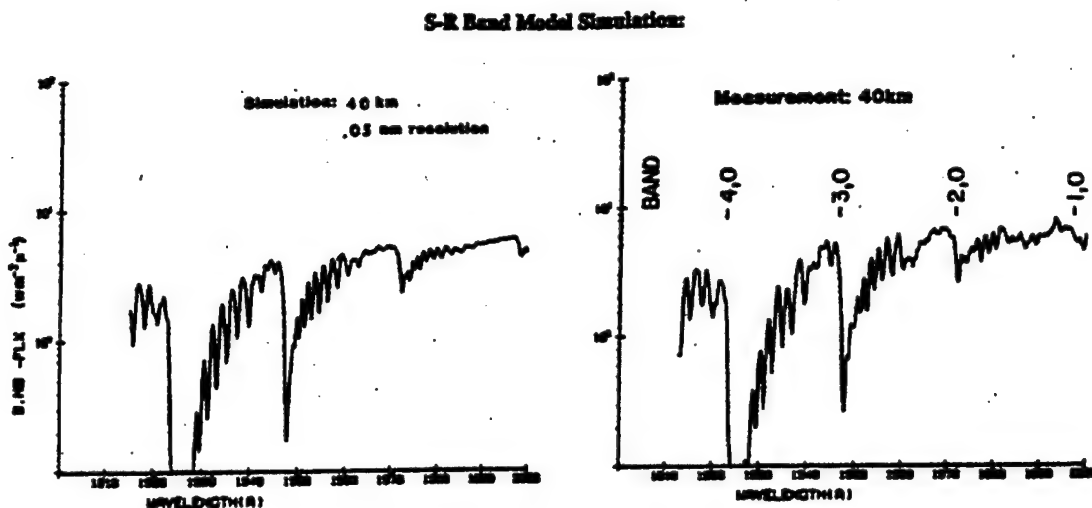
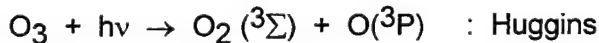


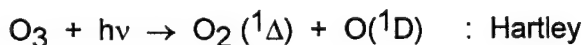
Figure 54. A Comparison of the LOWTRAN 7 Schumann-Runge Band Model Algorithm and an Actual Balloon-Borne Measurement of in situ Solar Irradiance. The Balloon Altitude was Approximately 40 km with the Sun at 24° Zenith Angle. The Model Easily Reproduces the 4-0, 3-0, 2-0 and 1-0 Band Heads.

by far the more efficient at production of the first excited state of atomic oxygen,  $O(^1D)$ , with approximately 88% efficiency, while the Huggins band fragmentation generally leads to the ground state product for atomic oxygen,  $O(^3P)$ :



$0.36 \mu\text{m} > \text{wavelengths} > 0.31 \mu\text{m}$

and:



$\text{wavelengths} < 0.31 \mu\text{m}$

The atomic oxygen excitation state is critical to subsequent photochemical reactions because  $O(^1D)$  is the energetically preferred partner. The Hartley band absorption is very strong, exhibiting only marginal structure and generally no temperature-dependence. The Huggins system has a much more pronounced band structure and moderate to strong temperature-dependence, although the features are still broad enough not to be amenable to detailed line-by-line representation (Figure 55).

Katayama<sup>264</sup> has established definitive vibrational assignments and inferred a band origin.

Research studies of the ozone absorption cross section have been available since the early 1900's. The relatively recent measurements of Bass and Paur<sup>27</sup> form the basis of MODTRAN 2 and FASCOD3 formulation. Their values, including quadratic temperature-dependence, are provided at 5 cm<sup>-1</sup> intervals from 41000 to 30000 cm<sup>-1</sup> (0.24 to 0.33 μm). Subsequent measurements of Molina and Molina<sup>28</sup> have been used in combination with those of Yoshino et.al.<sup>29</sup> to expand the temperature-dependent range to 0.34 μm, with a final extension to 0.36 μm using the values of Cacciani, et.al.<sup>30,265</sup>. At wavelengths less than 0.24 μm, the temperature-independent values of Molina and Molina were again adopted (between 0.18 and 0.24 μm). These various data sources agree very well (usually better than 3%) in the regions of overlap. All feature replication is real and suitable; that is, the small spectral features are represented at their natural resolution whereby a line-by-line calculation would not provide significantly greater detail.

#### Ozone Absorption Properties in the UV

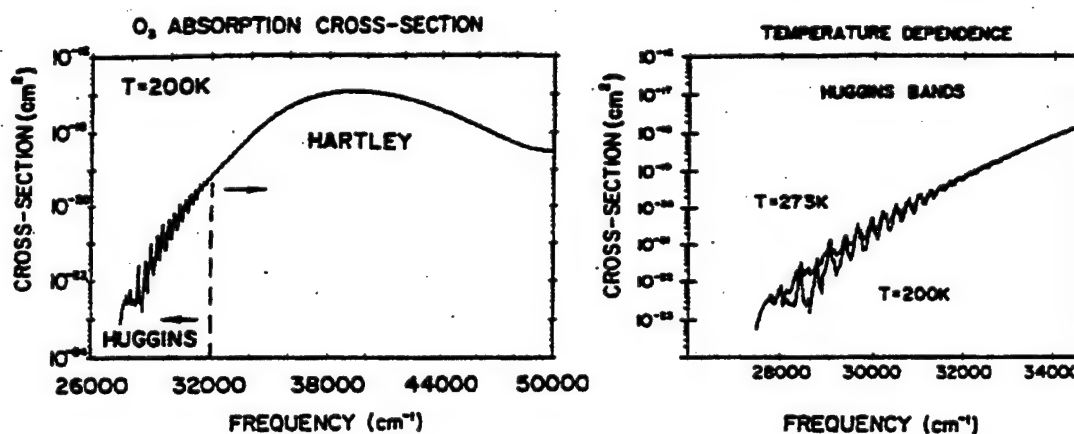


Figure 55. The Ozone Absorption Cross Sections as Available in MODTRAN. Structure at the Center of the Hartley System does not Appear in this Logarithmic Representation but is Provided in the Code.

### 4.6 Aerosol Transmittance

Within a given atmospheric layer of path length  $DS$ , in km, the transmittance,  $\tau(\nu)$ , due to aerosol extinction is given by

$$\bar{\tau}(\nu) = \text{EXP}[-\text{EXTV}(\nu) \cdot \text{HAZE} \cdot DS] \quad (100)$$

where  $EXTV(\nu)$  is the normalized extinction coefficient for the wavenumber  $\nu$  of the appropriate aerosol model and altitude. HAZE is the aerosol scaling factor (see section 2.3).

$EXTV(\nu)$  is found by interpolation of the values stored in the code for the required wavenumber and relative humidity. HAZE is determined by interpolation of the appropriate aerosol scaling-factor profiles according to the meteorological range and season.



## 5. ATMOSPHERIC RADIANCE

### 5.1 Radiative Transfer Equations

The radiance algorithm for MODTRAN 2 has been modified to specifically handle optically thick layers. Cornette<sup>266</sup> had reported on a possible correction for LOWTRAN 7.

Considering a single isolated layer, a direct application of the simple radiance equation leads to:

$$R = B d\tau \text{ or } R = (1 - \tau) \quad (101)$$

where  $R$  = Radiance,  $B$  = Planck Function, and  $d\tau = (1 - \tau)$ , the change in transmittance,  $\tau$  across the layer. The Planck Function is defined for a Curtis- Godson density-weighted temperature for the layer. For an optically thin case, the observed radiance in this scenario is independent of viewing direction. [Note that for typical lines-of-sight across a multi-layered atmospheric path, radiance is dependent on viewing direction while total transmittance remains independent of the observer's position.] However, if this single layer is optically thick and includes a directional temperature gradient, the observed radiance will be either larger (emanating from a warmer thermal region closer to the observer) or smaller (emanating from the closer cooler region). One approach in accommodating the opacity-imposed directionality consists of subdividing the layers into less optically thick entities. This approach is very awkward so various pragmatic solutions have been considered. Wiscombe<sup>267</sup> and Ridgway et.al.<sup>268</sup> recently suggested a method whereby the Planck Function and optical depth is assumed to vary linearly between the boundaries of the layer. Following this approach, Clough et al<sup>269</sup> produced an expression (his Eq. 13), dependent on the Planck ( $B$ ) functions for the Curtis-Godson temperature and the nearest boundary temperature, coupled with both the layer transmittance and optical depth:

$$R = (1 - \tau) \left\{ B_n + 2(B - B_n) \left[ \frac{1}{\tau} - \frac{\tau}{(1 - \tau)} \right] \right\} \quad (102)$$

where the subscript  $n$  implies the nearest boundary,  $t$  = layer optical depth between boundaries, and  $\tau$  = layer transmittance, for a single layer. For a multi-layer scenario, this local layer radiance becomes the input for its neighbor, and the full path solution is

reached through recursive calculations; (see Eq. 31 of Clough, et al<sup>14</sup>). The layer transmittance then becomes:  $\tau = \tau(b+1)/\tau(b)$  where  $\tau(b)$  and  $\tau(b+1)$  are the full path transmittances from observer to boundary  $b$  and  $(b+1)$ , respectively. The required optical depth term is an "effective" optical depth, due to the degraded  $2 \text{ cm}^{-1}$  resolution, and is derived from the ratios of adjacent full path transmittances at MODTRAN resolution:

$$T = -\ln \{ \tau(b+1)/\tau(b) \} \quad (103)$$

The radiance equation for a single layer (Eq. 102), including the "linear in tau" approximation, appears the same as the simple radiance equation (Eq. 101) if the bracketed quantity  $\{ \}$  is thought to contain an "equivalent" Planck function, defined by the optical depth weighting. This technique is fully implemented in MODTRAN 2 and provides excellent agreement with FASCOD3P results for optically thick calculations. Figure 56 depicts a comparison between FASCOD3P and MODTRAN 2 calculations in the optically thick  $15 \text{ } \mu\text{m}$   $\text{CO}_2$  band.

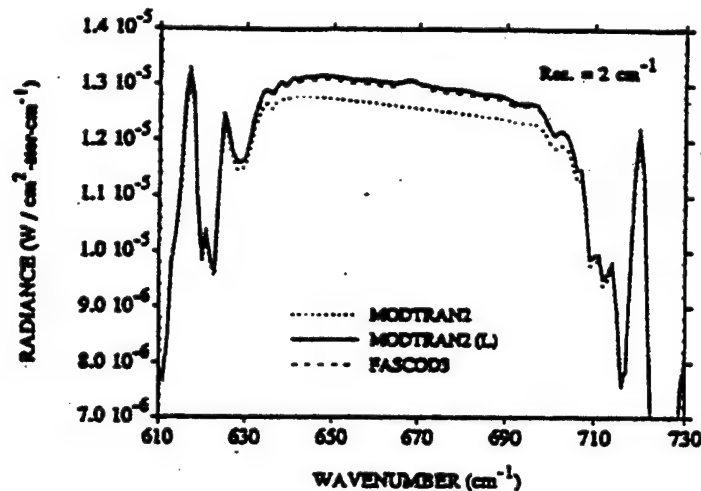


Figure 56. Radiance Calculations in the Optically Thick  $15 \text{ } \mu\text{m}$  Band for a Single  $1 \text{ km}$  Path with Boundary Temperatures of  $288.15\text{k}$  and  $281.15\text{k}$ , as Observed from the Warmer Boundary. The FASCOD3P Calculation Employs a Slightly Different Approximation to the "linear in tau" Algorithm used in MODTRAN 2. The Dotted Curve Represents the Old MODTRAN Calculation Which is Deficient Within the Band Center.

## 5.2 Improved Solar Source Function

An earlier version of LOWTRAN (Kneizys et al<sup>3</sup>) had included the solar spectrum (based on Thekeakara<sup>35</sup>) for calculating the single-scattered and/or directly transmitted

solar radiances. The data used for this spectrum was not at a resolution consistent with the treatment of molecular absorption in either LOWTRAN or MODTRAN. (Note - in LOWTRAN 6 the visible and UV ozone absorption were provided at 200 and 500  $\text{cm}^{-1}$  intervals respectively. Concerns have been raised in the literature on the accuracy of the Thekeakara<sup>35</sup> data (see Frhlich<sup>270</sup>, and the references therein).

These particular concerns led to the development of a new solar spectrum for LOWTRAN 7 and MODTRAN. The primary data sources used for the different spectral regions are summarized in Table 30.

**Table 30. Data Sources Used for the Solar Spectrum**

<u>Wavelength Range</u> ( $\mu\text{m}$ )	<u>Frequency Range</u> ( $\text{cm}^{-1}$ )	<u>Source</u>
0.17400 to 0.35088	28500 to 57470	VanHoosier et al. (1987) <sup>31</sup> (SUSIM)
0.35094 to 0.86806	11520 to 28495	Neckel & Labs (1984) <sup>33</sup>
0.86843 to 3.2258	3100 to 11515	Wehrli (1985) <sup>34</sup>
3.2258 to 3.4483	2900 to 3100	Smooth Transition between Wehrli and Thekeakara
3.4483 to $\infty$	0 to 2900	Thekeakara (1974) <sup>35</sup>

The smooth transition between the Thekeakara and Wehrli data was accomplished as follows:

$$S(x) = \left\{ \begin{array}{ll} \text{Thekeakara}, & x < 2900\text{cm}^{-1} \\ \frac{w(x) \bullet \text{Thekeakara} + [1 - w(x)] \bullet \text{Wehrli},}{\text{Wehrli},} & \begin{array}{l} 2900 < x < 3100\text{cm}^{-1} \\ 3100\text{cm}^{-1} < x \end{array} \end{array} \right\}$$

where:  $S(x)$  is the solar spectrum at a frequency,  $x$ ,

and  $w(x)$  is given by the expression:

$$w(x) = (x - b)^2 \frac{(2x - 3a + b)}{(b - a)^3} \quad (104)$$

This polynomial has the following properties:

$$w(a) = 1$$

$$w(b) = 0$$

$$w'(a) = w'(b) = 0$$

where:  $a = 2900 \text{ cm}^{-1}$  and  $b = 3100 \text{ cm}^{-1}$ .

In other words, over the interval from 'a' to 'b',  $w(x)$  goes from a value of one to zero, with the derivative equal to zero at the end points.

The individual data sets, from the different sources, were determined at a resolution compatible with the models by passing a  $20 \text{ cm}^{-1}$  triangular scanning function over the data values. This data is then tabulated at  $5 \text{ cm}^{-1}$  intervals for the frequency range of 0 to  $57495 \text{ cm}^{-1}$ , to ensure adequate sampling, and to maintain consistency within the models. Except for the SUSIM data (VanHoosier et al.)<sup>32</sup>, which was measured with a  $0.15 \text{ nm}$  resolution, the remaining data sets were all measured at a coarser resolution than  $20 \text{ cm}^{-1}$ . The low frequency data ( $x < 500 \text{ cm}^{-1}$ ) was tabulated directly as interpolated from the Thekeakara<sup>35</sup> values, since the strong decrease with frequency, causes a systematic increase of the values when smoothed with the  $20 \text{ cm}^{-1}$  scanning function.

Within the context of LOWTRAN and MODTRAN, the solar flux values have been stored in a look-up table. In an effort to reduce memory requirements, the effect on the accuracy of eliminating portions of the data and re-generating them by interpolation was examined. For the SUSIM data ( $x > 28500 \text{ cm}^{-1}$ ) the values were retained at a  $10 \text{ cm}^{-1}$  spacing. For the remainder of the data ( $x < 28500 \text{ cm}^{-1}$ ) the values were used with a  $20 \text{ cm}^{-1}$  spacing. A four-point Lagrange interpolation scheme was used. For the low frequencies ( $x < 100 \text{ cm}^{-1}$ ), the look-up table and interpolation were replaced with a simple power-law fit to the solar flux values. The scenario described here is implemented in the FORTRAN Function *FSUN*.

## 5.3 SOLAR/LUNAR SINGLE SCATTERING MODEL

### 5.3.1 Introduction

The radiation propagating through the atmosphere originates from the following sources: gaseous emission along the line-of-sight, transmitted extraterrestrial

(solar/lunar) sources or background emission (earth or target), and radiation scattered into the line-of-sight by aerosols or molecules.

Previous versions of LOWTRAN have calculated atmospheric radiance due only to gaseous and background emissions. While in many cases these two sources dominate the atmospheric radiance, there are other cases of interest where the scattered radiance is of equal or greater importance. Until now LOWTRAN has treated scattering only as a loss mechanism.

A number of techniques exist that include the full effects of scattering on atmospheric radiance: these include for example, Monte Carlo and "adding/doubling" techniques. These techniques take into account multiple scattering and can include both external and internal sources. These techniques however, tend to be computationally expensive and some of them are incompatible with the spectrally-averaged band model used in MODTRAN.

In many situations, a complete multiple scattering calculation is not necessary and the scattered radiation is dominated by solar radiation that has been scattered only once. Calculations of the single solar (or lunar) scattered radiation is relatively simple and fits well within the context and structure of MODTRAN.

Calculation of single scattering has been incorporated as an option in MODTRAN. The next two sections of this chapter develop the algorithm for single scattering and show the verification of the MODTRAN calculations against other methods. Then the phase functions for scattering by atmospheric aerosols and molecules will be explained. Next, sample calculations of solar scattering are shown that illustrate the conditions where the singly scattered radiation becomes significant compared to the emitted radiation. Finally, recommendations are given concerning the range of applicability of the single scattering model. For a more detailed discussion of the single scattering model, see Reference 271.

### 5.3.2 Radiative Transfer

Before proceeding further, it will be helpful to introduce the following nomenclature:

#### SUPERSCRIPTS;

A	aerosol
M	molecular

#### SUBSCRIPTS:

e	extinction
a	absorption
s	scattering

ps	primary solar path (sun to scattering point)
op	line-of-sight optical path (scattering point to observer)

## OTHER QUANTITIES:

k	monochromatic volumetric extinction, absorption, or scattering coefficient
$\tau = e^{-ks}$	monochromatic transmittance over a homogeneous path length is due to extinction absorption, or scattering
$P(\gamma)$	scattering phase function for a scattering angle $\gamma$
$I_{SUN}$	solar extraterrestrial intensity
$I_{MOON}$	lunar extraterrestrial intensity

**Note** that the dependence of most quantities on the spectral frequency  $\nu$  will be shown by a subscript  $\nu$ , although it will sometimes be suppressed for simplicity of notation when the concept is clear from context.

The monochromatic intensity (radiance) seen by an observer looking along a particular directional path is the sum of contributions from all sources lying along the line-of-sight. The sources are either primary sources (infrared emission) or scattering sources. The scattering source function  $J$  for scattering points along the observer's line-of-sight can be expressed in terms of the local incoming intensity at each point by  $I_\nu(\hat{n}')$  by

$$J_\nu(\hat{n}) = \int I_\nu(\hat{n}') (P_\nu^A k_s^A + P_\nu^M k_s^M) d\Omega' \quad , \quad (105)$$

where  $\hat{n}$  is the unit vector directed toward the observer and  $\hat{n}'(\Omega')$  is to be integrated over the solid angle denoted by  $\Omega'$ . With only single solar/lunar scattering included, the incident intensity  $I_\nu(\hat{n}')$  is given by:

$$I_\nu(\hat{n}') = I_\nu^{SUN} \tau_{e,ps}^{A+M} \delta(\hat{n}', \hat{n}_s') \quad (106)$$

where  $\hat{n}_s'$  is the direction of the incident solar/lunar radiation at the scattering point. A schematic of the scattering geometry for a particular sun/observer orientation is displayed in Figure 57. The path that the sunlight/moonlight takes in passing through the atmosphere prior to being scattered at any scattering point P will be called the 'primary solar' path. Other sources besides direct extraterrestrial illumination could of course contribute to the pre-scattered intensity  $I_\nu(\hat{n}')$ . One might include other direct sources such as gaseous emission and boundary surface radiation plus previously scattered radiation, but only un-scattered sunlight/moonlight is included in the present

scattering source function. The resulting source function is found by using EQ. (106) in EQ. (105) to obtain

$$J_v = \bar{I}_v^{SUN} \tau_{e,ps}^{A+M} (P_v^A(\gamma) k_s^A + P_v^M(\gamma) k_s^M) \quad (107)$$

Note that  $P^A$ ,  $P^M$ ,  $k_s^A$ , and  $k_s^M$  vary with altitude (atmospheric density and composition) and are generally slowly varying functions of frequency. Note also that the scattering angle  $\gamma = \arccos(\hat{n} \cdot \hat{n}_s')$  would be constant (independent of the particular scattering point) along a line-of-sight in the absence of refractive bending. Both the primary solar path and the line-of-sight optical path actually bend somewhat, so that  $\gamma$  can be expected to vary by as much as a few degrees along the line-of-sight.

The primary solar transmittance  $\tau_{e,ps}^{A+M}$  depends strongly on the optical path length of the primary solar path (prior to scattering), so that this factor can be expected to vary considerably from one scattering point to the next.

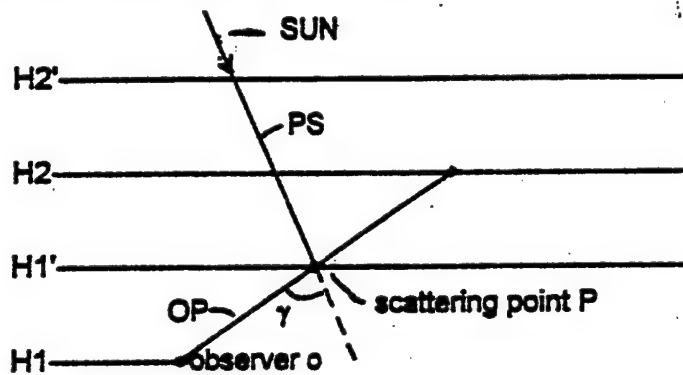


Figure 57. Schematic Representation of the Single Scattering Geometry. The Scattering Point at H1' is Shown for an Observer Looking up from an Altitude H1

The monochromatic intensity at the observer due to all of the single scattering sources within the line-of-sight is obtained by summing over the optical path, the product of the source function and the transmission function that gives

$$\begin{aligned} \bar{I}_v^{SCAT} &= \int J_v \tau_{e,op}^{A+M} ds_{op} \\ &= I_v^{SUN} \int \tau_{e,ps}^{A+M} \tau_{e,op}^{A+M} (P_v^A k_s^A + P_v^M k_s^M) ds_{op} \end{aligned} \quad (108)$$

The scattering optical depth increment  $k_s ds_{op}$  can be expressed in terms of the incremental transmittance for both aerosol and molecular scattering as

$$K_s^X ds_{op} = \frac{d\tau_{s,op}^X}{\tau_{s,op}^X}, \quad (109)$$

with X being either A or M. The intensity can therefore be written as:

$$I_\nu^{SCAT} = I_\nu^{SUN} \int \tau_{e,ps+op}^{A+M} \left[ P_\nu^A \frac{d\tau_{s,op}^A}{\tau_{s,op}^A} + P_\nu^M \frac{d\tau_{s,op}^M}{\tau_{s,op}^M} \right] \quad (110)$$

which includes two separate integrals covering aerosol and molecular scattering effects. The above equation, which provides for a monochromatic calculation at any frequency  $\nu$ , is now adapted for use with the molecular band transmission model used in LOWTRAN. The spectrally averaged intensity  $\bar{I}$  is formally defined in terms of a convolution of the spectral intensity with a triangular instrument shape function  $g(\nu)$  taken over a spectral width (half width at half maximum) of approximately  $\delta\nu = 10 \text{ cm}^{-1}$ , that is,

$$\bar{I}_\nu = \frac{1}{\delta\nu} \int I_\nu g(\nu - \nu') d\nu' \quad (111)$$

The spectrally averaged, scattered intensity can be expressed in terms of known LOWTRAN quantities provided that only the molecular absorption transmittance is a rapidly varying function of frequency. All other quantities are assumed to be constant over the spectral interval  $\delta\nu$ . The result is

$$\bar{I}_\nu^{SCAT} = \bar{I}_\nu^{SUN} \int \tau_{e,ps+op}^{-A+M} \left[ P_\nu^A \frac{d\tau_{s,op}^A}{\tau_{s,op}^A} + P_\nu^M \frac{d\tau_{s,op}^M}{\tau_{s,op}^M} \right] \quad (112)$$

The quantity  $\tau_{e,ps+op}^{-A+M}$  represents the spectrally averaged transmittance that is calculated in LOWTRAN. Therefore, the molecular band models and aerosol models of LOWTRAN provide a direct means of calculating the path transmittance required for each of the scattering points. In order to maintain compatibility with the spherical shell atmosphere of LOWTRAN, the integral over the path of scattering sources is replaced by a layer-by-layer sum along the line-of-sight.

For an optical path traversing N layers in an upward or downward direction this process gives



$$\begin{aligned} \bar{I}_\nu^{SCAT} = & \bar{I}_\nu^{SUN} \sum_{j=1}^N \left[ \left\langle \frac{\bar{\tau}_{e,ps+op}^{A+M} P_j^A}{\tau_{s,op}^A} \right\rangle j \Delta \tau_{s,op,j}^A \right. \\ & \left. + \left\langle \frac{\bar{\tau}_{e,ps+op}^{A+M} P_j^M}{\tau_{s,op}^M} \right\rangle j \Delta \tau_{s,op,j}^M \right] \end{aligned} \quad (113)$$

The quantity  $\Delta \tau_j$  is the change in molecular or aerosol scattering transmittance in passing through layer  $j$ , while  $\langle \rangle_j$  denotes an average value for that layer. Evaluating EQ. (113) requires the equivalent absorber amounts for both the line-of-sight and the primary solar paths associated with each scattering point, plus the scattering angle at each scattering point. The calculation of these amounts and angles is described in Appendix C of Ref. 3. The layer-by-layer sum of the singly scattered intensity is computed simultaneously with the existing direct thermal radiance using the following expression

$$\begin{aligned} \bar{I}_\nu^{SCAT} = & \bar{I}_\nu^{SUN} \sum_{i=1}^{n-1} \sum_{X=(A,M)} \left[ \tau_{s,op,i}^X - \tau_{s,op,i+1}^X \right] \cdot \\ & \frac{1}{2} \left[ \frac{\bar{\tau}_{e,ps+op,i}^{A+M} P_i^X}{\tau_{s,op,i}^M} + \frac{\bar{\tau}_{e,ps+op,i+1}^{A+M} P_{i+1}^X}{\tau_{s,op,i+1}^X} \right] \end{aligned} \quad (114)$$

where  $n$  is the number of scattering points (layer boundaries). The layer average  $\langle \rangle_j$  in EQ. (113) has been evaluated in EQ. (114) using the properties of only the two scattering points that bound each layer path segment. In this scheme, the observer position coincides with  $i = 1$  and the end of the line-of-sight with  $i = n$ .

If the optical path intersects the earth, then EQ. (114) has an additional term representing the sunlight reflected from the ground. The ground is assumed to be a diffuse Lambertian reflector. The irradiance at the ground is proportional to  $\cos(\theta)$ , where  $\theta$  is the solar zenith angle at the ground. The ground reflected sunlight is given by the term

$$\bar{I}_\nu^{SUN} \tau_{e,ps+op,n} A \cos(\theta) / 2\pi \quad (115)$$

where  $A$  is the ground albedo.

The ground albedo is assumed to be independent of frequency and is read in as an input to MODTRAN with a default of 0 (no reflection).

The extraterrestrial solar intensity  $\bar{I}_v^{SUN}$  is obtained from the data compiled by Thekaekara<sup>35</sup> The intensity is corrected for variation in the earth-to-sun distance due to the earth's elliptical orbit. The lunar extra-terrestrial intensity is obtained by reflecting the solar intensity off of the moon's surface as in Reference 272.

$$\bar{I}_v^{MOON} = 2.04472 * 10^{-7} \bar{I}_v^{SUN} \alpha_v P_{\gamma'}^{MOON}$$

Here  $\alpha_v$  is the wavenumber dependent geometric albedo of the moon<sup>273,274</sup> while  $P_{\gamma'}^{MOON}$  is the moon's phase function giving the relative intensity as a function of the phase angle  $\gamma'$  of the moon.<sup>275</sup> Note that  $P(\gamma' = 0) = 1$  for a full moon.

To ensure that the single scattering algorithm was correctly implemented, LOWTRAN calculations were compared to calculations of single scattered radiance by an independent, well-developed model. This model is a modification of the plane-parallel, monochromatic multiple scattering code described in Reference 276. This model, based on the adding/doubling technique, was modified to compute only single scattered radiance. Since LOWTRAN gaseous transmission functions do not obey Beer's Law, gaseous absorption was deleted in the calculations by setting the gaseous transmittances in LOWTRAN equal to 1.0. Statements were added to LOWTRAN to calculate and write total optical depths and albedos based on the remaining attenuation mechanisms. This data was then used in the modified adding/doubling programs. Comparisons were limited to cases where both the solar and line-of-sight zenith angles were within the range where the plane parallel approximation is valid.

An example of the comparisons is shown in Table 31. The optical path in this case is from ground to space with a zenith angle of 12.95°, the solar zenith angle is also 12.95°. A Henyey-Greenstein phase function was used [see Eqs. (117 and (118)]. The total optical depth for the optical path from ground to space is 0.183. The table presents the ratio of the LOWTRAN scattered radiance to the single scattered plane-parallel calculation for asymmetry factors  $g$  of 0 and 0.8 and for relative azimuthal angles of 0°, 90°, and 180°. The radiances shown are the upward radiances at 100 km, both the upward and downward radiance at 2 km, and the downward radiance at the ground. In

all cases, the LOWTRAN scattered radiance is within one percent of the radiance calculated by the adding/doubling program.

### 5.3.3 Phase Functions for Scattering by Atmospheric Aerosols and Molecules

The angular scattering of light by the atmosphere is specified by the phase function that gives the differential probability of the scattered radiation going in a given direction. The scattering by the aerosols and air molecules are treated separately using the appropriate phase function for each. The angular distribution from the two types of scattering are combined, weighted by the corresponding scattering coefficients so the integral over all possible scattering directions (that is, a sphere) is unity:

The phase functions as used in the program are normalized so the integral over all possible scattering directions (that is, a sphere) is unity:

$$\int \int_{4\pi} P(\gamma) d\Omega = 1 \quad (116)$$

with this normalization,  $P(\gamma) \Delta\Omega$  is the fraction of the scattered radiation that is scattered into a solid angle  $\Delta\Omega$  about an angle  $\gamma$  relative to the direction of the incident light

**Table 31** Ratio of Single Scattered Radiance, LOWTRAN, to an Adding/Doubling Technique (See Text for Description). The Geometry is illustrated in the lower part of the Figure.

TOP ↑	g	0.0	0.8	ψ
(100 km)		1.0022	1.0023	0°
			1.0024	90°
			1.0020	180°
			(a)	
2 km	g	0.0	0.8	ψ
		1.0015 ↑	1.0014	
		1.0000 ↓	1.0000	0°
			↑ 1.0014	
			↓ 0.9962	90°
			↑ 1.0015	
			↓ 0.9907	180°

			(b)	
Bottom ↓	g	0.0	0.8	$\psi$
		1.0003	1.0000	0°
			0.9957	90°
			0.9908	180°
			(c)	

All zenith angles are 12.95°.

↑ Radiation Propagation

g = asymmetry factor

$\psi$  = relative azimuth

SUN



100 km



Bottom

### 5.3.3.1 Aerosol Angular Scattering Function

The MODTRAN program offers the user three choices on handling the aerosol phase functions:

- (1) They can use the standard phase functions stored in the program for the various aerosol models;
- (2) They can use a Henyey-Greenstein type phase function, with a specified value for the asymmetry parameter;
- (3) They can input their own phase functions for the different altitude regions.

### 5.3.3.2 Standard MODTRAN Phase Functions

The standard aerosol phase functions stored in the MODTRAN program correspond to the different aerosol models available within the MODTRAN program. It is therefore recommended that this option be chosen whenever the MODTRAN aerosol models are used for solar scattering. These standard phase functions were originally developed to approximate the exact phase functions, within about 20 percent, for any of the various aerosol models available in LOWTRAN as a function of wavelength, between 0.2 and 40  $\mu\text{m}$ . The development of this standard set of approximate phase functions was

discussed in Appendix D,(Ref.3) along with details of their implementation in the LOWTRAN program.

The number of phase functions in this set represents a compromise between accuracy and memory requirements. The nominal accuracy of 20 percent is compatible with the other uncertainties in using the aerosol models (such as determining the concentration of the aerosols). If greater accuracy is desired in specifying the phase function, the phase functions for all aerosol models, for a number of wavelengths, is available as a supplemental data file from Phillips Laboratory / Geophysics Directorate's Simulation Branch of the Optical Environment Division. The phase functions are tabulated and discussed fully in a separate report by Shettle et al.<sup>277</sup>

### 5.3.3.3 Henyey-Greenstein Phase Function

In addition to the standard MODTRAN phase functions corresponding to the different aerosol models built into MODTRAN, the user has the option of specifying a Henyey-Greenstein scattering function be used. The Henyey-Greenstein <sup>278</sup> function is given by:

$$P_{HG}(\gamma) = \frac{1}{4\pi} \frac{(1-g^2)}{(1-2g \cos \gamma + g^2)^{3/2}} \quad , \quad (117)$$

where  $\gamma$  is the scattering angle and  $g$  is the asymmetry parameter,

$$g = \frac{\int \int_{4\pi} \cos \gamma P(\gamma) d\Omega}{4\pi} \quad , \quad (118)$$

with  $P(\gamma)$  normalized as in EQ. (116) The asymmetry parameter gives a measure of the asymmetry of the angular scattering. It has a value of +1 for complete forward scattering, 0 for isotropic or symmetric scattering, and -1 for complete backscattering.

### 5.3.3.4 User-Defined Phase Functions

The MODTRAN code allows the user to input their own phase functions for the different altitude regions. These scattering functions can be defined at up to 50 different angles, as specified by the user. The same angles must be used for all four altitude regions.

When inputting their own phase functions the user should make sure they are normalized as in EQ. (116). The literature is not standard on this convention, and other conventions are used, the most common alternate form has the integral (Eq. 116) equal to  $4\pi$ .

### 5.3.3.5 Molecular Scattering Phase Function

The angular distribution of light scattered by the air molecules is described by the Rayleigh scattering phase function

$$P(\gamma) = \frac{3}{16\pi} \cdot \frac{2}{2 + \delta} \left[ (1 + \delta) + (1 - \delta) \cos^2 \gamma \right], \quad (119)$$

where  $\delta$  is the depolarization factor that gives the correction for the depolarization effect of scattering from anisotropic molecules. When  $\delta$  goes to zero, that is, no depolarization, or symmetric molecules, EQ. (119) reduces to

$$P(\gamma) = \frac{3}{16\pi} [1 + \cos^2 \gamma], \quad (120)$$

which is a commonly used approximation for the Rayleigh phase function.

A value of  $\delta = 0.0295$  (Kasten)<sup>279</sup> is used in EQ. (119). Young<sup>280</sup> has given a value of  $\delta = 0.0279$  for dry air based on more recent measurements. With all constants evaluated, EQ. (119) becomes

$$P(\gamma) = 0.06055 + 0.05708 \cos^2 \gamma. \quad (121)$$

Figures 58 and 59 show some representative calculations from LOWTRAN using the single scattering option. In these figures, the solid line represents the radiance emitted by the atmosphere, the dashed line the path scattered radiance and the dotted line the ground reflected radiance (if any). The atmospheric profile in all cases is the 1976 U.S. Standard Atmosphere, and the rural aerosol model with 10-km meteorological range (VIS = 10km). The surface albedo is 0.05, independent of wavenumber corresponding to an emissivity of 0.95. The solar zenith angle is  $45^\circ$ ; results are shown for relative path azimuth angles of both  $0^\circ$  and  $180^\circ$ . (see Appendix C of reference 3 for a discussion of the scattering geometry).

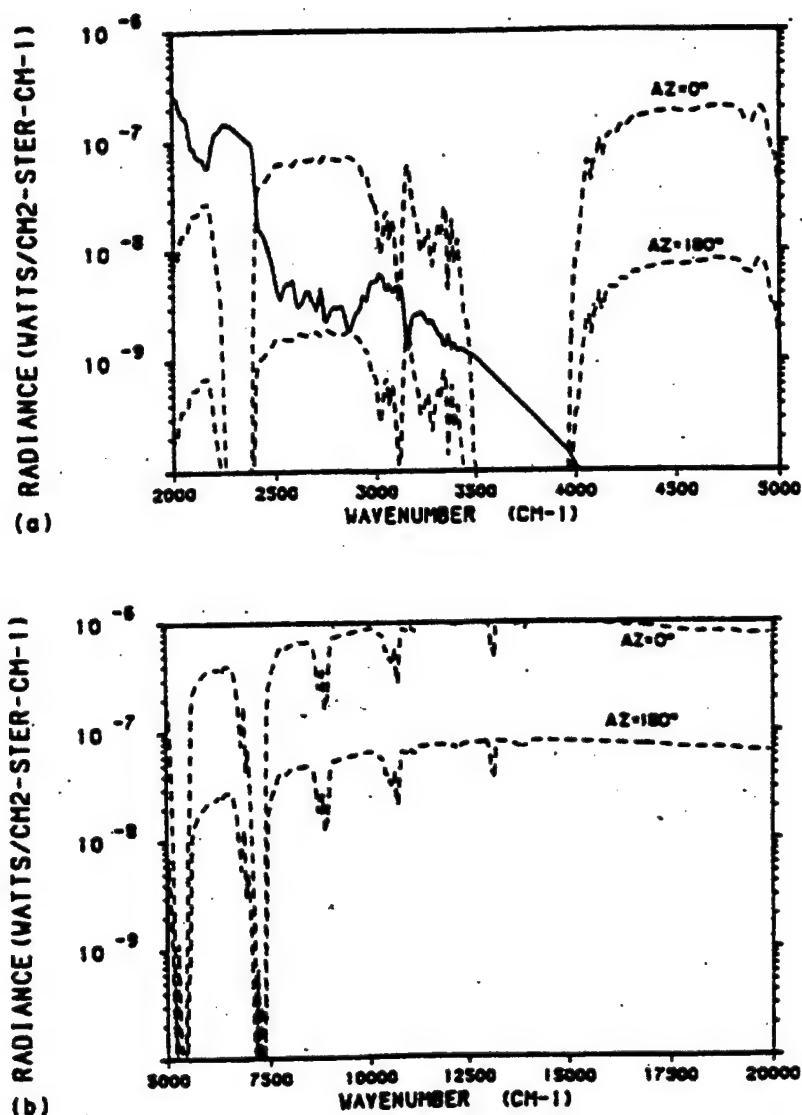


Figure 58. Calculated Radiances for the Following Conditions: Observer at the Ground Looking to Space with a Zenith Angle of  $30^\circ$ , Solar Zenith Angle of  $45^\circ$ , Relative Azimuths of  $0^\circ$  and  $180^\circ$ , U.S. Standard Atmosphere 1976, Rural Aerosol Model, VIS = 10km. Solid Line is Atmospheric Emission, Dashed Lines are Path Scattered Radiances. (a)  $2000 \text{ cm}^{-1}$  to  $5000 \text{ cm}^{-1}$ , (b)  $5000 \text{ cm}^{-1}$  to  $20000 \text{ cm}^{-1}$ .

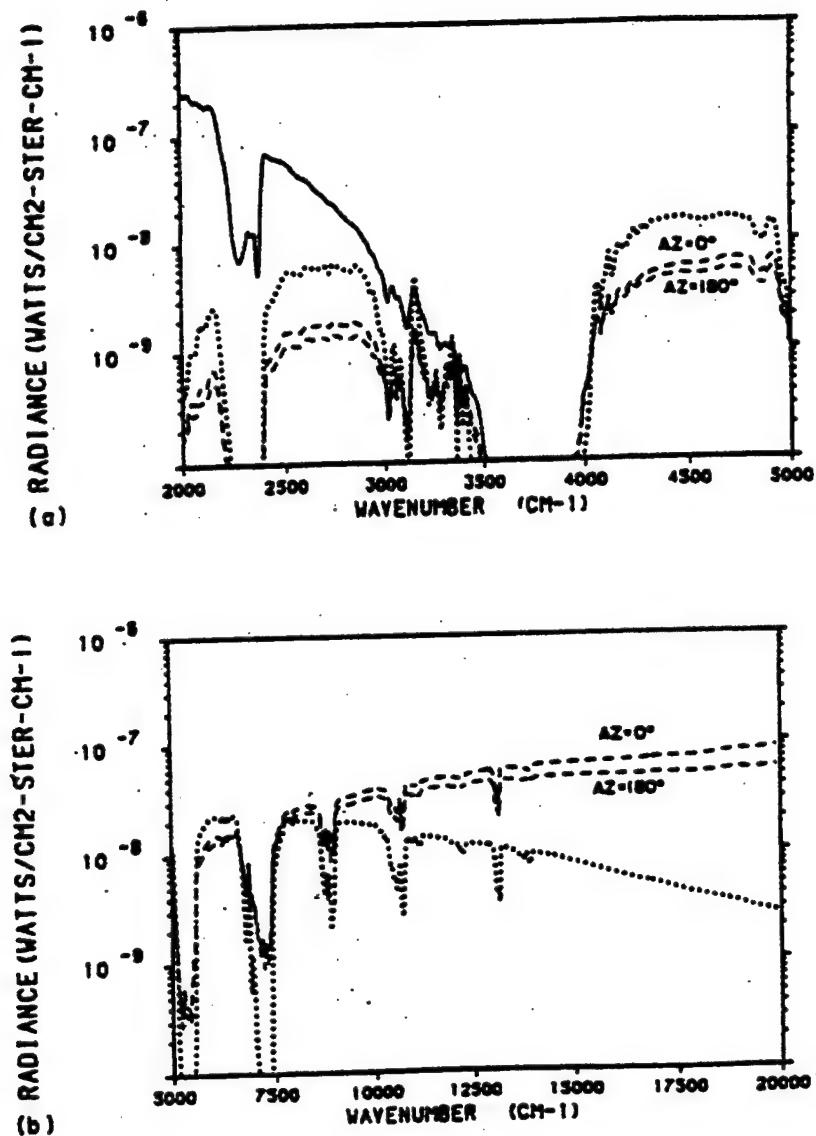


Figure 59. Calculated Radiances for the Following Conditions: Observer at 100km Looking at the Ground With a Zenith Angle at 100 km of  $150^\circ$ , Solar Zenith Angle is  $45^\circ$ , Relative Azimuths of  $0^\circ$  and  $180^\circ$ , Ground Albedo of 0.5, U.S. Standard Atmosphere 1976, Rural Aerosol Model VIS = 10 km. Solid Line is Atmospheric Emission, Dashed Lines are Path Scattered Radiances, Dotted Line is Ground Reflected Radiance. (a)  $2000 \text{ cm}^{-1}$  to  $5000 \text{ cm}^{-1}$  and (b)  $5000 \text{ cm}^{-1}$  to  $20000 \text{ cm}^{-1}$ .

In Figure 58, the observer is on the ground looking out to space with a zenith angle of  $30^\circ$ . The upper dashed line corresponds to a relative azimuth of  $0^\circ$  with a scattering angle of  $15^\circ$ , while the lower dashed line is  $180^\circ$  relative azimuth with a scattering angle of  $75^\circ$ . The figure shows that for the relative azimuth of  $0^\circ$ , the scattered radiance



dominates everywhere above  $2400\text{ cm}^{-1}$ , except around the strong  $\text{CO}_2$  absorption band centered at  $3700\text{ cm}^{-1}$ . For the relative azimuth of  $180^\circ$ , the scattered radiance is more than an order of magnitude less. This difference is due entirely to the difference in the scattering angles; the line-of-sight path and the scattering point-to-sun paths are otherwise identical. The reason for this difference is as follows: the bulk of the scattering occurs in the boundary layer where the rural aerosol model applies. The phase function for the rural aerosol model has a strong forward peak for these wavelengths. The large difference in the phase function between a scattering angle of  $15^\circ$  and  $75^\circ$  accounts for the large difference in the scattered radiance.

In Figure 59, the observer is at 100km looking down at the earth with a zenith angle of  $150^\circ$  (This is the reverse of the path in Figure 58). Again the upper dashed line corresponds to the relative azimuth of  $0^\circ$  with a  $105^\circ$  scattering angle and the lower one corresponds to  $180^\circ$  relative azimuth with a scattering angle of  $165^\circ$ . In this case the ground reflected solar radiance is greater than the path scattered radiance below  $5000\text{ cm}^{-1}$  and greater than the atmospheric emission above  $4000\text{ cm}^{-1}$ . The path scattered radiances for the two relative azimuths are now quite similar since the difference in the phase function between  $105^\circ$  and  $165^\circ$  is small. In the visible ( $\sim 17500\text{ cm}^{-1}$ ) the ground reflected radiance is more than an order of magnitude less than the path scattered radiance so that the ground is effectively obscured by the haze above it. Note, however, that the assumed albedo of 0.05 is low for the visible region of the spectrum.

### 5.3.4 Recommendations of Usage

The inclusion of single scattered solar radiance in LOWTRAN 6 is a significant improvement over previous versions that calculated the atmospheric emission only. The single scattering approximation is valid over a broad range of conditions found in the atmosphere. However, there are also conditions of interest in the atmosphere where multiple scattering and/or internal sources must be included to accurately calculate the atmospheric radiance. There is no simple indicator that predicts the conditions for which the single solar scattering approximation is acceptable: rather the range of applicability depends upon a large set of parameters including the atmospheric profile, the optical path, the solar geometry, the aerosol phase function, and the wavenumber region. The user will find some guidance in Section 4 of Ridgway et al. <sup>268</sup>. The following general comments, in part drawn from this source, may be useful. However, the user must be aware that they may not apply in all cases and are indicative only. Also, these

comments apply only to the validity of the single scattering approximation and not the uncertainties in the atmospheric data.

- 1... The single scattering approximation always underestimates the scattered radiance compared to multiple scattering.
- 2 The single scattering approximation becomes less valid with increasing scattering optical depth and with increasing single scattering albedo. For a scattering optical depth of less than about 0.7, the ratio of multiply scattered to singly scattered radiances should be less than 1.5. For scattering optical depths greater than about 2, the ratio may be much larger.
- 3 For an observer in space looking down at the ground in a window region where the total optical depth is less than 2, the ration of multiply scattered to singly scattered radiance is in most cases less than 2.0 and in many cases less than 1.5/ And contrary to intuition, the ratio decreases as the solar zenith angle increases and/or the path zenith angle decreases (note: a path zenith angle of 180° is straight down.
- 4...For an observer at the ground, the ratio of multiple to single scattered radiance increases with both the path and the solar zenith angle, and in general, single scattering is a poor approximation (error greater than a factor of 2) for cases where both the zenith angles are greater than 70.
- 5...Multiple scattering effects are dominant in clouds and thick fog.
- 6...Single scattering is a good approximation for early twilight cases, that is, where the sun is just below the horizon. For late twilight cases, multiple scattering becomes significant.
- 7...Single scattering is a good approximation when looking near the sun, since the scattering is dominated by the large forward peak.
- 8 In general, the aerosol scattering optical depth increases with wavenumber so that scattering in the infrared is less than that in the visible.

From a purely mechanical point-of-view, the single scattering option should not be used along with either the cirrus cloud model, or the rain model since the program does not

compute the scattered radiance from these aerosols. For an optical path looking directly at the sun, the single scattering model includes only the scattered radiance, and not the transmitted solar radiance.

### 5.3.5 Directly-Transmitted Solar Irradiance

An additional option has been provided to allow the user to compute the directly transmitted solar irradiance (flux), that is, the irradiance measured by an observer looking directly at the sun. This irradiance is given by:

$$\bar{I} = \bar{I}_\nu^{SUN} \tau_e^{A+M} \quad (122)$$

Note that all scattered light is lost and that no scattering into the path is included.

Instructions for using this option are in Section 3.2.3.1 of Ref. 2.

An example of the directly transmitted solar irradiance is given in Figure 60. The dashed line is the solar irradiance at the top of the atmosphere. The solid line is the transmitted irradiance for a vertical path from the ground, for the U.S. Standard Atmosphere 1962 and no aerosol extinction.

As mentioned in Section 5.2, the model now includes a new solar spectrum for calculating scattered and directly transmitted solar irradiances. The recent values of VanHoosier et.al.<sup>31</sup> have been adopted in the UV (0.2 to 0.35  $\mu\text{m}$ ) with a LOWTRAN compatible resolution (20  $\text{cm}^{-1}$ ). This data was obtained from the Shuttle platform (the Solar Ultraviolet Spectral Irradiance Monitor (SUSIM) on Spacelab 2) at 0.15nm resolution and subsequently converted to frequency for smoothing. The data stored in MODTRAN actually begins at 0.174  $\mu\text{m}$  recognizing that plans exist to extend the code into the UV. In the near UV to visible range (0.35 to 0.86  $\mu\text{m}$ ), the data of Neckel and Labs<sup>33</sup> have been adopted. Because these data have a resolution of 1-2 nm, they under-represent the actual variability in the solar Fraunhofer structure at the stated 20  $\text{cm}^{-1}$  resolution. Estimated accuracy of the composite MODTRAN compilation is 5-10% for the SUSIM spectral range (including feature replication at 20  $\text{cm}^{-1}$  resolution) and 5% for the near UV and visible range when degraded to 100  $\text{cm}^{-1}$  resolution.

NOTE: Because of general calibration difficulties in the UV, measured solar irradiances differ by as much as 10% in absolute magnitude<sup>258</sup>, while relative spectral detail is reproducible to much higher accuracy.

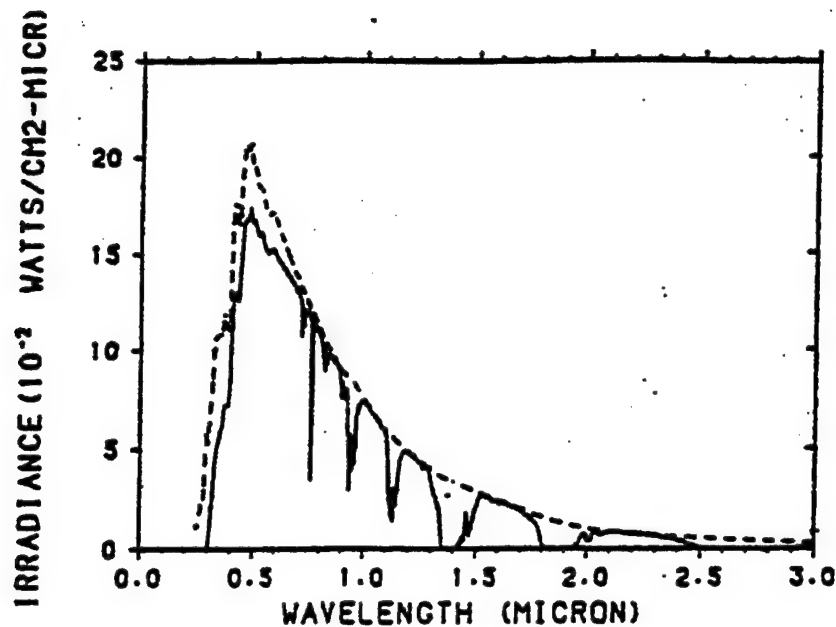


Figure 60. Solar Radiance (Dashed Line) and Directly Transmitted Solar Irradiance (Solid Line) for a Vertical Path, From the Ground, U. S. Standard Atmosphere 1976, No Aerosol Extinction.

## 5.4 NEW MULTIPLE SCATTERING ALGORITHM

### 5.4.1 Introduction

This description of the multiple scattering algorithm built into LOWTRAN 7 and MODTRAN 2 is a synopsis gleaned from the report by Isaacs et al.<sup>36</sup>

Optimal design and deployment of electro-optical (EO) remote sensing and communication systems requires accurate modeling and prediction of the effects of the ambient environment on atmospheric transmission. Atmospheric transmittance/radiance models such as AFGL's LOWTRAN (Kneizys et al.,<sup>2</sup>) and FASCODE (Anderson et al.,<sup>178</sup>) have been developed within this context to provide the capability to assess potential adverse environmental impacts on EO system performance.

In order to accurately predict atmospheric effects on the propagation of visible, infrared and microwave radiation, it is necessary to treat the extinction mechanisms including molecular scattering and absorption, and particle (aerosols, clouds and precipitation) scattering and absorption, characterizing the ambient atmosphere. In the present Phillips Laboratory's transmittance/radiance models, these processes are adequately included in the treatment of path transmission. However, simplified

treatments are employed to simulate the effects of scattering on the calculation of radiance. For thermal infrared and microwave radiation, for example, particle scattering in earlier versions of LOWTRAN had been treated as an enhancement to extinction but not as a source term. This approach leads to an underestimate of radiance for paths where multiple scattering is important (Ben-Shalom et al.,<sup>281</sup>). Earlier versions of LOWTRAN used the single scattering approximation for evaluating solar radiances (Ridgway et al.,<sup>268</sup>). While the single scattering implementation is straightforward, its application introduces errors which are functions of wavelength, sun/sensor geometry, and surface optical properties (see Isaacs and Özkaynak,<sup>282</sup> and Dave,<sup>283</sup>). These errors are primarily due to neglecting higher order scattering and surface reflection. In FASCODE, particle scattering has been treated as equivalent to absorption. All scattered radiation is thus re-emitted as if it were absorbed, i.e., the scattered radiation is conserved. This conservative scattering approach can lead to an overestimate of radiance.

In order to provide a more realistic simulation of radiation in spectral regions and along atmospheric paths where multiple scattering (MS) is a significant contribution to the source function, an efficient and accurate scattering parameterization has been incorporated into the MODTRAN and FASCODE models.

#### 5.4.2 Stream Approximation

Selection of an appropriate treatment of multiple scattering (MS) for application to the MODTRAN and FASCODE models is severely constrained by competing requirements of desired efficiency and accuracy, and limitations imposed by the inherent code structures of these models. Additionally, it was important to provide an approach which is uniformly applicable to all spectral regions considered and equally appropriate for implementation within both MODTRAN and FASCODE. Based on these considerations, the MS parameterization selected consisted of a finite stream approach (using two streams for simplicity) to approximate the scattering source function.

This approach could be implemented directly in FASCODE since it is essentially a monochromatic calculation. It is known, however, that there exist difficulties in calculating the transmittance/radiance averaged over a finite spectral interval in a non-gray gaseous absorber with multiple scattering because the commonly-used band models are not applicable (see Stephens,<sup>284</sup>). This was the driving factor for implementing an MS treatment within LOWTRAN. The best approach to solve this problem is the use of the k-distribution method, which decouples the multiple scattering from the gaseous spectral integration so that the available (monochromatic) multiple

scattering algorithms can be used directly. For LOWTRAN, the stream approximation is performed through an interface routine consisting of the k-distribution method. For practical purposes, this consists of decomposing the band model determined optical properties into a set of equivalent monochromatic calculations which are then summed to give the spectrally averaged results.

As mentioned earlier, the multiple scattering parameterization had to be accommodated by the existing MODTRAN/LOWTRAN and FASCODE code structures. This constraint is particularly important for FASCODE. In the FASCODE application, gaseous absorption is evaluated directly from the line-by-line calculation. Fluxes required for the stream approximation are calculated via the parameterized adding method. The adding method is particularly consistent with the code structure of both radiance/transmittance models since they treat one layer at a time.

In the FASCODE model, for example, the evaluation of layer optical properties always commences with that level in the selected path with the highest pressure and the selected spectral sampling interval decreases with pressure. This approach insures that the layer spectral resolution is consistent with the decrease of Voight line widths at higher altitudes. From the perspective of the line-by-line calculation, this method is computationally quite efficient. However, it is inconsistent with monochromatic multiple scattering treatments. In order to accommodate the sampling requirements of both the line-by-line and multiple scattering calculations, the FASCODE implementation employs the adding formalism to aid in the merging of the scattered fluxes from successive layers.

A generic outline of the basic theory is provided here. This prescription is modified slightly for specific application to the MODTRAN/LOWTRAN and FASCODE models.

#### 5.4.2.1 Radiance and Source Function

The desired radiance  $I_\nu$  at wavenumber  $\nu$  for an arbitrary path with zenith angle cosine and azimuth angle  $(\mu, \phi)$  is given by the solution to the radiative transfer equation (RTE):

$$\mu \frac{d}{d\tau} I_\nu(\tau, \mu, \phi) = I_\nu(\tau, \mu, \phi) - J_\nu(\tau, \mu, \phi) \quad (123)$$

Here  $\tau_\nu$  is the optical thickness,  $\mu$  is then cosine of the path zenith angle, and  $\phi$  is the azimuth angle relative to the sun's azimuth. Vertical optical depth,  $\tau_\nu$ , will depend on the relevant mechanisms determining the extinction of electromagnetic radiation for the

spectral region characterized by wavenumber  $\nu$ . In general these mechanisms include: (a) molecular absorption,  $k_a$ , (b) molecular scattering,  $k_s$ , (c) particulate absorption,  $\sigma_a$  and (d) particulate scattering,  $\sigma_s$ . Optical depth is given by integrating the relevant vertical extinction coefficient profiles according to:

$$\tau_\nu(z) = \int_z^\infty [k_a(z) + k_s(z) + \sigma_a(z) + \sigma_s(z)] dz \quad (124)$$

The general source function,  $J_\nu$ , including scattering of solar radiation and thermal emission, is given by:

$$J(\tau, \mu, \phi) = J_O(\tau, \mu, \phi) + J_{MS}(\tau, \mu, \phi) \quad (125)$$

where

$$J_O(\tau, \mu, \phi) = \frac{\omega_o(\tau)}{4\pi} \pi F e^{-\tau/\mu_o} P(\Omega; -\Omega_o) + [1 - \omega_o(\tau)] B[\Theta(\tau)] \quad (126)$$

and

$$J_{MS}(\tau, \mu, \phi) = \frac{\omega_o(\tau)}{4\pi} \int_\Omega P(\Omega; \Omega') I(\tau, \Omega') d\Omega' \quad (127)$$

Here,  $\omega_o$  is the single scattering albedo,  $P$  is the appropriate angular scattering or phase function, and  $B$  is the Planck function at temperature  $\Theta$ . The extraterrestrial solar irradiance is given by  $F$  and the path and solar directions are given by  $\Omega$  and  $\Omega_o$ , respectively. The first term in Equation 126 is the single scattering of solar radiation while the second is the local thermal emission.

Radiance solutions to the RTE (Eq. 123) are subject to boundary conditions at the top of the atmosphere ( $\tau = 0.0$ ) for downward radiance and at the earth's surface ( $\tau = \tau^*$ ) for upward radiance. At  $\tau = 0.0$ , downward diffuse radiance from space is zero (the direct solar irradiance is accounted for via the primary source function) resulting in:

$$I_b(0, -\mu, \phi) = 0.0 \quad (128)$$

(At millimeter wave frequencies a contribution due to emission at the cosmic background effective temperature of 2.7K may be included when high accuracy is required.)

Boundary conditions at the surface will depend on the nature of the surface reflectance/emittance properties. The most common assumption is that of Lambert reflectance, i.e. the upward isotropic flux given by a constant surface albedo,  $r$ , times the downward flux. Upward and downward fluxes  $F^\pm(\tau)$  at optical depth  $\tau$ , are defined respectively as:

$$F^\pm(\tau) = \int_0^{2\pi} \int_0^1 I(\tau, \pm\mu, \phi) \mu d\mu d\phi \quad (129)$$

This results in a lower boundary condition upward radiance of:

$$I_b(\tau^*, \mu, \phi) = \frac{r}{\pi} \left[ \pi F\mu_0 \exp(-\tau^*/\mu_0) + \int_0^{2\pi} \int_0^1 I(\tau^*, -\mu, \phi) \mu d\mu d\phi \right] + (1-r)B[T_s] \quad (130)$$

The three terms on the R.H.S. of Eq. 130 are respectively: (a) reflectance of attenuated solar irradiance (in UV, near IR spectral regions). (b) reflectance of downward scattered radiance field, and (c) thermal emission due to the surface at temperature,  $T_s$ . The surface emissivity is unity minus the surface albedo, i.e.,  $(1-r)$ .

MODTRAN requires that the surface albedo be specified, while FASCODE asks for the surface emissivity.

General radiance solutions to the RTE for upward and downward radiances, respectively, are:

$$I(\tau, +\mu, \phi) = I_b(\tau^*, \mu, \phi) e^{-(\tau^*-\tau)/\mu} + \int_{\tau}^{\tau^*} J(t, \mu, \phi) e^{-(t-\tau)/\mu} \frac{dt}{\mu} \quad (131)$$

$$I(\tau, -\mu, \phi) = I_b(0, -\mu, \phi) e^{-\tau/\mu} + \int_0^{\tau} J(t, \mu, \phi) e^{-(\tau-t)/\mu} \frac{dt}{\mu} \quad (132)$$



where the  $I_b$  are given by the boundary conditions Eq.'s 130 and 128 above, respectively. Incorporating these boundary conditions, the radiance solutions become:

$$I(\tau, \mu, \phi) = \left\{ \frac{r}{\pi} \left[ \pi \mu_o F e^{-\tau^*/\mu_o} + \int_0^1 \int_0^{2\pi} I(\tau^*, -\mu, \phi) \mu d\mu d\phi \right] \right. \\ \left. + (1-r) B[T(\tau^*)] \right\} \exp(-(\tau^* - \tau)/\mu) + \int_{\tau}^{\tau^*} J(t, \mu, \phi) e^{-(t-\tau)/\mu} \frac{dt}{\mu} \quad (133)$$

$$I(\tau, -\mu, \phi) = \int_0^{\tau} J(t, \mu, \phi) e^{-(\tau-t)/\mu} \frac{dt}{\mu} \quad (134)$$

In the stream approximation, the multiple scattering contribution to the source function (Eq. 127 above) is approximated by assuming constant scattered radiances  $I^+$  and  $I^-$  over upward ( $\Omega^+$ ) and downward ( $\Omega^-$ ) hemispheres, respectively, or from Eq. (127):

$$J_{MS}(\tau, \mu, \phi) \approx \frac{\omega_o(\tau)}{4\pi} \left[ I^+(\tau) \int_{\Omega^+} P(\Omega, \Omega^+) d\Omega^+ \right. \\ \left. + I^-(\tau) \int_{\Omega^-} P(\Omega, \Omega^-) d\Omega^- \right] \quad (135)$$

Integrating over the angular scattering functions for the resulting azimuthally averaged backscatter fractions,  $B(\mu)$ , as a function of zenith angle cosine and substituting the corresponding fluxes:

$$I^{\pm}(\tau) = F^{\pm}(\tau)/\pi \quad (136)$$

results in

$$J_{MS}(\tau, \pm\mu, \phi) \approx \frac{\omega_o(\tau)}{\pi} \{ F^{\pm}(\tau) [1 - \beta(\mu)] + F^m(\tau) \beta(\mu) \} \quad (137)$$

This simple expression for the multiple scattered contribution to the source function is added to the single scattering and thermal emission contributions for the general source function,  $J$  (Eq. (125) ). The source function is then integrated along with the desired path (as in Eqs. (133) or (134) ) to obtain the desired total radiance including the approximated MS contribution.

The evaluation of the approximated MS source function (Eq. 137) requires local fluxes  $F^+$  and  $F^-$ , backscatter fractions  $\beta(u)$ , and single scattering albedos,  $\omega_o$ . The backscatter fractions are given as functions of zenith angle cosine and asymmetry factor by Wiscombe and Grams <sup>285</sup> (see Figure 61). A small error is introduced by assuming these backscatter fractions for the equivalent Henyey-Greenstein phase function rather than integrating the actual function. The single scattering albedo,  $\omega_o(\tau)$ , for a given layer with total optical thickness  $\Delta\tau$  is:

$$\omega_o(\tau) = \Delta\tau_s / \Delta\tau \quad (138)$$

where  $\Delta\tau_s$  is the total scattering optical thickness of the layer. Discretizing equation (137) for a given layer,  $N$ , the contribution of multiple scattering is approximated as:

$$J_{SA}^N(\pm\mu) = J_o + \frac{\omega_o^N}{\pi} \left\{ F_N^\pm [1 - \beta^N(\mu, g^N)] + F_N^m \beta^N(\mu, g^N) \right\} \quad (139)$$

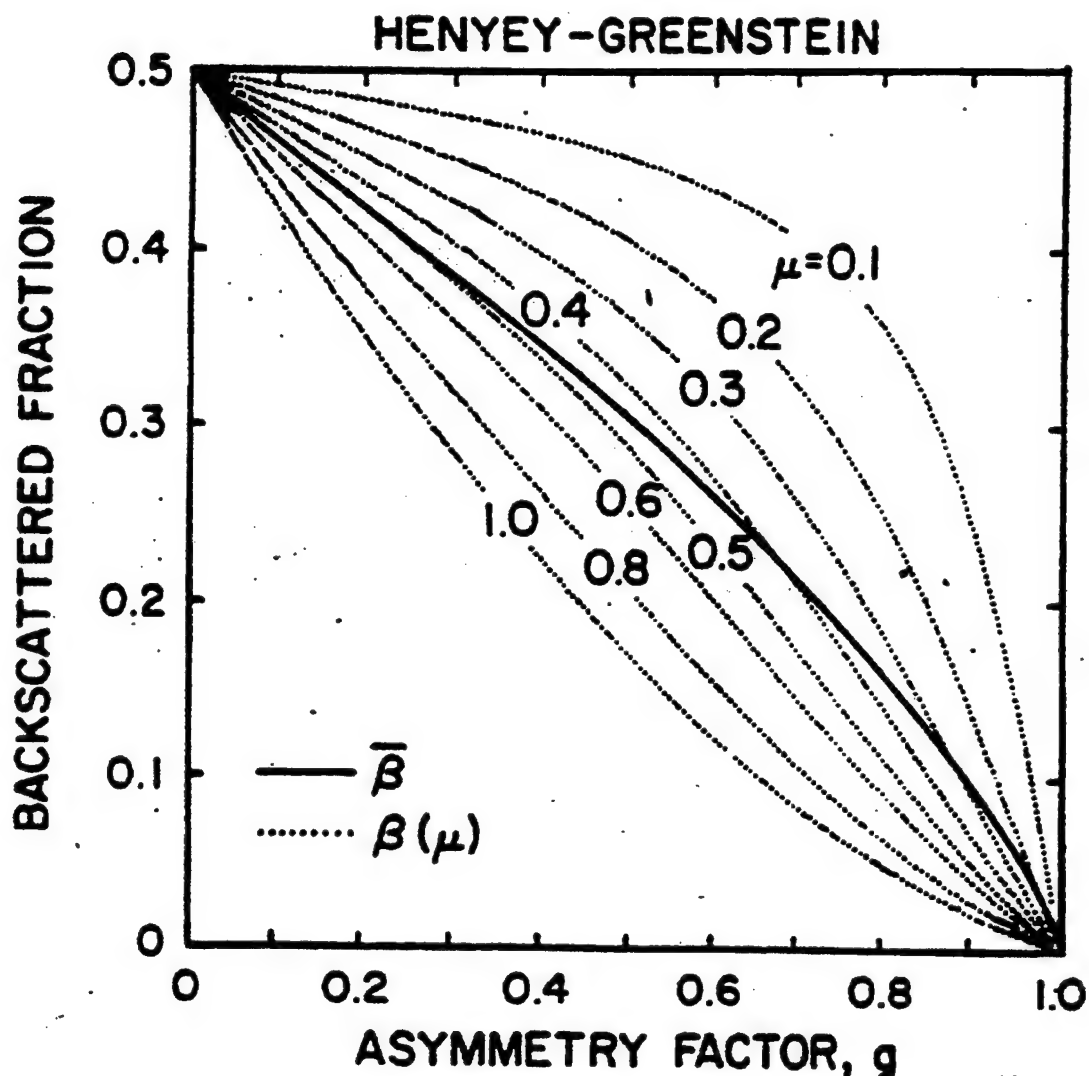


Figure 61. Backscattered Fractions  $\bar{\beta}$  and  $\beta(\mu)$  for the Henyey-Greenstein Phase Function Versus the Asymmetry Factor  $g$  for a Range of Values of  $\mu$  (Wiscombe and Grams,<sup>285</sup>)

Here the fluxes are taken as the layer mean quantities evaluated at a level halfway through the layer. The asymmetry factor,  $g$ , is a measure of the directional scattering and can be evaluated from the phase function.

Once the source function is approximated, the path radiance can be evaluated. Along a path consisting of layers ( $N$ ) and the layer above ( $N+1$ ) with transmissions  $T_N$  and  $T_{N+1}$ , respectively, for example, the emission,  $E$ , depends on the path integral of the total source function:

$$E_{N+1}^+ = E_N^+ T_{N+1} + J_{SA}^{N+1} (+\mu)(1 - T_{N+1}) \quad (140)$$

for downward looking and:

$$E_{N+1}^- = E_N^- + (1 - T_{N+1}) J_{SA}^{N+1} (-\mu) T_N \quad (141)$$

for upward looking, where the intrinsic layer emission is:

$$E_N^\pm = (1 - T_N) J_{SA}^N (\pm\mu) \quad (142)$$

#### 5.4.2.2 Layer Fluxes

Fluxes approximate the required radiances for evaluation of the multiply scattered source function. Upward and downward fluxes ( $F^+$  and  $F^-$  respectively) for individual isolated layers are evaluated using an appropriate flux parameterization. For example, for solar scattering, the hybrid modified delta Eddington approximation (Meador and Weaver, 286) is used. The chosen flux parameterization also provides intrinsic layer reflection and transmission functions,  $R$  and  $T$ . These fluxes are calculated using standard two stream parameterization approaches. To accommodate the flux parameterizations, optical properties for the whole atmosphere (i.e., surface to space) are required. This approach for calculating fluxes thus consists of two steps: (1) evaluating local layer (i.e., intrinsic) fluxes for each atmospheric layer, and (2) combining these to obtain the actual flux profiles using the adding method.

Upward and downward layer fluxes for solar radiation are given by:

$$F^+ = Ae^{k\tau} + Be^{-k\tau} + Ce^{-\tau/\mu_0} \quad (143)$$

$$F^- = \frac{1}{\gamma_2} \{ A(\gamma_1 - k)e^{k\tau} + B(\gamma_1 + k)e^{-k\tau} + Ye^{-\tau/\mu_0} \} \quad (144)$$

Where the appropriate constants are given by :

$$\begin{aligned} k &= \sqrt{(\gamma_1^2 - \gamma_2^2)} \\ A &= [B(\gamma_1 + k) + Y]/(k - \gamma_1) \\ B &= (E_1 e^{k\tau^*} + E_2 e^{-\tau^*/\mu_0}) / (E_3 e^{k\tau^*} + E_4 e^{-k\tau^*}) \end{aligned} \quad (145)$$

$$C = \pi\omega_o \left\{ \frac{\beta(\mu_o)}{\mu_o} - \gamma_1\beta(\mu_o) - \gamma_2[1-\beta(\mu_o)] \right\} \left( \frac{\mu_o^2}{1-k^2\mu_o^2} \right)$$

$$Y = C \left( \gamma_1 + \frac{1}{\mu_o} \right) - \pi F \omega_o \beta(\mu_o)$$

and additionally:

$$E_1 = Y[1/(\gamma_1 - k) - r/\gamma_2]$$

$$E_2 = \left[ -C + \pi F \mu_o r + \frac{rY}{\gamma_2} \right]$$

$$E_3 = (\gamma_1 + k)[1/(k - \gamma_1) + r/\gamma_2]$$

$$E_4 = [1 - r(\gamma_1 + k)/\gamma_2] \quad (146)$$

$$\gamma_1 = \frac{-\{1 - g^2 - \omega_o(4 - 3g) - \omega_o g^2(4\beta_o + 3g - 4)\}}{4[1 - g^2(1 - \mu_o)]}$$

$$\gamma_2 = \frac{\{7 - 3g^2 - \omega_o(4 + 3g) + \omega_o g^2(4\beta_o + 3g)\}}{4[1 - g^2(1 - \mu_o)]}$$

Here,  $r$  is the Lambert surface albedo and the solar zenith angle cosine is  $\mu_o$

The transmission and reflection functions used later in the flux adding are given by:

$$R = F^+ / \mu_o \pi F$$

$$T = F^- / \mu_o \pi F + \exp^{(-\tau/\mu)} \quad (147)$$

For the thermal fluxes, a linear Planck function relation across an atmospheric layer is used. In so doing, the parameterized two-stream solutions for emission from the layer top and layer bottom, and for total transmission and reflection are:

$$\begin{aligned}
 F^+ &= a(PB_t - mQ - B_b)/D \\
 F^- &= a(PB_b + mQ - B_t)/D \\
 T &= a/D \\
 R &= uv(e^{\tau_1} - e^{-\tau_1})/D
 \end{aligned} \tag{148}$$

where  $B_t$  and  $B_b$  are the Planck intensity at the layer top and bottom and:

$$\begin{aligned}
 a^2 &= 1 - \omega_o \\
 m &= (B_b - B_t)/\tau \\
 P &= ve^{\tau_1} + ue^{-\tau_1} \\
 Q &= ve^{\tau_1} - ue^{-\tau_1} - a \\
 D &= v^2 e^{\tau_1} - u^2 e^{-\tau_1} \\
 u &= (1 - a)/2 \\
 v &= (1 + a)/2 \\
 \tau_1 &= \sqrt{3} a\tau
 \end{aligned} \tag{149}$$

The optical thickness  $\tau$  and the single scattering albedo  $\omega_o$  are given by:

$$\begin{aligned}
 \tau &= ku + \tau_s(1 - g) + \tau_a \\
 \omega_o &= \tau_s(1 - g)/\tau
 \end{aligned} \tag{150}$$

Here  $k$  is the gas absorption coefficient (for a particular wavelength and probability interval),  $u$  is the gas amount,  $\tau_s$  is the scattering optical thickness,  $\tau_a$  is the absorption optical thickness and  $g$  is the asymmetry factor for the particulate matter in the layer.

### 5.4.2.3 Flux Adding Method

To obtain the actual flux profile throughout the atmosphere, intrinsic layer fluxes are combined algebraically using the adding method. In this method, fluxes, reflections, and transmissions are used to add individual layers together. Composite upward fluxes,  $F_N^+$ , and reflection functions  $R_N^+$ , obtained upon adding two isolated layers, N and (N-1) are given by:

$$F_N^+ = F_N^+ + T_N(1_{F_{N-1}^+} + F_N^- R_{N-1}^+)(1 - R_N^+ R_{N-1}^+)^{-1} \quad (151)$$

$$R_N^+ = R_N^+ + R_{N-1}^+ T_N^2 (1 - R_N^+ R_{N-1}^+)^{-1} \quad (152)$$

Analogous equations provide composite downward fluxes and reflection functions,  $F_N^-$  and  $R_N^-$ , respectively. The composite upward and downward fluxes provide the actual upward and downward fluxes at layer interfaces including the effects of all layers above and below. For example, the upward and downward fluxes at the boundary between layers N and (N+1) are given by:

$$2_{F_N^+} = (1_{F_N^+} + 1_{F_{N+1}^-} R_N^+)(1 - R_N^+ R_{N+1}^-)^{-1} \quad (153)$$

$$2_{F_{N+1}^-} = (1_{F_{N+1}^-} + 1_{F_N^+} R_{N+1}^-)(1 - R_N^+ R_{N+1}^-)^{-1} \quad (154)$$

Once obtained, these fluxes are substituted into Eq. (139) above to provide the approximation of the MS source function.

### 5.4.2.4 Band Model Considerations

For LOWTRAN, it is necessary to integrate the spectral radiance values over a finite spectral interval ( $\sim 20 \text{ cm}^{-1}$ ). The basic problem encountered in the calculation of radiative transfer in low spectral resolution in a hazy or cloudy atmosphere is the coupling between the processes of scattering and absorption and absorption due to cloud/aerosol particles and absorption by atmospheric gases. The main difficulty is that the integration over frequency cannot be properly accounted for by the usual band model technique for gaseous absorption because they do not allow for multiple-scattering. A direct line-by-line integration over frequency would be very time consuming. One alternative way of carrying out the frequency integration is to use the "k-distribution method" for homogeneous layers (Arking and Grossman, 287) and the

"correlated k-distribution approximation" for inhomogeneous atmospheres (cf. Wang and Ryan, 288).

For gaseous absorption, the k-distribution method is comparable to line-by-line calculations (Arking and Grossman, 287). This method is equivalent to the exponential-sum fitting method (see Wiscombe and Evans, 289) and to the path length distribution method (see Bakan et al., 290). However, in general, the latter two methods use scaling approximations to account for atmospheric inhomogeneity while the correlated-k approximation assumes certain relationships between k values at different pressure and temperature levels. The accuracy of the approximation is excellent for the 9.6  $\mu\text{m}$   $\text{O}_3$  band thermal radiation calculations (see Lacis et al., 291).

Yamamoto et al. (292,293) used finite sums of exponentials to describe the non-grey nature of water vapor absorption and carried out solutions of the equation of transfer for homogeneous band layers using both Chandrasekhar's principles of invariance as well as the discrete ordinate technique. Both techniques require extensive numerical calculations. On the other hand, two stream approximations together with the correlated-k approximation have been used to study the radiative effects of aerosols (see Hansen et al., 294).

As summarized recently by Stephens on efficient and accurate radiation parameterizations ( pg. 862 of the paper<sup>284</sup>): "...Only the k-distribution approach can be readily incorporated into scattering models..."

In a homogenous gas layer, the k-distribution function is formally related to the mean transmission function  $T_{\Delta\nu}(u)$ ,

$$\begin{aligned}
 T_{\Delta\nu}(u) &\equiv \frac{1}{\Delta\nu} \int_{\Delta\nu} e^{-ku} d\nu \equiv \int_0^\infty f(k) e^{-ku} dk \\
 &\equiv \int_0^1 e^{-ku} dg = \sum_{i=1}^n e^{-k_i u} \Delta g_i
 \end{aligned} \tag{155}$$

where  $\Delta\nu$  is the narrow repeated interval (20  $\text{cm}^{-1}$  in LOWTRAN) and  $u$  is the gas amount. The  $f(k)$  for a given gas at a specified  $\Delta\nu$  is the probability density function such that  $f(k)dk$  is the fraction of the frequency interval for which the absorption coefficient is between  $k$  and  $k+dk$ . Eq. (155) reveals that the transmission depends on the distribution of k-values within  $\Delta\nu$ , but not on the ordering of the values. The



cumulative k-distribution function is  $g(k)$ , while  $(k_i, \Delta g_i)$  are the discrete sets of values to approximate the integral.

By expressing the band model transmission as the sum of exponentials, the multiple scattering calculation for each component can be performed independently as if it were a monochromatic problem. These are weighted and summed (as in Eq. (155)) to recover the essential band model character of the problem.

The fit of Wiscombe and Evans<sup>289</sup> has been used for the two LOWTRAN transmission functions of water vapor/uniformly mixed gases, and ozone. The accuracy of the fitting is in general within a few percent for  $T > 0.1$ . For inhomogeneous atmospheres, we adopt the same scaling approximation used in LOWTRAN, i.e.,

$$k_i(P, \Theta) = k_i(P_o, \Theta_o) \frac{P}{P_o} \sqrt{\frac{\Theta_o}{\Theta}} \quad (156)$$

where  $\Theta_o$  and  $P_o$  are reference temperatures and pressures, respectively.

#### 5.4.3 Implementation in MODTRAN 2 and LOWTRAN 7

This section describes the technical details of incorporating the multiple scattering treatment into MODTRAN along with the required k-distribution method needed by LOWTRAN 7.

##### 5.4.3.1 Modified k-Distribution Method (LOWTRAN 7 Only)

Because of the complicated molecular absorption band structure of the gases, a rigorous frequency integration would require a line-by-line integration which clearly is very time consuming and therefore unacceptable for implementation in the LOWTRAN model. Instead, the application of the absorption coefficient ( $k$ ) distribution method (Wang and Ryan<sup>288</sup> and Stephens<sup>284</sup>) has been adopted for LOWTRAN 7. In a homogeneous gas layer, the k-distribution function is formally related to the mean transmission function  $T_{\Delta\nu}(u)$ , by:

$$\begin{aligned} T_{\Delta\nu}(u) &\equiv \frac{1}{\Delta\nu} \int_{\Delta\nu} e^{-ku} d\nu \equiv \int_0^\infty f(k) e^{-ku} dk \\ &\equiv \int_0^1 e^{-ku} dg = \sum_{i=1}^n e^{-k_i u} \Delta g_i \end{aligned} \quad (157)$$

where  $\Delta\nu$  is the narrow repeated interval ( $20 \text{ cm}^{-1}$  in LOWTRAN) and  $u$  is the gas amount. The  $f(k)$  for a given gas at a specified  $\Delta\nu$  is the probability density function of the frequency interval for which the absorption coefficient is between  $k$  and  $k + dk$ . Equation 151 reveals that the transmittance depends on the distribution of  $k$ -values within  $\Delta\nu$  but not on the ordering of the values. The cumulative  $k$ -distribution function is  $g(k)$ , while  $(k_i, \Delta g_i)$  are the discrete set of values to approximate the integral.

For the summation in Eq. 151 to be useful with LOWTRAN, values for  $k$  and  $\Delta g$  must be found to fit the LOWTRAN transmission data for water vapor, the uniformly mixed gases and ozone. The transmission for water vapor/uniformly mixed gases and ozone may be expressed as:

$$T_1 = T(H_2O^+) = \sum_{i=1}^M e^{-k_i u_1} \Delta g_i \quad (158)$$

$$T_2 = T(O_3) = \sum_{j=1}^N e^{-k_j u_2} \Delta g_j \quad (159)$$

The problem of fitting LOWTRAN transmission data (previous versions before LOWTRAN 7) as an exponential sum had been handled successfully by Wiscombe and Evans<sup>289</sup>, using 10  $k$  and  $\Delta g$  values for  $H_2O^+$  and six for  $O_3$ . Making use of the Wiscombe and Evans exponential sum fit of the LOWTRAN transmission data, Isaacs et al.<sup>36</sup> modified this method and reduced the necessary number of  $k$ 's to six.

It is important to remember that the  $k$ -distribution transmittances are only employed in the determination of the multiply scattered source function. The adding of radiances based on the source function depends on the original LOWTRAN transmittances. Thus, errors in the combined  $k$ -distribution/stream approximation approach for multiple scattering are not propagated beyond the approximate multiple scattering approach.

#### **Coordination of the new LOWTRAN 7 band model with the $k$ -distribution.**

The development of the new band model formulation utilized in LOWTRAN 7 (explained fully in section 4.1), necessitated further refinements in the proposed

k-distribution method. The Pierluissi<sup>13</sup> double exponential band model formulation is given by:

$$\tau_p(x, a) = e^{-(x)^a} \quad (160)$$

where  $x = CW$  and  $C$  is the band model absorption coefficient, while:

$$= \left( \frac{P}{P_o} \right)^n \left( \frac{T_o}{T} \right)^m U \quad (161)$$

$U = PL$  which equals the true layer amount, and  $W$  is the scaled absorber amount. The band model parameters  $a$ ,  $n$  and  $m$  are listed in Table 32 as a function of molecule and specific spectral band for that molecule.

For multiple scattering calculations of layer fluxes, Abreu and Kneizys modified the k-distribution method, replacing the Isaacs et al<sup>36</sup> six k method with a three term k-distribution, capable of accommodating the Pierluissi band model. This three term k-distribution is described as:

$$\tau_k(x, a) = G_1 e^{-k_1 x} + G_2 e^{-k_2 x} + G_3 e^{-k_3 x} \quad (162)$$

The constants  $G_1$ ,  $G_2$ ,  $G_3$  and  $k_1$ ,  $k_2$ ,  $k_3$  were determined from a non-linear least squares fit to  $\tau_p$  as a function of  $a$  and  $x$  with a constraint of the ratio's of the k's.

The G's are listed in Table 33 and the k's are listed in Table 34, as a function of molecule and specific spectral band. When more than one molecule absorbs at the same frequency, we neglect the cross terms in the k-distribution representation (in order to minimize computational time).

Table 32. Band Model Parameters for each Absorbing Molecule.

ABSORBER	SPECTRAL RANGE (cm <sup>-1</sup> )	a	n	m
Ammonia (NH <sub>3</sub> )	0 - 385	0.4704	0.8023	- 0.9111
	390 - 2150	0.6035	0.6968	0.3377
Carbon	425 - 835	0.6176	0.6705	- 2.2560
Dioxide (CO <sub>2</sub> )	840 - 1440	0.6810	0.7038	- 5.0768
	1805 - 2855	0.6033	0.7258	- 1.6740
	3070 - 3755	0.6146	0.6982	- 1.8107
	3760 - 4065	0.6513	0.8867	- 0.5427
	4530 - 5380	0.6050	0.7883	- 1.3244
	5905 - 7025	0.6160	0.6899	- 0.8152
	7395 - 7785	0.7070	0.6035	0.6026
	8030 - 8335	0.7070	0.6035	0.6026
	9340 - 9670	0.7070	0.6035	0.6026
Carbon	0 - 175	0.6397	0.7589	0.6911
Monoxide (CO)	1940 - 2285	0.6133	0.9267	0.1716
	4040 - 4370	0.6133	0.9267	0.1716
Methane (CH <sub>4</sub> )	1065 - 1775	0.5844	0.7139	- 0.4185
	2345 - 3230	0.5844	0.7139	- 0.4185
	4110 - 4690	0.5844	0.7139	- 0.4185
	5865 - 6135	0.5844	0.7139	- 0.4185
Nitric Oxide (NO)	1700 - 2005	0.6613	0.5265	- 0.4702
Nitrogen Dioxide (NO <sub>2</sub> )	580 - 925	0.7249	0.3956	- 0.0545
	1515 - 1695	0.7249	0.3956	- 0.0545
	2800 - 2970	0.7249	0.3956	- 0.0545
Nitrous Oxide (N <sub>2</sub> O)	0 - 120	0.8997	0.3783	0.9399
	490 - 775	0.7201	0.7203	- 0.1836
	865 - 995	0.7201	0.7203	- 0.1836
	1065 - 1385	0.7201	0.7203	- 0.1836
	1545 - 2040	0.7201	0.7203	- 0.1836
	2090 - 2655	0.7201	0.7203	- 0.1836
	2705 - 2865	0.6933	0.7764	1.1931
	3245 - 3925	0.6933	0.7764	1.1931
	4260 - 4470	0.6933	0.7764	1.1931
	4540 - 4785	0.6933	0.7764	1.1931
	4910 - 5165	0.6933	0.7764	1.1931

Table 32. (continued) Band Model Parameters for each Absorbing Molecule.

ABSORBER	SPECTRAL RANGE (cm <sup>-1</sup> )	Band Model Parameters		
		a	n	m
Oxygen	0 - 265	0.6011	1.1879	2.9738
(O <sub>2</sub> )	7650 - 8080	0.5641	0.9353	0.1936
	9235 - 9490	0.5641	0.9353	0.1936
	12850 - 13220	0.5641	0.9353	0.1936
	14300 - 14600	0.5641	0.9353	0.1936
	15695 - 15955	0.5641	0.9353	0.1936
	49600 - 52710	0.4704	0.9353	0.1936
Ozone	0 - 200	0.8559	0.4200	1.3909
(O <sub>3</sub> )	515 - 1275	0.7593	0.4221	0.7678
	1630 - 2295	0.7819	0.3739	0.1225
	2670 - 2845	0.9175	0.1770	0.9827
	2850 - 3260	0.7703	0.3921	0.1942
Sulfur	0 - 185	0.8907	0.2943	1.2316
Dioxide	400 - 650	0.8466	0.2135	0.0733
(SO <sub>2</sub> )	950 - 1460	0.8466	0.2135	0.0733
	2415 - 2580	0.8466	0.2135	0.0733
Water	0 - 345	0.5274	0.9810	0.3324
Vapor	350 - 1000	0.5299	1.1406	- 2.6343
(H <sub>2</sub> O)	1005 - 1640	0.5416	0.9834	- 2.5294
	1645 - 2530	0.5479	1.0443	- 2.4359
	2535 - 3420	0.5495	0.9681	- 1.9537
	3425 - 4310	0.5464	0.9555	- 1.5378
	4315 - 6150	0.5454	0.9362	- 1.6338
	6155 - 8000	0.5474	0.9233	- 0.9398
	8005 - 9615	0.5579	0.8658	- 0.1034
	9620 - 11540	0.5621	0.8874	- 0.2576
	11545 - 13070	0.5847	0.7982	0.0588
	13075 - 14860	0.6076	0.8088	0.2816
	14865 - 16045	0.6508	0.6642	0.2764
	16340 - 17860	0.6570	0.6656	0.5061

Table 33. k-Distribution Band Model Parameters for each Absorbing Molecule.

ABSORBER	SPECTRAL RANGE (cm <sup>-1</sup> )	Model a	G1	G2	G3
Ammonia (NH <sub>3</sub> )	0- 385	0.4704	0.2858	0.2698	0.4444
	390- 2150	0.6035	0.1342	0.3539	0.5119
Carbon	425- 835	0.6176	0.1203	0.3482	0.5315
Dioxide (CO <sub>2</sub> )	840- 1440	0.6810	0.0697	0.3035	0.6268
	1805- 2855	0.6033	0.1344	0.3540	0.5116
	3070- 3755	0.6146	0.1232	0.3496	0.5272
	3760- 4065	0.6513	0.0909	0.3272	0.5819
	4530- 5380	0.6050	0.1327	0.3534	0.5139
	5905- 7025	0.6160	0.1218	0.3489	0.5293
	7395- 7785	0.7070	0.0543	0.2807	0.6650
	8030- 8335	0.7070	0.0543	0.2807	0.6650
	9340- 9670	0.7070	0.0543	0.2807	0.6650
Carbon	0- 175	0.6397	0.1004	0.3353	0.5643
Monoxide (CO)	1940- 2285	0.6133	0.1245	0.3502	0.5253
	4040- 4370	0.6133	0.1245	0.3502	0.5253
Methane (CH <sub>4</sub> )	1065- 1775	0.5844	0.1544	0.3577	0.4879
	2345- 3230	0.5844	0.1544	0.3577	0.4879
	4110- 4690	0.5844	0.1544	0.3577	0.4879
	5865- 6135	0.5844	0.1544	0.3577	0.4879
Nitric Oxide (NO)	1700- 2005	0.6613	0.0833	0.3196	0.5971
Nitrogen Dioxide (NO <sub>2</sub> )	580- 925	0.7249	0.0453	0.2642	0.6905
	1515- 1695	0.7249	0.0453	0.2642	0.6905
	2800- 2970	0.7249	0.0453	0.2642	0.6905
Nitrous Oxide (N <sub>2</sub> O)	0- 120	0.8997	0.0017	0.0956	0.9027
	490- 775	0.7201	0.0476	0.2687	0.6837
	865- 995	0.7201	0.0476	0.2687	0.6837
	1065- 1385	0.7201	0.0476	0.2687	0.6837
	1545- 2040	0.7201	0.0476	0.2687	0.6837
	2090- 2655	0.7201	0.0476	0.2687	0.6837
	2705- 2865	0.6933	0.0621	0.2929	0.6450
	3245- 3925	0.6933	0.0621	0.2929	0.6450
	4260- 4470	0.6933	0.0621	0.2929	0.6450
	4540- 4785	0.6933	0.0621	0.2929	0.6450
	4910- 5165	0.6933	0.0621	0.2929	0.6450

Table 33. (Continued) k-Distribution Band Model Parameters for each Absorbing Molecule.

ABSORBER	SPECTRAL RANGE (cm <sup>-1</sup> )	Model		k-Distribution Parameters		
		a	G1	G2	G3	
Oxygen	0- 265	0.6011	0.1367	0.3547	0.5086	
(O <sub>2</sub> )	7650- 8080	0.5641	0.1771	0.3554	0.4675	
	9235- 9490	0.5641	0.1771	0.3554	0.4675	
	12850-13220	0.5641	0.1771	0.3554	0.4675	
	14300-14600	0.5641	0.1771	0.3554	0.4675	
	15695-15955	0.5641	0.1771	0.3554	0.4675	
	49600-52710	0.4704	0.2858	0.2698	0.4444	
Ozone	0- 200	0.8559	0.0067	0.1380	0.8553	
(O <sub>3</sub> )	515- 1275	0.7593	0.0309	0.2317	0.7374	
	1630- 2295	0.7819	0.0233	0.2100	0.7667	
	2670- 2845	0.9175	0.0005	0.0785	0.9210	
	2850- 3260	0.7703	0.0270	0.2212	0.7518	
Sulfur	0- 185	0.8907	0.0025	0.1043	0.8932	
Dioxide	400- 650	0.8466	0.0082	0.1471	0.8447	
(SO <sub>2</sub> )	950- 1460	0.8466	0.0082	0.1471	0.8447	
	2415- 2580	0.8466	0.0082	0.1471	0.8447	
Water	0- 345	0.5274	0.2193	0.3349	0.4458	
Vapor	350- 1000	0.5299	0.2164	0.3369	0.4467	
(H <sub>2</sub> O)	1005- 1640	0.5416	0.2063	0.3433	0.4504	
	1645- 2530	0.5479	0.1962	0.3486	0.4552	
	2535- 3420	0.5495	0.1945	0.3498	0.4557	
	3425- 4310	0.5464	0.1985	0.3475	0.4540	
	4315- 6150	0.5454	0.1985	0.3475	0.4540	
	6155- 8000	0.5474	0.1962	0.3486	0.4552	
	8005- 9615	0.5579	0.1841	0.3534	0.4625	
	9620-11540	0.5621	0.1794	0.3549	0.4657	
	11545-13070	0.5847	0.1541	0.3576	0.4883	
	13075-14860	0.6076	0.1301	0.3525	0.5174	
	14865-16045	0.6508	0.0913	0.3275	0.5812	
	16340-17860	0.6570	0.0865	0.3229	0.5906	

Table 34. k-Distribution Band Model Parameters for each Absorbing Molecule.

ABSORBER	SPECTRAL RANGE (cm <sup>-1</sup> )	Model a	k-Distribution Parameters		
			K1	K2	K3
Ammonia (NH <sub>3</sub> )	0- 385	0.4704	19.9507	1.7956	0.2993
	390- 2150	0.6035	27.8458	2.5061	0.4177
Carbon	425- 835	0.6176	29.4277	2.6485	0.4414
Dioxide (CO <sub>2</sub> )	840- 1440	0.6810	37.0842	3.3376	0.5563
	1805- 2855	0.6033	27.8241	2.5042	0.4174
	3070- 3755	0.6146	29.0834	2.6175	0.4363
	3760- 4065	0.6513	33.4608	3.0115	0.5019
	4530- 5380	0.6050	28.0093	2.5208	0.4201
	5905- 7025	0.6160	29.2436	2.6319	0.4387
	7395- 7785	0.7070	40.1951	3.6176	0.6029
	8030- 8335	0.7070	40.1951	3.6176	0.6029
	9340- 9670	0.7070	40.1951	3.6176	0.6029
Carbon	0- 175	0.6397	32.0496	2.8845	0.4807
Monoxide (CO)	1940- 2285	0.6133	28.9354	2.6042	0.4340
	4040- 4370	0.6133	28.9354	2.6042	0.4340
Methane (CH <sub>4</sub> )	1065- 1775	0.5844	25.8920	2.3303	0.3884
	2345- 3230	0.5844	25.8920	2.3303	0.3884
	4110- 4690	0.5844	25.8920	2.3303	0.3884
	5865- 6135	0.5844	25.8920	2.3303	0.3884
Nitric Oxide (NO)	1700- 2005	0.6613	34.6834	3.1215	0.5203
Nitrogen Dioxide (NO <sub>2</sub> )	580- 925	0.7249	42.2784	3.8051	0.6342
	1515- 1695	0.7249	42.2784	3.8051	0.6342
	2800- 2970	0.7249	42.2784	3.8051	0.6342
Nitrous Oxide (N <sub>2</sub> O)	0- 120	0.8997	59.3660	5.3429	0.8905
	490- 775	0.7201	41.7251	3.7553	0.6259
	865- 995	0.7201	41.7251	3.7553	0.6259
	1065- 1385	0.7201	41.7251	3.7553	0.6259
	1545- 2040	0.7201	41.7251	3.7553	0.6259
	2090- 2655	0.7201	41.7251	3.7553	0.6259
	2705- 2865	0.6933	38.5667	3.4710	0.5785
	3245- 3925	0.6933	38.5667	3.4710	0.5785
	4260- 4470	0.6933	38.5667	3.4710	0.5785
	4540- 4785	0.6933	38.5667	3.4710	0.5785
	4910- 5165	0.6933	38.5667	3.4710	0.5785



Table 34. (Continued) k-Distribution Band Model Parameters for each Absorbing Molecule.

ABSORBER	SPECTRAL RANGE (cm <sup>-1</sup> )	Model		k-Distribution Parameters		
		a	K1	K2	K3	
Oxygen (O <sub>2</sub> )	0- 265	0.6011	27.5869	2.4828	0.4138	
	7650- 8080	0.5641	24.1314	2.1718	0.3620	
	9235- 9490	0.5641	24.1314	2.1718	0.3620	
	12850-13220	0.5641	24.1314	2.1718	0.3620	
	14300-14600	0.5641	24.1314	2.1718	0.3620	
	15695-15955	0.5641	24.1314	2.1718	0.3620	
	49600-52710	0.4704	19.9507	1.7956	0.2993	
Ozone (O <sub>3</sub> )	0- 200	0.8559	55.6442	5.0080	0.8347	
	515- 1275	0.7593	46.1189	4.1507	0.6918	
	1630- 2295	0.7819	48.5155	4.3664	0.7277	
	2670- 2845	0.9175	60.7802	5.4702	0.9117	
	2850- 3260	0.7703	47.2982	4.2568	0.7095	
Sulfur Dioxide (SO <sub>2</sub> )	0- 185	0.8907	58.6298	5.2767	0.8794	
	400- 650	0.8466	54.8078	4.9327	0.8221	
	950- 1460	0.8466	54.8078	4.9327	0.8221	
	2415- 2580	0.8466	54.8078	4.9327	0.8221	
Water Vapor (H <sub>2</sub> O)	0- 345	0.5274	21.8352	1.9652	0.3275	
	350- 1000	0.5299	21.9588	1.9763	0.3294	
	1005- 1640	0.5416	22.4234	2.0181	0.3364	
	1645- 2530	0.5479	22.9517	2.0657	0.3443	
	2535- 3420	0.5495	23.0750	2.0768	0.3461	
	3425- 4310	0.5464	22.8262	2.0544	0.3424	
	4315- 6150	0.5454	22.8262	2.0544	0.3424	
	6155- 8000	0.5474	22.9517	2.0657	0.3443	
	8005- 9615	0.5579	23.6654	2.1299	0.3550	
	9620-11540	0.5621	23.9774	2.1580	0.3597	
	11545-13070	0.5847	25.9207	2.3329	0.3888	
	13075-14860	0.6076	28.2957	2.5466	0.4244	
	14865-16045	0.6508	33.3998	3.0060	0.5010	
	16340-17860	0.6570	34.1575	3.0742	0.5124	

### 5.4.3.2 Inhomogeneous Atmosphere

For inhomogeneous atmospheres, we adopt the same scaling approximation used in LOWTRAN (see Eq. 156):

$$k_i(P, \Theta) = k_i(P_o, \Theta_o) \frac{P}{P_o} \sqrt{\Theta_o / \Theta}$$

The adding method (as discussed in Section 3.1.2 of the Isaacs report<sup>36</sup>) is used for calculating the thermal radiation flux in an inhomogeneous atmosphere. Basically, the parameters used are  $F^+$ ,  $F^-$ ,  $T$ , and  $R$ , as presented in Section 3.1.2 of the Isaacs report.

### 5.4.3.3 Stream Approximation, Source Function, and Radiance Calculation

Again, we use the same procedures discussed in Section 3.1.3 of the Isaacs report<sup>36</sup> to calculate the radiance from the source function and stream approximation.

The multiple scattered contribution to the source function is approximated by (Eqs. 137, 125, 126, 133 and 134)

$$J_{MS}(\tau, \pm\mu, \phi) \approx \frac{\omega_o(\tau)}{\pi} \{F^\pm(\tau)[1 - \beta(\mu)] + F^m(\tau)\beta(\mu)\}. \quad (163)$$

The total source function is:

$$J(\tau, \mu, \phi) = J_o(\tau, \mu, \phi) + J_{MS}(\tau, \mu, \phi) \quad (164)$$

where:

$$J_o(\tau, \mu, \phi) = \frac{\omega_o(\tau)}{4\pi} \pi F e^{-\tau/\mu_o} P(\Omega; -\Omega_o) + [1 - \omega_o(\tau)] B[\Theta(\tau)] \quad (165)$$

The single scattered contribution to  $J_o$  above is taken directly from the single scattering algorithm used in earlier versions of LOWTRAN. (Actually the summed multiply scattered radiance is added to the summed singly scattered radiance).

One essential difference between the multiple scattering radiance implementation and the previous single scattering version is the treatment of surface reflection.

Through the surface boundary condition, surface reflection affects the flux profile and hence the source function throughout the atmosphere. From the radiance solutions:

$$I(\tau, \mu, \phi) = \left\{ \frac{r}{\pi} \left[ \pi \mu_o F e^{-\tau^*/\mu_o} + \int_0^1 \int_0^{2\pi} I(\tau^*, -\mu, \phi) \mu d\mu d\phi \right] + (1-r) B[T(\tau^*)] \right\} \exp(-(\tau^* - \tau)/\mu) + \int_{\tau}^{\tau^*} J(t, \mu, \phi) e^{-(t-\tau)/\mu} \frac{dt}{\mu} \quad (166)$$

$$I(\tau, -\mu, \phi) = \int_0^{\tau} J(t, \mu, \phi) e^{-(\tau-t)/\mu} \frac{dt}{\mu} \quad (167)$$

It can be seen that surface reflection can increase both upward and downward radiances through the source function. For upward radiances, there is a more drastic difference between the single scattering treatment and the implemented multiple scattering version. This concerns reflection of downward scattered radiance from the surface and back to a downward looking observer (the second term in the brackets in Eq. (166)). This contribution is not included in standard single scattering calculations, although the reflected attenuated direct solar term is (i.e., the first term in Equation 166).

The addition of multiple scattering to MODTRAN was made with a minimum of changes to the source code and input deck. Only one new input parameter, IMULT, was added. IMULT, read as the fourth variable on card 1, is set to one for multiple scattering calculations. If aerosols are not included (clear sky case), calculations are performed independent of the value of IMULT.

The main program has been altered to allow the path geometry calculations (called from subroutine GEO) to be accessed twice, once for the original single scatter path and once for the entire atmosphere, required for computation of the multiply scattered radiance. The reason for the second path geometry call is that the thermal and solar source functions used to determine the multiply scattered radiance contribution are functions of the upward and downward flux at each layer. The Multiply scattered flux at a given layer will, in part, be determined by radiation from all atmospheric layers, even those above or below the layers between the observer and target. To calculate the fluxes at each layer, it is therefore necessary to add the flux contributions from the surface up to space, and back down to the surface again. This adding procedure, executed in the new subroutine FLXADD, is discussed in detail in Section 3.1.2.1 and 3.1.2.2 of the Isaacs report<sup>36</sup>.

A flag (variable ITEST) has been incorporated into RFPATH for the purpose of isolating the refracted viewing path zenith angle for each layer, as opposed to the solar zenith angle, calculated for the solar cases in a later pass through RFPATH.

A number of changes were incorporated into subroutine TRANS. After calculating the cumulative path parameters used in the original scattering routines, it calls MSRAD, where the aerosol scattering and extinction, H<sub>2</sub>O continuum and Rayleigh scattering optical thickness for each layer are calculated. The asymmetry factor for each layer is also calculated based on model extinction and absorption data added to EXABIN, AEREXT, and EXTDTA, and aerosol effective absorber amounts for the four vertically spaced aerosol regions. MSRAD calls subroutine FLXADD.

Subroutine FLXADD calculates the six degraded k components of the H<sub>2</sub>O/uniformly mixed gas transmission for each layer, as well as the molecular absorption optical thickness (see section 5.4.3 for a detailed description of the necessary modifications needed to accommodate the Pierluissi<sup>13</sup> double exponential formulation). It is then added to the continuum, aerosol extinction, and molecular scattering optical thickness from MSRAD to provide the total optical thickness for each layer and k-value, as well as the corresponding single scatter albedo. The diffuse flux contribution for each isolated layer and k-value is computed from the applicable two-stream approximation, either solar or thermal, and combined in the flux adding routine to determine the total upward and downward flux for each layer for each k value. The diffuse solar downward flux is summed over k value and returned to evaluate the surface reflected downward diffuse solar flux. Function PLANCK returns the black body radiance for a particular wavenumber and temperature in units of Wcm<sup>-2</sup> strad<sup>-1</sup>/cm<sup>-1</sup>, while subroutine ALEVEL returns the layer number corresponding to a particular height, the top layer of the atmosphere is layer 1. Knowing the upward and downward fluxes as well as the backscatter parameter  $\beta$  returned from function BETABS, the multiple scattered source function can be determined.

Returning to MSRAD, the radiance is summed over the viewing path (between H1 and H2) and k-values to provide the multiply scattered diffuse radiance contribution. For a downward looking (upward radiance) calculation, the multiply scattered radiance at the upper boundary may be expressed by

$$I^+(n_t) = \sum_{k=1}^6 \left\{ (1 - T'_{n_t}) S(k, n_t) + \sum_{i=n_t}^{n_b-1} (T'_{i+1} - T_i) S(k, i+1) \right\} \Delta g_k + I_s \quad (168)$$

where  $n_b$  is the bottom layer,  $n_t$  the top layer,  $S(k, i)$  the source function for a particular k value and layer i.  $T'_i$  is the transmission from the upper boundary (H2) through layer i along the viewing path. The total upward radiance also includes  $I_s$ , a direct solar reflection surface contribution or surface thermal emission term, which includes the contribution due to the reflection of the single and multiple scattered solar radiance.

For a thermal case,

$$I_s = B_s T_t \varepsilon \quad (169)$$

where  $B_s$  is the black body function for a given surface temperature and frequency,  $T_t$  is the total atmospheric transmissivity, and  $\varepsilon$  is the surface emissivity. For the single scatter solar case,

$$I_s = a_s \mu_o T_t S / \pi, \quad (170)$$

where  $a_s$  is the surface albedo,  $\mu_o$  the cosine of solar zenith angle at the surface, and  $S$  the direct solar intensity at the surface. With multiple scattering (IMULT=1), the single and multiple scatter reflection terms are added, so that:

$$I_s = a_s \mu_o T_t S / \pi + a_s F_s^- T_t / \pi, \quad (171)$$

where  $F_s^-$  is the downward diffuse flux at the surface.

For an upward looking (downward radiance) case, the multiply scattered radiance is expressed by:

$$I^-(n_b) = \sum_{k=1}^3 \left\{ (1 - T_{n_b}) S(k, n_b) + \sum_{i=n_b}^{n_t+1} (T_i - T_{i-1}) S(k, i-1) \right\} \Delta g_k \quad (172)$$

where  $T_i$  is the transmission from the lower boundary (H1) through layer  $i$  along the viewing path. At this point, the path parameters are reloaded, and TRANS is executed once more for the single scattering case. The single scatter diffuse radiance is added to the multiple scatter term and the boundary radiance contributions (if any) to yield the total thermal radiance, while the solar/lunar radiance is the sum of the single and multiple scatter terms plus a surface reflection term where applicable. MSRAD and FLXADD are not called for the MODTRAN single scatter case.

#### 5.4.3.4 Notes on the Operation of Codes with Multiple Scattering

Unlike the earlier LOWTRAN models, the new MODTRAN/LOWTRAN 7 requires a complete atmospheric profile (surface to surface) to properly calculate the multiple scattering contribution to the radiance. For a calculation involving a path from 0-1 km, for example, it is still necessary to choose the desired stratospheric as well as higher level aerosol distribution set by IVULCN on card 2. For a 3-20 km path, the boundary layer aerosols, set using IHAZE, on card 2 or user-defined via card 2D, will now affect the calculated radiance. The earlier versions of LOWTRAN, performing single scattering calculations, required aerosol information only along the path between the observer and target.

When the models are run for solar single scattering only, (IMULT = 0), the output for a solar case includes the reflected attenuated direct solar radiance under the heading GROUND REFLECTED. However, in many cases, the ground reflected diffuse

radiance due to single and multiple scattering is of the same order of magnitude as the direct reflected radiance. The output with multiple scattering activated (IMULT =1) has therefore been altered to include both the total (diffuse single and multiple scattered and direct) and direct reflection terms.

Running MODTRAN with multiple scattering results in a several-fold increase in CPU time. The atmospheric profile and path being used may not produce a significant multiple scattering contribution, possibly resulting in wasted computer time. Both the total (single and multiple) and single scattered radiance are included under the heading PATH SCATTERED RADIANCE. If in doubt, the user can run a multiple scattering calculation to determine the relative size (s) of the single and multiple scatter contributions. If multiple scattering is negligible, future calculations may be made with the more economical single scatter (IMULT = 0) option.

#### 5.4.4 Comparison to Exact Calculations

##### 5.4.4.1 Solar Multiple Scattering

In order to verify the correct operation of the implemented multiple scattering treatment for both solar and thermal regimes, comparisons were made to exact results.

In the case of solar multiple scattering, exact results were obtained for a variety of cases during the trade-off analysis summarized in Appendix A of the Isaacs report<sup>36</sup>. Exact solutions to the radiative transfer equation for solar multiple scattering were obtained using the Gauss-Seidel iterative method based on a code by Dave<sup>283</sup>. This algorithm evaluates the fluxes and radiances for inhomogeneous atmospheres with arbitrary vertical distributions of anisotropically scattering aerosol overlying a Lambertian reflecting surface.

A number of special modifications of LOWTRAN were necessary to accommodate the comparison. These included reading in the same aerosol extinction and absorption coefficients, asymmetry factor, and phase function as were used for the Dave model runs, and forcing LOWTRAN to use the quantities with the same vertical distribution as the Dave code. (Ordinarily, user supplied aerosol data read into LOWTRAN will only be used in the lowest 2 km of the atmosphere). These changes made the comparison as close as possible to a direct one. The LOWTRAN code was run at 0.55  $\mu\text{m}$  with the sun at a zenith angle of 60°.

The first test of the LOWTRAN implementation is whether the adding method is calculating the correct fluxes for use in the stream approximation of the multiply scattered source function. Table 35 compares the emergent fluxes calculated by the

exact code and LOWTRAN. For simplicity, all fluxes and radiances plotted in the Isaacs report<sup>36</sup> (pages 81-85) have been normalized to correspond to  $\pi$  units of incident solar irradiance. To obtain the appropriate engineering units ( $\text{watts/cm}^2 \text{ cm}^{-1}$ , and  $\text{watts/cm}^2 \text{ str cm}^{-1}$ , for flux and radiance, respectively), the normalized values can be multiplied by  $1.719 \times 10^{-6}$ . As can be seen from the results, the solar two stream approximation and flux adding procedure in LOWTRAN is reproducing the exact values quite well throughout the range of optical thicknesses and surface albedos examined. The errors, on the order of a few percent, are to be expected from the two stream approximation.

**Table 35. Comparison of Solar Multiply Scattered Emergent Fluxes**  
(Normalized to  $\pi$  Units of Incident Irradiance) from  
FLXADD Subroutine (L) and Exact calculation (E).

$\pi^*$	Upward Flux $F^+(\pi=0)$		Downward Flux $F^-(\pi=\pi^*)$	
	$r=0.0$	$r=0.4$	$r=0.0$	$r=0.4$
	L / E	L / E	L / E	L / E
0.25	.188 / .191	.611 / .634	.323 / .316	.367 / .371
0.50	.244 / .256	.562 / .584	.503 / .489	.536 / .544
1.00	.316 / .324	.492 / .515	.599 / .567	.605 / .615

A good comparison between the exact radiance calculation as a function of path zenith angle (theta) and those obtained from using either the solar single scattering option or the multiple scattering option can be seen in the Isaacs<sup>36</sup> report (Figures 4-9 to 4-12, pgs. 81-84). Plotted are the normalized emergent upward and downward radiances for an optical depth of 0.5 and surface albedos of 0.0 and 0.4. The plots extend to a maximum zenith angle of  $60^\circ$  since at larger angles the effects of refraction in the MODTRAN code make it difficult to compare to the plane parallel exact results. In all cases it can be seen that the addition of the multiply scattered contribution to path radiance in MODTRAN has considerably improved the simulation as compared to that obtained from the exact code. The improvement is considerable, especially for upward radiance when there is surface reflection (see Figure 4-11). This is because although the single scatter version of LOWTRAN included the surface reflection of the attenuated direct solar beam, it contained no provision to treat the reflected downward scattered radiance. This contribution (which is the second term in the brackets in Equation (166)) may be considerable when multiple scattering is a factor and the MS option is included in the calculation, since the downward scattered flux is calculated as a result of the adding method.

The relative accuracies as a function of path zenith angle expressed as percent errors obtained in the comparison between MS calculations and the exact calculations for all optical depths evaluated are summarized in (Figures 4-13 and 4-14, Pg. 85-86 of the Isaacs report<sup>36</sup>) for surface albedos of 0.0 and 0.4, respectively. In general, the solar multiple scattering approach implemented within the models underestimates radiance by 10 or 20 percent. These accuracies are consistent with those obtained off line in the trade-off analysis.

#### **5.4.4.2 Thermal Multiple Scattering**

The MODTRAN/LOWTRAN thermal multiple scattering method was compared to the thermal multiple scattering routine in FASCODE. The FASCODE MS had been compared to exact multiple scattering using the discrete ordinate method. In general, the degraded FASCODE calculations are within 10% of the answers obtained when using MODTRAN.

A significant problem with the previous treatment of thermal scattering within earlier versions of LOWTRAN, was the failure to provide a source function to introduce multiply scattered radiance contributions along the observed path. As a consequence, LOWTRAN seriously underestimated path radiance for long paths near the horizon where multiple scattering contributes significantly (Ben-Shalom et al.,<sup>281</sup>). For a good comparison of this effect see the Isaacs report<sup>36</sup> (pgs. 79-92, Figures 4-17 to 4-20).



## 6. Validation and Applications

Throughout the development of the MODTRAN model it has been meticulously compared to FASCODE calculations. It is of course extremely important to compare any model to actual measurements. An interferometric measurement by a Bomem FTS taken on 2 July 1992 at Sudbury, Ma; is compared with a MODTRAN 2 calculation in Figure 62. Possible differences may arise from several factors; errors in the forward calculations, the input profiles of temperature and water vapor supplied by supporting radiosonde data, and the instrumental calibration. The actual agreement, except for the 10 micron ozone, is within a few % RMS. This instrument, a Double Beam Interferometer Sounder (DBIS), was designed and operated by the Defense Research Establishment Valcartier (DREV), Canada. The instrument and the calibration are described fully in a paper by Theriault et al.<sup>295</sup>

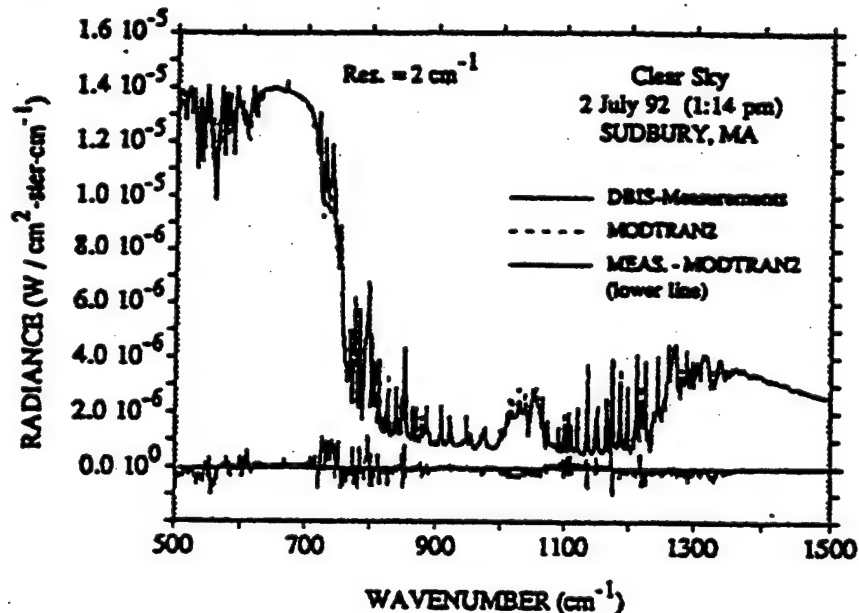


Figure 62. Atmospheric Up-looking Emission Spectra as Measured and Calculated by the DBIS Interferometer and MODTRAN 2 Calculations. Input Specifications for MODTRAN were Provided by Supporting Radiosonde Profiles of Temperature and Water Vapor.

The Theriault paper describes the development of a successful simultaneous (temperature and water vapor profile) retrieval algorithm, based primarily on FASCOD3 forward calculations, with accompanying derivative matrices. Traditionally the derivative matrices required for the least square residual technique embody time-consuming forward runs of full-path FASCODE radiance predictions, each run differing from the

preceding run by a single small perturbation,  $x = x_0 + x'$ , where  $x = T(K)$  or  $H_2O(g/m^3)$ , for each layer,  $l$ . The Jacobian matrix is then defined as the set of differences in total radiance:

$$\frac{dR(x,1)}{dx} = \frac{R(x,1) - R_0}{x'} \quad (173)$$

where:  $R_0$  is the unperturbed total radiance and

$R(x,1)$  is the total radiance with a single perturbation ( $x = x_0 + x'$  and  $x' = T'$  or  $H_2O'$ ) at layer 1

The size of the original matrix is  $j$  by  $k$ , where  $j$  is the number of spectral channels, dependent on spectral resolution, and  $k$  is (at minimum) the number of atmospheric layers or boundaries times the number of constituents undergoing perturbation in the simultaneous retrieval.

Moncet and colleagues<sup>296</sup> have recently devised a method which greatly optimizes calculations of the Jacobian elements, principally based on FASCODE. However, even with these modifications, this task will still consume a formidable amount of computer time. This has prompted an investigation into the feasibility of employing MODTRAN 2 for the Jacobian calculations. The task did not require a modification of MODTRAN, instead the outline above was followed: each full path radiance calculation was carried out with and without the perturbation at each layer over the spectral range of the DBIS instrument. The subsequent derivative matrix elements were then compared to the equivalent FASCODE elements. The agreement, as seen in Figures 63,64 and 65 (all typical), is remarkably good for both temperature and water vapor perturbations. The RMS differences in the Jacobian radiances (Eq. 173 with the denominator set to unity) are of the order of  $1.0E-08$  to  $1.0E-10$  compared to an average radiance of  $3.0E-06$   $W/(cm^2\text{-ster}\text{-}cm^{-1})$ , smaller than 3 parts in 1000.

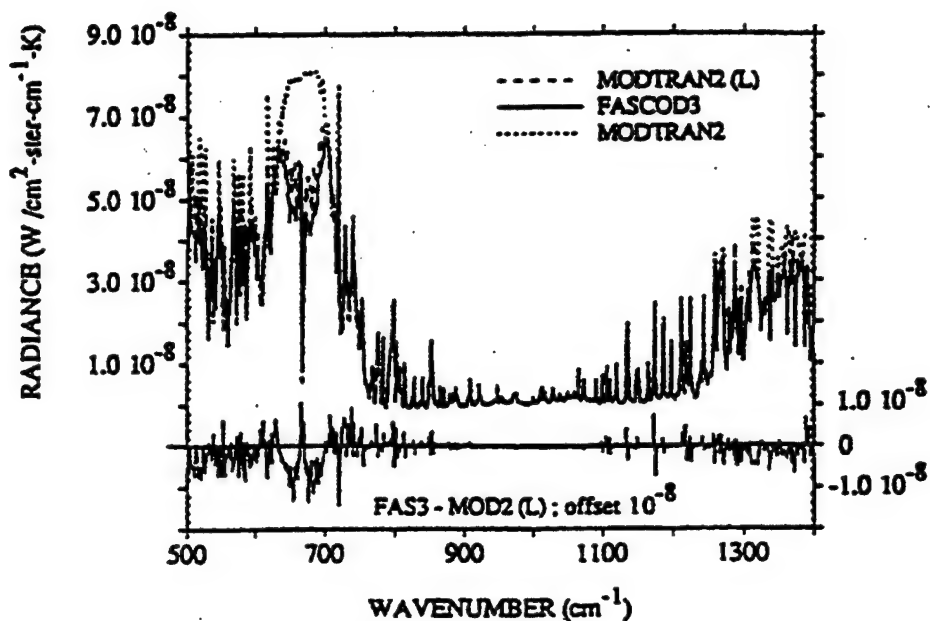


Figure 63. Temperature Jacobians for a 2 K Temperature Perturbation Centered at 0.2 km, where the Original Temperature and Water Vapor Profiles Correspond to the Supporting Radiosonde Data for Figure 62. Note that MODTRAN 2, without the "linear in Tau" Approximation Cannot Follow the Sensitivity of FASCOD3 and MODTRAN 2(L) when the Transmittance is Optically Thick Due to CO<sub>2</sub> and H<sub>2</sub>O.

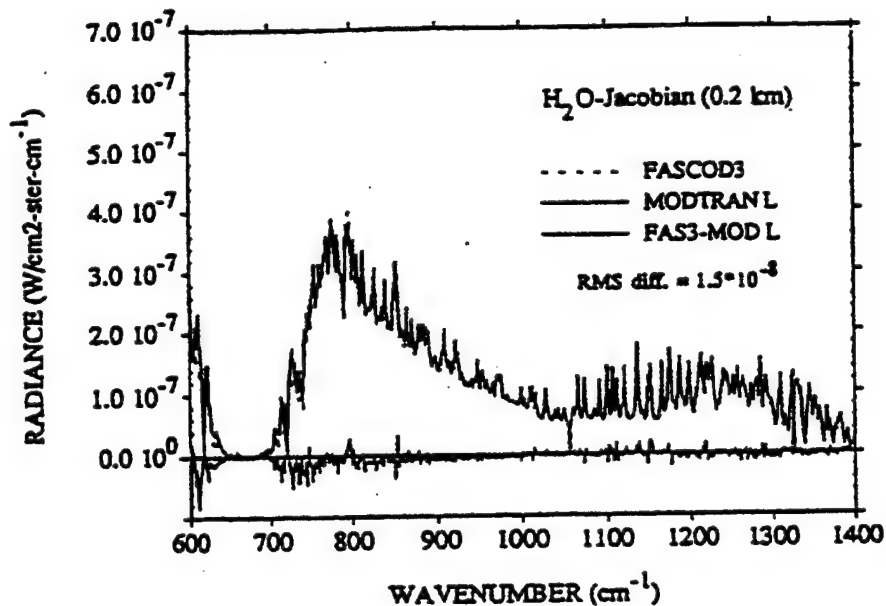


Figure 64. Water Vapor Jacobians for a 0.1 g/m<sup>3</sup> Perturbation at 0.2 km for

the same Conditions as in Figure 63. Note the Magnitude of the RMS Deviations Relative to the Maximum in the Jacobian and the Corresponding Total Radiance in Figure 62.

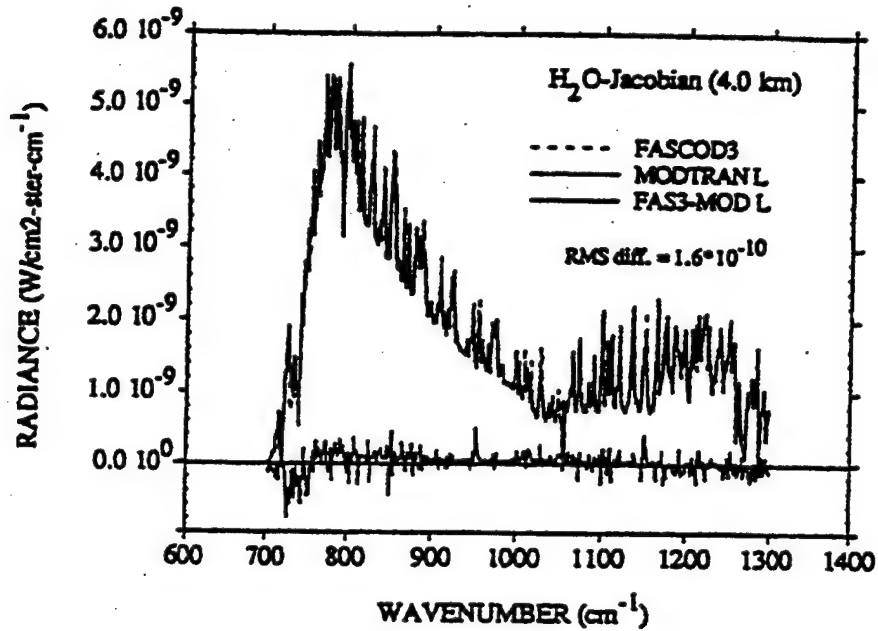


Figure 65. Same Calculations as in Figure 64 Except that the Perturbation Occurs at 4 km. While the Maximum Magnitude of the Jacobian has Fallen by two Orders of Magnitude, the Relative RMS Differences with FASCODE Remain Unchanged.

Another way of looking at the "second order" noise imposed by substituting MODTRAN-derived Jacobian elements for FASCODE's Jacobian's is that the RMS noise in the system is potentially increased by a factor of 1.05 over that previously calculated for the line-by-line Jacobian noise. This number is approximated by:

$$\left[ \frac{(RMS \text{ noise})/R(v')}{[J(v')/R(v')]} \right] \approx \frac{1}{20} \quad (174)$$

where  $v'$  denotes the frequency of the Jacobian ( $J$ ) maximum. That is, the inherent signal/noise ratio of MODTRAN Jacobians is approximately 20 for these three typical cases. It should be noted that the magnitude of any particular Jacobian element represents (in these cases) that layer's contribution to the total radiance. Therefore, the  $H_2O$  Jacobian at 4km, with a maximum value of  $5.0E-09$  (at  $800 \text{ cm}^{-1}$ ) compared to a total radiance of  $2.5E-06$ , contributes less than 0.2% to the total signal, while the Jacobian at 0.2km contributes approximately 12% to the signal. However, the additional

RMS MODTRAN induced noise in the Jacobians is approximately the same fraction for each; for instance, the S/N is 26 at 4km and 20 at 0.2km. Therefore, there appears to be no systematic altitude-dependent impact when substituting MODTRAN for FASCOD3 Jacobians.

A pair of inversions for the above mentioned DBIS measurement (2 July 1992) have been performed using the Theriault-Moncet algorithm with similar channel selection and damping factors, as described by Theriault, et al.<sup>295</sup>. Figure 66 displays the first guess inputs, the radiosonde profiles, and the inverted profiles, using both the FASCOD3 and MODTRAN-derived Jacobian matrices. The differences in the inverted profiles are typically small but not insignificant. The MODTRAN Jacobians introduce an additional oscillation, particularly in the H<sub>2</sub>O profile. A preliminary attempt to account for a 5% increase in system noise introduced by MODTRAN (by adopting a slightly larger damping) reduced the oscillation appropriately, but not without a parallel loss in information content. This accounting of noise sources can, of course, be documented according to the definitions of Rodgers<sup>297</sup>. However, the initial success in reproducing accurate Jacobians, substituting them directly into an existing inversion algorithm, and retrieving realistic profiles is very promising.

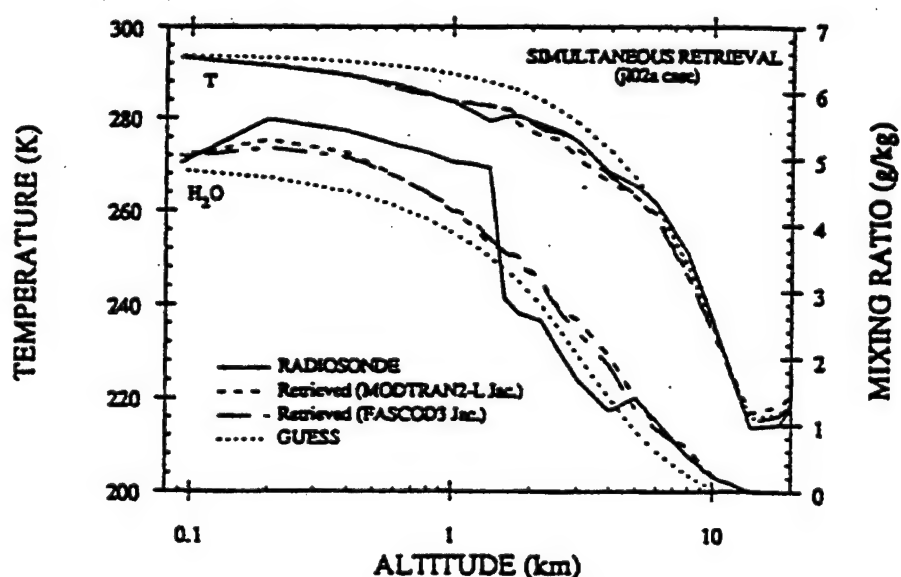


Figure 66. Simultaneous Retrieval of Temperature and Water Vapor Profiles for Conditions Appropriate to Figure 62., Using Both FASCOD3- and MODTRAN-Derived Jacobians. In each Instance, FASCOD3, with the Exact Profiles, was used for the Forward Radiance Simulation, while the Inversion was Initialized with the "Guess" Profiles.

## 7. Discussion of Future Modifications

The capabilities of the MODTRAN 2 model have yet to be fully exploited. The increased accuracy of the newly developed band model parameters (HITRAN92 compatible), coupled with the LOWTRAN 7 and FASCOD3 common elements (see Chapter 2) for e.g.; coarse continua CO<sub>2</sub>, H<sub>2</sub>O, N<sub>2</sub>, O<sub>2</sub>, etc.), spherical refractive geometry, default constituent profiles for gases, clouds, aerosols, fogs, rain models and thermal multiple scattering, combined with "ease of use", suggest that MODTRAN 2 may be an effective tool throughout the fields of atmospheric remote sensing and radiative transfer. For most observational conditions and spectral domains, the accuracy of MODTRAN 2 transmittance calculations fall within a few percent of FASCOD3 predictions, both statistically and in spectral detail. The agreement is sufficiently good that, for simulations at 2 cm<sup>-1</sup> and greater resolution, MODTRAN 2 may be substituted for FASCOD3 for most applications. In addition, layer-specific radiance contributions, represented by the detailed agreement in the Jacobian comparisons (see Chapter 6), suggest that MODTRAN 2 may also be appropriate for broader applications. Further studies that continue to explore these layer-specific attributes, based on flux-divergence quantities (leading to rapid estimates of up- and down-welling fluxes, heating/cooling rates, and photodissociation rates) will be conducted in the future.

The speed, accuracy and user-friendliness of MODTRAN make it extremely attractive for enhancements and vectorization. Near term plans include the addition of new molecular cross sections, including IR chloro-fluorocarbons (CFC's) and additions to the UV (specifically, SO<sub>2</sub> and NO<sub>2</sub>). These additions will allow MODTRAN to effectively calculate heating and cooling rates, as well as photochemical photo-dissociation rate calculations, both are required inputs for pollution and climate change studies. Longer term plans call for the evolution of several new models based on or appended to MODTRAN; e.g. AURIC E<sup>298,299</sup> ( a MODTRAN extension to 0.1 microns), an expanded model MOSART<sup>300</sup> (combining MODTRAN with improved surface reflectance and enhanced cloud models from the APART 7 model<sup>301</sup>).

In the upper atmosphere (above 120 km) a chemical treatment for the effects of non-local thermodynamic equilibrium conditions (NLTE) is a necessity. A new model combining MODTRAN 2 and the SHARC-3 model<sup>302</sup> is currently being developed into a model called SAMM<sup>303</sup>. MODTRAN, FASCOD3 and LOWTRAN are also included in the new all-inclusive radiative transfer model, PLEXUS<sup>304</sup>.

## REFERENCES

1. Berk, A., Bernstein, L.S., Robertson, D.C., "MODTRAN: A Moderate Resolution Model for LOWTRAN 7", GL-TR-89-0122, 1989. ADA214337
2. Kneizys, F.X., Shettle, E.P., Abreu, L.W., Chetwynd, J.H., Anderson, G.P., Gallery, W.O., Selby, J.E.A. and Clough, S.A. (1988), Users Guide to LOWTRAN 7, AFGL-TR-88-0177, (NTIS AD A206773).
3. Kneizys, F.X., Shettle, E.P., Gallery, W.O., Chetwynd, J.H., Abreu, L.W. Selby, J.E.A., Clough, S.A. and Fenn, R.W. (1983), Atmospheric Transmittance/Radiance: Computer Code LOWTRAN 6, AFGL-TR-83-0187, (NTIS AD A137796).
4. Kneizys, F.X., Shettle, E.P., Gallery, W.O., Chetwynd, J.H., Abreu, L.W., Selby, J.E.A., Fenn, R.W., and McClatchey, R.A. (1980), Atmospheric Transmittance/Radiance: Computer Code LOWTRAN 5, AFGL-TR-80-0067, (NTIS AD A 088215) .
5. Robertson, D.C., Bernstein, L.S., Haimes, R., Wunderlich, J. and Vega, L.,  $5\text{ cm}^{-1}$  Band Model Option to LOWTRAN 5, Appl. Opt., 20: 3218 (1981)
6. Selby, J.E.A., Kneizys, F.X., Chetwynd, Jr., J.H., and McClatchey, R.A. (1978) Atmospheric Transmittance/Radiance: Computer Code LOWTRAN 4, AFGL-TR-78-0053, AD A058643.
7. Selby, J.E.A., Shettle, E.P., and McClatchey, R.A. (1976) Atmospheric Transmittance from 0.25 to  $28.5\text{ }\mu\text{m}$ : Supplement LOWTRAN 3B, AFGL-TR-76-0258, AD A040701.
8. Selby, J.E.A. and McClatchey, R.A. (1975) Atmospheric Transmittance from 0.25 to  $28.5\text{ }\mu\text{m}$ : Computer Code LOWTRAN 3, AFCRL-TR-75-0255, AD A017734.
9. Selby, J.E.A. and McClatchey, R.A. (1972) Atmospheric Transmittance from 0.25 to  $28.5\text{ }\mu\text{m}$ : Computer Code LOWTRAN 2, AFCRL-TR-72-0745, AD A763721
10. Anderson, G.P., Clough, S.A., Kneizys, F.X., Chetwynd, J.H., and Shettle, E.P. (1986) AFGL Atmospheric Constituent Profiles (0-120 km), AFGL-TR-86-0110, AD A175173.

11. NASA (1966), U.S. Standard Atmosphere Supplements, 1966, U.S. Government Printing Office, Washington, D.C .
12. NASA (1976), U.S. Standard Atmosphere Supplements, 1976, U.S. Government Printing Office, Washington, D.C .
13. Pierluissi, J.H. and Maragoudakis, C.E. (1986) Molecular Transmission Band Models for LOWTRAN, AFGL-TR-86-0272, AD A180655
14. Clough, S.A., Kneizys, F.X., Rothman, L.S. and Gallery, W.O., (1981) Atmospheric Spectral Transmittance and Radiance: FASCOD1B, SPIE vol 277/Atmospheric Transmission.
15. Burch, D.E. and Alt. R.L. (1984) Continuum Absorption by H<sub>2</sub>O in the 700-1200 cm<sup>-1</sup> and 2400-2800 cm<sup>-1</sup> Windows, AFGL-TR-84-0128 AD A147391
16. Burch, D.E. (1985) Absorption by H<sub>2</sub>O in Narrow Windows between 3000 and 4200 cm<sup>-1</sup>, AFGL-TR-85-0036, AD A166648.
17. Devir, A.D., Ben-Shalom, A., Lipson, S.G., Oppenheim, U.P., and Ribak, E. (1985) Atmospheric Transmittance Measurements: Comparison with LOWTRAN 6 Report RAA/99-85, Technion-Israel Institute of Technology, Haifa 32000, Israel.
18. Jacor, I.M. H<sub>2</sub>O cont WL/LL report ???
19. Anderson, G.P., Chetwynd, J.H., Theriault, J.-M., Acharya, P.K., Berk, A., Robertson, D.C., Kneizys, F.X., Hoke, M.L., Abreu, L.W., and Shettle, E.P. (1993) MODTRAN 2: Suitability for Remote Sensing, SPIE, Vol 1968, 514-523
20. Rothman, L.S., Gamache, R.R., Tipping, R.H., Rinsland, C.P., Smith, M.A.H., Benner, D.C., Malathy Devi, V., Flaud, J.-M., Camy-Peyret, C., Perrin, A., Goldman, A., Massie, S.T., Brown, L.R., and Toth, R.A. (1992) The HITRAN Molecular Database: Editions of 1991 and 1992, J. Quant. Spectrosc. Radiat. Transfer, vol 48 no. 5/6, pp. 469-507



21. Acharya, P.K., Robertson, D.C., and Berk, A. (1993), Upgraded Line-of-Sight Geometry Package and Band Model Parameters for MODTRAN, PL-TR-93-2127, ADA280952.
22. Yoshino, K., Cheung, A.S-C, Esmond, J.R., Parkinson, W.H., Freeman, D.E., Guberman, S.L., Jenouvrier, A., Coquart, B., and Merienne, M.F. (1988) Improved Absorption Cross Sections of Oxygen in the Wavelength Region 205-240 nm of the Herzberg Continuum, Planet. Space Sci. 36: 1469-1475.
23. Johnston, H.S., Paige, M., and Yao, F. (1984) Oxygen Absorption Cross Sections in the Herzberg Continuum and between 206 and 327K, J. Geophys Res. 89: 11661-11665.
24. Shardanand (1977) Nitrogen-Induced Absorption of Oxygen in the Herzberg Continuum, J. Quant. Spectrosc. Radiat. Transfer 18:525-530.
25. Frederick, J.E. and Hudson, R.D. (1979) Predissociation Linewidths and Oscillator Strengths for the (2-0) to (13-0) Schumann-Runge Bands of O<sub>2</sub>, J. Molec. Spectrosc. 74:247-258.
26. Yoshino, K., Freeman, D.E., and Parkinson, W.H. (1984) Atlas of the Schumann-Runge Absorption bands of O<sub>2</sub> in the Wavelength Region 175-205 nm., J. Phys. Chem. 13:207.
27. Bass, A.M. and Paur, R.J. (1985) The Ultraviolet Cross-Sections of Ozone. Measurements in Atmospheric Ozone, Proceedings of the Quadrennial Ozone Symposium in Halkidiki, Greece, edited by C. Zeferos and A. Ghaz, pp. 606-616 D. Reidel, Inc.
28. Molina, L.T. and Molina, M.J. (1986) Absolute Absorption Cross Sections of Ozone in the 185-350 nm Wavelength Range, J. Geophys. Res 91:14501-14509.
29. Yoshino K., Freeman, D.E., Esmond, J.R., and Parkinson, W.H. (1988) Absolute Absorption Cross Section Measurements of Ozone in the Wavelength Region 238-335 nm and the Temperature Dependence, Planet. Space Sci. 36:395-398.

30. Cacciani, M., diSarra, A., and Fiocco, G. (1987) Laboratory Measurements of the Ozone Absorption Coefficients in the Wavelength Region 339-362 nm at Different Temperatures, Dept. of Physics, University of Roma - La Sapienza, Italy, Internal Note No. 882.
31. VanHoosier, M.E., Bartoe, J.D., Brueckner, G.E., and Prinz, D.K. (1988) Absolute Solar Spectral Irradiance 120 nm-400 nm : Results from the Solar Ultraviolet Spectral Irradiance Monitor (SUSIM) Experiment on Board Spacelab 2, Astro. Lett. and Communications 27:163-168.
32. VanHoosier, M.E. and Brueckner, G.E. (1987) Solar Ultraviolet Spectral Irradiance Monitor (SUSIM): Calibration Results from Spacelab 2, Proceedings of the 8th Workshop on Vacuum Ultraviolet Radiometric Calibration of Space Experiments, 19 March 1987.
33. Neckel, H. and Labs, D. (1984) The solar radiation between 3300 and 12500 Å, Solar Phys. 90:205-258.
34. Wehrli, Ch. (1985) Extra-Terrestrial Solar Spectrum, Publication No. 615, July 1985, Physikalisch-Meteorologisches Observatorium and World Radiation Center, CH-7260 Davos-Dorf, Switzerland.
35. Thekeakera, M.P. (1974) Extra-Terrestrial Solar Spectrum, 3000-6100 Å° at 1 Å° Intervals, Appl. Opt. 13:518-522.
36. Isaacs, R.G., Wang, W-C., Worsham, R.D. and Goldenberg, S. (1986) Multiple Scattering Treatment for use in the LOWTRAN and FASCODE Models, AFGL-TR-86-0073, AD A173990.
37. Isaacs, R.G., Wang, W-C., Worsham, R.D. and Goldenberg, S. (1987) Multiple Scattering LOWTRAN and FASCODE Models, Appl. Opt 26:1272-1281.
38. Gathman, S.G., de Leeuw, G., Davidson, K.L., and Jensen, D.R. (1989) The Naval Oceanic Vertical Aerosol Model: Progress Report, AGARD Conference Proceedings No. 454, Atmospheric Propagation in the UV, Visible, IR, and mm-Wave Region and Related Systems Aspects, Copenhagen, Denmark.

39. Falcone, V.J., Abreu, L.W. and Shettle, E.P. (1979) Atmospheric Attenuation of Millimeter and Submillimeter Waves: Models and Computer Code, AFGL-TR-79-0253, ADA084485
40. Clough, S.A., Kneizys, F.X., Shettle, E.P., and Anderson, G.P. (1986) Atmospheric Radiance and Transmittance: FASCOD2, Proc. of the Sixth Conference on Atmospheric Radiation, Williamsburg, VA. American Meteorological Society, Boston, MA. 141-144.
41. Longtin, D.R., Shettle, E.P., Hummel, J.R., and Pryce, J.D. (1988) A Desert Aerosol Model for Radiative Transfer Studies, pg. 261-269 in Aerosols and Climate, ed. by P.V. Hobbs and M.P. McCormick, A. Deepak Publishing, Hampton, VA.
42. Longtin, D.R., Shettle, E.P., Hummel, J.R., and Pryce, J.D. (1988) A Wind Dependent Desert Aerosol Model: Radiative Properties, AFGL-TR-88-0112.
43. Hummel J.R., Shettle, E.P. and Longtin, D.R. (1988) A New Background Stratospheric Aerosol Model for Use in Atmospheric Radiation Models, AFGL-TR-88-0166, ADA210110
44. Gallery, W.O., Kneizys, F.X., and Clough, S.A., (1983) Air Mass Computer Program for Atmospheric Transmittance/Radiance Calculations: FSCATM, AFGL-TR-83-0065. (NTIS AD A132108).
45. Edlen, K. (1966) The Refractive Index of Air, Metrologia 2: 12
46. Burch, D.E., and Gryvnak, D.A. (1979) Method of Calculating H<sub>2</sub>O Transmission Between 333 and 633 cm<sup>-1</sup>, AFGL-TR-79-0054, (NTIS AD A072850)
47. Burch, D.E., and Gryvnak, D.A. (1978) Infrared Absorption by CO<sub>2</sub> and H<sub>2</sub>O, AFGL-TR-78-0154, (NTIS AD A060079)
48. Burch, D.E., Gryvnak, D.A., and Pembroke, J.D. (1971) Investigation of Absorption by Atmospheric Gases, AFCRL-71-0124, (NTIS AD A882876)

49. Burch, D.E. (January 1970) Semi-Annual Technical Report, Aeronutronic Report No. U-4784.
50. Smith, M.A.H. (1982) Compilation of Atmospheric Gas Concentration Profiles from 0-50 km, NASA Tech Mem 83289, 70 pp.
51. W.M.O. (1982) The Stratosphere 1981: Theory and Measurements, Report No. 11, NASA, Greenbelt, MD.
52. W.M.O. (1986) Atmospheric Ozone 1985: Assessment of Our Understanding of the Processes Controlling its Present Distribution and Change, WMO Report No. 16, W.M.O., Geneva, Switzerland.
53. Brasseur, G. and Solomon, S. (1984) Aeronomy of the Middle Atmosphere D. Reidel Publishing Co, Dordrecht, Holland, Chapter 5: Composition & Chemistry, 440 pp.
54. Russell III, J.M., Gille, J.C., Remsberg, E.E., Gordley, L.L., Bailey, P.L., Fischer, H., Girard, A., Drayon, S.R., Evans, W.F.J. and Harries, J.E. (1984b) Validation of Water Vapor Results Measured by the LIMS Experiment on Nimbus 7, J. Geophys. Res. 89, 5115-5120.
55. Keating, G.M. and Young D.F. (1985) Interim Reference Ozone Models for the Middle Atmosphere, Interim COSPAR Reference Atmosphere for Altitudes 20 -120 km,
56. Jones, R.L. and Pyle, J.A. (1984) Observations of CH<sub>4</sub> and N<sub>2</sub>O by the Nimbus 7 SAMS: A Comparison with In Situ Data and Two-Dimensional Numerical Model Calculations, J. Geophys. Res. 89, 5263-5379.
57. Solomon, S., Garcia, R.R., Olivero, J.J., Bevilacqua, R.M., Schwartz, P.R., Clancy, R.T. and Mahleman, D.O. (1985) Photochemistry and Transport of CO in the Middle Atmosphere, J. Atmos. Sci., 42: 1072-1083.
- 58 WMO and COSPAR
59. CIRA 1972, (1972) Ed, A.C. Strickland, Akademie-Verlag, Berlin, 450 pp.

60. Shettle, E.P. and Fenn, R.W., (1979) Models of the Aerosols of the Lower Atmosphere and the Effects of Humidity Variations on Their Optical Properties, AFGL-TR-79-0214, 17 September 1979. ADA085951
61. Johnson, R.W., Hering, W.S., Gordon, J.I., and Fitch, B.W. (1979) Preliminary Analysis and Modeling Based upon Project OPAQUE Profile and Surface Data, AFGL-TR-79-0285.
62. Huschke, R.E. (editor) (1959) Glossary of Meteorology, American Meteorological Society, Boston, MA, 638 pp.
63. Middleton, W.E.K. (1952) Vision Through the Atmosphere, University of Toronto Press, 250 pp.
64. Blifford, I.H., and Ringer, L.D. (1969) The Size and Number Distribution of Aerosols in the Continental Troposphere, J. Atmos. Sci. 26: 716-726.
65. Hoffman, R.J., Rosen, J.M., Pepin, T.J., and Pinnick, R.G. (1975) Stratospheric Aerosol Measurements I: Time Variations at Northern Latitudes, J. Atmos. Sci. 32: 1446-1456.
66. Elterman, et. al. (1969) Features of Tropospheric Dust, Appl. Opt. 8: 893-903.
67. Jursa, A.S., Scientific Editor, Handbook of Geophysics and the Space Environment (1985) AFGL Publication.
68. Hänel, G. (1976) The Properties of Atmospheric Aerosol Particles as Functions of the Relative Humidity at Thermodynamic Equilibrium with the Surrounding Air, in Advances in Geophysics, Vol 19 pp. 73-188, Edited by H.E. Landsberg, J. Mieghem, Academic Press, New York.
69. Hänel, G. (1972) Computation of the Extinction of Visible Radiation by Atmospheric Aerosol Particles as a Function of the Relative Humidity, Based upon Measured Properties, Aerosol Sci. 3: 377-386.

70. Hale, G.M., and Querry, M.R. (1973) Optical Constants of Water in the 200-nm to 200- $\mu$ m Wavelength Region, Appl. Opt. 12: 555-563.
71. Volz, F.E. (1972) IR Absorption by Aerosol Substances, JGR. 77: 1017-1031.
72. Volz, Frederic E. (1973) Infrared Optical Constants of Ammonium Sulfate, Sahara Dust, Volcanic Pumice, and Flyash, Appl. Opt. 12: 564-568.
73. Whitby, K.T., and Cantrell, B. (1975) Atmospheric Aerosols-Characteristics and Measurement, International Conf. on Environmental Sensing and Assessment, Vol. 2, Las Vegas, Nev., 14-19 sep 1975.
74. Twitty, J.T., and Weinman, J.A. (1971) Radiative Properties of Carbonaceous Aerosols, J. Appl. Meteor. 10: 725-731.
75. Junge, Christian E. (1963) Air Chemistry and Radioactivity, 382 pp. Academic Press, New York.
76. Junge, C. E. (1972) Our Knowledge of the Physico-Chemistry of Aerosols in the Undisturbed Marine Environment, J. Geophys. Res. 77: 5183-5200.
77. Volz, Frederic E. (1972) Infrared Refractive Index of Atmospheric Aerosol Substance, Appl. Opt. 11: 755-759.
78. Byers, H.R. (1959) General Meteorology, 540 pp., McGraw Hill, New York
79. Silverman, B.A., and Sprague, E.D. (1970) Airborne Measurement of In-Cloud Visibility, 271-276, Second National Conference on Weather Modification, Santa Barbara, CA, 6-9 April 1970, American Meteorological Society.
80. Dyanchenko, P.V. (1962) Experimental Application of the Method of Mathematical Statistics to Microstructural Fog and Cloud Research, Translated by A.I. Voyekova, Main Geophysical Observatory.
81. Longtin, D.R., Shettle, E.P., Hummel, J.R. and Pryce, J.D., (1988), A Wind Dependent Desert Aerosol Model: Radiative Properties, AFGL-TR-88-0112, ADA201951

82. Shettle, E. P. (1984) Optical and Radiative Properties of a Desert Aerosol Model, IRS '84: Current Problems in Atmospheric Radiation, G. Fiocco, Ed., A. Deepak Publishing, Hampton, VA, 74-77.
83. World Climate Research Programme (1983) Report of the Experts Meeting on Aerosols and Their Climatic Effects, A. Deepak and H. E. Gerber, eds. World Climate Programme Publication WCP-55, December 1983.
84. d'Almeida, G. and Schutz, L. (1983) Number, Mass and Volume Distributions of Mineral Aerosol and Soils of the Sahara, Climate and Appl. Meteor., 22: 233-243.
85. Patterson, E.M., and Gillette, D. A. (1977) Commonalities in Measured Size Distributions for Aerosols Having a Soil-Derived Component, J. Geophys. Res., 82: 2074-2082
86. Schutz, L. and Jaenicke, R. (1974) Particle Number and Mass Distributions Above 10 cm Radius in Sand and Aerosols of the Sahara Desert, J. Appl. Meteor., 13: 863-870.
87. Levin, Z., and Lindberg, J. A. (1979) Size Distribution, Chemical Composition, and Optical Properties of Urban and Desert Aerosols in Israel, J. Geophys. Res., 84: 6941-6950.
88. Kushelevsky, A., Shani G., and Haccoun A. (1983) Effect of Meteorologic Conditions on Total Suspended Particulate (TSP) Levels and Elemental Concentration of Aerosols in a Semi-Arid Zone, Beer-Sheva, Israel), Tellus, 35B: 55-64.
89. Cahill, T. A., Kusko, B. H., Ashbaugh, L. L., Barone, J. B., Eldred, R. A. and Walther, F. G. (1981) Regional and Local Determinations of Particulate Matter and Visibility in the Southwestern United States During June and July, 1979, Atmospheric Environment, 15: 2011-2016.
90. Annegarn, H. J., Van Greiken, R. E., Bibby, D. M. and Von Blotnitz., F. (1983) Background Aerosol Composition in the Namib Desert, Southwest Africa, Namibia, Atmospheric Environment, 17: 2045-2053.

91. Pinnick, R. G., Jennings, S. G., and Fernandez, G. (1987) Volatility of Aerosols in the Arid Southwestern United States, J. Atmos. Sci., 44: 562-576.
92. Levin, Z., Joseph, J. H. and Mekler, Y. (1980) Properties of Sharav (Khamsin) Dust: Comparison of Optical and Direct Sampling Data, J. Atmos. Sci., 37: 882-891.
93. Malm, W. C. and Johnson, C. E. (1984) Optical Characteristics of Fine and Coarse Particulates at Grand Canyon, Arizona, Atmospheric Environment, 18: 1231-1237.
94. Otterman, J., Fraser, R. S., and Bahethi, O. P. (1982) Characterization of Tropospheric Desert Aerosols at Solar Wavelengths by Multispectral Radiometry from Landsat, J. Geophys. Res., 87: 1270-1278.
95. Junge, C. and Jaenicke, R. (1971) New Results in Background Aerosols, Studies from the Atlantic Expedition of the R. V. Meteor, Spring 1969, Aerosol Science, 2: 305-314.
96. Savoie, D. L. and Prospero, J. M. (1977) Aerosol Concentration Statistics for the Northern Tropical Atlantic, J. Geophys. Res., 82: 5954-5964.
97. Schmidt, M., Specht, H. and Fabian, P. (1978) Aerosol Measurements at the Algarve Coast of Portugal, Tellus, 30: 449-457.
98. Ganor, E. and Mamane, Y. (1982) Transport of Saharan Dust Across the Eastern Mediterranean, Atmospheric Environment, 16: 581-587.
99. Chester, R., Sharples, E. J., Sanders, G. S. and Saydam, A. C. (1984) Saharan Dust Incursion Over the Tyrrhenian Sea, Atmospheric Environment, 18: 929-935.
100. Shaw, G. E. (1980) Transport of Asian Desert Aerosol to the Hawaiian Islands, J. Appl. Meteor., 19: 1254-1259.
101. Jaenicke, R., and Schutz, L. (1978) A Comprehensive Study of Physical and Chemical Properties of the Surface Aerosols in the Cape Verde Islands Region, J. Geophys. Res., 83: 3583-3598.



102. d'Almeida, G. A. and Jaenicke, R. (1981) The Size Distribution of Mineral Dust, J. Aerosol Sci., 12: 160-162.
103. Gillette, D. A., Blifford, Jr., I. H. and Fryrear, D. W. (1974) The influence of wind Velocity on the Size Distributions of Aerosols Generated by the Wind Erosion of Soils, J. Geophys. Res., 79: 4068-4075.
104. Gillette, D. A. (1978) Tests with a Portable Wind Tunnel for Determining Wind Erosion Threshold Velocities, Atmospheric Environment, 12: 2309-2313.
105. Gillette, D. A., Blifford, Jr., I. H. and Fenster, C. R. (1972) Measurements of Aerosol Size Distributions and Vertical Fluxes of Aerosols on Land Subject to Wind Erosion, J. Appl. Meteor., 11: 977-987.
106. Gillette, D. A. (1978) A Wind Tunnel Simulation of the Erosion of Soil: Effect of Soil Texture, Sandblasting, Wind Speed, and Soil Consolidation on Dust Production, I, Atmospheric Environment, 12: 1735-1743.
107. Reiter, E. R. (1971) Atmospheric Transport Processes Part 2: Chemical Tracers, U. S. Atomic 382 pp.
108. Volz, F. E. (1975) Distribution of Turbidity after the 1912 Katmai Eruption in Alaska, J. Geophys. Res. 80: 2643-2648.
109. Volz, F. E. (1975) Burden of Volcanic Dust and Nuclear Debris after Injection into the Stratosphere at 40°-58°N., J. Geophys. Res. 80: 2649-2652.
110. Rosen, J.M., Hofmann, D.J., and Laby, J. (1975) Stratospheric Measurements II: the Worldwide Distribution, J. Atmos. Sci. 32: 1457-1462.
111. Cunnold, D.M., Gray, C.R., and Merritt, D.C. (1973) Stratospheric Aerosol Layer Detection, J. Geophys. Res. 78: 920-931.
112. Pepin, T.J., (1977) Inversion of Solar Extinction Data from the Apollo-Soyuz Test Project Stratospheric Aerosol Measurement (ASTP/SAM) Experiment, pp. 529-554 in Inversion Methods in Atmospheric Remote Sounding. A workshop sponsored by Old

Dominion University and the NASA Langley Research Center, Hampton, VI, 15-17  
December 1976, NASA-CP-004.

113. Ivlev, L.S. (1967) Aerosol Model of the Atmosphere, Prob. Fiz. Atmos., No. 7, Leningrad, pp. 125-160, translated by Foreign Science and Technology Ctr., Dept of the Army, available from U.S. NTIS (AD 760-393).

114. Ivlev, L.S. (1969) Atmospheric Aerosol, pp. 28-42 in Radiation Characteristics of the Atmosphere and the Earth's Surface, Ed. K. Ya Kondratev, Amerind Publishing Co., New Delhi, available from U.S. NTIS (no. TT-71-58003).

115. Rozenberg, G.V. (1966) Twilight: A Study in Atmospheric Optics, Plenum Press, New York, NY, 358 pp.

116. Clemesha, B.R., and Nakamura, Y. (1972) Dust in the Upper Atmosphere, Nature 237: 328-329.

117. Poultney, S.K. (1972) Laser Radar Studies of Upper Atmosphere Dust Layers and the Relation of Temporary Increases in Dust to Cometary Micrometeoroid Streams, Space Research 12: 403-421.

118. Rossler, F. (1968) The Aerosol Layer in the Stratosphere, Space Research 8: 633-636.

119. Rossler, F. (1972) Aerosol Layers in the Atmosphere, Space Research 12: 423-431.

120. Fogle, G., and Haurwitz, B. (1972) Noctilucent Clouds, Space Sci. Rev. 6, 279-340.

121. WCP (1986) A preliminary Cloudless Standard Atmosphere for Radiation Computation, WCP-112, WMO/TD-NO 24, World Climate Research Programme, International Association of Meteorology and Atmospheric Physics/Radiation Commission.

122. Remsberg, E. E. (1971) Radiative Properties of Several Probable Constituents of

Atmospheric Aerosols, PhD. Thesis, Department of Meteorology, University of Wisconsin, Madison.

123. Remsberg, E. E. (1973) Stratospheric Aerosol Properties and their Effects on Infrared Radiation, J. Geophys. Res., 78: 1401-1407.
124. Palmer, K. F. and D. Williams (1975) Optical Constants of Sulfuric Acid; Application to the Clouds of Venus?, Applied Optics, 14: 208-219.
125. Volz, F. E. (1973) Infrared Optical Constants of Ammonium Sulfate, Sahara Dust, Volcanic Pumice and Flyash, Appl. Opt., 12: 564-568.
126. Pinkley, L. W. and Williams, D. (1976) The Infrared Optical Constants of Sulfuric Acid at 250 K, J. Opt. Soc. Am., 66: 122-124.
127. Reiter, R., Jager, H., Carmuth, W., and Funk, W. (1979) The Stratospheric Aerosol Layer Observed by Lidar since October 1976. A Contribution to the Problem of Hemispheric Climate, Arch. Met. Geoph. Biokl., Ser. B, 27: 121-149.
128. D'Altorio, A., Viconti, G., and Fiocco, G. (1981) Lidar Detection of Volcanic Aerosols in the Atmosphere following the Mount St. Helen Eruption, Geophys. Res. Let., 8: 63-65.
129. Clemesha, B. R. and Simmonich, D. M. (1978) Stratospheric Dust Measurements, 1970-1977, J. Geophys. Res., 83: 2403-2408.
130. Iwasaka, Y., Hayashida, S., and Ono, A. (1983) Increasing Backscattered Light from the Stratospheric Aerosol Layer Radar after Mt. El Chichon Eruption, Laser Radar Measurement at Nagoya (35°N, 137°E), Geophys. Res. Let., 6: 440-442.
131. Hirono, M., Fujiwara, M., Shibata, T., and Kugumiya, N. (1981) Lidar Observations of Mt. St. Helens in May 1980, Geophys. Res. Let., 9: 1019-1022.
132. McCormick, M. P., Swissler, T. J. (1983) Stratospheric Aerosol Mass and Latitudinal Distribution of the El Chicon Eruption Cloud for October 1982, Geophys. Res. Let., 9: 877-880.

133. Clemesha, B. R. and Simmonich, D. M. (1983) Lidar Observations of the El Chicon Dust Cloud at 23°S, Geophys. Res. Let., 10: 321-324.
134. Hirono, M., Fujiwara, M., and Shibata, T. (1981) Lidar Observation of Sudden Increases of Aerosols in the Stratosphere Caused by Volcanic Injections: I. Soufriere 1979 event, J. Atmos. Terr. Phy., 43: 1127-1131.
135. Hirono, M., Fujiwara, M., and Shibata, T. (1982) Lidar Observation of Sudden Increases of Aerosols in the Stratosphere Caused by Volcanic Injections: II. Sierra Negra Event, J. Atmos. Terr. Phy., 44: 811-818.
136. Hirono, M. and Shibata, T. (1983) Enormous Increase of Stratospheric Aerosols over Fukuoro due to Volcanic Eruption of El Chicon in 1982, Geophys. Res. Let. 10: 152-154.
137. D'Altorio, A. and Visconti, G. (1983) Lidar Observations of Dust Layers' Transience in the Stratosphere Following the El Chichon Volcanic Eruption, Geophys. Res. Let., 10: 27-30.
138. Rosen, J. M., Hofmann, D. J., and Laby, J., (1975) Stratospheric Aerosol Measurements, II, Worldwide Distribution, J. Atmos. Sci., 32: 1457-1462.
139. Hofmann, D. J., and Rosen, J. M., (1982) Balloon-borne Observations of Stratospheric Aerosol and Condensation Nuclei During the Year Following the Mt. St. Helens Eruption, J. Geophys. Res., 87: 11039-11061.
140. Hofmann, D. J., and Rosen, J. M., (1983) Stratospheric Sulfuric Acid Fraction and Mass Estimate for the 1982 Volcanic Eruption at El Chichon, Geophys. Res. Let., 10: 313-316.
141. Hofmann, D. J., and Rosen, J. M., (1984) On the Temporal Variation of Stratospheric Aerosol Size and Mass During the First 18 Months Following the 1982 Eruption of El Chichon, J. Geophys. Res., 89: 4883-4890.
142. Pinnick, R. G., Rosen, J. M., and Hofmann, D. J., (1976) Stratospheric Aerosol

Measurements, III, Optical Model Measurements, J. Atmos. Sci., 33: 304-314.

143. Oberbeck, V. R., Farlow, N. H., Fong, W., Snetsinger, K. G., Ferry, G. V. Ferry and Hayes, D. M., (1982) Mount St. Helens Aerosol Evolution, Geophys. Res. Let., 9: 1089-1092.

144. Knollenberg, R. G., and Huffmann, D., (1983) Measurements of the Aerosol SizeDistributions in the El Chichon Cloud, Geophys. Res. Let., 10: 1025-1028.

145. Oberbeck, V. R., Danielsen, E. F., Snetsinger, K. G., Ferry, G. V., Fong, W., Hayes, D. M., (1983) Effect of the Eruption of El Chichon on Stratospheric Aerosol Size and Composition, Geophys. Res. Let., 10: 1021-1024.

146. Wilson, J. C., Blackshear, E. D., and Hyun, J. H., (1983) Changes in the sub-2.5 micron Diameter Aerosol Observed at 20 km Altitude after the Eruption of El Chichon, Geophys. Res. Let., 10: 1029-1032.

147. Witteborn, F. C., O'Brien, K., Crean, H. W., Pollack, J. B., and Bilski, K. H., (1983) Spectroscopic Measurements of the 8- to 13- Micrometer Transmission of the Upper Atmosphere Following the El Chichon Eruptions, Geophys. Res. Let., 10: 1009-1012.

148. Dutton, E., and DeLuisi, J., (1983) Extinction of Solar Radiation by the El Chichon Dust Cloud, Geophys. Res. Let., 10: 1013-1016.

149. Woods, D. C., and Chuan, R. L., (1983) Size-Specific Compositions of Aerosols in the El Chichon Volcanic Cloud, Geophys. Res. Let., 10: 1041-1044.

150. Patterson, E. M. (1981) Measurements of the Imaginary Part of the Refractive index Between 300 and 700 nanometers for Mount St. Helens Ash, Science, 211: 36-838.

151. Patterson, E. M., Pollard, C. O., and Galindo, I., (1983) Optical Properties of the Ash from El Chichon, Geophys. Res. Let., 10: 317-320.

152. Mossop, S.C., (1964) Volcanic Dust Collected at an Altitude of 20 km, Nature 203: 824-827.

153. Newkirk, G. Jr., and Eddy, J.A. (1964) Light Scattering by Particles in the Upper Atmosphere, J. Atmos. Sci. 21: 35-60.
154. Rosen, J.M. (1969) Stratospheric Dust and its Relationship to the Meteoric Influx Space Sci. Rev. 9: 58-89.
155. Poultney, S. K. (1974) Times, Locations and Significance of Cometary Micro Meteoroid Influxes in the Earth's Atmosphere, Space Res. 14: 707-708.
156. Divari, N.B., Zaginalio, Yu. I., and Koval'chuk, L.V. (1973) Meteoric Dust in the Upper Atmosphere, Solar System Res. 7: 191-196. (Translated from Astronomicheskii Vestnik 7: 223-230).
157. Shettle, E. P., and Volz, F. E. (1976) Optical Constants for a Meteoric Dust Aerosol Model, in Atmospheric Aerosols: Their Optical Properties and Effects, a Topical Meeting on Atmospheric Aerosols Sponsored by Optical Society of America and NASA Langley Research Center, Williamsburg, Virginia, 13-15 December 1976, NASA CP-2004.
158. Gaffey, M.J. (1974) A Systematic Study of the Spectral Reflectivity Characteristics of the Meteorite Classes with Applications to the Interpretation of Asteroid Spectra for Mineralogical and Petrological Information, Ph. D Thesis, M.I.T.
159. Farlow, N.H. and Ferry, G.V. (1972) Cosmic Dust in the Mesosphere Space Res. 2: 369-380.
160. Kornblum, J.J. (1969) Micro-meteoroid Interaction with the Atmosphere J. Geophys. Res. 74: 1893-1907.
161. Kornblum, J.J. (1969) Concentration and Collection of Meteoric Dust in the Atmosphere, J. Geophys. Res. 74: 1908-1919.
162. National Aeronautics and Space Administration (1969) Meteoroid Environment Model, 1969 (Near Earth to Lunar Surface), NASA SP-8013 (March 1969).

163. Soberman, R. K., and Hemenway C. L. (1965) Meteoric Dust in the Upper Atmosphere, J. Geophys. Res 70: 4943-4949.
164. Lindblad, B.A., Arinder, G., and Wiesel, T. (1973) Continued Rocket Observations of Micro-Meteorites, Space Res. 13: 1113-1120.
165. Filippov, V. L., and Mirumyants, S. O. (1972) Aerosol Extinction of Visible and Infrared Radiation as a Function of Air Humidity, Izv. Atmos. Oceanic Phvs. 8: 571-574.
166. Kasten, F. (1968) Falling Speed of Aerosol Particles, J. Appl. Meteor. 7: 944-947.
167. Diermendjian, D. (1973) On Volcanic and Other Turbidity Anomalies, Advances in Geophys. 16: 267-296.
168. Fitzgerald, J. W. (1978) On the Growth of Aerosol Particles With Relative Humidity, NRL Memo Rpt. 3847.
169. Hänel, G. (1971) New Results Concerning the Dependence of Visibility on Relative Humidity and their Significance in a Model for Visibility Forecasts, Contrib. Atmos. Phys. 44: 137-167.
170. Larson, R.E., and Bressan, D.J. (1980) Air Mass Characteristics over Coastal Areas as Determined by Radon Measurements, Preprint of Second Conference on Coastal Meteorology, 30 January - 1 February 1980, Los Angeles, CA.; published by A. M. S., Boston, Mass.
171. Heaps, M. G. (1982) A Vertical Structure Algorithm for Low Visibility/Low Stratus Conditions, ASL-TR-0111, US Army Atmospheric Sciences Laboratory, White Sands Missile Range, N.M.
172. Heaps, M. G. , and Johnson, R. D. (1983) An Empirical Algorithm for the Vertical Structure of Atmospheric Extinction, ASL-TR-0142, US Army Atmospheric Sciences Laboratory, White Sands Missile Range, N.M.

173. Lindberg, J.D. (1982) Early Wintertime Fog and Haze. Report on Project Meppen 80, ASL-TR-0108, US Army Atmospheric Sciences Laboratory, White Sands Missile Range, N.M.
174. Hoihjelle, D. L., Pinnick, R. G., Lindberg, J. D., Loveland, J R. B., Stenmark, E. B., and Petracca, C. J. (1976) Balloon-borne Aerosol Particle Counter Measurement Made in Wintertime at Grafenwohr, West Germany ECOM-DR-76-3, US Army Atmospheric Sciences Laboratory, White Sands Missile Range, N.M.
175. Pinnick, R. G., Hoihjelle, D. L., Fernandez, G., Stenmark, E. B., Lindberg, J. D., Jennings, S. G., and Hoidale, G. B. (1978) Vertical Structure in Atmospheric Fog and Haze and Its Effect on IR Extinction, ASL-TR-0010, US Army Atmospheric Sciences Laboratory, White Sands Missile Range, N.M.
176. Duncan, L D, Lindberg, J. D., and Loveland, R. B. (1980) An Empirical Model of the Vertical Structure of German Fogs, ASL-TR-0071, US Army Atmospheric Sciences Laboratory, White Sands Missile Range, N.M.
177. Marshall, J.S., and Palmer, W.M.K. (1948) The Distribution of Raindrops with Size, J. Meteorol. 5: 165-166.
178. Anderson, G.P., Clough, S.A., Kneizys, F.X., Shettle, E.P., Abreu, L.W. Chetwynd, J.H. and Hall, L.A. (1988) FASCOD3: Spectral Simulation, I.R.S. 1988 International Symposium, Lille, France, pg. 372-375.
179. Shettle, E. P., and Robert W. Fenn, (1979) Models for the Aerosols of the Lower Atmosphere and the Effects of Humidity Variations on Their Optical Properties, AFGL-TR-79-0214, ADA085951
180. Joss, J., and Waldvogel, A. (1969) Raindrop Size Distributions and Sampling Size Errors, J. Atmos. Sci. 26: 566-569.
181. Sekhon, R. S., and Srivastava, R. C. (1971) Doppler Radar Observations of Drop-Size Distributions in a Thunderstorm, J. Atmos. Sci. 28: 983-984.



182. Berry, F.A., Bollary, E., and Beers, N.R. (1945) Handbook of Meteorology, Chapter 11, McGraw Hill.
183. Mason, B.J. (1971) The Physics of Clouds, Clarendon Press, Oxford.
184. Borovikov, A.M., Khrgian, A.K.H., et. al. (1963) Cloud Physics, US Dept of Commerce, Office of Technical Services.
185. Carrier, L.W., Cato, G.A., and von Essen, K.J. (1967) The Backscatter and Extinction of Visible and Infrared Radiation by Selected Major Cloud Models, App. Optics 6: 1209-1216.
186. Luke, J.D. (1968) Penetrability of Haze, Fogs, Clouds and Precipitation by Radiant Energy over the Spectral Range 0.1 micron to 10 centimeters, NAVWAG Study 61, AD A847658.
187. Diem, M. (1948) Messurngen der Grosser von Wolkenelementen II, Meteorologische Rundeschen 9/10: 261-273.
188. Weickman, H.K. and Aufra Kampe, H.J. (1953) Physical Properties of Cumulus Clouds, J. Meteor. 16: 204-211.
189. Durbin, W. (1959) Droplet Sampling in Cumulus Clouds, Tellus 7: 202-215.
190. Gates, D., and Shaw, C. (1960) Infrared Transmission of Clouds, J. Opt. Sci. Am. 50: 876-882.
191. Squires, P. and Twomey, S. (1960) The Relation Between Cloud Droplet Spectral and the Spectrum of Cloud Nuclei, Amer. Geophys. Uni. 15: 211-219.
192. Silverman, B.A. and Sprague, E.D. (1970) Airborne Measurements of In-Cloud Visibility, Natl. Conf. on Weather Modification of the A.M.S., April 6-9, Santa Barbara, CA.
193. Blau, H.H., Fowler, M.G., Chang, D.T., and Ryan, R.T. (1972) Cloud Microstructure Studies, ERT P-375 Final Report NASA Contract NAS 5-21696.

194. Mie, G. (1908) Beitrage zur Optik Truber Median, Speziell Kollodaler Metallosungen, Ann der Ohys. **25**: 377-445.
195. Ray, P.S. (1972) Broadband Complex Refractive Indices of Ice and Water, App. Opt. **11**: 1836-1844.
196. World Meteorological Organization (1956) International Cloud Atlas, vol. 1, Geneva, Switzerland.
197. Rothman, L.S., Rinsland, C.P., Goldman, A., Massie, S.T., Edwards, D.P., Flaud, J.-M., Perrin, A., Dana, V., Mandin, J.-Y., McCann, A., Gamache, R.R., Wattson, R.B., Yoshino, K., Chance, K.V., Jucks, K.W., Brown, L.R., Nemtchinov, V., and Varanasi, P., The HITRAN Molecular Database: Editions of 1996, J. Quant. Spectrosc. Radiat. Transfer, in publication
198. Wattson, O.B., and Rothman, L.S., A Direct Numerical Diagonalization: Wave of the Future, JQSRT **48**, 763-780 (1992).
199. Toth, N.A., J.Opt.Soc.Am. **B8**, 2236 (1991).
200. Giver, T.P., Brown, L.R., Wattson, R.B., Spencer, M.N., and Chackerian, C. Jr., Proceedings of the Fiftieth International Symposium on Molecular Spectroscopy, Ohio State Univ., Columbus, Ohio (June 12-16, 1995), p. 311.
201. Giver, A., Chackerian, C., Jr., Spencer, M.N., Brown, L.R., and Wattson, R.B., J.Molec.Spectrosc. **175**, 104 (1996).
202. Rinsland, R.P., Smith, M.A.H., Malathy Devi, V., Perrin, A., Flaud, J.-M., and Camy-Peyret, C. J.molec.Spectrosc. **149**, 474 (1991).
203. Flaud, S.-M., Camy-Peyret, C., Perrin, A., Malathy Devi, V., Barbe, A., Bouazza, S., Plateaux, J.J., Rinsland, C.P., Smith, M.A.H., and Goldman, A., J.molec.Spectrosc. **160**, 378 (1993).

204. Farrenq, O., Guelachvili, G., Sauval, A.J., Grevesse, N., and Farmer, C.B., Improved Dunham Coefficients for CO from Infrared Solar Lines of High Rotational Excitation, J.Molec.Spectrosc. **149**, 375-390 (1991).
205. Chackerian, F., and Tipping, R.H., A Vibration-Rotational and Rotational Intensities for CO Isotopes, J.Molec.Spectrosc. **99**, 431-449 (1983).
206. Tarrago, T., Restelli, G., and Cappellani, J.Molec.Spectrosc. **129**, 326-332 (1988).
207. Ouardi, W., Hilico, J.C., O., Loëte, M., and Brown, L.R., The hot bands of methane between 5 and 10 mm, J.Molec.Spectrosc. **180**, 311-322 (1996).
208. Gamache, A., Goldman, A., and Rothman, L.S., AN Improved Spectral Parameters for the Three Most Abundant Isotopomers of the Oxygen Molecule, @ in press, JQSRT (1997).
209. Rouillé, R., Millot, G., Saint-Loup, R., and Berger, H., J.Molec.Spectrosc. **154**, 372 (1992).
210. Ritter, E.J., and Wilkerson, T.D., J.Molec.Spectrosc. **121**, 1 (1987).
211. Dana, I., Mandin, J.-Y., et. al., J.Molec.Spectrosc. **165**, 525-540 (1994).
212. Lafferty, S.J., Pine, A.S., et. al., The  $n_1+n_3$  and  $2n_1+n_3$  band systems of SO<sub>2</sub>: line positions and intensities, J.Molec.Spectrosc. **176**, 280-286 (1996).
213. Chu, T.M., Wetzel, S.J., et. al., Line intensities for the 8mm bands of SO<sub>2</sub>, @ Submitted for publication in J.Molec.Spectrosc. (1997).
214. Perrin, H., Flaud, J.-M., et. al., The interacting bands of NO<sub>2</sub>: line positions and intensities, J.Molec.Spectrosc. **154**, 391-406 (1992).
215. Malathi Devi, E., Fridovitch, B., et. al., Tunable diode laser spectroscopy of NO<sub>2</sub> at 6.2  $\mu\text{m}$ , J.Molec.Spectrosc. **93**, 179-195 (1982).

216. Kleiner, B., Tarrago, G., and Brown, L.R., Analysis of  $3n_2$  and  $n_2+n_4$  of  $^{14}\text{NH}_3$  near 4 mm, J.Molec.Spectrosc. **173**, 120-145 (1995).
217. Guelachvili, E., Abdulah, A., et. al., J.Molec.Spectrosc. **133**, 345 (1989).
218. Sirota, S.M., Weber, M., et. al.,  $\text{HNO}_3$ : Absolute line intensities for the  $n_6$  fundamental, J.Molec.Spectrosc. in press (1997).
219. Coudert, T.H., and Perrin, A., Accounting for the torsional splitting in the  $n_5$  and  $2n_9$  bands of nitric acid, J. Molec., Spectrosc., **172**, 352-368 (1995)
220. Ludwig, C.B., Malkmus, W., Reardon, J.E., and Thomson, J.A.L., Handbook of Infrared Radiation from Combustion Gases, NASA Report SP-3080 (1980).
221. Curtis, A.R., Q. J. R. Meteorol. Soc., **78**: 165 (1952)
222. Godson, W.L., J. Meteorol., **12**: 123 (1955)
223. Anding, D. Band Model Methods for Computing Atmospheric Slant-Path Molecular Absorption, Rpt. No. 7142-12-T, Willow Run Laboratories, Institute of Science and Technology, University of Michigan, Ann Arbor, MI (1967)
224. LaRocca, A.J., and Turner, R.E., Atmospheric Transmittance and Radiance: Methods of Calculation, Rpt. No. 107600-10-T, Environmental Research Institute of Michigan, Ann Arbor, MI (June 1975)
225. Penner, S.S., Quantitative Molecular Spectroscopy and Gas Emissivities, (Addison Wesley, London, 1959).
226. Sharma, R.D., Sundberg, R.L., Bernstein, L.S., Duff, J.W., Gruninger, J.H., Robertson, D.C. and Healey, R.J. (1991) Description of SHARC-2, The Strategic High Altitude Atmospheric Radiance Code, PL-TR-91-2071, ADA239008
227. Pierluissi, J.H., Tomiyama, K., and Gomex, R.B., (1979) Analysis of the LOWTRAN Transmission Functions, Appl. Opt. **18**: 1607.

228. Gruenzel, R.R., (1978) Mathematical Expressions for Molecular Absorption in LOWTRAN 3B, Appl. Opt. 17: 2591.
229. Pierluissi, J.H., and Gomez, R.B., (1984) Study of Transmittance Models for the 15 micron-CO<sub>2</sub> Band, Proceedings of the Sixth Conference on Aerospace and Aeronautical Meteorology (American Meteorological Society, Boston, Ma.
230. Elsasser, W.M., (1942) Heat Transfer by Infrared Radiation in the Atmosphere Harvard Meteorological Studies 6 (Howard U.P., Cambridge, Ma.).
231. Goody, R.M., (1952) A Statistical Model for Water Vapor Absorption, Q.J.R. Meteorological Society, 78: 165.
232. Smith, W.L., (1969) Polynomial Representation of Carbon Dioxide and Water Vapor Transmission, NESC-47 (Natl. Environ. Sat. Center, Washington, D.C.
233. Valley, S.L., (1965) Handbook of Geophysics and Space Environments, (McGraw-Hill, New York, NY).
234. Rothman, L.S. (1981) AFGL Atmospheric Line Parameters Compilation: 1980 Version, Appl. Opt. 20: 791.
235. Rothman, L.S., Goldman, A., Gillis, J.R., Gamache, R.R., Pickett, H.M., Poynter, R.L., Husson, N., and Chedin, A. (1983b), AFGL Trace Gas Compilation: 1982 Version, Appl. Opt., 22: 1616-1627.
236. Burch, et al., (1962) Infrared Absorption by Carbon Dioxide, Water Vapor and Minor Atmospheric Constituents, AFCRL-TR-62-698.
237. Burch, D.E., et al., (1975) Infrared Absorption by H<sub>2</sub>O, NO<sub>2</sub> and N<sub>2</sub>O<sub>4</sub>, AFCRL-TR-75-0420, (Ad A019686).
238. France, W.L., Williams, D., (1966) Total Absorptance of Ammonia in the Infrared, J. Opt. Soc. Am. 56: 70.

239. Ford, D.L., and Shaw, J.H., (1965) Total Absorptance of the NO Fundamental Band, Appl. Opt. 4: 1114.
240. Burch, D.E., and Gryvnak, D.A., (1976) Strengths, Widths and Shapes of the Oxygen Lines Near 7600 Angstroms, U-4076, Philco-Ford Corp., Newport Beach, CA.
241. Burch, D.E., Gryvnak, D.A., and Williams, D., (1962) Total Absorptance of Carbon Dioxide in the Infrared, Appl. Opt. 1: 759.
242. Burch, D.E., Gryvnak, D.A., and Petty, R.R., (1968) Absorption of Infrared Radiation by CO<sub>2</sub> and H<sub>2</sub>O, II. Absorption by CO Between 8000 and 10000 cm<sup>-1</sup> (1-1.25 microns), J. Opt. Soc. of Am. 158: 335.
243. Burch, D.E. et al., (1969) Absorption of Infrared Radiant Energy by CO<sub>2</sub> and H<sub>2</sub>O, IV. Shapes of Collisioned-Broadened CO<sub>2</sub> Lines, J. Opt. Soc. of Am. 59: 267.
244. Burch, D.E., Pembroke, J.D., and Gryvnak, D.A., (1971) Absorption and Emission by SO Between 1050 and 1800 cm<sup>-1</sup> (9.5-7 m), U-4947, Philco-Ford Corp., Newport Beach, Ca.
245. Pierluissi, J.H., and Maragoudakis, C.E., (1984) Molecular Transmission Band Models for the Uniformly Mixed and the Trace Gases, AFGL-TR-84-0320, (NTIS AD A160442).
246. Goldman A., Kyle, T.G., and Bonomo, F.W. (1971) Statistical Band Model Parameters and Integrated Intensities for the 5.9-μ, 7.5-μ, and 11.3-μ bands of HNO<sub>3</sub> Vapor, Appl. Opt. 1: 65.
247. Reddy, S.R., and Cho, C.W. (1965) Canada J. Physics 43: 2331.
248. Shapiro, M.M., and Gush, H.P. (1966) Canada J. Physics 44: 949.
249. McClatchey, R.A., Fenn, R.W., Selby, J.E.A., Volz, F.E., and Garing, J.S. (1972) Optical Properties of the Atmosphere (Third Edition), AFCRL-72-0497 (NTIS AD A753075).

250. Lewis, B.R., Berzins, L., and Carver, J.H. Oscillator strengths for the Schumann-Runge bands of O<sub>2</sub>, JQSRT 36, 209-232 (1986).
251. Lewis, B.R., Berzins, L., Dedman, C.J., Scholz, T.T., and Carver, J.H. Pressure broadening in the Schumann-Runge system of molecular oxygen, JQSRT 39, 271-282 (1988).
252. Minschwaner, K., Anderson, G.P., Hall, L.A., and Yoshino, K., Polynomial coefficients for calculating O<sub>2</sub> Schumann-Runge cross sections at 0.5 cm<sup>-1</sup> resolution, J.Geophys.Res. 97, 10103-10108 (1992).
253. Yoshino, K., Freeman, D.E., Esmond, J.R., and Parkinson, W.H. High resolution absorption cross section measurements and band oscillator strengths of the (1,0)-(12,0) Schumann-Runge bands of O<sub>2</sub>, Planet.Space Sci. 31, 339-353 (1983).
254. Yoshino, K., Esmond, J.R., Cheung, A.S., Freeman, D.E., and Parkinson, W.H., AHigh Resolution Absorption Cross Sections in the Transmission Window Region of the Schumann-Runge Bands and Herzberg continuum of O<sub>2</sub>, Planet. Space Sci. 40, 185-192 (1992).
255. Watanabe, K., (1958) Ultraviolet Absorption Processes in the Upper Atmosphere, Advances in Geophysics 5, 153-221.
256. Frederick, J.E., (1982) Solar Irradiance in the Stratosphere: Implications for the Herzberg Continuum Absorption of O<sub>2</sub>, Geophys. Res. Lett. 9, 461-464.
257. Anderson, G.P. and Hall, L.A. (1983) Attenuation of Solar Irradiance in the Stratosphere: Spectrometer Measurements Between 191 and 207 nm, J. Geophys. Res., 88, 6801-6806.
258. Anderson, G.P. and Hall, L.A. (1989) Solar Irradiance Between 2000 and 3100Å With Spectral Band Pass of 1Å, J. Geophys. Res. 94, 6435-6441.

259. Cann, M.W.P., Shin, J.B., and Nicholls, R.W. (1984) Oxygen Absorption in the Spectral Range 180-300nm for Temperatures to 3000K and Pressures to 50 Atmospheres, Can. J. Phys., **62**, 1738-1751.
260. Trakhovsky, E.A., Ben-Shalom, A., Oppenheim, U.P., Devir, A.D., Balfour, L.S., and Engel, M. (1989) Contribution of Oxygen to Attenuation in the Solar Blind UV Spectral Region, Appl. Opt. **28**, 1588-1591.
261. Yoshino, K., Freeman, D.E., and Parkinson, W.H., (1983) High Resolution Absorption Cross Section Measurements and Band Oscillator Strengths of the (1-0)-(12-0) Schumann-Runge Bands of O<sub>2</sub>, Planet. Space Sci., **31**, 339-353.
262. Anderson, G.P. and Hall, L.A. (1986) Stratospheric Determination of O<sub>2</sub> Cross Sections and Photodissociation Rate Coefficients: 191-215nm, J. Geophys. Res. **91**, 14509-14514.
263. Steinfeld, J.I., Adler-Golden, S.M., and Gallagher, J.W., (1987) Critical Survey of Data on the Spectroscopy and Kinetics of Ozone in the Mesosphere and Thermosphere, J. Phys. Chem. Ref. Data, **16**, 911-942.
264. Katayama, D.H. (1979) New Vibrational Quantum Number Assignments for the UV Absorption Bands of Ozone Based on the Isotope Effect, J. Chem. Phys. **71**, 815-820.
265. Cacciani, M., diSarra, A., Fiocco, G., and Amoruso, A. (1989) Absolute Determination of the Cross Sections of Ozone in the Wavelength Region 339-355nm at Temperatures 220-293K, J. Geophys. Res. **94**, 8485-8490.
266. Cornette, W.M. (1992) Robust Algorithm for Correcting the Layer Problem in LOWTRAN, Appl. Opt. **31**, 5767.
267. Wiscombe, W.J. (1976) Extension of the Doubling Method to Inhomogenous Sources, J. Quant. Spectrosc. Radiat. Transfer **16**, 477.
268. Ridgway, W.L., Harshvardan, and Arking, A. (1991) Computation of Atmospheric Cooling Rates by Exact and Approximate Methods, J. Geophys. Res. **96**, 8969.



269. Clough, S.A., Iacono, M.J., and Moncet, J.-L. (1992) Line-by-Line Calculations of Atmospheric Fluxes and Cooling Rates: Application to Water Vapor, J. Geophys. Res. 97, 15761.
270. Frhlich, C. (1983) Data on Total and Spectral Solar Irradiance: Comments, Appl. Opt. 22: 3928.
271. Ridgeway, W.L., Moose, R.A., and Cogley, A.C. (1982) Single and Multiple Scattered Radiation, AFGL-TR-82-0299, (NTIS AD A126323).
272. Turner, R.E., et al (1975) Natural and Artificial Illumination in Optically Thick Atmospheres, Environmental Research Institute of Michigan, Report No. 108300-4-F
273. Condrón, T.P., Lovett, J.J., Barnes, W.H., Marcotte, L., and Nadile, R. (1968) Gemini 7 Lunar Measurements, AFCRL-68--0438, AD A678099.
274. Lane, A.P., and Irvine, W.M. (1973) Astron. J. 78.
275. Bullrich, K. (1948) Ber. Deutsch. Wettered, U.S. Zone No. 4.
276. Sharma, S. (1980) An Accurate and Computationally Fast Formulation for Radiative Fields and Heat Transfer in General, Plane-Parallel, Non-Grey Media With Anisotropic Scattering, PhD Thesis, University of Illinois at Chicago
277. Shettle, E.P., Turner, V.D., and Abreu, L.W., (1983) Angular Scattering Properties of the Atmospheric Aerosols, Fifth Conference on Atmospheric Radiation, October 31-November 4, Baltimore, MD, A.M.S.
278. Henyey, L.G., and Greenstein, J.L. (1941) Diffuse Radiation in the Galaxy, Astrophys. J. 93:70-83
279. Kasten, F. (1968) Rayleigh-Cabannes Streuung in Trockener Luft Unter Berücksichtigung Neuerer Depolarisations-Messungen, Optik, 27: 155-166.
280. Young, A.T. (1980) Revised Depolarization Corrections for Atmospheric Extinction, Appl. Opt. 19: 3427-3428.

281. Ben-Shalom, A., Barzilia, B., Cabib, D., Devir, A.D., Lipson, S.G. and Oppenheim U.P. (1980) Appl. Opt. 19: 6, 838.
282. Isaacs, R.G. and Özkaynak (1980) Uncertainties Associated with the Implementation of Radiative Transfer Theory within Visibility Models, Second Joint Conference on Applications of Air Pollution Meteorology, New Orleans, LA, 24-27 March 1980, 362-369. A.M.S., Boston, MA.
283. Dave, J.V. (1981) Transfer of Visible Radiation in the Atmosphere, Atmos. Env., 15: 10/11, 1805-1820.
284. Stephens, G. (1984) The Parameterization of Radiation for Numerical Weather Prediction and Climate Models, Mon. Weather Rev. 112: 826-867.
285. Wiscombe, W.J. and Grams, G.W. (1976) The Backscattered Fraction in Two-Stream Approximations, J. Atmos. Sci. 33: 2440-2451.
286. Meador, W.E. and Weaver, W.R. (1980) Two-Stream Approximations to Radiative Transfer in Planetary Atmospheres: A Unified Description of Existing Methods and a New Improvement, J. Atmos. Sci. 37: 630-643.
287. Arking, A. and Grossman K. (1972) The Influence of Line shape and Band Structure on Temperatures in Planetary Atmospheres, J. Atmos. Sci. 29: 937.
288. Wang, W.-C. and Ryan, P.B. (1983) Overlapping Effect of Atmospheric H<sub>2</sub>O, CO<sub>2</sub> and O<sub>3</sub> on the CO<sub>2</sub> Radiative Effect, Tellus, 35B: 81-91.
289. Wiscombe, W.J. and Evans, J.W. (1977) Exponential-Sum Fitting of Radiative Transmission Functions, J. Comput. Phys. 24: 416-444.
290. Bakan, S., Koepke, P. and Quenzel, H. (1978) Radiation Calculations in Absorption Bands: Comparison of Exponential Series and Path Length Distribution Method, Beit. Physics der. Atmos. 51: 28-30.

291. Lacis, A.A., Wang, W.-C. and Hansen, J.E. (1979) Correlated k-Distribution Method for Radiative Transfer in Climate Models: Application to Effect of Cirrus Cloud on Climate, NASA Publ. 2076, E.R. Kreins, Ed., 416 pp.
292. Yamamoto, G., Tanaka, M. and Asano, S. (1970) Radiative Transfer in Water Clouds in the Infrared Region, J. Atmos. Sci. 27: 282-292.
293. Yamamoto, G., Tanaka, M. and Asano, S. (1971) Radiative Heat Transfer in Water Clouds in the Infrared Radiative, J. Quant. Spectrosc. Radiat. Trans. 11: 697-708.
294. Hansen, J.E., Lacis, A.A., Lee, P. and Wang, W.-C., (1980) Climatic Effects of Atmospheric Aerosol, Aerosols: Anthropogenic and Natural Sources and Transport, Ann. N.Y. Acad. Sci. 338: 575-587.
295. Theriault, J.-M., Anderson, G.P., Chetwynd, J.H., Qu, Y., Murphy, E., Turner, V., Cloutier, M., and Smith, A. (1993) Retrieval of Tropospheric Profiles from IR Emission Spectra: Investigations with the Double Beam Interferometer Sounder (DBIS), Optical Remote Sensing of the Atmos. Tech. Digest 5, 78.
296. Moncet, J.-L. (1993) Atmospheric and Environmental Research Inc., Private Communication.
297. Rodgers, C.D. (1987) A General Error Analysis for Profile Retrieval, Advances in Remote Sensing Retrieval Methods, pg. 285.
298. Anderson, G.P., Hall, L.A., Minschwaner, K., Yoshino, K., Betchley, C., and Conant, J.A. (1992) Ultraviolet O<sub>2</sub> Transmittance: AURIC Implementation, Proc. of the Soc. Photo. Opt. Instrum. Eng., 1764, 108.
299. Link, R., Strickland, D.J. and Daniell, R.E., (1992) AURIC Airglow Modules: Phase 1 Development and Application, Proc. of the Soc. Photo. Opt. Instrum. Eng., 1764, 132.
300. Anderson, G.P. (1994) MOSART (Moderate Spectral Atmospheric Radiance Transmittance Code), combining MODTRAN 2 and APART 7, under development by PL/GPOS.

301. Cornette, W.M., (1990) Atmospheric Propagation and Radiative Transfer (APART) Computer Code (Version 7.0), R-075-90, Photon Research Assoc., San Diego, CA.

302. Sharma, R.D., Sundberg, R.L., Bernstein, L.S., Healey, R.J., Gruninger, J.H., Duff, J.W. and Robertson, D.C. (1991) Description of SHARC-2, The Strategic High-Altitude Atmospheric Radiance Code, PL-TR-91-2071. ADA239008

303. SAMM (SHARC and MODTRAN Merged), (1994), Under Development by PL/GPOS; POC: R.D. Sharma.

304. PLEXUS, an Umbrella Architecture for PL/GP Radiance and Background Codes, (1994) Under Development by PL/GPOC; POC: F.O. Clark.

## Appendix A MODTRAN 3 User Instructions

Prepared for:

Phillips Laboratory, Geophysics Directorate  
PL/GPOS  
29 Randolph Road  
Hanscom AFB, MA 01731-3010

**Under Contract**  
**Ms. Gail Anderson Technical Representatives**

Prepared by:

Spectral Science, Incorporated  
99 South Bedford Street #7  
Burlington, MA 01803-5169

Tel: (USA)-617-273-4770 Fax: (USA)-617-270-1161

This description is based on Section 3 from the original LOWTRAN 7 Users Manual; plus the "Readme" files on the MODTRAN 3 "ftp" site and the MODTRAN report:

Users Guide to LOWTRAN 7

AFGL-TR-88-0177

16 August 1988

MODTRAN: A Moderate Resolution Model

LOWTRAN 7 GL-TR-89-0122

30 April 1989

The scientific differences between the codes will be outlined in the Scientific Report due for publication in early 1996.

### A3. INSTRUCTIONS FOR USING MODTRAN 3

The instructions for using MODTRAN 3 are similar to those for the earlier LOWTRAN 7 version. However, some new parameters have been added, necessitating the addition of one new card, and minor modifications to two other cards. The new parameters (appearing on required CARD 1A), are principally required to govern: (1) a second multiple scattering option (based on the multiple stream DISORT algorithm, after Stamnes et al. 1988); (2) a new high resolution solar irradiance (based on a full calculated irradiance, after Kurucz 1995) with an optional triangular smoothing function; and (3) a "one-step" update to the CO<sub>2</sub> mixing ratio. This last option is offered because, for historic calibration studies, the 330 ppmv for CO<sub>2</sub> has been preserved in the code. However, CO<sub>2</sub> increases by approximately 1/2 % per year, and is currently 355-360 ppmv.

The most important altered card is the vital CARD 4 from the LOWTRAN sequence, governing the beginning and ending frequencies, the frequency step size on output, and spectral resolution (based on a triangular slit function). The format for these variables has changed from real to integer values. In addition, MODTRAN performs all of its calculations at 1 cm<sup>-1</sup> intervals (for frequencies between 0 22000 cm<sup>-1</sup>), independent of the choice of output step size and triangular resolution. The new MODTRAN 1 cm<sup>-1</sup> band models, the primary upgrade from LOWTRAN, provide much improved spectral accuracy and will still run very rapidly. For frequencies beyond the current band model upper limit (22000-50000 cm<sup>-1</sup>), MODTRAN uses a fixed 5 cm<sup>-1</sup> step size, with the transition occurring automatically. Note that the option to "incorrectly" request an un-smoothed large step size, particularly as used in the solar regime, is no longer available.

The second "altered" card involves two new provisions on CARD 1. First, the SALB parameter now provides access to spectral vectors (wavelength, emissivity, and reflectivity) from a selection of default options stored on a file called "refbkg". Negative values from -1 through -16 (with values of -7 through -12 available for user- specification) will pick up any of an assortment of surface properties, including snow, forest, farm, desert, ocean, cloud deck and 4 sample grass models. The size of these vectors is variable and the format is in ASCII. (Ref. Robertson, SSI).

Second, the MDEF value on CARD 1 was previously limited to a value of 1, selecting the single set of prestored molecular profiles for species for which MODEL (1...6) do not pertain (O<sub>2</sub>, NO, SO<sub>2</sub>, NO<sub>2</sub>, NH<sub>3</sub> and HNO<sub>3</sub>). Now, when MDEF=2, the user will be allowed to specify the profiles for the new heavy molecules for which cross-sections have been specified. These include nine chloro-fluorocarbons (CFC's), plus CLONO<sub>2</sub>, HNO<sub>4</sub>, CCL<sub>4</sub>, and N<sub>2</sub>O<sub>5</sub>, with the databases stored in 'UFTAPX.asc'. The specification of user-defined profiles is modeled after the MODEL=7 option in LOWTRAN, but only one set of units can be used for the whole set of heavy species. The "default" profiles for these heavy molecules are stored in BLOCK DATA XMLATM and are based on 1990 photochemical predictions (after M. Allen, JPL). Since some of the CFC's have increased by as much as 8%/year, the user might well wish to redefine these values. Note that both CFC11 and CFC12 are now as much as 80% larger than the default profiles.

In general, for standard atmospheric models, six input cards are now required to run MODTRAN for a given problem. For any specific problem a combination of several of the fifteen additional optional control cards are possible. The formats for the six main cards, fifteen optional cards, and definitions of the input parameters are given below. Because of the similarity between the MODTRAN and LOWTRAN instructions, the changes will be highlighted and the numbering scheme will be altered.

### A3.1 Input Data and Formats

The use of the word 'CARD' is equivalent to editing with 80 columns.

The program is activated by submission of a **six** (or more) card sequence as follows:

**CARD 1:**    **L**MODTRN, MODEL, ITYPE, IEMSC, IMULT, M1, M2, M3, M4, M5, M6  
                   **M**DEF, IM, NOPRT, TBOUND, **S**ALB  
                   **F**ORMAT (L1, I4, 12I5, F8.3, F7.2)

**CARD1A:**    **L**DISORT, ISTRM, LSUN1, ISUN, CO2MIX  
                   **F**ORMAT (L1, I4, L1, I4, F10.3)

**CARD 2:**    IHAZE, ISEASN, IVULCN, ICSTL, ICLD, IVSA, VIS, WSS, WHH,  
                   RAINRT, GNDALT  
                   **F**ORMAT (6I5, 5F10.3)

## OPTIONAL CARDS

CARD 2A: CTHIK, CALT, CEXT, ISEED (If ICLD=18, 19, or 20)

FORMAT (3F10.3, I10)

CARD 2B: ZCVSA, ZTVSA, ZINVSA (If IVSA=1)

FORMAT (3F10.3)

CARD 2C: ML, IRD1, IRD2, TITLE (If MODEL=0 or 7, and IM=1)

FORMAT(3I5, 18A4)

CARDS 2C1 through 2C3 (as required) repeated ML times.

CARD 2C1: ZMDL, P, T, WMOL(1), WMOL(2), WMOL(3), JCHAR, **JCHARX**

FORMAT (F10.3, 5E10.3, 15A1, **1X, A1**)

CARD 2C2: (WMOL(J), J=4, 12) (If IRD1=1)

FORMAT (8E10.3)

CARD 2C2X: (XMOL(J), J=1,13) (If MDEF=2)

**FORMAT (8E10.3)**

CARD 2C3: AHAZE, EQLWCZ, RRATZ, IHA1, ICLD1, IVUL1,

ISEA1, ICHR1 (If IRD2=1)

FORMAT (10X, 3F10.3, 5I5)

CARD 2D: IREG (1 TO 4) (If IHAZE=7 or ICLD=11)

FORMAT (4I5)

CARD 2D1: AWCCON, TITLE

FORMAT (E10.3, 18A4)

CARD 2D2: (VX(I), EXTC(N,I), ABSC(N,I), ASYM(N,I), I=1, 47)

(If IHAZE=7 or ICLD=11)

FORMAT (3(F6.2, 2F7.5, F6.4))

CARD 3: H1, H2, ANGLE, RANGE, BETA, RO, LEN

FORMAT (6F10.3,I5)

ALTERNATE CARD 3:

H1, H2, ANGLE, IDAY, RO, ISOURC, ANGLEM (If IEMSCT=3)

FORMAT (3F10.3, I5, 5X, F10.3, I5, F10.3)

## OPTIONAL CARDS:

CARD 3A1: IPARM, IPH, IDAY, ISOURC (IEMSCT=2)

FORMAT (4I5)

CARD 3A2: PARM1, PARM2, PARM3, PARM4, TIME, PSIPO, ANGLEM, G



FORMAT (8F10.3) (If IEMSCT=2)

CARD 3B1: NANGLS (If IPH=1)

FORMAT (15)

CARD 3B2(1 TO NANGLS): (If IPH=1)

(ANGF (I), F(1,I), F(2,I), F(3,I), F(4,I), I=1, NANGLS)

FORMAT (5E10.3)

**CARD4:** IV1, IV2, IDV, IRES

FORMAT (4I10)

**CARD 5:** IRPT

FORMAT (15)

Definitions of these quantities will be discussed in Section 3.2.

### A3.2 Basic Instructions

The various quantities to be specified on each of the six control cards along with the fifteen optional cards (summarized in Section 3.1) will be discussed in this section.

**A3.2.1 CARD 1: LMODTRN, MODEL, ITYPE, IEMSCT, IMULT, M1, M2, M3, M4, M5, M6, MDEF, IM, NOPRT, TBOUND, SALB**

FORMAT (L1, I4, 12I5, F8.3, F7.2)

**LMODTRN** selects MODTRAN or LOWTRAN run options; LMODTRN = "T" runs MODTRAN, LMODTRN = "F" or blank runs LOWTRAN.

**LMODTRN** = "logical" T or F.

**MODEL** selects one of the six geographical-seasonal model atmospheres or specifies that user-defined meteorological data are to be used.

MODEL = 0 If meteorological data are specified (horizontal path only)

1 Tropical Atmosphere

2 Midlatitude Summer

3 Midlatitude Winter

- 4 Subarctic Summer
- 5 Subarctic Winter
- 6 1976 US Standard
- 7 If a new model atmosphere (e.g. radiosonde data) is to be read in or IR1 0 or

MDEF=2.

(NOTE: MODEL = 0 Used for horizontal path only)

ITYPE Indicates the type of atmospheric path.

- ITYPE =
- 1 For a horizontal (constant-pressure) path
  - 2 Vertical or slant path between two altitudes
  - 3 For a vertical or slant path to space

IEMSCT Determines the mode of execution of the program.

- IEMSCT =
- 0 Program execution in transmittance mode
  - 1 Program execution in thermal radiance mode
  - 2 Program execution in radiance mode with solar/lunar single scattered radiance included
  - 3 Program calculates directly transmitted solar irradiance

IMULT Determines execution with multiple scattering

- IMULT =
- 0 Program executed without multiple scattering
  - 1 Program executed with multiple scattering
- (NOTE: IEMSCT must equal 1 or 2 for multiple scattering)

M1, M2, M3, M4, M5, and M6 are used to modify or supplement the altitude profiles of temperature and pressure, water vapor, ozone, methane, nitrous oxide and carbon monoxide from the atmospheric models stored in the program.

MDEF Uses the default (U.S. Standard) profiles for the remaining species if, and only if, MDEF=0, "b", or 1. If MDEF=2 the user will be allowed to specify the profiles for the new heavy molecules for which cross-sections have been specified. These include nine chloro-fluorocarbons (CFC's), plus ClONO<sub>2</sub>, HNO<sub>4</sub>, CCl<sub>4</sub>, and N<sub>2</sub>O<sub>5</sub>, with the databases stored in 'UFTAPX.asc'. The specification of user-defined profiles is modeled after the MODEL=7 option in LOWTRAN, but only one unit definition (see JCHAR definitions for CARD 2C1) can be used for the whole set of heavy species. The "default" profiles for these heavy molecules are stored in BLOCK DATA XMLATM and are based on 1990 photochemical predictions (after M. Allen, JPL). Since some of the CFC's have increased by as much as 8%/year, the user might well wish to redefine these values. Note that both CFC11 and CFC12 are now as much as 80% larger than the default profiles.

For normal operation of program (MODEL 1 to 6)

Set  $M1=M2=M3=0$ ,  $M4=M5=M6=MDEF=0$

These parameters are reset to default values by MODEL (1 to 6) when they are equal to zero

When  $M1 = 0$        $M1$  reset to 'MODEL'

When  $M2 = 0$        $M2$  reset to 'MODEL'

When  $M3 = 0$        $M3$  reset to 'MODEL'

When  $M4 = 0$        $M4$  reset to 'MODEL'

When  $M5 = 0$        $M5$  reset to 'MODEL'

When  $M6 = 0$        $M6$  reset to 'MODEL'

When  $MDEF = 0$   $MDEF$  reset to 1 for all remaining species (not needed with MODEL 1 to 6).

If  $MODEL=0$  or 7 and if:

- a.  $M1$  through  $M6$  are zero then the JCHAR parameter on card 2C.1 should be utilized to supply the necessary amounts.

or

- b.  $M1$  through  $M6$  are non-zero then the chosen default profiles will be utilized provided the specific JCHAR option is blank.

$M1 = 1$  to 6 Default temperature and pressure to specified model atmosphere

$M2 = 1$  to 6 Default  $H_2O$  to specified model atmosphere

$M3 = 1$  to 6 Default  $O_3$  to specified model atmosphere

$M4 = 1$  to 6 Default  $CH_4$  to specified model atmosphere

$M5 = 1$  to 6 Default  $N_2O$  to specified model atmosphere

$M6 = 1$  to 6 Default  $CO$  to specified model atmosphere

$MDEF = 1$  Use default profiles for  $CO_2$ ,  $O_2$ ,  $NO$ ,  $SO_2$ ,  $NO_2$ ,  $NH_3$ ,  $HNO_3$ ,

(not needed with MODEL 1 to 6).

or

$MDEF = 2$  User-defined control of heavy molecules

(CFC's will be updated; requires  $MODEL=0$  or 7)

If  $MODEL=0$  or  $MODEL=7$ , the program expects to read user supplied atmospheric profiles. Set:  $IM=1$  for first run. To then rerun the same user-atmosphere for a series of cases set  $IM=0$ ; MODTRAN will reuse the previously read data.

$IM = 0$  For normal operation of program or when subsequent calculations are to be run with the

$MODEL$  data set last read in.

$= 1$  When user input data are to be read initially.

$NOPRT = 0$  For normal operation of program. Controls TAPE6 output

$= 1$  To minimize printing of transmittance or radiance table and atmospheric profiles

= -1 Controls Tape 8 output (see subsequent options)

**TBOUND=** Boundary Temperature (°K), used in the radiation mode (if IEMSCT=1 or 2) for slant paths that intersect the earth or terminate at a grey boundary (for example, cloud, target). If TBOUND is left blank and the path intersects the Earth, the program will

use

the temperature of the first atmospheric level as the boundary temperature.

**SALB =** Surface albedo of the Earth at the location and average frequency of the calculation (0.0 to 1.0). If SALB is left blank the program assumes the surface is a blackbody (with emissivity equal to 1; for example, SALB=0), or

**SALB < 0** Negative values allow the user to access prestored spectrally variable surface albedos; values from -1 to -16 with -7 to -12 open for "user-specification".

The choices for negative SALB include: -1 = fresh snow, -2 = forest, -3 = farm, -4 = desert, -5 = ocean, -6 = cloud deck, -7 to -12 = "open for user specification", -13 = old grass, -14 = decayed grass, -15 = maple leaf, and -16 = burnt grass. These are only meant to be representative of the types of options available; the user is encouraged to add to the set.

Table 7 summarizes the use of the eight control parameters LMODTRN, MODEL, ITYPE, IEMSCT, IMULT, MDEF, NOPRT and SALB on CARD 1.

### A3.2.1B CARD 1A LDISORT, ISTRM, LSUN, ISUN, CO2MIX

**LDISORT**, **ISTRM**, **LSUN1**, **ISUN**, and **CO2MIX** are principally required to govern: (1) a second multiple scattering option (based on the multiple stream DISORT algorithm, after Stamnes et al. 1988); (2) a new high resolution solar irradiance (based on a full calculated irradiance, after Kurucz, 1995) with an optional triangular smoothing function; and (3) a "one-step" update to the CO2 mixing ratio. This last option is offered because, for historic calibration studies, the 330 ppmv for CO2 has been preserved in the code. However, CO2 increases by approximately 1/2 % per year, and is currently 355-360 ppmv.

**LDISORT** = "logical" T or F; requires that IMULT = 1, "T" will activate DISORT multiple scattering algorithm.  
"F" will continue with original Isaacs two-stream.

**ISTRM** = 2, 4, 8, 16 streams, the number of streams to be used by DISORT. This is a time-intensive operation, so if ISTRM=2, run Isaacs model. ISTRM= 8 is recommended at this time, but improvement in accuracy is NOT guaranteed.

- LSUN1** = "logical" Tor F; F uses "default solar irradiance, as embedded in MODTRAN Block Data; T reads 1 cm-1 binned solar irradiance from the file "sun2" and requires the ISUN scanning definition. Both irradiances are based on work of R. Kurucz, Harvard-Smithsonian Astrophysical Observatory.
- ISUN** > 2; will run a triangular smoothing filter over the SUN vector, in wavenumber.
- CO2MIX** = replacement CO2 mixing ratio; default value is 330 ppmv; current recommended values (1995) are 355-360 ppmv. Units must be in ppmv.

## Appendix C

Table 7. MODTRAN CARD 1 Input Parameters: LMODTRAN, MODEL, ITYPE, IEMSCT, IMULT, MDEF, NOPRT and SALB

CARD 1		LMODTRN, MODEL, ITYPE, IEMSCT, IMULT, M1, M2, M3, M4, M5, M6, MDEF, IM, NOPRT, TBOUND, SALB FORMAT (L1, I4, I2I5, F8.3, F7.2)						
LMODTRN (COL 1)		MODEL (COL 2)	ITYPE (COL 6)	IEMSCT (COL 11)	IMULT (COL 16)	MDEF (COL 51)	NOPRT (COL 61)	SALB (COL 74)
T	MODTRAN run	0 User- defined*	1 Horizontal path	0 Transmittance	0 Without Multiple Scattering	1 for MODEL=0,7 Default for minor species**	-1 TAPE8 Output	-1 snow
F	LOWTRAN run	1 Tropical	2 Slant path H1 to H2	1 Radiance	1 With Multiple Scattering	2 for MODEL=0,7 User control of heavy molecules	0 TAPE6 Normal Output	-2 forest
b	LOWTRAN run	2 Midlatitude summer	3 Slant path to space	2 Radiance with solar/lunar scattering			1 TAPE6 Short Output	-3 farm
		3 Midlatitude winter		3 Transmitted solar irradiance			-4 desert	
		4 Subarctic summer		-5 ocean				
		5 Subarctic winter		-6 cloud deck				
		6 1976 U.S. Standard		-7 to -12 open				
		7 User- defined*		-13 old grass				
				-14 decayed grass				
				-15 maple leaf				
				-16 burnt grass				
M1, M2, M3, M4, M5, M6, MDEF, IM, TBOUND, SALB are left blank for standard cases. *Options for non-standard models.   **CO2, O2, NO, SO2, NO2, NH3, HNO3.								

### A3.2.2 CARD 2: IHAZE, ISEASN, IVULCN, ICSTL, ICLD, IVSA, VIS, WSS, WHH, RAINRT, GNDALT

#### FORMAT (615, 5F10.3)

IHAZE, ISEASN, IVULCN, and VIS select the altitude and seasonal-dependent aerosol profiles and aerosol extinction coefficients. IHAZE specifies the aerosol model used for the boundary-layer (0 to 2 km) and a default-surface meteorological range. The relative humidity dependence of the boundary-layer aerosol extinction coefficients is based on the water vapor content of the model atmosphere selected by MODEL. ISEASN selects the seasonal dependence of the profiles for both the tropospheric (2 to 10 km) and stratospheric (10 to 30 km) aerosols. IVULCN is used to select both the profile and extinction type for the stratospheric aerosols and to determine transition profiles above the stratosphere to 100 km. VIS, the meteorological range, when specified, will supersede the default meteorological range in the boundary-layer aerosol profile set by IHAZE.

IHAZE selects the type of extinction and a default meteorological range for the boundary-layer aerosol models only. If VIS is also specified, it will override the default IHAZE value. Interpolation of the extinction coefficients based on relative humidity is performed only for the RURAL, MARITIME, URBAN, and TROPOSPHERIC coefficients used in the boundary layer (0 to 2 km altitude).

IHAZE = 0	no aerosol attenuation included in the calculation
= 1	RURAL extinction, default VIS = 23 km
= 2	RURAL extinction, default VIS = 5 km
= 3	NAVY MARITIME extinction, sets own VIS (wind and relative humidity dependent)
= 4	MARITIME extinction, default VIS = 23 km (LOWTRAN model)
= 5	URBAN extinction, default VIS = 5 km
= 6	TROPOSPHERIC extinction, default VIS = 50 km
= 7	User defined aerosol extinction coefficients. Triggers reading cards 2D, 2D1 and 2D2 for up to 4 altitude regions of user defined extinction, absorption and asymmetry parameters.
= 8	FOG1 (Advection Fog) extinction, 0.2-km VIS
= 9	FOG2 (Radiative Fog) extinction, 0.5-km VIS
= 10	DESERT extinction, sets own visibility from wind speed (WSS)

ISEASN selects the appropriate seasonal aerosol profile for both the tropospheric and stratospheric aerosols. Only the tropospheric aerosol extinction coefficients are used with the 2 to 10 km profiles.

ISEASN = 0      season determined by the value of MODEL;  
                     SPRING-SUMMER for MODEL = 0, 1, 2, 4, 6, 7  
                     FALL-WINTER for MODEL = 3, 5  
       = 1      SPRING-SUMMER  
       = 2      FALL-WINTER

The parameter IVULCN controls both the selection of the aerosol profile as well as the type of extinction for the stratospheric aerosols. It also selects appropriate transition profiles above the stratosphere to 100 km. Meteoric dust extinction coefficients are always used for altitudes from 30 to 100 km.

IVULCN= 0,1 BACKGROUND STRATOSPHERIC profile and extinction  
       = 2      MODERATE VOLCANIC profile and AGED VOLCANIC extinction  
       = 3      HIGH VOLCANIC profile and FRESH VOLCANIC extinction  
       = 4      HIGH VOLCANIC profile and AGED VOLCANIC extinction  
       = 5      MODERATE VOLCANIC profile and FRESH VOLCANIC extinction  
       = 6      MODERATE VOLCANIC profile and BACKGROUND  
                     STRATOSPHERIC extinction  
       = 7      HIGH VOLCANIC profile and BACKGROUND STRATOSPHERIC  
                     extinction  
       = 8      EXTREME VOLCANIC profile and FRESH VOLCANIC extinction

Table 8 shows the value of IVULCN corresponding to the different choices of extinction coefficient model and the vertical distribution profile.

ICSTL is the air mass character (1 to 10), only used with the Navy maritime model (IHAZE = 3). Default value is 3.

ICSTL = 1      open ocean  
                     .  
                     .  
                     .  
                     10      strong continental influence

ICLD specifies the cloud models and rain models used.



Table 8. MODTRAN CARD 2 Input Parameter: IVULCN

	VERTICAL DISTRIBUTION			
	BACKGROUND STRATO-SPHERIC	MODERATE VOLCANIC	HIGH VOLCANIC	EXTREME VOLCANIC
BACKGROUND STRATOSPHERIC	0,1	6	7	-
AGED VOLCANIC	-	2	4	-
FRESH VOLCANIC	-	5	3	8

The rain profiles decrease linearly from the ground to the top of the associated cloud model. The program cuts off the rain at the cloud top.

ICLD = 0      No clouds or rain

- = 1      Cumulus cloud;    base 0.66 km,    top 3.0 km
- = 2      Altostratus cloud;    base 2.4 km, top 3.0 km
- = 3      Stratus cloud:        base 0.33 km,    top 1.0 km
- = 4      Stratus/Strato Cu;    base 0.66 km,    top 2.0 km
- = 5      Nimbostratus cloud:    base 0.16 km,    top 0.66 km
- = 6      2.0 mm/hr Drizzle (modeled with cloud 3)  
rain 2.0 mm/hr at 0 km to 0.22 mm/hr at 1.5 km
- = 7      5.0 mm/hr Light rain (modeled with cloud 5)  
rain 5.0 mm/hr at 0 km to 0.2 mm/hr at 2.0 km
- = 8      12.5 mm/hr Moderate rain (modeled with cloud 5)  
rain 12.5 mm/hr at 0 km to 0.2 mm/hr at 2.0 km

- = 9      25.0 mm/hr Heavy rain (modeled with cloud 1)  
rain 25.0 mm/hr at 0 km to 0.2 mm/hr at 3.0 km
- = 10     75.0 mm/hr Extreme rain (modeled with cloud 1)  
rain 75.0 mm/hr at 0 km to 0.2 mm/hr at 3.5 km
- = 11     Read in user defined cloud extinction and absorption. Triggers reading  
Cards 2D, 2D1 and 2D2 for up to 4 altitude regions of user defined  
extinction, absorption, and asymmetry parameters
- = 18     Standard Cirrus model
- = 19     Sub-visual Cirrus model
- = 20     NOAA Cirrus model (LOWTRAN 6 Model)

IVSA selects the use of the Army Vertical Structure Algorithm (VSA) for aerosols in the boundary layer.

IVSA = 0    not used

= 1    Vertical structure algorithm

VIS specifies the surface meteorological range <sup>\*36,37,38</sup> (km) overriding the default value associated with the boundary layer chosen by IHAZE. If set to zero uses default value specified by IHAZE.

VIS > 0    user specified surface meteorological range (km)

= 0    uses the default meteorological range set by IHAZE (See Table 10),

WSS specifies the current wind speed for use with the Navy maritime and desert aerosol models.

WSS =      current wind speed (m/s). Used with the Navy maritime model (IHAZE=3)  
or the DESERT model (IHAZE=10).

WHH specifies the 24 hour average wind speed for use with the Navy maritime model.

WHH =    24-hr average wind speed (m/s). Only used with the Navy maritime model (IHAZE=3)

For the Navy Maritime model if WSS=WHH=0, default wind speeds are set according to the value of MODEL, see Table 9. For the Desert aerosol model (IHAZE=10), if WSS<0, the default wind speed is 10 m/s.

Table 9. Default Wind Speeds for Different Model Atmospheres Used with the Navy Maritime Model  
(IHAZE=3)

MODEL	Model Atmosphere	WSS and WHH Default Wind Speed (m/s)
0	User-defined (Horizontal Path)	6.9
1	Tropical	4.1
2	Midlatitude summer	4.1
3	Midlatitude winter	10.29
4	Subartic summer	6.69
5	Subartic winter	12.35
6	U. S. Standard	7.2
7	User-defined	6.9

RAINRT Specifies the rain rate

RAINRT = Rain rate (mm/hr) default value is zero.

Used to top of cloud when cloud is present;

When no clouds rain rate used to 6km

GNDALT specifies the altitude of the surface relative to sea level

GNDALT = Altitude of surface relative to sea level (km)

Used to modify aerosol profiles below 6 km altitudes

Table 10 summarizes the use of the control parameters IHAZE, ISEASN, and IVULCN on card 2 and  
Table 11 summarizes the use of the parameter ICLD.

## Appendix C

Table 10. MODTRAN CARD 2 Input Parameters: IHAZE, ISEASN, VULCN, VIS.

Card 2	IHAZE, ISEASN, IVULCN, ICSTL, ICLD, IVSA, VIS, WSS, WHH, RAINRT, GNDALT FORMAT (615, 5F10.3)									
<u>IHAZE</u>			<u>ISEASN</u>		<u>IVULCN</u>					
COL 5	VIS* (KM)	EXTINCTION	COL 10	SEASON	COL 15	SEASON	PROFILE	EXTINCTION	PROFILE/ EXTINCTION	
0										
1	23	RURAL	0	Set by model		Set by model			Meteoric dust extinction	
2	5		1	Spring- summer		Spring- summer				
3	**	Navy maritime	2	Fall- winter		Fall- winter				
4	23	LOWTRAN maritime	Tropospheric profile/  tropospheric extinction		0  1		Background  stratospheric	Background stratospheric	Normal  atmospheric profile	
5	5	URBAN			2		Moderate volcanic	Aged volcanic	Transition profiles  - volcanic to normal	
6	50	Tropospheric			3		High volcanic	Fresh volcanic		
7	23	User- defined			4		High volcanic	Aged volcanic		
8	0.2	Fog 1			5		Moderate volcanic	Fresh volcanic		
9	0.5	Fog 2			6		Moderate volcanic	Background stratospheric		
10	**	Desert			7		High volcanic	Background stratospheric		
					8		Extreme Volcanic	Fresh Volcanic		
0 to 2 km					2 to 10 km		10 to 30 km			
* Default VIS, can be overridden by VIS > 0 on CARD 2 ** Sets own default VIS										

Table 11. MODTRAN CARD 2 Input Parameter: ICLD

CARD 2	IHAZE, ISEASN, IVULCN, ICSTL, <u>ICLD</u> , IVSA, VIS, WSS, WHH, RAINRT, GNDALT FORMAT (615, 5F10.3)
<u>ICLD</u>	FOR CLOUD AND OR RAIN OPTION
0	NO CLOUDS OR RAIN
1	CUMULUS CLOUD
2	ALTOSTRATUS CLOUD
3	STRATUS CLOUD
4	STRATUS/STRATO CUMULUS
5	NIMBOSTRATUS CLOUD
6	2.0 MM/HR DRIZZLE (MODELED WITH CLOUD 3)
7	2.0 MM/HR LIGHT RAIN (MODELED WITH CLOUD 5)
8	12.5 MM/HR MODERATE RAIN (MODELED WITH COULD 5)
9	25.0 MM/HR HEAVY RAIN (MODELED WITH CLOUD 1)
10	75.0 MM/HR EXTREME RAIN (MODELED WITH CLOUD 1)
11	USER DEFINED CLOUD EXTINCTION AND ABSORPTION
18	STANDARD CIRRUS MODEL
19	SUB VISUAL CIRRUS MODEL
20	NOAA CIRRUS MODEL (LOWTRAN 6 MODEL)

**A3.2.2.1 Optional Cards Following CARD 2**

Optional input cards after CARD 2 selected by the parameters ICLD, IVSA, MODEL, and IHAZE on CARDS 1 and 2.

CARD 2A CTHIK, CALT, CEXT, ISEED (If ICLD=18, 19 or 20)  
FORMAT (3F10.3, I10)

Input card for cirrus altitude profile subroutine when ICLD = 18, 19, or 20

CTHIK is the cirrus thickness (km)

If CTHIK = 0 use thickness statistics  
> 0 user defined thickness

CALT is the cirrus base altitude (km)

CALT = 0 use calculated value  
> 0 user defined base altitude

CEXT is the extinction coefficient ( $\text{km}^{-1}$ ) at 0.55  $\mu\text{m}$

CEXT      = 0    use  $0.14 * \text{CTHIK}$   
             > 0    user defined extinction coefficient

ISEED is the random number initializing flag.

ISEED      = 0    use default mean values for cirrus.  
             > 0    initial value of seed for random number generator, function RANF  
                     (SEED), (different values of SEED produce different random number  
                     sequences). This provides for statistical determination of cirrus base  
                     altitude (CALT) and thickness (CTHIK).

**NOTE:** Random number generator is system dependent.

CARD 2B   ZCVSA, ZTVSA, ZINVSA    (If IVSA = 1)  
             FORMAT (3F10.3)

Input card for Army VSA subroutine when IVSA = 1. The case is determined by the parameters VIS, ZCVSA, ZTVSA, and ZINVSA.

CASE 1: cloud/fog at the surface; increasing extinction with height from cloud/fog base to  
             cloud/fog top. Selected by VIS  $\leq 0.5$  km and ZCVSA = 0.

Use case 2 or 2' below cloud and case 1 inside it.

CASE 2: hazy/light fog; increasing extinction with height up to the cloudbase. Selected  
             by  $0.5 < \text{VIS} \leq 10$  km, ZCVSA = 0.

CASE 2': clear/hazy; increasing extinction with height, but less so than case 2, up to the  
             cloudbase. Selected by VIS  $> 10$  km, ZCVSA = 0.

CASE 3: no cloud ceiling but a radiation fog or an inversion or boundary layer present;  
             decreasing extinction with height up to the height of the fog or layer. Selected  
             by ZCVSA  $< 0$  ZINVSA  $\geq 0$ .

CASE 4: no cloud ceiling or inversion layer; constant extinction with height. Selected by  
             ZCVSA  $< 0$ .

ZCVSA is the cloud ceiling height (km):

If ZCVSA    > 0.0 the known cloud ceiling height;  
                   = 0.0 height unknown: the program will calculate one for case 2, and  
                     default is 1.8 km for case 2'; or  
                   < 0.0 no cloud ceiling (cases 3 and 4).

ZTVSA is the thickness of the cloud (case 2) or the thickness of the fog at the surface (case 1) (km):

If ZTVSA > 0.0 the known value of the cloud thickness;  
 = 0.0 thickness unknown; default is 0.2 km.

ZINVSA is the height of the inversion or boundary layer (km):

If ZINVSA > 0.0 the known height of the inversion layer;  
 = 0.0 height unknown: default is 2 km, 0.2 km for fog;  
 < 0.0 no inversion layer (case 4, if ZCVSA < 0.0 also).

## OPTIONAL USER INPUT CARDS 2C, 2C1, 2C2 and 2C3

If the value of MDEF has been set to 2, then the user has declared that a "user-specified" set of CFC's will be supplied. This will be accompanied by the setting of MODEL to 0 or 7 and usually will be accompanied by an IRD1=1, the specification of "user-defined" molecular species. Instructions and formats for the CFC's follow the same rules as the following discussion. A new parameter, JCHARX, governs the units for all CFC's. The following cards handle user input data.

Cards 2C and 2C1 are always read for MODEL 0 or 7.

CARD 2C ML, IRD1, IRD2, TITLE (MODEL=0/7, IM=1)

FORMAT (315, 18A4)

Additional atmospheric model (MODEL 0/7)

New model atmospheric data can be inserted provided the parameters

'MODEL' and 'IM' are set equal to 0/7 and 1 respectively on card 1.

ML = Number of atmospheric levels to be inserted (Maximum of 34)

IRD1 Controls reading WN20, WCO... and WNH3, WHNO3 (CARD 2C2)

IRD1=0 No read

IRD1=1 Read CARD 2C2

IRD2 Controls reading AHAZE, EQLWCZ, ... (CARD 2C3)

IRD2=0 No read

IRD2=1 Read CARD 2C3

TITLE = Identification of new model atmosphere

CARD 2C1 ZMDL, P, T, WMOL(1), WMOL(2), WMOL(3), (JCHAR(J), J=1, 14), JCHARX

FORMAT (F10.3, 5E10.3, 15A1, 1X, A1)

CARD 2C2 (WMOL(J), J=4, 12)

FORMAT (8E10.3)

## CARD 2CX (XMOL(J), J=1, 13)

FORMAT (8E10.3)

ZMDL           = Altitude of layer boundary (km)  
 P               = Pressure of layer boundary  
 T               = Temperature of layer boundary  
 WMOL(1-12) = Individual molecular species (see Table 11A for species)  
 JCHAR(1-14) = Control variable on units selection for profile input  
                  (P, T and molecular constituents, see Table 11A.)  
 JCHARX       = Single control variable for selection of units for entire set of CFC's and  
                  other heavy molecules. (See Table 11B for order and identification of  
                  these species.)

By utilizing a choice of values for the JCHAR(J) control variable (where J = 1,14) the user can designate specific units or accept defaults for the various molecular species and for the temperature and pressure. If JCHAR(J) is left blank the program will default to the values chosen by M1, M2, M3, M4, M5, M6 and MDEF when the given amount is zero. If the amount is non-zero and the JCHAR(J) is blank, the code assumes the first option on units: mb for pressure, K for temperature, and ppmv on constituents. The single unit option, JCHARX, follows the same rules, and for each altitude specified on card 2C1, the code will expect to find a full set (2 card images) containing values for the 13 species in the order specified by Table 11B. These values are required only if MDEF=2.

## For JCHAR(1)

A   indicates Pressure in (mb)  
 B   indicates Pressure in (atm)  
 C   indicates Pressure in (torr)  
 1-6 will default to specified atmospheric value



Table 11A. The Association of the JCHAR(J) Index (J=1,14)  
with the Variables P, T and WMOL

J	VARIABLE	
1	P	pressure
2	T	temperature
3	WMOL(1)	water vapor (H <sub>2</sub> O)
4	WMOL(2)	carbon dioxide (CO <sub>2</sub> )
5	WMOL(3)	ozone (O <sub>3</sub> )
6	WMOL(4)	nitrous oxide (N <sub>2</sub> O)
7	WMOL(5)	carbon monoxide (CO)
8	WMOL(6)	methane (CH <sub>4</sub> )
9	WMOL(7)	oxygen (O <sub>2</sub> )
10	WMOL(8)	nitric oxide (NO)
11	WMOL(9)	sulphur dioxide (SO <sub>2</sub> )
12	WMOL(10)	nitrogen dioxide (NO <sub>2</sub> )
13	WMOL(11)	ammonia (NH <sub>3</sub> )
14	WMOL(12)	nitric acid (HNO <sub>3</sub> )

For JCHAR(2)

A indicates Ambient temperature in deg (K)

B indicates Ambient temperature in deg (C)

1-6 will default to specified atmospheric value

Table 11B. The New Heavy Molecules, (XMOL(J), J=1,13) Nomenclature

	(1)	(2)	(3)
1	CFC-11	F11	CCl <sub>3</sub> F
2	CFC-12	F12	CCl <sub>2</sub> F <sub>2</sub>
3	CFC-13	F14	CClF <sub>3</sub>
4	CFC-14	F14	CF <sub>4</sub>
5	CFC-22	F22	CHClF <sub>2</sub>
6	CFC-113	F113	C <sub>2</sub> Cl <sub>3</sub> F <sub>3</sub>
7	CFC-114	F114	C <sub>2</sub> Cl <sub>2</sub> F <sub>4</sub>
8	CFC-115	F115	C <sub>2</sub> ClF <sub>5</sub>
9	ClONO <sub>2</sub>		
10	HNO <sub>4</sub>		
11	CHCl <sub>2</sub> F		
12	CCl <sub>4</sub>		
13	N <sub>2</sub> O <sub>5</sub>		

For JCHAR(3-14)

- A indicates Volume mixing ratio (ppmv)
- B indicates Number density ( $\text{cm}^{-3}$ )
- C indicates Mass mixing ratio (gm/kg)
- D indicates Mass density ( $\text{gm/m}^3$ )
- E indicates Partial pressure (mb)
- F indicates Dew point temp (TD in T (K)) -  $\text{H}_2\text{O}$  only
- G indicates Dew point temp (TD in T (C)) -  $\text{H}_2\text{O}$  only
- H indicates Relative humidity (RH in percent) -  $\text{H}_2\text{O}$  only
- I is available for user definition
- 1-6 will default to specified model atmosphere

CARD 2C3 is read when IRD2 is set to 1 on CARD 2C.

CARD 2C3 AHAZE, EQLWCZ, RRATZ, IHA1, ICLD1, IVUL1, ISEA1, ICHR1  
 FORMAT (10X, 3F10.3, 515)

- AHAZE Aerosol or cloud scaling factor (equal to the visible [wavelength of  $0.55 \mu\text{m}$ ] extinction coefficient [ $\text{km}^{-1}$ ] at altitude ZMDL)  
 [NOTE: only one of AHAZE or EQLWCZ is allowed]
- EQLWCZ Equivalent liquid water content ( $\text{gm/m}^3$ ) at altitude ZMDL for the aerosol, cloud or fog models
- RRATZ Rain rate (mm/hr) at altitude ZMDL

Only one of IHA1, ICLD1 or IVUL1 is allowed

- IHA1 Aerosol model extinction and meteorological range control for the altitude, ZMDL See IHAZE (CARD 2) for options
- ICLD1 Cloud extinction control for the altitude, ZMDL, See ICLD (Card 2) for options. When using ICLD1 it is necessary to set ICLD (CARD 2) to the same value as the initial input of ICLD1.
- IVUL1 Stratospheric aerosol profile and extinction control for the altitude ZMDL, see IVULCN (CARD 2) for options

The precedent order of these parameters (IHA1, ICLD1 and IVUL1) is as follows:

- If (IHA1>0) then others ignored
- If (IHA1=0) and (ICLD1>0) then use ICLD1
- If (IHA1=0) and (ICLD1=0) then use IVUL1

If AHAZE and EQLWCZ are both zero, default profile loaded from IHA1, ICLD1, IVUL1

- ISEA1 Aerosol season control for the altitude, ZMDL, see ISEASN (CARD 2) for options.
- ICHR1 Used to indicate a boundary change between 2 or more adjacent user defined aerosol or cloud regions at altitude ZMDL (required for IHAZE=7 or ICLD=11).
- ICHR1 =0 no boundary change in user defined aerosol or cloud regions (regions are not adjacent).
- =1 signifies the boundary change in adjacent user defined aerosol or cloud regions.

**NOTE:** ICHR1 internally defaults to 0 if (IHA1 7) or (ICLD1 11).

## OPTIONAL CARDS 2D, 2D1, 2D2

The following cards allow the user to specify their own attenuation coefficients for any or all four of the aerosol regions. They are only read if IHAZE=7 or ICLD=11 are specified on card 2 (pages 24 and 26).

CARD 2D (IREG (II), II=1,4) (IHAZE=7 or ICLD=11 input)  
FORMAT (415)

IREG Specifies which of the four altitude regions a user defined aerosol or cloud model is used (IHAZE=7/ICLD=11)

(**NOTE:** Regions default to 0-2, 3-10, 11-30, 35-100 km and can be overridden with 'IHA1' settings in MODEL 7)

IREG (II) = 0 Use default values for region II

IREG (II) = 1 Read extinction, absorption, and asymmetry for a region

CARD 2D1 AWCCON, TITLE  
FORMAT (E10.3, 18A4)

AWCCON is a conversion factor from equivalent liquid water content ( $\text{gm}/\text{m}^3$ ) to extinction coefficient ( $\text{km}^{-1}$ ). It is numerically equal to the equivalent liquid water content corresponding to an extinction coefficient of  $1.0 \text{ km}^{-1}$ , at a wavelength of  $0.55 \mu\text{m}$ . AWCCON has units of ( $\text{km-gm-m}^{-3}$ ).

TITLE for an aerosol or cloud region (up to 72 characters)

CARD 2D2 (VX(I), EXTC(N, I), ABSC(N, I), ASYM(N, I), I=1,47)  
FORMAT (3(F6.2, 2F7.5, F6.4))

Where  $N=II$  when  $IREG(II)=1$  for up to 4 altitude regions. User defined aerosol or cloud extinction and absorption coefficients when  $IHAZE=7$  or  $ICLD=11$

$VX(I)$  = Wavelengths for the aerosol or cloud coefficients (not used by program but should be the same as the wavelengths defined in array  $VX2$  in routine  $EXTDTA$ , see Table 12)

$EXTC(N, I)=$  Aerosol or cloud extinction coefficients, normalized so that  $EXTC$  for a wavelength of  $0.55 \mu m$  ( $I=4$ ) is  $1.0 km^{-1}$

$ABSC(N, I)=$  Aerosol or cloud absorption coefficient, normalized so that  $EXTC$  for a wavelength of  $0.55 \mu m$  ( $I=4$ ) is  $1.0 km^{-1}$

$ASYM(N, I)=$  Aerosol or cloud asymmetry parameter

### A3.2.3 CARD 3: H1, H2, ANGLE, RANGE, BETA, RO, LEN

#### FORMAT (6F10,3, 15)

CARD 3 is used to define the geometrical path parameters for a given problem.

$H1$  = initial altitude (km)

$H2$  = final altitude (km) (for  $ITYPE = 2$ )

$H2$  = tangent height(km) (for  $ITYPE = 3$ )

It is important to emphasize here that in the radiance mode of program execution ( $IEMSCT = 1$  or  $2$ ),  $H1$ , the initial altitude, always defines the position of the observer (or sensor).  $H1$  and  $H2$  cannot be used interchangeably as in the transmittance mode.

$ANGLE$  = initial zenith angle (degrees) as measured from  $H1$

$RANGE$  = path length (km)

$BETA$  = earth center angle subtended by  $H1$  and  $H2$  (degrees)

$RO$  = radius of the earth (km) at the particular latitude at which the calculation is performed.

If  $RO$  is left blank, the program will use the midlatitude value of 6371.23 km if  $MODEL$  is set equal to 7. Otherwise, the earth radius for the appropriate standard model atmosphere (specified by  $MODEL$ ) will be used as shown in Table 13.

For an  $ITYPE = 2$  path for which  $H1 > H2$  (and by necessity,  $ANGLE > 90^\circ$ ), two paths are possible: the long path from  $H1$  through a tangent height to  $H2$  and the short path from  $H1$  to  $H2$ .  $LEN$  selects the type of path in these cases.

$LEN$  = 0 short path (default)

= 1 long path through the tangent height.

Table 12. The VX Array with the Required Wavelengths for the Multiply Read Card 2D2

INDEX	WAVELENGTH	INDEX	WAVELENGTH
1	.2000	25	9.0000
2	.3000	26	9.2000
3	.3371	27	10.0000
4	.5500	28	10.5910
5	.6943	29	11.0000
6	1.0600	30	11.5000
7	1.5360	31	12.5000
8	2.0000	32	14.8000
9	2.2500	33	15.0000
10	2.5000	34	16.4000
11	2.7000	35	17.2000
12	3.0000	36	18.5000
13	3.3923	37	21.3000
14	3.7500	38	25.0000
15	4.5000	39	30.0000
16	5.0000	40	40.0000
17	5.5000	41	50.0000
18	6.0000	42	60.0000
19	6.2000	43	80.0000
20	6.5000	44	100.0000
21	7.2000	45	150.0000
22	7.9000	46	200.0000
23	8.2000	47	300.0000
24	8.7000		

Table 13. Default Values of the Earth Radius for Different Model Atmospheres

MODEL	Model Atmosphere	Earth Radius, RO (km)
1	User-defined (Horizontal Path)	Not used
2	Tropical	6,378.39
3	Midlatitude summer	6,371.23
4	Midlatitude winter	6,371.23
5	Subarctic summer	6,356.91
6	Subarctic winter	6,356.91
7	U. S. Standard	6,371.23
	User-defined	6,371.23

It is not necessary to specify every variable on CARD 3; only those that adequately describe the problem according to the parameter ITYPE (as described below). (See Table 14).

- (1) Horizontal Paths (ITYPE = 1)
  - (a) Specify H1, RANGE
  - (b) If non-standard meteorological data are to be used, that is, if MODEL = 0 on CARD 1, then refer to Section 3.3 for a detailed explanation.
- (2) Slant Paths Between Two Altitudes (ITYPE = 2)
  - (a) specify H1, H2, and ANGLE
  - (b) specify H1, ANGLE, and RANGE
  - (c) specify H1, H2, and RANGE
  - (d) specify H1, H2, and BETA
- (3) Slant Paths to Space (ITYPE = 3)
  - (a) specify H1 and ANGLE
  - (b) specify H1 and H2 (for limb-viewing problem where H2 is the tangent height or minimum altitude of the path trajectory).

For case 2(b), the program will calculate H2, assuming no refraction; then proceed as for case 2(a). The actual slant path range will differ from the input value. This method of defining the problem should be used when refraction effects are not important; for example, for ranges of a few tens of km at zenith angles less than 80°. For case 2(c), the program will calculate BETA and then proceed as for case 2(d). For case 2(d), the program will determine the proper value of ANGLE (including the effects of refraction) through an iterative procedure. This method can be used when the geometrical configuration of the source and receiver is known accurately, but the initial zenith angle is not known precisely due to atmospheric refraction effects. Beta is most frequently determined by the user from ground range information.

Table 14 lists the options on CARD 3 provided to the user for the different types of atmospheric paths.

### A3.2.3.1 Alternate CARD 3 for Transmitted Solar or Lunar Irradiance (IEMSCT = 3)

For calculating directly transmitted solar or lunar irradiance, an ITYPE = 3 path is assumed and CARD 3 has the following form:

## ALTERNATE CARD 3

H1, H2, ANGLE, IDAY, RO, ISOURC, ANGLEM

FORMAT (3F10.3, 15, 5X, F10.3, 15, F10.3)

Table 14. Allowable Combinations of Slant Path Parameters

Case		ITYPE	H1	H2	ANGLE	RANGE	BETA	LEN (Optional)
2a	(1)	2	*	*	*			(*)
2b	(2)	2	*		*	*		
2c	(3)	2	*	*		*		
2d	(4)	2	*	*			*	
3a		2	*		*			
3b	(5)	2	*	*				
<p>(1) LEN option is available only when <math>H1 &gt; H2</math> and <math>ANGLE &gt; 90^\circ</math>. Otherwise, LEN is set in the program.</p> <p>(2) H2 calculated assuming no refraction. Calculated RANGE will differ from the input value.</p> <p>(3) BETA calculated assuming no refraction.</p> <p>(4) Exact ANGLE is calculated by iteration of the path calculation.</p> <p>(5) H2 is interpreted as the tangent height. If H2 and ANGLE are both zero, Case 3a is assumed with <math>ANGLE = 0</math> (that is vertical path). For a path tangent at the earth's surface, read in a small number for H2, for example, 0.001 km.</p>								

H1 = altitude of the observer

H2 = tangent height of path to sun or moon

ANGLE = apparent solar or lunar zenith angle at H1

IDAY = day of the year, used to correct for variation in the earth to sun distance

RO = radius of earth (default according to MODEL)

ISOURC = 0 extraterrestrial source is the sun

= 1 extraterrestrial source is the moon

ANGLEM = phase angle of the moon, that is, the angle formed by the sun, moon,

and earth (required if ISOURE = 1)

Either H2 or ANGLE should be specified. If both are given as zero, then a vertical path (ANGLE = 0°) is assumed. If IDAY is not specified, then the mean earth to sun distance is assumed.

If the apparent solar zenith angle is not known for a particular case, then the solar scattering option (IEMSCT = 2) may be used along with, for instance, the observers location, day of the year and time of day to determine the solar zenith angle (see section 3.2.3.2 of the user instructions). Note that the apparent solar zenith angle is zenith angle at H1 of the refracted path to the sun and is less than the astronomical solar zenith angle. The difference between the two angles is negligible for angles less than 80°.

### A3.2.3.2 Optional Cards Following CARD 3

Optional input cards after CARD 3 are selected by parameters IEMSCT on CARD 1 and IPH on CARD 3A1.

CARD3A1 IPARM, IPH, IDAY, ISOURE (if IEMSCT = 2)

FORMAT (415)

Input card for solar/lunar scattered radiation when IEMSCT = 2.

IPARM = 0, 1, 2 controls the method of specifying the solar/lunar geometry on CARD 3A2.

IPH = 0 Henyey-Greenstein aerosol phase function (see CARD 3A2)  
 = 1 user-supplied aerosol phase function (see CARD 3B)  
 = 2 MIE-generated internal database of aerosol phase functions  
 for the MODTRAN models

IDAY= day of the year, that is, from 1 to 365 used to specify the earth to sun distance and (if IPARM = 1) to specify the sun's location in the sky. (Default value is the mean earth to sun distance, IDAY=93).

ISOURE= 0 extraterrestrial source is the sun  
 = 1 extraterrestrial source is the moon

CARD 3A2 PARM1, PARM2, PARM3, PARM4, TIME, PSIPO, ANGLEM, G (IEMSCT = 2)

FORMAT (8F10.3)

Input card for solar/lunar scattered radiation when IEMSCT = 2. Definitions of PARM1, PARM2, PARM3, PARM4 determined by value of IPARM on CARD 3A1, (See Table 14A.).



For IPARM = 0

PARM1 = observer latitude (-90 to +90 )

(Note that if ABS(PARM1) is greater than 89.5° the observer is assumed to be at either the north or south pole. In this case the path azimuth is undefined. The direction of line-of-sight must be specified as the longitude along which the path lies. This quantity rather than the usual azimuth is read in.)

PARM2 = observer longitude (0 to 360 , west of Greenwich)

PARM3 = source (sun or moon) latitude

PARM4 = source (sun or moon) longitude

For IPARM = 1

**Note:** The parameters IDAY and TIME must be specified. This option cannot be used with ISOURC = 1.

PARM1 = observer latitude (-90 to +90 )

PARM2 = observer longitude (0 to 360 , west of Greenwich)

PARM3, PARM4 are not required

(Note: that the calculated apparent solar zenith angle is the zenith angle at H1 of the refracted path to the sun and is less than the astronomical solar zenith angle. The difference between the two angles is negligible for angles less than 80 degrees.)

For IPARM = 2

PARM1 = azimuthal angle between the observers line-of-sight and the observer to sun path, measured from the line of sight, positive east of north, between -180 and 180.

PARM2 = the sun's zenith angle

PARM3, PARM4 are not required

Table 14A. Card 3A2; Options for Different Choices of IPARM

IPARM=			
PARM1	Observer Latitude (-90 to +90 )	Observer Latitude (-90 to +90 )	Azimuth Angle Between Observer LOS & Observer to Sun Path
PARM2	Observer Longitude (0 to 360 West of Greenwich)	Observer Longitude (0 to 360 West of Greenwich)	Solar Zenith Angle
PARM3	Source Latitude		
PARM4	Source Longitude		
TIME		Greenwich Time (Decimal Hours)	
PSIPO	Path Azimuth Angle (degrees East of Due North)	Path Azimuth Angle (degrees East of Due North)	
ANGLEM (only if ISOURC=1)	Lunar Phase Angle		Lunar Phase Angle
G (only if IPH=0)	Asymmetry Parameter (-1 to +1) for use with Henyey- Greenstein Phase Function	Asymmetry Parameter (-1 to +1) for use with Henyey- Greenstein Phase Function	Asymmetry Parameter (-1 to +1) for use with Henyey- Greenstein Phase Function

## REMAINING CONTROL PARAMETERS

TIME = Greenwich time in decimal hours, that is, 8:45 am is 8.75, 5:20 pm is 17.33  
etc. (used with IPARM = 1)

PSIPO = path azimuth (degrees east of north, that is, due north is 0.0 due east is  
90.0 etc. (used with IPARM = 0 or 1)

ANGLEM = phase angle of the moon, that is, the angle formed by the sun, moon, and

earth (required only if ISOURC = 1)

G = asymmetry factor for use with Henyey-Greenstein phase function (only used with IPH = 0), e.g., +1 for complete forward scattering, 0 for isotropic or symmetric scattering, and -1 for complete backscattering.

CARD 3B1 NANGLS (Only if IPH = 1 on card 3A1)

FORMAT (15)

Input card for user-defined phase functions when IPH = 1.

NANGLS = number of angles for the user-defined phase functions (maximum of 50)

CARD 3B2 (1 to NANGLS)

(ANGF(I), F(1,I), F(2,I), F(3,I), F(4,I), I = 1, NANGLS)

FORMAT (5E10.3)

Input card for user-defined phase functions when IPH = 1.

ANGF(I) = scattering angle in decimal degrees (0.0 to 180.0)

F(1,I) = user-defined phase function at ANGF(I), boundary layer (0 to 2 km default altitude region)

F(2,I) = user-defined phase function at ANGF(I), troposphere (2 to 10 km default altitude region)

F(3,I) = user-defined phase function at ANGF(I), stratosphere (10 to 30 km default altitude region)

F(4,I) = user-defined phase function at ANGF(I), mesosphere (30 to 100 km default altitude region)

The default altitude regions may be overridden by the parameters IHA1, ICLD1 or IVUL1.

## A3.2.4 Card 4: IV1, IV2, IDV, IRES

FORMAT (4I10)

The spectral range and increment of the calculation.

IV1 = initial frequency in integer wavenumber ( $\text{cm}^{-1}$ )

IV2 = final frequency in integer wavenumber ( $\text{cm}^{-1}$ ), where  $V2 > V1$

IDV = frequency increment or step size ( $\text{cm}^{-1}$ ), maximum =  $50 \text{ cm}^{-1}$

(Note: that  $\nu = 10^4/\mu$ , where  $\nu$  is the frequency in  $\text{cm}^{-1}$  and  $\mu$  is the wavelength in  $\mu\text{m}$ , and that DV can only take on integer  $\text{cm}^{-1}$  values.

IRES = triangular slit function; minimum of 2 will insure proper sampling, max = 50.

Table 15 above summarizes the user-control parameters on CARD 4 and CARD 5.

Table 15. MODTRAN CARD 4 and CARD 5 Input Parameters: IV1, IV2, IDV, IRES.

CARD 4	IV1, IV2, IDV, IRES Format (4I10)			
	IV1 (cm <sup>-1</sup> )	IV2 (cm <sup>-1</sup> )	IDV (cm <sup>-1</sup> )	IRES (cm <sup>-1</sup> )
CARD 5	IRPT Format (I5)			
COL5	IRPT			
0	End of program.			
1	Read new CARDS 1, 2, 3, 4, and 5.			
2	Not used (stops program).			
3	Read new CARDS 3 and 5.			
4	Read new CARDS 4 and 5.			

## A3.2.5 CARD 5: IRPT

### FORMAT (15)

The control parameter IRPT causes the program to recycle. so that a series of problems can be run with one submission of MODTRAN.

- IRPT = 0 to end program
- = 1 to read all new data cards (1, 2, 3, 4, 5)
- = 2 not used
- = 3 read new CARD 3 (the geometry card) and CARD 5
- = 4 read new CARD 4 (frequency) and CARD 5
- > 4 or IRPT = 2 will cause program to STOP

Thus, if for the same model atmosphere and type of atmospheric path the reader wishes to make further transmittance calculations in different spectral intervals V1' to V2' etc., and for a different step

size (DV etc.), then IRPT is set equal to 4. In this case, the card sequence is as follows and can be repeated as many times as required.

```
CARD 5  IRPT = 4
CARD 6  IV1', IV2', IDV', IRES'
CARD 7  IRPT = 4
CARD 8  IV1", IV2", IDV", IRES"
CARD 9  IRPT = 0
```

The final IRPT card should always be a blank or zero. When using the IRPT option, the wavelength dependence of the refractive index is not changed (use the IRPT = 1 option if this is required).

**NOTE:** IRPT=3 cannot be used when running multiple scattering cases or solar single scattering. Use IRPT=1.

### A3.3 Non-Standard Conditions

Several options and combination of choices are available if atmospheric transmittance/radiance calculations are required for non-standard conditions. Here non-standard refers to conditions other than those specified by the parameters MODEL, IHAZE, and ICLD on CARDS 1 and 2. These options enable the user to insert:

- (1) An additional atmospheric model (MODEL = 7), which can be in the form of radiosonde or other source data. It is not necessary to duplicate the altitudes used in MODTRAN 3.
- (2) Meteorological conditions for a given horizontal path calculation (MODEL = 0)
- (3) A combination of any or all of the 12 gases can be input for each layer boundary with default choices interleaved with user supplied data.
- (4) Aerosol vertical distributions can be input at specified altitudes by the use of AHAZE, EQLWCZ, and/or IHA1 on CARD 2C3 when IRD2 is set to 1 on CARD 2C.
- (5) Cloud liquid water contents and or rain rates can be input at specified altitudes by the use of EQLWCZ, RRATZ and/or ICLD1 on CARD 2C3 when IRD2 is set to 1 on CARD 2C.

- (6) Any combination of the one to four Aerosol altitude regions can be replaced by reading in specific values of extinction and absorption coefficients and asymmetry parameters for specific regions by utilizing CARDS 2D, 2D1 and 2D2. The parameters can be for aerosols and for clouds.

### A3.3.1 ADDITIONAL ATMOSPHERIC MODEL (MODEL = 7)

A new model atmosphere can be inserted by the use of CARD 2C and the required multiples of card 2C1, provided the parameters MODEL and IM are set to 7 and I respectively on CARD 1. The number of atmospheric levels to be inserted (ML) must also be specified on CARD 2C.

The appropriate meteorological parameters and the format are given below:

CARD 2C ML, IRD1, IRD2, TITLE  
FORMAT (3I5, 18A4)

CARD 2C1 ZMDL, P, T, WMOL(1), WMOL(2), WMOL(3), (JCHAR(J), J = 1,14), JCHARX  
FORMAT (F10.3, 5E10.3, 15A1, 1X, A1)

See section 3.2.2.1 above for a detailed description of each variable.

### A3.3.2 HORIZONTAL PATHS (MODEL = 0)

If known meteorological data are to be used for horizontal path atmospheric transmittance/radiance calculations, then set MODEL = 0 and IM = 1 on CARD 1. Proceed to read the meteorological conditions utilizing CARDS 2C and 2C1 as described above. In this instance the parameter ML must be set to 1.

### A3.3.3 USER INSERTED VALUES FOR ATMOSPHERIC GASES (MODEL 0 OR 7)

The user may wish to enter specific values of any or all of the atmospheric gases. This can be accomplished by utilizing CARDS 2C, 2C1 and 2C2. On CARD 2C set IRD1 = 1. The specific gas amounts for individual gases can be entered on CARDS 2C1 and 2C2 and by utilizing the parameter JCHAR on CARD 2C1. The user has a choice of entering data in several different sets of units (eg. volume mixing ratio, number density, . . . etc.), or defaulting to one of the model atmospheric gases at the specified altitude.

### A3.3.4 USER INSERTED VALUES FOR AEROSOL VERTICAL DISTRIBUTION (MODEL = 0 OR 7)

The capability exists for the user to be able to replace aerosol distributions at specific altitudes. In order to accomplish this the user must set IRD2 to 1 on CARD 2C. Then specify the altitudes on

CARDS 2C1 along with the variables, defaults and or units by utilizing the parameters as explained in section 3.2.2.1

On CARD 2C3 the aerosol scaling factor for a given altitude can be entered by using the variable AHAZE, or an appropriate value for EQLWCZ, or defaulted by using the variable IHA1.

### A3.3.5 USER INSERTED VALUES FOR CLOUD AND OR RAIN RATES

**(MODEL = 0 OR 7)**

The same capability exists permitting the user to replace cloud liquid water contents and or rain rates at specific altitudes as described in the above section. This is accomplished by setting IRD2 to 1 on CARD 2C. Then the specific altitudes may be entered on CARDS 2C1 along with the variables, defaults and or unit selection by using the remaining parameters of CARD 2C1 as described earlier.

On CARD 2C3 the variables EQLWCZ and/or RRATZ can be used to enter the intended value of equivalent liquid water content of a cloud and/or the rain rate at the specified altitude, or the cloud attenuation can be specified by using AHAZE, The user may default at the specified altitude to one of the built-in cloud and/or rain model values by using ICLD1.

### A3.3.6 REPLACEMENT OF AEROSOL OR CLOUD ATTENUATION MODELS

**(IHAZE = 7 AND/OR ICLD = 11)**

The aerosols or cloud model utilized in any or all of the four altitude regions may be replaced by a user input model, The built-in regions are 0-2 km, > 2-10 km, > 10-30 km and > 30-100 km. These regions may be modified by the use of the parameters IHA1, ICLD1 or IVUL1. This option is initialized by setting IHAZE = 7 or ICLD = 11.

On CARD 2D the variable IREG (1, 4) determines which of the altitude regions will have replacement values read in. The user is required to enter a conversion factor, AWCCON ( $\text{km gm m}^{-3}$ ), on card 2D1, which converts aerosol or cloud profiles specified in terms of equivalent liquid water content, EQLWCZ ( $\text{gm m}^{-3}$ ), to an extinction coefficient ( $\text{km}^{-1}$ ). This conversion factor (AWCCON) is only used if the aerosol or cloud concentration are specified by EQLWCZ instead of by the visible extinction, AHAZE. The LOWTRAN values for this variable are stored as DATA statements in subroutine EXABIN. (See DATA statements ELWCR, ELWCM, ELWCU, ELWCT, AFLWC, RFLWC, CULWC, ASLWC, STLWC, SCLWC, SNLWC, BSLWC, FVLWC, AVLWC, and MDLWC.)

The multiply read CARDS 2D2 (13 cards) consist of four variables, VX, EXTC, ABSC and ASYM. The first variable VX is the wavelength of the data points which should correspond to the wavelengths used in the program (defined in array VX2 in Subroutine EXTDTA, see table 12). The next three variables EXTC, ABSC, and ASYM are the aerosol or cloud extinction, absorption coefficients and the asymmetry parameters respectively. As stated previously the variable IREG (1-4) will determine if the user is reading in 1, 2, 3, or 4 sets of CARDS 2D1-2D2. Additionally, by utilizing the variables IVUL1

and ISEA1 the user can substitute for stratospheric aerosol profiles and can change the seasonal profile values.

The values of  $EXTC(N,I)$  and  $ABSC(N,I)$  should be normalized so that  $EXTC(N,4) = 1.0$  (i.e., the extinction for wavelength 0.55  $\mu$ m is normalized to 1.0).